Distribution Agreement

In presenting this thesis or dissertation as a partial fulfillment of the requirements for an advanced degree from Emory University, I hereby grant to Emory University and its agents the non-exclusive license to archive, make accessible, and display my thesis or dissertation in whole or in part in all forms of media, now or hereafter known, including display on the world wide web. I understand that I may select some access restrictions as part of the online submission of this thesis or dissertation. I retain all ownership rights to the copyright of the thesis or dissertation. I also retain the right to use in future works (such as articles or books) all or part of this thesis or dissertation.

Signature:

___Holly Christopher Lewis___ ___July 28, 2017_____
[Student's name typed] Date

Approval Sheet

Aromatics & Exosomes: The Translation of Cell Therapy

By

Holly Christopher Lewis
A.B. Harvard University, 2009

Graduate Division of Biological and Biomedical Science
Immunology and Molecular Pathogenesis

_____
Jacques Galipeau
Advisor

_____
Daniel Kalman
Committee Member

_____
Sean Stowell
Committee Member

_____
Brian Evavold
Committee Member

_____
Iñaki Sanz
Committee Member

Accepted:

_____
Lisa A. Tedesco, Ph.D.
Dean of the James T. Laney School of Graduate Studies

_____
Date

Abstract Cover Page

Aromatics & Exosomes: The Translation of Cell Therapy

By

Holly Christopher Lewis

A.B. Harvard University, 2009

Graduate Division of Biological and Biomedical Science

Immunology and Molecular Pathogenesis

Advisor: Jacques Galipeau MD

A dissertation submitted to the Faculty of the

James T. Laney School of Graduate Studies of Emory University

in partial fulfillment of the requirements for the degree of

Doctor of Philosophy

in Graduate Division of Biological and Biomedical Science

Immunology and Molecular Pathogenesis

2017

Abstract

Aromatics & Exosomes: The Translation of Cell Therapy

By Holly C. Lewis

Mesenchymal stromal cells (MSCs) are a low-frequency population in the adult bone marrow. These self-renewing pluripotent stem cells can be easily expanded *ex vivo*, generating clinical quantities of personalized cell therapeutics. Despite showing biologic efficacy in a variety of mammalian studies and clinical trials, the mechanisms by which MSCs exert their bioactivity have been incompletely described.

One of the principle mechanisms we and others have shown as crucial for MSC efficacy is the enzyme indoleamine 2,3-dioxygenase (IDO). This enzyme catalyzes the key reaction in tryptophan metabolism. The synthetic drug 1-methyl tryptophan is a selective inhibitor of IDO enzymatic activity that is being tested in cancer immunotherapy trials, particularly for patients with IDO+ tumors. Based on its chemical structure, we hypothesized 1MT might also activate the aryl hydrocarbon receptor (AHR). AHR is a widely-expressed transcription factor that is classically understood as the receptor for 2,3,7,8-tetrachlorodioxin, a potent environmental toxin. Such a mechanism of action for 1MT suggests its application for a wider range of patients, irrespective of tumor IDO expression. Such observations support a novel paradigm by which AHR-activating compounds like 1MT may be used in cancer immunotherapy to stimulate a pro-inflammatory response.

Collaborations with our lab have recently shown that MSC-conditioned culture medium

(CM) can maintain healthy peripheral-blood-derived antibody-secreting cells (ASCs) for up to 30 days *in vitro*. We hypothesized that some of this *in vitro* support was due to nanoscale extracellular membrane vesicles, or exosomes. We interrogated exosome production from replicating and irradiated, growth- arrested MSCs to model the physiology of endogenous-mobilized or quiescent marrow MSCs. We found that exosomes were able to reproduce the *in vitro* support to ASCs observed with unfractionated CM. Purified exosomes from both replicating and growth-arrested MSCs were comparable in their ability to support ASCs. To elucidate factors accounting for the *in vitro* ASC support, we performed proteomics on exosomes derived from replication-competent and growth- arrested MSCs, identifying factors involved in the vesicle-mediated delivery of immune signaling proteins. Taken together, these findings indicate that MSC-derived exosomes can serve as a model for cell-free cell therapy.

Cover Page

Aromatics & Exosomes: The Translation of Cell Therapy

By

Holly Christopher Lewis
A.B. Harvard University, 2009
Graduate Division of Biological and Biomedical Science
Immunology and Molecular Pathogenesis

Advisor: Jacques Galipeau MD

A dissertation submitted to the Faculty of the
James T. Laney School of Graduate Studies of Emory University
in partial fulfillment of the requirements for the degree of
Doctor of Philosophy
in Graduate Division of Biological and Biomedical Science
Immunology and Molecular Pathogenesis
2017

Acknowledgements

There are a great many people that I must thank for helping me every step of the way towards this doctoral degree. I wish to begin by thanking my parents Wayne and Dorothy Lewis, who birthed me, named me and directed the earliest developments of my life, inspiring me to achieve the highest levels that I could. They wouldn't take no for an answer, and always pushed me to challenge myself. I thank my siblings, Jake, Katie and Dave for always supporting me, no matter what. Likewise, I thank my grandparents, aunts, uncles, cousins, and everyone who saw inner talent in me. To the same degree, I thank many unnamed chosen-family; those intimately-close folks who have stuck by me, especially this past decade of marital, gender and professional struggle, helping me achieve the triumph I feel today.

I thank Dr. Kohn, the speech pathologist who I first saw as an infant, and then later my elementary school speech pathologist Ms. Corcoran. Pitied or spurned by shoppers in the grocery stores, and later insulted by classmates as a deficient child who was unable to communicate, it was their training in the science of language that gave me voice. It was that confidence that empowered me to study Spanish and Latin in high school (thank you to Ms. Qualey, Ms. Kames, Ms. Murray, Ms. Curran, the Moscas) and that would help me go on to graduate Harvard University with a secondary degree in Romance Languages and Literatures, fluent in Spanish, Catalan and Portuguese, that I parlayed into medical internships in Barcelona, Cuba and Puerto Rico (thank you, Silvia Bonamusa, Luis Girón-

Negrón, Doris Sommer among many others). And again, I thank my mother for tirelessly bringing me to every session of speech therapy, standing up for me in public and parochial schools to get the care I deserved. Her stick-to-it-iveness has been a life-long-lesson in advocacy that I draw upon every day on behalf of marginalized folx of every gender, sexuality, race and ability.

I thank Miss Margaret of Vero Beach, Florida, who worked with me as a diffident adolescent, terrified of swimming in chest-deep water, teaching me to rely on my own abilities to float, push and then soar. It was her training that enabled me to pursue lifeguard training two years later, thence onward to become a Red Cross-certified swimming and diving instructor. It was my experiences as Head Lifeguard at New Silver Beach in Falmouth, Massachusetts that would inspire me to a career in medicine. Having studied and trained for years to develop swimming, first aid and CPR abilities, I have pushed relentlessly towards my professional degrees, seeking to understand the practical application of biomedical knowledge.

I thank Dr. Eileen Shaughnessy, Harvard-trained chemist who inexplicably taught at my public vocational/technical high school in Weymouth, a blue-collar town about ten miles south of where I was born in Dorchester. It was her junior-year class that first showed me the beauty of arrow-pushing chemistry, inspired me to develop an independent studies in biochemistry and advanced physics the next year, and led me to concentrate in the same department that awarded her doctoral degree, Harvard's Chemistry & Chemical

Biology. Others who inspired me in those years were my history teacher Mr. Tortora, and my English teachers Mr. Porro and Mr. Pappas, each of whom taught me to question everything.

At Harvard, I had amazing privileges, setting into motion a career I could not have imagined. I was advised by Dr. Gregg Tucci, who comforted me in my first year, weeping when I got the first two C's I'd ever seen on a report card, terrified that I'd never be a doctor. Dr. Ahamindra Jain, the director of undergraduate laboratories, fortunately never saw my transcripts, but only me, excitedly synthesizing spearmint and banana oils (chiral enantiomers of each other, a key concept in my dissertation), and he saw something in me that my grades did not reveal. He invited me to participate in an elite sophomore seminar in organic synthesis, where I worked with Nobel laureate E.J. Corey, developing a new synthesis of Tamiflu, to combat the 2006 H1N1 influenza pandemic. I'll never forget the day my little brother was hit by a car in front of our high school; I was in the lab, running my first Tamiflu isolates through a silica column. Dr. Jain finished the extraction for me that day, as I anxiously ran to catch the Red Line south, arriving at the hospital that night to visit David (who survived, badly contused & concussed but unbroken, though it did end his football career). Dr. Jain did not, dying the next year from a very rapid case of pancreatic cancer, and I struggled at his memorial service, unable to tell his widow and child what their father meant to me.

That summer I presented my organic synthesis at the American Chemical Society, and was delighted to see Dr. Shaughnessy there too, presenting her own research. My entrée to academic science was assured, and I began work that year at the Harvard School of Public Health. My grandfather was nearby at the Beth Israel Hospital, dying of complications from a liver iron-storage disease that afflicts most of my family…my eyes tear up now as I remember visiting him in those days, while I was learning to grow mouse cells with the same mutation. Under the very patient advising of a professor of Nutritional Biochemistry, Dr. Marianne Wessling-Resnick, I discovered this iron signaling defect was intricately linked to the pathogenesis of tuberculosis and the anemia of chronic disease. I worked every day at the lab with Dr. Erin Johnson, my first queer science mentor, who taught me to grow cells in a plastic dish, shaking her head and laughing when I killed my first plate of cells, and doing so with an incredibly confident and badass attitude that it would take me years to appreciate. It was my first time culturing deadly bacteria on agar plates and my first time working with mice, donning a spacesuit/ventilator to enter the BL3 lab on Huntington Avenue, to watch the sad animals coughing blood. It was Erin who first taught me to grow leukocytes on piece of glass, using immunologic histochemistry to observe sub-cellular protein trafficking, a technique that would become instrumental for my dissertation.

After college, I joined the Division of Immunology at Boston Children's Hospital, under the patient guidance of Dr. Michiko Oyoshi. Michiko refused to hire me for twelve months, lest I only complete a lackluster research post-bacc…her insistence that I take 2 years to

work in basic science was difficult to explain to my parents, as a dream-deferred would require taking the MCAT again due to a time-expired score. I have no regrets. Michiko trained me to become an independent scientist, to present data at lab meetings, to keep an assiduous notebook, and how to design experiments with my analyses in mind from the start. Dr. Lisa Bartnikas and Dr. Janet Chou let me come with them on rounds, where we saw children with atopic dermatitis and food allergies, the same diseases I was learning to induce in my Balb/c mice. I showed Lisa how to count spleen-derived lymphocytes, and she showed me how to test a child's back for skin allergies. Translational medicine at its finest, and I am forever grateful for those experiences. My first immunology tattoo was an eosinophil, forever emblazoning the life lessons I learned from Michiko, and the first time I appeared in PubMed.

At Emory, I gained an amazing assemblage of new advisors, scientists, clinicians and inspiring humanists at every turn. The dean of admission, Dr. Ira Schwartz, saw through my middling grades at Harvard in a way the NIH F30 study sections never would, embracing me as a passionate clinician-scientist, searching for a home to develop into who I have become. I was embraced and inspired by Dr. Nick Krawiecki, the first Emory pediatrician I studied under, who taught always the value of ethics and patient-centered care. Likewise for Dr. Flavia Mercado, who has been a staunch ally of mine, in the clinics and *calles* of Puerto Rico, from the Consulates of Honduras & Brazil, to the International Clinic of Grady; she has never doubted for a second that a white-skinned femme-leaning medical student could do valuable translational work in any culture or language setting.

Ditto for Dr. Dabney Evans, who shared with me her expertise in Cuban public health, through words and actions, helping me arrange that amazing summer in 2012, traveling the socialist island as I sought to understand its secrets for public health.

In my third year of PhD research, I wept disconsolately and was comforted by Mary Horton, MD/PhD program director, as I told her I'd have to take some time off. I had just come out as queer/trans, my wife had left me, and the world around me was echoing with the ricochets of an exploded seven-year relationship and a ten-month marriage. Since my earliest days at Emory, she has been one of the strongest advocates I've had in the School of Medicine, and I am so grateful to her for everything. Ditto for Dr. Schwartz, who was there for me in my darkest hours, and though he did not yet understand the circumstances, he nonetheless assured me that divorce would not define me, in the same way my mistakes at Harvard have not.

Dr. Galipeau. He accepted and embraced any scientist who could do the work. Shala Yuan, Seema Patel, Spencer Ng, Andrea Pennati, Ian Copland, Marco Garcia, Wayne Harris, Hilary Rosenthal, Raghavan Chinnadurai and Jiusheng Deng…each lab member inspired me in profound ways, teaching me with words and with actions, what it means to be a professional scientist. A very special thank you is due to Seema, who not only taught me everything I know about flow cytometry, but also, supported me and believed in me through any number of personal, scientific and relationship crises. Ditto for Spencer, whose friendship I will also treasure for my entire life. Dr. Galipeau gave me the freedom

to define my project, the freedom to build hypotheses, and the freedom to develop collaborations across the schools and continents in a way I never thought possible. Under his guidance, I learned the true value of scientific openness and collaboration. A cell therapist, a clinician, a scientist, a Québécois-speaking man-of-the-world, Dr. Galipeau's mentorship has been everything an aspiring physician-scientist could hope for. I wept in his office too, struggling with failed experiments ("it is always challenging to cut through the forest. No-one yet has been there to build a path," he said) and also when I had to take two weeks off to meet the soon-to-be-ex-wife in Cambridge to discuss the divorce terms. I put the exosome experiments on pause, saw about that ugly business, and came right back to work. In the science I found meaning, purpose and a clear direction ahead, and Dr. Galipeau has never flagged in supporting me. Though I was saddened by his Emory departure, he assured me he would only leave once he'd been sure to set me up for success. In the past year of dissertating, I have relied greatly upon the kindness of Dr. Eun-Hyung Lee, Dr. Steve Bosinger, Dr. Greg Tharpe, Dr. Gary Miller, Dr. Mike Caudle, Dr. Sean Stowell, and Dr. Haydn Kissick. A special thanks to Dr. Dan Kalman, who supported me in a time of dark tribulations, and simply refused to let me give up on myself. Warm thank-yous are also due to the other members of my thesis committee, Dr. Iñaki Sanz, Dr. Brian Evavold, each of whom has been supportive in their own important ways.

A special thanks goes to Dr. Galipeau for also allowing me the freedom to develop my skills as an educator, working under Dr. Megan Cole, to teach six semesters of pre-med lab biology for Emory college students. Though I taught much, I learned more from those

students than they may imagine, for as St. Francis of Assis reportedly said, it is in giving that we receive.

In a bizarre way, I thank the ex-wife, as she freed me in ways to discover and define myself anew. One of those ways was allowing this newly-single grad student to begin a relationship with a chemistry PhD student and public science advocate named Marika. My work with Marika, Tayla, Constance were pivotal in my life; so too was a loving relationship with a one person. Blossoming out into the Atlanta area, I met a whole new community of artists, scientists and radical activists, that helped me develop the award-winning *Sickle & Flow.* Leveraging my basic science skills, community health outreach and navigating the queer activist spaces of Atlanta, I finally realized that I am most whole when I am living my whole self. Ditto for Critical Junctures 2016, and 2017: The Work of Art, leveraging science, gender and disability studies to, among other inspiring events, bring the head of the NIH's LGBTQ research office to campus, exploring ways to connect basic science, public health and the humanities.

I thank also my queer science and public health mentors in Atlanta, Representative Park Cannon, Dr. Bettina Love, Dr. Anne Pollock, Dr. Deboleena Roy, Dr. Manu Platt, and others who have helped me synergize health sciences and humanities: Dr. Nael McCarty, Dr. Hughes Evans, Dr. Angelika Bammer, Dr. Jennifer Sarrett, Dr. Jennifer Singh, Dr. Maria Carrión. It's been a long strange trip, but I know I'll continue to thrive if I collaborate like these folks have taught me. Lastly, I thank the advocates who have helped me navigate

this past year of intense transitions (medical, scientific, and personal): Dr. Izzy Lowell, Dr. Bill Eley, Dr. Lisa Tedesco, Dr. Larry Boise, Dr. Don Batisky, Dr. Joanna Bonsall, Dr. Ann Chahroudi, Dr. TJ Murphy, Dr. Anita Corbett, Dr. Cathy Quiñones-Maeso, Ms. Laura Hopkins, Dr. Sheryl Heron, Dr. Maura George, Dr. Kim Manning, Rebecca Masel, Jenny O'Neil, Barbara Powley, Erica Weaver, Maxine Thompson, Shelby Smith, Danielle Bruce Steele and Megan Pendleton.

Table of Contents

List of Figures

Foreword:

Defense Program Abstract

Mesenchymal stromal cells (MSCs) are a low-frequency population in the adult bone marrow, comprising one in 10,000 of all mononuclear cells harvested from an iliac crest aspirate under local anesthesia. These self-renewing pluripotent stem cells can be easily expanded ex vivo, generating clinical quantities of personalized cell therapeutics that we and others have utilized for a variety of first-in-human trials. MSCs have been deployed in clinical trials as immune-modifying therapies for Crohn's disease, multiple sclerosis, lupus, and engraftment during sickle cell transplantation therapy in addition to regenerative applications for ischemic stroke or cardiomyopathy. Despite showing biologic efficacy in a variety of mammalian studies and clinical trials, the mechanisms by which MSCs exert their bioactivity have been incompletely described. A number of reports have shown that contact-dependent factors and the release of soluble factors are both implicated in MSC therapy.

One of the principle mechanisms we and others have shown as crucial for MSC efficacy is the enzyme indoleamine 2,3-dioxygenase (IDO). This enzyme catalyzes the key reaction in tryptophan metabolism, generating a class of bioactive molecules called kynurenines, known to be involved in tolerance signaling. The synthetic drug 1-methyl tryptophan is a selective inhibitor of IDO enzymatic activity that is being tested in cancer immunotherapy trials, particularly for patients with IDO+ tumors. Based on its chemical structure, we

hypothesized 1MT might also activate the aryl hydrocarbon receptor (AHR). AHR is a widely-expressed transcription factor that is classically understood as the receptor for 2,3,7,8-tetrachlorodioxin, a potent environmental carcinogen that can be found in cigarette smoke, contaminated ground water, and Agent Orange. We demonstrate MSCs express the AHR protein, and that in vitro treatment with 1MT causes AHR activation as observed by RNA, immunologic, and bioinformatics techniques. These findings for 1MT are consistent with its MSC- and immune-stimulating reputation, yet uncoupled from the expression or catalytic function of IDO. Such a mechanism of action for 1MT suggests its application for a wider range of patients, irrespective of tumor IDO expression. These observations support a novel paradigm by which AHR-activating compounds like 1MT may be used in cancer immunotherapy to stimulate a pro-inflammatory response.

An understanding of the stromal cues that enable marrow-resident B cells to maintain immunologic memory is crucial not only for vaccine design, but also in cell therapy platforms that seek to expand patient lymphocytes. Emerging cancer immunotherapies using chimeric antigen-receptor T cells have shown great promise in the clinic, due in part to a historically-thorough understanding of T cell growth requirements, buttressed with novel genetic engineering techniques. However, the development of clinical-grade B cell therapy platforms lags due to incomplete knowledge of how to keep such cells functional without introducing cancer-derived genes. For example, the development of monoclonal antibody (mAb) biologics often relies upon fusing a customized B cell with a cancerous myeloma cell. Infusions of such hybridomas is therapeutically impossible, due to a high

risk of cancer in recipients. Only their cell-free mAb byproducts—traditionally derived from animal ascites or more often today via recombinant bacteria—are approved for safe clinical use in humans. Likewise, induced pluripotent stem (IPS) cells or embryonic stem cells both carry a non-zero risk for carcinogenesis in recipients. In contrast, the clinical effect of MSCs relies upon their inherent immune-modifying character, require no genetic manipulation, and have led to virtually no reports of MSC-linked malignancies in cell therapy trials.

Collaborations with our lab have recently shown that MSC-conditioned culture medium (CM) can maintain healthy peripheral-blood-derived antibody-secreting cells (ASCs) for up to 30 days in vitro. When we treated MSC CM with a liposome-disrupting agent, plasma cell antibody-secretion was greatly diminished; leading us to hypothesize that some of this in vitro support was due to nanoscale extracellular membrane vesicles, or exosomes. We interrogated exosome production from replicating and irradiated, growth-arrested MSCs to model the physiology of endogenous-mobilized or quiescent marrow MSCs. Electron microscopy (EM) and immunologic techniques demonstrated that irradiation of the MSCs altered neither the structural morphology nor the overall yield of exosomes. We found that exosomes were able to reproduce the in vitro support to ASCs observed with unfractionated CM. Purified exosomes from both replicating and growth-arrested MSCs were comparable in their ability to support ASCs. To elucidate factors accounting for the in vitro ASC support, we performed proteomics on exosomes derived from replication-competent and growth-arrested MSCs, identifying factors involved in the

vesicle-mediated delivery of immune signaling proteins. Taken together, these findings indicate that MSC-derived exosomes can serve as a model for cell-free cell therapy.

This written dissertation encompasses all work pursued by the author in the pursuit of her PhD degree, as a dual degree candidate in the Laney Graduate School and the School of Medicine. The reader should note that all figures and tables are based on data and experiments of her own design. As a dually-enrolled student, fully-engaged with basic science investigations, she also worked to stay abreast of clinical and translational outcomes for this type of research. To wit, an interlude chapter found within this written dissertation describes her award-winning community outreach non-profit organization, *Sickle & Flow.*

Chapter 1: An Introduction to Mesenchymal Cell Therapy

Endogenous and ex vivo-cultured MSCs

In vertebrates, the majority of post-natal hematopoiesis occurs in the marrow of the long bones. Each day, the marrow of adult humans releases hundreds of millions of new blood cells into circulation [1], but the profound proliferative capacity of this system must be kept in check by a variety of mechanisms: dysregulated marrow is the genesis of autoimmune disease and hematologic dyscrasias, both benign and malignant. The hematopoietic stem cell (HSC) is the multipotent self-renewing progenitor that gives rise to all cells of the lymphoid (i.e. T cell, B cell, natural killer cell) and myeloid (i.e. erythrocyte, monocyte, granulocyte, platelet) lineages.

A bone marrow aspirate reveals the stromal tissue of mammalian bone marrow to be a complex structure, punctuated by blood cell progenitors of varying maturity, interspersed with adipocytes as well as the bone-remodeling osteoclasts and osteoblasts. In the highly vascularized endosteal niche, the stromal cell network surrounds and coordinates the development of HSCs. If a healthy human bone marrow aspirate is put into tissue culture plates, after a week of culture, a population of plastic-adherent spindle-shaped cells will manifest. This process of *ex vivo* expansion is necessary in order to generate appreciable amounts of cells, for in the native marrow, these cells are vanishingly rare—and can be found at a frequency of approximately 1 out of 10,000 cells[2]. These are mesenchymal stromal cells, a progenitor population that can differentiate into a number of mesoderm-

derived tissues, such as adipose, cartilage and osteocytes. It is this mesenchymal progenitor feature that serves loosely as rationale for the term "stem cell", but to prevent confusion with HSCs, and in reference to their stromal derivation, we and others refer to these as mesenchymal stromal cells, though MSC abbreviates both terms.

MSCs Coordinate HSC Development

Within the vascularized marrow compartment, fate-mapping and parabiosis experiments have elucidated different MSC classes that interact with HSCs to coordinate hematopoiesis [3-7]. Although MSC surface and intracellular markers vary in the literature, such variance is thought to reflect the different microenvironments in which the cells reside (i.e. skin, lung, fat, marrow) rather than distinct cell lineages [7]. One of the more well-described marrow-resident MSCs is the CXCL12-abundant reticular (CAR) stromal cell. Named for their reticuloid processes as well as their chemokine production, CAR stromal cells have been shown to be essential for functional hematopoiesis. CXCL12 is produced by stromal cells in the marrow and is required for normal lymphopoeisis—the development of a functionally mature T and B cell compartment. Recent work using conditional knockout mice has elucidated the connection between CAR stromal cells and committed lymphoid progenitors (CLPs) in the marrow. Using a *Cre-lox* system, Greenbaum and colleagues show that when CXCL12 is deleted only from CAR stromal cells, animals exhibit a sharp drop in the numbers of pre-pro B cells, and have fewer marrow CLPs [6]. CAR stromal cells are also principal sources of stem cell factor (SCF, a.k.a. Kit ligand), a cytokine which is presented on the stromal cell membrane. SCF is the ligand

for the receptor tyrosine kinase c-Kit (CD117) which transduces important pro-survival signals to developing HSCs [8, 9]. As such, CAR stromal cell-derived signals are indispensable for normal hematopoiesis. Using an inducible knockout system in mice, Omatsu and colleagues have shown that short-term ablation of CAR stromal cells decreases the self-renewing cell cycling of HSCs, as well as reducing the numbers of both lymphoid and erythroid progenitor cells [4].

MSCs and Central Tolerance in the Bone Marrow

Lymphopoeisis is a complex process, wherein T and B cell progenitors generate a unique antigen receptor via the recombination of hundreds of different gene segments. Immunologists have calculated that on the order of 10^{18} different antigen receptors could be stochastically made, although certain mechanisms (allelic exclusion, the preponderance of certain TCR β-chains) revise this number downward [10]. Nonetheless, gene segment recombination endows a healthy vertebrate with an extremely diverse immune repertoire, poised to respond to a vast array of proteins, lipids or carbohydrates. Occasional lymphocytes are generated whose receptors target against self antigens. Left unchecked, such T or B cells may escape to the periphery, and under certain conditions, initiate a pathologic autoimmune process. The body has a number of mechanisms whereby it evades autoimmune disease, but these can be grouped into two general classes: central tolerance and peripheral tolerance. By central tolerance, we refer to events occurring in the primary lymphoid organs—the bone marrow, thymus or spleen—

whereas peripheral tolerance may be induced anywhere leukocytes are found in the body.

In the marrow, lymphoid progenitors with newly-generated antigen receptors are in constant contact with the stromal cell network. It is important to note that although lymphoid progenitors begin this process in the marrow, T cells migrate to the thymus in order to undergo maturation. In a process termed positive selection, new lymphocytes ensure that their receptor is capable of recognizing peptides presented by endogenous antigen-presenting cells. In negative selection, lymphocytes that vigorously auto-react to self antigens are neutralized to so-called clonal ignorance, anergy or undergo apoptosis, here termed deletion. Thymic stroma help coordinate positive and negative selection, thereby serving as primary enforcers of central tolerance. Studies using human cells as well as murine models have shown that MSCs can be isolated from the thymus, and that they contribute to the development of normal T cell compartment [11, 12]. Towards the coordination of such lymphopoiesis, MSCs, like professional antigen presenting cells, can express the diverse human leukocyte antigen (HLA) molecules: Class I, presenting mainly intracellular-derived peptides, and Class II, presenting extracellular-derived peptides. If the lymphocyte is unable to recognize, or if it auto-reacts too vigorously to the HLA-presented peptides, that lymphocyte clone is deprived of pro-survival signals (i.e. CXCL12, other growth factors) and is deleted.

In addition to Class I and II, less variable HLA molecules are expressed by mesenchymal stromal cells, including HLA-G. Initially discovered on trophoblastic tissues, HLA-G prevents maternal immune infiltration of the semi-allogeneic fetus. When expressed by MSCs, HLA-G confers an immunosuppressive signal by activating immunotyrosine inhibitory motifs (ITIMs) on lymphocytes and monocytes. In the marrow, HLA-G signaling dampens the activity of bone-remodeling osteoclasts (monocyte-derived), whereas in the periphery, lymphocytes respond to HLA-G on membranous vesicles [13, 14].

Ex vivo, MSCs have been defined using conventional flow cytometric techniques by the International Society for Cellular Therapy (ISCT) [15]. These cells must stain positively for CD73 (ecto-5'-nucleotidase), CD90, and CD105 (endoglin), but lack staining for the following lymphomyeloid markers: CD11b, CD14, CD19, CD34, CD45, CD79a, or of MHC class II[16].

MSCs can be isolated from a variety of non-hematopoietic tissues including lung, fat, kidney, skin and muscle. Indeed, some reports indicate that MSCs can be derived and propagated from any organ tissue, and that the amount of MSCs present is proportional to the blood vessel density per end-organ [17]. The role of MSCs as precursors for angiogenesis has become appreciated as recent reports show a shared phenotype with vascular pericytes. Though beyond the scope of present discussion of immune-mediated application, MSCs have been much-explored in the field of regenerative medicine, particularly in cardiovascular and wound-healing models [18-22].

Cell Biology of MSCs in Culture

Since their initial discovery in bone marrow, MSCs have been studied by translational scientists in attempts to harness their regenerative and immunomodulatory abilities. The stem nature of MSCs—and their proven ability to differentiate into cartilage, bone and fat cells—has spurred research efforts to regenerate these tissues. A number of studies have utilized MSCs to regrow musculoskeletal tissues, including craniofacial defects [23], repair of ruptured tendons [24], or to correct the congenital bone disease osteogenesis imperfecta [25]. The regenerative nature of MSCs has not been without controversy, however, as published reports have claimed the ability to repair transected spinal cords, myocardial infarcts and even autism. Such controversy may speak to the variability inherent to performing *in vitro* differentiation with stem cells, by which different laboratory culture media and cell processing protocols can be at variance.

MSCs and B cell Immunosuppression

Whereas the regenerative capacity of MSCs may remain a question of tissue culture recipes, the immunomodulatory capabilities of these cells has been borne out in a variety of assay systems. From a teleological perspective, the role of MSCs in hematopoiesis affords us the best lens to view the mechanisms by which stromal cells suppress the proliferation and effector function of potentially pathologic leukocytes. After an immature B cell has undergone gene recombination and expresses its novel antigen receptor, marrow stromal cells mediate positive and negative selection. Through this

process, autoreactive B cells are either silenced or deleted, thereby maintaining central tolerance. For autoreactive B cells that do escape the marrow, mechanisms of peripheral tolerance exist to limit immunopathology. Given the complexities of observing central and peripheral tolerance *in situ,* a number of techniques have been developed to model how MSCs and pathologic B cells interact.

In a 2008 paper, our group explored a mouse model of hemophilia A, a coagulopathy that arises from an inherited deficiency in clotting Factor VIII (FVIII) [26]. After years of FVIII replacement therapy, it is common for human patients to develop allo-antibodies to FVIII, complicating treatment and causing significant morbidity. Our team utilized both *in vivo* and *in vitro* techniques to show that murine MSCs induced plasma cells to re-express Pax5 via the protein phosphatase-dependent inhibition of STAT3, causing a systemic decrease in anti-FVIII antibodies. Our protocol was repeated in healthy mice immunized to ovalbumin protein (OVA), after which we observed similarly decreased anti-OVA immunoglobulin production by B cells. Other studies using B cells and MSCs from healthy human donors have shown that MSC co-culture attenuates the production of IgA, IgM and IgG via *in vitro* assay systems [27]. A recent study by Ma and colleagues has explored the utility of MSC therapy for idiopathic thrombocytopenic purpura (ITP), a hematologic disease characterized by spontaneous bleeding, petechiae, and purpura [28]. Although not all cases of ITP are proven autoimmune in nature, both T and B cells with specificity to platelet surface antigens have been implicated in its pathogenesis [29]. Via *ex vivo* culture systems of primary cells from ITP patients, Ma and team show a marked

decrement in platelet destruction after MSC co-culture (although they are unable to pinpoint a specific causative relation, instead citing a number of possibilities).

T cells and Central Tolerance

Though they begin development as CLPs in the bone marrow, T cells must migrate to the thymus to complete their maturation. In the thymus, signals from both local tissue-resident and marrow-derived cells guide the developing T cells through positive and negative selection [30]. Medullary thymic epithelial cells (mTECs) express the transcription factor AutoImmune Regulator (AIRE), enabling the cells to express self-derived antigens. Recent research has shown that mTECs can also transfer this antigen for indirect presentation by thymus-resident dendritic cells [31]. In the thymus, autoreactive T cells can be converted to so-called 'natural' regulatory T cells, be deleted or otherwise deprived of survival signals, and become anergic. These mechanisms of central tolerance, enforced by the thymus, suffice to keep a healthy individual free of autoimmune disease. Autoreactive T cells can be tolerized to self antigen in the periphery, thereby becoming 'induced' regulatory T cells. The precise mechanisms by which these conversions occur are an area of intense interest, with changes in cellular metabolism, co-stimulatory and co-inhibitory surface molecules all being investigated [32, 33].

MSC and T cell Co-culture Assays

Different *in vitro* systems have been utilized to observe the mechanisms whereby MSCs can regulate, suppress or limit the inflammatory damage of pathologic T cells. One of the

principal ways that MSC-mediated immunosuppression can be observed is via co-culture with peripheral blood mononuclear cells, or purified T cells. In order to activate the T cells toward proliferation and effector differentiation, the T cell markers CD3 and CD28 must be ligand-stimulated. These stimuli reproduce the so-called Signal 1 and Signal 2 of T cell activation: Signal 1, in which a T cell receptor (TCR) encounters its cognate antigen presented by the HLA molecule of an antigen-presenting cell (APC), and Signal 2, whereby CD80 or CD86 on the APC delivers co-stimulation to the CD28 on the T cell. Whether affixed to beads or in solution, anti-CD3/anti-CD28 stimulation to PBMCs or purified T cells induces activation and proliferation that is polyclonal in nature. We and others have used this technique in combination with *in vitro* co-culture to demonstrate the suppressive effects mediated by MSCs [34-36]. Other techniques for polyclonal activation of T cells include the use of mitogenic stimuli, such as phytohemagglutinin (PHA) [37] and the superantigen Staphylococcal enterotoxin B (SEB) [36].

To assess proliferation, and thereby judge the degree of MSC immunosuppression, different groups employ the generational dilution of carboxyfluorescein succinimidyl ester (CFSE) [38], an increase in ^{3}H-thymidine incorporation [38], or intracellular flow cytometric staining for Ki67 [36]. The classical mixed lymphocyte reaction (MLR) has also been utilized to assess the degree by which MSCs modulate T cell allo-proliferation. Given a high degree of HLA-mismatch, responder T cells proliferate in an allo-specific fashion, generationally diluting their CFSE concentration. MSCs can be plated beneath the MLR allowing the researcher to tease apart tolerance-conferring mechanisms [39].

MSCs have been shown to suppress the proliferation of activated T cells using a variety of mechanisms, and both contact-dependent and soluble factors have been implicated. Soluble factors include prostaglandin E2 (PGE2), transforming growth factor-β (TGF-β), hepatocyte growth factor and HLA-G, released on membranous bodies as described above. These and other mechanisms have been reviewed by others [15, 16, 40-42] so our discussion will instead focus on translationally important findings whereby stromal cells suppress the activity of T cells.

For researchers in transplantation and autoimmune disease, the word 'tolerance' evokes the categorical good: immunosuppressive pharmacotherapies are thus employed to avert rejection of allografted organs or host tissues under autoimmune infiltration. However, tolerance can also be maladaptive, a consequence engendered by the stromal environment where benign tumors first become malignant cancers. By understanding the mechanisms of cancer-associated maladaptive tolerance, immunologists stand to gain valuable insight for next-generation immunomodulatory therapies.

It is now appreciated that cancer is not one syndrome, but rather a collection of diseases marked by dysregulated proliferation of the body's endogenous cells. The last century has advanced our understanding of carcinogenic toxins, inherited or acquired mutations, and chronic inflammatory changes that can all incite cells to become cancerous. In the process, one or all of the following systems becomes dysregulated: a cell can undergo loss of function (e.g. of a tumor-suppressing factor like *Rb*), it can gain a competitive growth advantage (e.g. the constitutive growth triggered by *Bcr-abl*), it can become ignorant to

apoptotic signals (e.g. mutations in *Bcl-2*), and lastly, it gains the ability to metastasize beyond its normal niche (e.g. the loss of *E-cadherin*)[43]. These changes may not occur sequentially in every cancer, but *in vitro*, each is sufficient for a human cell to acquire immortality. In the healthy body, it is appreciated that such dysregulations occur at a basal level, but are kept in check by a variety of homeostatic mechanisms. The concept of immune surveillance has been described as the mechanisms by which circulating lymphocytes detect pre-malignant changes and subsequently kill the mutated cell [44]. A number of studies have demonstrated the ability of lymphocytes to perform tumoricidal immune surveillance [45, 46]. However, in instances where cancer does arise, recent discoveries indicate that tumor stromal tissue exerts immunosuppressive mechanisms that neuter the potentially cancer-fighting effects of tumor-infiltrating lymphocytes (TILs) [47].

PD-L1 and Immunosuppression by Tumors

After receiving Signal 1, Signal 2, and being exposed to inflammatory cytokines, newly-activated T cells—$CD4^+$ T helper cells and $CD8^+$ cytotoxic lymphocytes (CTLs)—upregulate adhesion molecules and then traffic to inflamed areas by following chemokine gradients. The activation process for T cells involves the maturation of effector function (i.e. the ability to release cytokines such as IFN-γ or Granzyme B), after which they lose dependence upon the co-stimulatory Signal 2. For example, when CTLs arrive at an inflamed area, they serially kill any cell that displays the cognate antigen-HLA complex. In addition to gaining effector function, T cell activation induces the upregulation of

inhibitory receptors that include Programmed Death-1 (PD-1) [48]. Although we have described the process of T activation, it is important to note that PD-1 expression is also upregulated on activated B cells. PD-1 is a transmembrane protein that contains an ITIM motif, which upon ligation recruits tyrosine phosphatases that inactivate a number of signaling molecules, including Syk, ZAP-70, and PI3K [48]. Such changes induce the anergy or apoptosis of T cells and B cells, tempering the late immune response towards resolution.

The principal ligands for PD-1 are PD-L1 (also called B7-H1) and PD-L2 (also called B7-DC). Early studies of PD-L1 indicated that the molecule was commonly found on primary human cancer cells [49], although subsequent work has also located the molecule on benign hematopoeitic and non-hematopoietic cells [48]. Likewise, PD-L2, first identified on human cancer cell lines [50], has been since identified on antigen-presenting cells and some non-hematopoietic cells [48]. The finding that PD-L1 was associated with cancerous human tissues generated a flurry of research in the first decade of the new millennium, as scientists explored new avenues of cancer immunotherapy. Antibodies to blockade PD-1 and PD-L1 have shown great promise in pre-clinical models [51, 52], later spurring the development of clinical trials for cancer immunotherapy [53-55]. In late 2014, the FDA approved pembrolizumab, a monoclonal antibody drug targeting PD-1, as the newest therapeutic for metatstatic melanoma [56].

PD-L1 and Immunosuppression by MSCs

Among the contact-dependent factors implicated in immunosuppression by MSCs, PD-L1 has emerged as a potentially important mediator. As discussed above, the role of PD-L1 has been explored in oncology research, and found to dampen the effects of tumoricidal lymphocytes. Such findings have furthered efforts to improve immunomodulatory MSC therapy, via a deepened mechanistic understanding of immune tolerance. In 2005, just a few years after the first characterizations of PD-1, surface expression of PD-L1 by marrow-derived MSCs was described to mediate immunosuppression [57]. Augello and colleagues showed that resting, marrow-derived MSCs only contained mRNA for PD-L1, but could be induced to express the protein on the cell surface by inflammatory stimuli. The researchers showed MSCs inhibit the proliferation of both B cells and T cells in a MLR or after PHA stimulation, and that this effect could be reversed by a blocking antibody to PD-L1. A 2008 study used MLR, mitogens and also anti-CD3/anti-CD28 stimulation to show that lymphocyte-derived IFN-γ was responsible for the induction of PD-L1 on the surface of MSCs [58].

Recent studies have further elucidated the role of PD-L1 in MSC immunosuppression. In a 2012 study, Luz-Crawford and team explored how MSCs utilize PD-L1 to inhibit both proliferation and effector capacity of T cells [59]. Using established protocols for *in vitro* T cell skewing, the researchers generated inflammatory T_H1 and T_H17 cells, confirmed by canonical transcription factors and cytokine expression (*T-bet* and IFN-γ, *RORγt* and IL-17, respectively). They show that MSCs are able to suppress cytokine release from both types of inflammatory T cells, which was reversed by antibody blockade of PD-L1. Of particular

note was the finding that although soluble factors play a role in the immunosuppression, T_H17 cells were especially sensitive to contact-dependent inhibition via PD-L1. Subsequent work by the same researchers suggests that MSCs can re-program T_H17 cells into regulatory T cells [60], though the exact role of PD-L1 remains to be fully described.

In a 2014 report, our research group explored the differential effects of MSC immunosuppression after inhibition of indoleamine 2,3-dioxygenase (IDO) or PD-L1 [36]. Primary human MSCs were shown capable of inhibiting both the proliferation and effector function (cytokine release) of T cells after treatment with the superantigen SEB or anti-CD3/anti-CD28 stimulation. We showed that although IDO was associated with suppression, treatment with the enzymatic inhibitor 1-MT did not fully reverse this effect. However, siRNA-mediated knockdown of PD-L1 or PD-L2 was shown to reverse the inhibitory potential of MSCs. These results suggest that MSCs may rely on a number of factors—soluble factors, IDO catalysis and PD-L1/PD-1 signaling—to mediate their immunosuppression in complementary, non-overlapping mechanisms.

IDO and Immunosuppression by Tumors

The enzyme indoleamine 2,3-dioxygenase (IDO) is an important enzyme that is known to be associated with the conferrance of immunologic tolerance. It catalyzes the rate-limiting step in the biochemical degradation of tryptophan, yielding a group of metabolites collectively termed kynurenines [61]. A 2012 report identified IDO in trophoblast-derived macrophages, where it is associated with the maintenance of

maternal-fetal tolerance [62]. IDO-expressing dendritic cells have likewise been found to be tolerance-inducing in a heart transplantation model [63]. Although these recent discoveries speak to the tolerogenic stimuli sought by the transplant field, the enyzmatic activity of IDO was first indirectly observed in the field of oncology. In a 1956 study, patients with advanced bladder cancer were found to have abnormally high excretion of kynurenines, which could be modulated by supplementation of tryptophan or other chemical analogs [64]. Viewed from a modern lens, it is likely that IDO-expressing cells in the cancerous bladder wall augmented local tryptophan degradation, rendering any TILs impotent in their attempt to eradicate the tumor.

Various models have been proposed to explain how IDO can suppress the immune response, and block the anti-tumor effect of TILs. One model holds that local deprivation of tryptophan prevents the phosphorylation of TCR zeta-chains, thereby preventing further activation of T cells [40]. Other studies have examined the role of IDO-generated kynurenines and how they may act directly or indirectly to re-program effector T cells into tolerogenic regulatory T cells [65]. Perhaps an echo of the 1956 cancer studies, enzymatic inhibitors of IDO have been developed as an effort to abrogate its downstream immunosuppressive effects. The most promising of these inhibitors is 1-methyl-tryptophan, a structural analog that blocks the catalytic site of IDO, and is being tested in clinical trials for breast cancer, brain tumors and melanoma [66]. As such studies continue, the mechanistic switches that govern maladaptive tolerance to cancer will better inform future IDO-targeted therapies.

IDO and Immunosuppression by MSCs

Although not basally expressed in resting MSCs, upon treatment with IFN-γ, the expression of IDO greatly increases in MSCs, as confirmed via messenger RNA (mRNA) levels and Western blot protein analysis [67, 68]. A number of studies have shown that in human MSCs, the IDO enzyme is a key correlate of immunosuppressive ability [69, 70]. Using bone marrow-derived MSCs from a variety of different donors, we showed that immunosuppressive potency was correlated with the expression of IDO protein [70]. Others have explored the downstream effects of IDO-catalyzed changes in target cells, and noted decreased levels of tryptophan, as well as increased production of kynurenines [34]. The mechanisms whereby MSCs and kynurenines together suppress leukocyte inflammation are an area of active research [42]. In a 2011 study, our group showed a link between IDO catalysis and MSC reprogramming of inflammatory macrophages (conventional or M1 macrophages) into an anti-inflammatory, or M2 phenotype. The contributions of M2 macrophages have become increasingly appreciated as key players in wound healing, and post-inflammatory resolution [42]. Such reprogramming of peripheral macrophages may be a recapitulation of MSCs in the marrow, which are known to modulate the bone-resorptive activity of monocyte-derived osteoclasts [13]. Crosstalk between MSCs and M2 macrophages has been demonstrated by a number of recent studies [71-73], further suggesting this axis of immunosuppression may be important for *in vivo* efficacy.

In addition to monocytes, IDO catalysis has been found to an important factor in the reprogramming of inflammatory T cells into a regulatory phenotype. This was first suggested in a 2004 report in which MSCs were shown to inhibit the proliferation of T cells in a human MLR via IDO-catalyzed production of kynurenines [74]. More recently, these studies have been expanded through the use of animal models that co-transplant organs with allogeneic MSCs [75]. The presence of IDO, as well as increased production of kynurenines were both shown to be associated with long-term graft tolerance, as well as increased frequency of both peripheral and tissue-resident regulatory T cells [76].

MSC Response to Inflammatory Signals: Licensing and Integration

Having considered the cellular biology of MSCs as observed via *in vitro* methodologies, as well as appreciating their endogenous role in normal hematopoietic niche, we now turn to how MSCs functionality is altered by inflammatory signals. Much of the basic and clinical research occurring with MSCs explores these cells' unique immunomodulation, and how it changes before, during and after *in vitro* culture expansion. Tissue culture experiments are vital to the furtherance of all MSC cell biology work, as rigorous reductionist methods teach us with each new data point. When such work is predicated on endogenous observations, it affords better perspective on how MSCs function in patients currently being treated with this cellular therapeutic.

We described above the role of MSCs in the hematopoietic niche, where these cells integrate a variety of signaling paradigms—CXCL12, SCF, adrenergic stimuli—to regulate

the development of lymphoid and myeloid cells that defend and oxygenate all tissues. In addition, MSCs have been observed to exert immune control in the peripheral tissues, suppressing immune activation and tipping the inflammatory milieu back towards resolution. As stromal cells, MSCs are poised to respond to environmental cues—in the marrow, adipose or other vascularized tissues—and thence exert immunomodulatory abilities [7]. The mechanisms by which MSCs sense inflammation, integrate stimuli and modulate the immune response depend upon basic cellular biology. That is to say the response of MSCs is determined by the identity of activating ligands, the presence of the relevant receptor, and the activation state of diverse adaptors that transduce, amplify or otherwise allow MSCs to coordinate the local immune response.

As tissue-resident stromal cells, MSCs can respond to inflammatory stimuli via a diversity of receptors. One of the most important classes of innate sensing molecules possessed by MSCs are the highly-conserved pattern recognition receptors (PRRs). These are surface or intracellular sensing molecules that detect inflammatory changes early in the course of infection or injury. MSCs possess a number of PRRs that enable them to sense and migrate towards an inflammatory nidus, and help coordinate the influx of innate and adaptive immune cells. We will sequentially discuss the effects of inflammatory signaling on MSC phenotype and behavior, as it pertains to a number of different ligand classes. However, it is essential that the reader understand that *in vivo*, all such signaling happens simultaneously, and it is via the integration of local and long-range signals that stromal

cells and leukocytes together cooperate to inflame, defend, and then repair the tissue microenvironment.

Let us consider as an example a chronically non-healing wound, such as a stasis ulcer that can arise in poorly-controlled diabetes mellitus. Although a variety of endocrine and cardiovascular factors contribute to such pathology, over time endothelial cells and capillary-associated cells locally release inflammatory cytokines and chemokines in response to poor perfusion, leading to pathologic degradation of extracellular matrix. One key cytokine in this process is TNF-α, which we will discuss at length below, but for now it should be noted that its local action in capillary beds causes vasodilatation, enabling the local diapedesis of leukocytes [77]. The exposed endothelium causes platelet activation, release of additional inflammatory mediators and the formation of clots in the microvasculature, attempting containment of the insult. An increasing body of literature has appreciated the diverse secretome of platelet activation, including cytokine growth factors such as PDGF, VEGF and TGF-β, eicosanoids like TXA_2, as well as fibrinolytic and anti-fibrinolytic enzymes.

MSCs and Complement

The complement system is an early innate immune defense mechanism, comprised of plasma proteins that interact with membrane surfaces. Elements of the complement system were first identified by their 'complementary' role in antibody-mediated lysis of pathogens. However, a modern evolutionary understanding of these proteins reveals

their early innate action, long before the adaptive immune system begins antibody production. Indeed, the alternative and lectin pathways demonstrate that from sea urchins to man, the complement system functions to detect foreign invaders [78]. In the case of the inflammatory ulcer described above, breach of the tissue with the outside environment introduces a host of pathogens. Complement proteins are deployed in the process of opsonization, to coat invading pathogens, either lysing or delivering them up to phagocytic cells for destruction. Through the deposition of complement proteins onto pathogen surfaces, the cleavage of reactive thioester bonds generates split products, such as C3a, C4a, and C5a. Listed in order of increasing inflammatory potential, these anaphylatoxins ligate G-protein coupled receptors on leukocytes to enhance phagocytosis, antigen-processing and presentation.

MSCs have been shown to express the C3a receptor (C3aR) as well as C5aR, and to migrate chemotactically to *in vitro* gradients of C3a and C5a. The mechanisms of C3aR ligation were shown to be linked to receptor translocation and prolonged ERK1/2 phosphorylation within primary human MSCs [79]. Others have shown that anaphylatoxin generation and even complement deposition on MSC surfaces is important in activating and enabling MSC immunosuppression in MLRs [80]. Moll and colleagues show this effect was associated with expression of the surface membrane protein CD59, which prevents complement-mediated lysis of MSCs. Together, such results suggest that MSCs are poised to respond to local complement activation and modulate the early inflammatory response to injury or infection.

MSCs and TLRs

When in the loss of epithelial integrity (such as in the lesions of inflammatory bowel disease) microbes entering into the wound may be of commensal origin, living at host tissues without causing overt disease, though upon entry to the subcutaneous niche become pathogenic. Such microbes are referred to as pathobionts, in that they have the ability to cause disease when in conjunction with other damage-associated markers[81]. The highly-conserved molecular patterns of microbes are called pathogen-associated molecular patterns or PAMPs and those released from damaged tissues (such as heat-shock proteins or uric acid) are called damage-associated molecular pattern molecules (DAMPs). A variety of immune-competent cells, including MSCs, express receptors for such molecules, sensing microenvironmental changes to help coordinate the immune response [82]. In addition to the soluble defense mechanisms (e.g. complement, ficolins and C-reactive protein), invading pathogens are sensed by pattern recognition receptors (PRRs). Evolutionarily ancient in origin, PRRs recognize conserved patterns common in microbes, such as the formylated methionine residues found in bacteria, and detected by f-MLF receptor. In considering the role of PRRs in MSC biology, the most well-characterized class is the Toll-like receptor (TLR) family. Initially discovered as innate sensing molecules in *Drosophila*, TLRs can be found on the cell surface or on intracellular membrane surfaces of a variety of vertebrate and invertebrate cells. There have been eleven TLRs described in humans (thirteen in mice) and together, these molecules are able to detect and transduce danger signals associated with pathogenic lipoproteins,

lipopolysccahride (LPS), flagellin, double- or single-stranded RNA, and unmethylated CpG DNA motifs [82, 83]. It is important to note that TLRs do not just sense invading microbes, but also host-derived molecules indicative of inflammatory or necrotic processes. Accordingly, TLRs have been described to respond to uric acid, heat shock proteins, intracellular cell debris or fragments of extracellular matrix [82].

The pattern-sensing TLR domain contains about twenty leucine-rich repeats, which facilitates in ligand detection via homo- or hetero- dimerization. Depending on the class of ligand being sensed, a TLR will recruit different adaptor molecules to its signaling region, the 200-residue Toll-IL-1-R (TIR) domain. The TIR domain is shared with IL-1R, demonstrating the importance of this cytokine in tuning and responding to inflammatory events. TLR dimerization patterns, as well as a diversity of adaptor molecules (MyD88, TIRAP, TRAF, TRAM) help to explain how only a dozen or so molecules can transduce a diversity of signals that vary according to the level of threat posed by each pathogen- or host-derived ligand. These signals feed into the nuclear factor κB (NF-κB), mitogen-activated protein (MAP)-kinase or Caspase pathways, resulting in immune activation, proliferation or apoptosis [83].

The presence and function of TLRs on MSCs has been interrogated in a number of studies, exploring primary murine and human MSCs derived from a variety of tissue sources. Such reports have identified some degree of expression for TLR families 1-6, although TLR3 and TLR4 are the only classes that reach expression levels comparable to that seen in

hematopoietic-derived cells [84]. In one such study, researchers identified that stimulation of MSCs with the well-characterized TLR4 ligand LPS abrogated the ability of MSCs to exert immunosuppressive modulation on *in vitro* T cell proliferation assays. Likewise, treatment of MSCs with poly(I:C) (a synthetic dsRNA analog and TLR3 ligand), prevented the immunosuppression observed in controls. Treatment of MSCs with either LPS or poly(I:C) induced NF-κB activation, as well MSC downregulation of the protein Jagged-1. Jagged-1 is a ligand for the T cell receptor Notch, and MSC signaling via Notch and Jagged-1 has been implicated in MSC immunosuppression of T cells [84]. Our research group followed these studies to show that TLR3 or TLR4 ligands cause MSCs to produce greater amounts of IL-1β, IL-6, CXCL8, CCL5, and IL-12p75 [85]. Furthermore, we showed that treatment of MSCs with interferon alpha (IFN-α) increased expression of TLR3. Type I interferons (IFN-α or IFNβ) function as early innate mediators, and activate defenses including protein kinase R, and RIG-I, key systems that block viral proliferation in host cells. In the same experimental system we found that treatment with the Type II interferon, IFN-γ, increased MSC expression of both TLR3 and TLR2. The observations that TLR ligands prevent MSC immunosuppression are nonetheless consistent with their coordinating role for the early immune response. By analogy, TLR ligands have been shown to activate DCs, priming them to perform antigen-presentation to engage the adaptive immune system. Much as DCs modulate the immune response, tissue-resident MSCs can be seen as responsive to microenvironmental cues, engendering early inflammation but later tipping the balance back to resolution and repair.

IFN-γ in the Immune Response

The role of IFN-γ is classically most well-understood as a cytokine involved in the coordination of the immune response, specifically that driven by T_H1 cells. The first descriptions of T_H1 and T_H2 cells, performed by Mossman and Coffman in 1986, showed that T cell subsets respond to stimulation differently, and can be characterized by their specific cytokine secretion [86]. Today, some degree of plasticity is appreciated to exist, wherein T cells may secrete multiple cytokines or be reprogrammed to different subsets. However, the role of IFN-γ derived from T_H1 cells spurred many studies exploring this cytokine's effect on the immune response. Like the type I interferons (IFN-α and IFN-β), IFN-γ was noted early on for its ability to 'interfere' with viral replication. It is now thought that the T_H1 response is most well-adapted to a variety of intracellular pathogens, such as *Mycobacteria* and *Listeria*, as well as protozoans and viruses. As it is derived chiefly from activated T cells, it does not arise until later in the inflammatory process, after innate immune cells—both resident and immigrant—have sounded the alarm. This is an important point, for the persistence of IFN-γ in the cytokine milieu signifies ongoing, inflammatory changes in the microenvironment.

In a successful immune response, the immune infiltrates will defeat the pathogen, and a shift towards immunosuppression, wound healing and repair must occur, otherwise risk the development of a chronic, non-healing wound. From this perspective, we can appreciate how and why inflammatory signals (such as IFN-γ) can deploy the anti-inflammatory effect of MSCs, both *in vitro* and *in vivo*.

MSCs and IFN-γ

In the past decade, a number of studies have sought to identify the most important factors involved in immunomodulation by MSCs. Both IDO and PD-L1, described above, have been found to be essential in conferring on MSCs the ability to suppress T cell proliferation and effector function. Resting MSCs, that is, cells derived from primary tissue sources and maintained via *in vitro* culture, are only partially effective at suppressing T cell proliferation. Pre-treatment with an inflammatory mediator will 'license,' or greatly augment the immune veto effects of the MSCs. Among the mediators described thus far, IFN-γ has been the most-well explored and characterized MSC licensing agent. A number of studies have demonstrated that IFN-γ markedly enhances the ability of human MSCs to suppress alloproliferation in MLRs, as well as mitogen-driven immune proliferation [87-89]. After ligating the IFNgR, Janus-family kinase 1 (Jak1) and Jak2 both associate with the intracytoplasmic tails of the receptor. Following this, signal transducer and activator of transcription 1 (STAT1) homodimerizes and is phosphorylated, enabling it to traffic to the nucleus to initiate transcription of IFN-γ responsive genes. In MSCs, IFN-γ treatment results in STAT1 phosphorylation, and the upregulation of a number of genes, including IDO. It has been shown that in response to IFN-γ, primary human MSCs increase expression of Class I HLA, and begin to express *de novo* Class II HLA as well as PD-L1 [36, 90]. The importance of IFN-γ and IDO in enabling MSC immunosuppression has been demonstrated through the use of blocking antibodies to the IFNgR, as well as siRNA-mediated knockdown experiments targeting IDO, after which the MSCs are not able to

suppress as well. The increased expression of HLA molecules is consistent with antigen-presentation, which may be a way to recapitulate the endogenous role of MSCs as enforcers of self- tolerance (described above).

TNF-α in the Immune Response

Tumor necrosis factor-α (TNF-α) is a cytokine that is classically associated with both acute and chronic inflammatory responses. As a component of the acute phase response, TNF-α signaling triggers containment of infection, while also initiating vasodilatation in the area of inflammation. However, systemic release of TNF-α (either induced experimentally or observed in patients) results in a clinical syndrome not unlike septic shock. The discovery of TNF-α followed the characterization of a hormone known as cachectin, which had been at high levels in patients with cachexia, a clinical syndrome with extreme muscle and fat wasting, common in late-stage cancer patients. In 1985, Bruce Beutler performed the first studies showing that TNF-α and cachectin were in fact the same molecule [91]. It is now appreciated the signaling via TNF receptors (TNFR) is crucial for a vast array of processes, beyond the shaping of acute and chronic inflammation. As an example, TNFR signaling is essential during the development of secondary lymphoid organs, particularly those of the gut, including Peyer's patches and mesenteric lymph nodes, via the extrinsic and intrinsic transduction of apoptotic or survival cues [92, 93].

We will only describe the extrinisic or death receptor pathway, as it is so vital to immune system function; additionally, its membrane-bound activation affords perspective on how

cell-to-cell TNF signalling can induce target cell death. Upon ligation, the TNFR homotrimerizes and its intracellular death domain (DD) moieties, which, in the case of TNFR-1, associate with TRADD. Depending on the ligand-receptor class, TRADD can then associate with FADD, and activate the initiator Caspase-8, leading to eventual apopotsis (driven by the executioner caspases, Casp-3, Casp-6, and Casp-7). Alternatively, recruitment of adaptor TRAF will instead lead to activation of the transcription factors NF-κB, as well as the kinase c-Jun, part of the AP-1 complex which leads to cell survival, proliferation or immune activation [94].

Synergy of IFN-γ, TNF-α in MSCs

MSC licensing has been explored through a number of studies, utilizing both human and mouse MSCs in a variety of assay systems. The T cell suppression assay, described above, is perhaps the most reductionist method to study the pre-treatments by which MSC immunomodulation can be altered. It was through such studies that Ren and colleagues demonstrated a synergistic effect after treating murine MSCs with both IFN-γ and TNF-α [102]. In this 2008 study, murine MSCs were found to depend on IFN-γ signals for activation, as MSCs lacking the IFNgR were unable to suppress T cell proliferation. An important note in the MSC field is that murine MSCs do not utilize IDO at all; rather, the enzyme most correlated with IFN-γ-induced licensing is inducible nitric oxide synthase (iNOS). Ren and colleagues demonstrate that upon treatment with IFN-γ—plus addition of either TNF-α or IL-1—murine MSCs induce the highest levels of iNOS, chemoattract and suppress the proliferation of T cells more robustly than in mono-treatment. In 2010, our

research group sought to explore the connection between synergistic cytokine licensing and the antigen-presenting capacity of MSCs [103]. As mentioned above, MSCs may be induced to express both Class I and Class II HLA molecules, and have also been observed to perform cross-presentation, akin to dendritic cells. Upon treating MSCs with both IFN-γ and TNF-α, we observed enhanced antigen-presenting capacity, as well as reduced activation and proliferation among co-cultured T cells. As others have noted, and we described above, Ren and team show the source of these cytokines to be the activate T cells, leading to a feedback loop in which the inflammatory milieu primes MSCs into a regulatory, immunosuppressive phenotype.

Strength of Signal and Integration

Some controversy has arisen regarding MSCs in clinical trials, as results have not been uniform in replicating promising *in vitro* findings. We and others have pointed out that this may be due to differences in cell source and processing at trial sites[104]. Such challenges could be inherent to cell therapeutics, suggesting they will remain the purview of academic or biomedical research centers, equipped for such protocols.

However, some of these heterogeneous results may in fact be explained by the MSCs themselves. Within a tissue culture system, MSCs typically adopt a fibroblast-like morphology but as culture conditions change, differences can be perceived. At low culture densities, MSCs exhibit a small, round morphology characterized by rapid self-renewal. In this state, MSCs express surface proteins that maintain the mesenchymal

state: thereby promoting motility, and inhibiting cell adhesion. After continued culture towards confluence, the cells adopt an extended fibrous shape while some of their mesenchymal plasticity and surface Ag expression is lost. This bimodal distribution is referred to as Type 1 or Type 2 MSCs. Type 1 MSCs are the smaller, self-renewing and robustly pluripotent cells. Type 2 MSCs have reduced proliferative capacity and may be less desirable as a cellular therapeutic [15].

If MSC1 and MSC2 represent different temporal states of MSC populations *in vitro*, it may help to explain the differential behavior of MSCs upon infusion into human patients. In the early phases of an inflammatory insult, tissue-resident MSCs can behave like classical APCs. In response to acute phase stimuli (such as IL-1, TNFα or TLR agonists) they upregulate HLA molecules to coordinate with the influx of first-responder leukocytes. MSCs have been shown *in vitro* to present both soluble and intracellular antigens on Class I and Class II molecules, in addition to cross-presentation, just as a classically activated dendritic cell (DC)[105-107]. Whether unmanipulated MSCs are capable of upregulating CCR7, and thereby trafficking to secondary lymphoid organs, remains controversial [108-110]. Nonetheless, their antigen-presenting role in early inflammatory response plays an important role in tissue maintenance.

As inflammatory stimuli persist, the ingress of activated T cells, particularly IFNγ-releasing T_H1 cells, will alter the stromal tissue cytokine milieu in which leukocytes and MSCs interact. T_H1 cells are known to be pathologic in a number of chronic inflammatory

conditions, and have associated with aberrant wound repair and immune activation, such as observed in sarcoidosis and cutaneous ulcers [111, 112]. As discussed above, increasing levels of IFNγ act upon MSCs in a STAT1-dependent fashion, upregulating the enzyme IDO, the cell surface marker PD-L1, and other changes. Poised as stroma-resident immune coordinators, MSCs may integrate the signals initiated by inflammatory products, and, in physiologic conditions, tip the local balance back towards resolution and repair. Immunosuppression, so often demonstrated through *in vitro* assays, may play a crucial role *in vivo* by dampening the proliferative capacity of pathologic T cells (IDO-catalyzed changes), contact-dependent deletion (PD-L1) and the paracrine release of factors (TSG-6, PGE2, antagonistic mpCCL2) with anti-inflammatory properties.

In vitro culture as a model for clinical efficacy

Discussion of the mechanistic cellular biology of MSCs is an important endeavor, for any efforts aimed at future development of this therapeutic must be based on scientific data. The studies described heretofore posit elegant models that seek to define the *modus operandi* for MSCs. We now turn our attention to recently-generated data from larger-scale clinical trials examining the therapeutic utility of MSCs in immune ailments, sponsored by governmental and industry-based organizations in a variety of settings worldwide. We frame our discussion by the general platform by which clinical researchers are deploying the MSC product, and analyze these results vis-à-vis the putative mechanisms by which they are thought to act. It is our hope the reader may thereby gain

contextual framework to better understand the biology of these immunomodulatory cells.

Random-donor, industrial-scale

Osiris Therapeutics, Inc. is a company based in Columbia, Maryland, U.S.A., and their MSC product, named Prochymal, has been explored in a variety of clinical studies. Though much of their pre-clinical data has been encouraging, a recent Phase III randomized placebo-controlled study failed to meet its primary endpoint in a study of graft versus host disease (GvHD) after hematopoietic stem cell transplant (HSCT) [113]. In this study, overall 100-day response rate of patients receiving MSCs was 82%, compared to 73% in the placebo group. Given other encouraging results using MSCs for immune-mediated diseases (notably from trials discussed below), it bears exploring some of the variations that may cause their product to achieve sub-optimal results. We have discussed this specific trial and its failure in a separate publication [104], to which the reader is referred for a more comprehensive discussion; what follows is abbreviated therefrom.

Recognizing that the development of autologous, or patient-derived cells can sometimes be a challenge to generate large-scale doses for patients in geographically-diverse clinical trials, Osiris had sought to employ instead a so-called universal, or random donor marrow source for their MSC product. According to the company website and other papers published by the group [114], Osiris used MSCs from 4 different human sources, isolated, expanded and archived according to good manufacturing practices (GMP), the

designation by the FDA for handling of cellular-based therapeutics. Many individualized dose-units were then stored in cryopreservation, and shipped out to infusion centers at healthcare institutions participating in clinical trials using the Prochymal product. Given our discussions above regarding the differential behavior of MSC in different cell niches, and their temporal abilities to respond to environmental cues, such a platform may be disadvantageous to clinical success. Using a massively-expanded universal lot of cells could bias the overall population towards a clonal homogeneity that poorly reflects their in vivo niche; clinical response by patients may therefore be blunted by infusion of sub-optimal cells.

Lastly, and perhaps most importantly, for convenience of product distribution, Prochymal is shipped as a frozen bag, and infused as a just-thawed product into patients. In their methods description[114], the study authors state the cells are ascertained to have 70% viability, presumably by Trypan blue exclusion, though this is not specified. It remains an open question whether viability is the best determinant of MSC immunomodulatory abilities. This has been borne out in studies by our group and others, showing that cryopreservation and immediate infusion of thawing cells can cause dramatic loss of immune veto function [115-117].

Notably, in late 2013, Osiris sold their entire platform for MSC-based therapy (including all intellectual property rights) to an Australian company, Mesoblast [118]. Mesoblast continues to oversee the expansion of the Prochymal product, having recently received

provisional approval for GvHD and Crohn's disease by regulatory bodies in Canada and New Zealand, aiming a full commercial launch for 2016. Additionally, the company states they have begun filing for similar approvals with the U.S. FDA, with a projected launch of 2016[119].

Other studies have continued to explore using third-party MSCs for prophylaxis as well as therapy in GvHD arising after HSCT. However, literature discrepancies exist regarding the definitions of response after treatment (including varied time-point assessment intervals) as well as different pharmacotherapy regimens (before, after and during MSC infusion), as well as patient age and severity of GvHD. GvHD is appreciated to be a complex syndrome, and each of the variables just mentioned can drastically alter the immunologic environment into which the MSCs are infused[120]. As perspective, the earlier-described cellular biology research explores MSC function and effect through *in vitro* or animal models, but without addressing patient co- morbidities or concomitant immunomodulatory therapy. Due to variable GvHD presentations and cellular processing, it is difficult to truly compare large meta-analyses of MSC therapies[121]; a different approach may be to examine the results of such studies in consideration of their contextual framework.

One illustrative example comes from a European group in 2013, who treated a cohort of 37 children with severe (grade III-IV) GvHD using HLA-mismatched MSCs from cryopreserved third-party stocks[122]. These children had developed acute GvHD

following HSCT, and were treated with three MSC doses. Of these patients, 69% demonstrated a complete response, with the majority of those children alive and well after a 3-year median follow-up period. The aforementioned review[121] by Introna and Rambaldi analyzes the recent developments in using MSCs immediately after HSCT, as prophylaxis for GvHD (again, in conjunction with standard pharmacotherapy regimens). One such study, from a Russian group in 2012, infused MSCs sourced from the same donor as the transplanted HSCs in order to prevent the development of GvHD[123]. Their cellular formulations are of interest; some MSC doses were delivered fresh, others were given as thawed cellular preparations, but all cells were culture-expanded in human platelet lysate, rather than fetal calf serum. Theirs was a randomized, prospective study of 37 patients, mostly adults diagnosed with hematologic malignancies. The researchers demonstrate both safety and efficacy for prophylaxis, with 5% of the MSC-therapy group developing acute GvHD, compared with 38% of the control group.

Allogeneic MSCs, low passage

The function of MSCs in maintaining the hematopoietic niche in a healthy state, and the multi-level signaling that maintains central tolerance was described mechanistically above. It is this very attribute of MSCs, their tolerance-enforcing role, that has motivated their application in a number of autoimmune diseases. Systemic lupus erythematosus (SLE) is a complex disease with a diverse symptomatology, with prominent pathologic signs that imperil the gut, skin, kidneys and nervous system. Although not found in every patient case, antibodies that react with self antigens have been shown to be critical to its

pathogenesis. Either in the periphery or the marrow, lymphocytes that react against self-tissues are not re-programmed into death or ignorance, and instead proliferate and wreak havoc across the body [124]. Given its immune-mediated nature, a number of research teams have sought to employ MSCs as a disease-modifying therapy in lupus.

One such study is a 2010 report that sought to treat lupus patients using autologous MSCs derived from patients' own marrow, which failed to show significant clinical benefit in treated patients, despite apparent increases in regulatory T cells [125]. Hypothesizing that a tolerogenic defect may exist in the MSCs derived from lupus patients, a different team led by Lingyun Sun has instead sought to utilize allogeneic MSCs. In a 2013 paper, Sun and colleagues describe the results of four years' worth of clinical trial data conducted at their hospital in Nanjing, treating 87 patients with severe or drug-refractory lupus [126]. In their clinical trials, MSCs are harvested from marrow or umbilical cord, culture-expanded for no more than 5 *in vitro* passages, and infused into patients while still in a fresh, living state. Standard phenotyping and differentiation assays are performed to confirm MSC identity, but invasive studies aimed at mechanistic questions were not performed in these patients. Nonetheless, their data showed induction of clinical remission and improvement in renal function, irrespective of marrow or umbilical source.

These same researchers released a study in 2014 that sought to go further in identifying the mechanistic links whereby MSCs effect clinical improvement [127]. In a series of carefully reductionist experiments, the team replicates their allo-MSC data using *in vitro*

assays that culture lymphocytes and/or MSCs derived from healthy donors or patients with lupus. They demonstrate that it is the CD8 compartment of T cells that produces large amounts of IFN-γ, and that this in turn results in increased expression and enzymatic activity of IDO in healthy MSCs. Conversely, lupus patient-derived MSCs are deficient in IDO activity, a measure which is defined as IDO catalysis of tryptophan into kynurenines. By careful comparisons of *in vitro* assays with the patient-centered trials, such reports demonstrate how basic cellular biology can synergize with clinical medicine, to further our understanding of such cell-based therapies.

Autologous MSCs for Autoimmune Disease

Crohn's Disease (CD) is an autoimmune disease characterized by inflammatory lesions that can occur anywhere along the gastrointestinal tract, from mouth to anus. Along with ulcerative colitis (UC), these two forms of inflammatory bowel disease (IBD) cause a spectrum of painful and damaging symptoms, including enterocutaneous fistulas, intestinal bleeding episodes, diarrhea and malnourishment [128]. Although the precise etiology is not confirmed for all cases, it is generally accepted that CD arises in patients with a genetic predisposition, and may represent a dysregulated immune response in the gut. The naturally tolerogenic balance of immune cells, gut tissues and commensal flora is lost in these patients, and inflammatory cytokines such as IL-6, IL-23 and TNF-α have all been identified to play a role in its pathogenesis [129]. Although IBD can be described as an autoimmune disease, frankly self-reactive T cells or B cells are not uniformly found in

all patients; nonetheless, syndromic inflammatory damage to the gastrointestinal system is a hallmark of both UC and CD.

The immunologic component of IBD has been appreciated for some time, and a number of disease-modifying immunotherapies have been developed, and are now in clinical use. These include anti-TNF-α antibodies such as infliximab, and lymphocyte depletion drugs drawn from the realm of chemotherapy, including azathioprine. Cellular-based therapies have also been explored, including the transplant of hematopoietic stem cells, as well as MSC-based therapies. The rationale by which MSC therapies are thought to improve IBD lies in their profound immunosuppressive effects, which have been described for a variety of *in vitro* and animal model systems. A number of ongoing clinical trials are now exploring MSC platforms as a therapy for CD. As above, interpreting these clinical data and the mechanisms by which the cells are thought to act affords us excellent perspective on how to further improve MSC-based therapies for immune-mediated diseases.

In 2010, a Dutch group led by Hommes and Duijvestein released a report in which they described results from infusing ten CD patients with autologous, bone marrow-derived MSCs [130]. Hommes and colleagues harvested MSCs from the patients, cultured the cells no more than three passages, and then cryopreserved the cells prior to infusion. Patients received two infusions of cells, separated one week apart. One of the distinctive aspects of this study is the battery of immunologic assays the team employed to characterize patient response. In addition to assessing symptom scores using the Crohn's

Disease Activity Index, the trial included endoscopic examination of lesional changes, as well as biopsies to assess T cell subsets and cytokine levels present in gut tissues. Additionally, they performed *ex vivo* T cell suppression assays, using peripheral blood mononuclear cells (PBMCs) and MSCs derived from the same set of CD patients. Their *in vitro* experiments show that MSCs derived from CD patients are not inferior to MSCs from healthy donors in suppressing the proliferation or cytokine secretion of CD3/CD28-stimulated PBMCs. As many of the patients receive simultaneous pharmacologic treatments, the team added these drugs to co-culture systems, observing an additive effect on MSC immunosuppression. Biopsies from patients after MSC infusions showed trends of improvement, as suggested by regulatory T cell numbers and cytokine levels in lesional areas, but none of the patients in the study entered true long-term clinical remission. This study is nonetheless an important benchmark in MSC therapy for CD in part because of the investigative mechanisms explored by the research team. By exploring the *in vivo* mechanisms by which MSCs have been shown to act *in vitro,* further insights are sure to follow.

Chapter 1: Figure 1:
Licensing of MSCs Activates their Immunomodulatory Capabilities

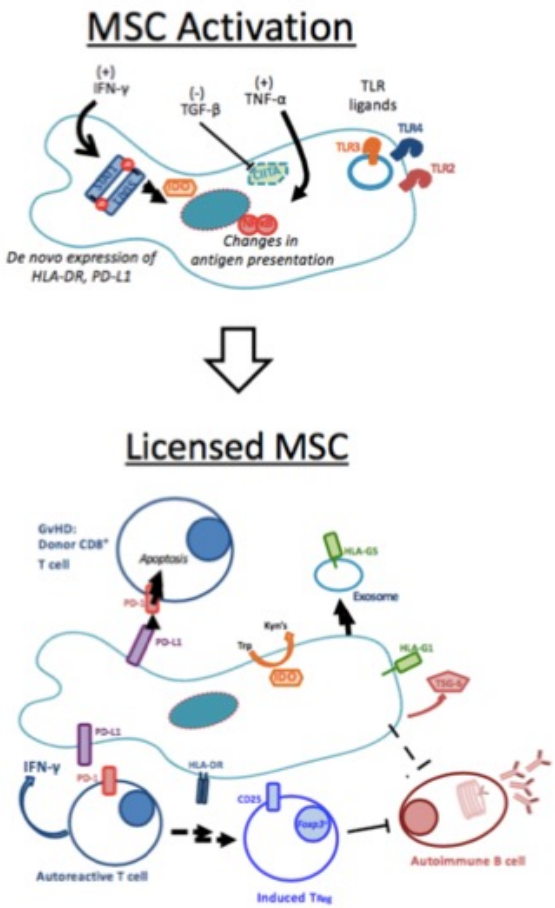

Chapter 1: Figure 1:
Licensing of MSCs Activates their Immunomodulatory Capabilities:

Exposure to inflammatory stimuli causes mesenchymal stromal cells (MSCs) to undergo a number of RNA- and protein-level changes, activating their immunomodulatory capabilities. This includes the *de novo* expression of PD-L1, HLA-DR, as well as increased expression of Class I HLA molecules. TNF-α signaling causes a number of NF-κB-mediated signaling events, consistent with immune activation. TGF-β treatment abrogate expression of HLA-DR via CIITA inhibition [92]. After *in vitro* licensing, MSCs have been shown to more efficiently suppress the function and proliferative capacity of T and B cells. In the setting of cellular therapy, it is thought that inflammatory factors in the patient can activate these same mechanisms, resulting in immunomodulation by the transfused MSCs.

Chapter 2: AHR Signaling as a Model for MSC Bioactivity

Chapter Abstract

The catabolism of tryptophan (Trp) by indoleamine 2,3-dioxygenase (IDO) is a key step in tolerance effected by a variety of cell types, including mesenchymal stromal cells (MSCs). Trp catabolism generates molecules known as kynurenines, whose tolerance mechanisms involve activation of the Aryl Hydrocarbon Receptor (AHR). A synthetic analog of Trp, 1-methyl tryptophan (1MT), is a selective inhibitor of IDO enzymatic activity being utilized in cancer immunotherapy trials. We hypothesized 1MT might activate AHR independently of its effects on IDO. We demonstrate MSCs express AHR protein, and that *in vitro* treatment with 1MT causes AHR nucleotranslocation. Upon analyzing mRNA, we observed transcriptional upregulation of cytochrome p450 1a1 and 1b1 by 1MT racemic mixture (R-MT), consistent with AHR-activation. RNA-sequencing identified Nrf2, MAPK12 and IL-1a as downstream targets of 1MT. We demonstrate 1a1 and 1b1 activation by 1MT in IDO+ MSC following interferon-γ (IFN-γ) activation, suggesting AHR signaling is uncoupled from IDO catalytic function. Such a mechanism of action for 1MT may extend its usage to a wider range of patients, irrespective of tumor IDO expression. These observations support a novel paradigm by which AHR-activating compounds like 1MT can be used in cancer immunotherapy to stimulate a pro-inflammatory response.

Introduction

Recent studies in cancer immunology have explored the role of tolerance inside the tumor microenvironment, enabling cancers to evade immune surveillance [1]. Cells that mediate tumor-associated suppression include myeloid suppressor cells or tumor-associated macrophages. Such cells have been shown to facilitate tumor progression by the accumulation of regulatory T cells [1]. One of the principle mechanisms whereby tumor-resident cells mediate this immunomodulation is the catabolism of tryptophan (Trp) by indoleamine 2,3-dioxygenase (IDO). It has been shown that IDO is a crucial determinant of the immunomodulatory abilities of mesenchymal stromal cells (MSCs) [2]. Immune-suppressing cells with IDO expression engender a tolerogenic tumor microenvironment [3] providing a rationale for pharmacologically blocking IDO activity with 1MT for cancer immunotherapy. IDO catalytic activity leads to the deprivation of Trp and has been shown in biochemical studies to dampen the proliferation of T cells by limiting ζ-chain activation [4]. However, the Trp-deprivation model has been questioned by studies showing IDO-catalyzed Trp catabolites bind to and activate the aryl hydrocarbon receptor (AHR) [5]. Much of our understanding of aryl hydrocarbons comes from studies with 2,3,7,8-tetrachlorodibenzodioxin (TCDD). First described as the TCDD receptor, ligand-activation of AHR causes a conformational shift, allowing it to bind its chaperone protein, AHR nuclear translocator (ARNT). ARNT contains a nuclear-localization-signal (NLS) in residues 39-61 [6] which allows the complex entry to the nucleus, whereupon it activates transcription at AHR response elements (AHREs) [1, 7]. Signaling at AHREs has been

implicated in carcinogenesis studies with aromatic hydrocarbons like benzopyrene [8, 9]. In such studies, ligand-activation of AHR is often shown by the upregulation of cytochrome p450 (Cyp) enzymes, Cyp1a1 and Cyp1b1 [10]. However, the evolutionary conservation of AHR signaling (including invertebrates with no such hepatic biotransformation of toxins [11]) suggests a broader homeostatic function for AHR signaling, beyond just toxin-processing. Indeed, the finding that endogenous kynurenines can activate the AHR suggests this transcription factor may have broadly-acting immunomodulatory effects [12]. Like Trp and Kyn, 1MT is also an aromatic hydrocarbon, but 1MT is currently the focus of more than a dozen clinical oncology trials [13], where its use is rationalized on the basis of its irreversible inhibition of IDO catalysis. Since immune-competent cells, such as MSCs and dendritic cells, can co-express AHR and IDO under inflammatory conditions [14], it suggests that the effects of 1MT ascribed to selective inhibition of IDO may also arise from activation of the AHR pathway. We here demonstrate that AHR+ MSCs with IDO competency deploy a robust inflammatory molecular genetic response to 1MT, even in the absence of IDO expression. These data provide important insights that may expand the clinical indications for 1MT as a cancer immunotherapy, and it that may be therapeutic even in IDO-null tumors, through activating AHR-mediated mechanisms.

Results

Immunophenotype of marrow-derived human Mesenchymal Stromal Cells

We performed flow cytometry to confirm that MSCs expressed conventional cell surface

markers, using guidelines from the International Society for Cellular Therapy [15]. Figure 1A presents the flow cytometry gating strategy used to confirm the presence of these markers for one MSC donor, in comparison with relevant matched-isotype control samples. Figure 1B compares three distinct MSC samples, analyzed using the same gating strategy. These findings are representative of all MSCs used in subsequent analyses.

MSCs constitutively express AHR but inducibly express IDO

The Trp derivative 1MT has been classically described as an enzymatic inhibitor of the IDO1 enzyme. As IDO is an important protein for MSC function, we sought to assess the effects of 1MT on MSCs. Resting MSCs (rMSCs) are immunoregulatory at baseline, but not nearly as effective as MSCs that have been pre-licensed with inflammatory stimuli such as interferon-γ (IFN-γ). IFN-γ activates a STAT1-mediated signaling cascade that causes *de novo* mRNA transcription and protein expression of IDO1 [16]. Figure 1C confirms this, showing that rMSCs are IDO-negative and that IFN-γ induces robust IDO protein upregulation. Treatment with any of the enantiomer mixtures of 1MT does not induce IDO expression (Figure 1C). As the AHR protein has been described as being constitutively present in the cytoplasm at baseline [17], we sought to confirm that our MSCs expressed this protein. Figure 1D summarizes these findings, in which the antibody localizes the AHR protein near the 100 kDa marker. Notably, these two immunblots demonstrate that 1MT alone does not induce IDO expression, nor alter the level of AHR expression.

1MT causes AHR nucleotranslocation

Upon ligand binding, the AHR associates with ARNT, only upon which will the protein enter the nucleus, where it acts as a transcription factor at AHREs. To generate evidence that 1MT could induce this pathway of activation, we used a protein-based tracking method, to document a shift of AHR protein from cytoplasm-to-nucleus, after treatment with test drugs [18, 19]. Figures 2A-B demonstrate that at baseline, MSCs exhibit a cytoplasmic signal for AHR, and nuclei that are devoid of the green immunofluorescent signal. This is readily observed when comparing the untreated cells (NoRx) to the isotype-stained cells (Isotype). After 5h of TCDD treatment, an increase in nuclear-staining can be appreciated, consistent with its classification as a *bona fide* AHR ligand. We performed this experiment using three enantiomeric mixtures of 1MT, and then utilized Leica software packages to numerically quantify the resultant changes in immunofluorescence (Figure 2C). We performed a one-way ANOVA test, affording a p-value of 0.0003, indicating that the nuclear shift in AHR signal induced by 1MT was comparable to that induced by TCDD. Taken together, these data demonstrate 1MT activates a similar cellular response as the most well-understood AHR ligand.

Known AHR ligands and Trp derivatives activate the AHR response

As discussed above, *bona fide* AHR ligands bind the molecule and activate its nucleotranslocation, resulting in the induction of genes that contain an AHRE. The most well-characterized sentinel genes of such AHR activation are Cyp1a1 and Cyp1b1 [8, 20, 21]. We cultured MSCs in the presence of two validated AHR ligands, TCDD and 6-formylindolo[3,2-b]carbazole (FICZ), well-characterized molecules known to ligate the

receptor [22]. Additionally, we included two IDO-catabolized Trp byproducts, kynurenine and kynurenic acid, both of which have been explored for their AHR bioactivity. Kynurenic acid in particular has been documented as a verified AHR ligand that results in more potent cytochrome induction that kynurenine [23]. Untreated controls were included in each experiment, and Fold-Induction of each Cyp gene was calculated relative to baseline expression of GAPDH. Figure panels 3A-3D plot the induction of Cyp1a1 and Cyp1b1 following 6h or 24h timepoints. We note that racemic 1MT (R-MT) induces significant induction for Cyp1a1, and that the other test ligands responded with the prototypic AHR response. Although the induction of Cyp1b1 by R-MT did not achieve statistical significance, we note that the magnitude of cytochrome induction for known ligands FICZ and kynurenic acid are similar to that effected by racemic 1MT.

1MT induces dose-dependent response for AHR activation in MSCs

We used a fixed time point to further explore the 1MT-mediated mRNA-induction of Cyp1a1 and Cyp1b1 [8, 20, 21] using clinically-relevant ranges of 1MT concentrations, with three different enantiomeric preparations. In current clinical trials with 1MT, patients are dosed orally up to 2000mg, achieving peak plasma concentrations of 1200 ng/ml (5.5 µM) [24, 25], and *in vitro* studies use 1mM dosing to inhibit IDO activity [2, 3]. As different publications explore different enantiomers of 1MT for IDO activity, we sought to assess if these three preparations would show different AHR activity profiles, at concentrations ranging from 5000 µM to 0.1 µM (Figure 3E-F). Untreated controls were included in each experiment, and Fold-Induction of each cytochrome gene was calculated

as above. These data were fitted to linear regression models, which were then compared for difference in slope, affording statistically-significant p-values, suggesting the racemic mixture (R-MT) may be more AHR-bioactive than either of the pure enantiomers. Taken together, these results indicate that over a variety of sub-clinical and clinical doses, all three mixtures of 1MT can induce the canonical AHR-driven response.

Interferon-γ licensing of MSCs does not modify AHR response

Our initial experiments showed that resting MSCs, negative for the IDO protein, were able to demonstrate robust upregulation of the downstream AHR signaling pathway in response to 1MT. However, it is conceivable that IDO+ cells might occupy equivalents of 1MT in the active site of the IDO protein, leaving none available to activate the AHR response [26]. To address this, we pre-treated MSCs with IFN-γ for 24h, which is sufficient to induce robust IDO protein expression [16]. Following, the IFN-γ was washed off and cells were treated with a fixed dose (1mM) of the 1MT enantiomeric preparations. Figure 4A is an immunoblot demonstrating that the amount of IDO protein expressed by MSCs does not alter when cells were also treated with 1MT. Figure 4B-G shows the induction of the cytochrome genes when IFN-γ pre-stimulation was followed by 1MT, at a variety of dose titrations. A peak in Cyp1a1 induction occurred for at 100μM for D-MT and R-MT, but one was not observed for L-MT until 2.5 mM. We used linear regression and found that IFN-γ licensing of MSCs does not consistently alter the magnitude of cytochrome enzyme induction to a significant degree. This pattern is particularly important to note near 5.5 μM, which is the plasma concentration seen in humans dosed therapeutically

with 1MT [24, 25]. These data indicate that 1MT can activate the AHR-driven response in MSCs in a comparable fashion, irrespective of IDO expression.

RNA-seq shows 1MT and TCDD activate similar gene sets

Given that 1MT is known to be effective in cancer immunotherapy, we sought to use RNA profiling to identify novel immune signals induced by 1MT, and how those might be similar to the transcriptome of a verified AHR ligand. Five independent MSC samples were exposed for 24h to racemic 1MT, TCDD, or treated with vehicle only (NoRx); we then performed RNAseq analysis. We focused on differentially-expressed genes (DEGs) that were most significantly changed upon treatment with R-MT or TCDD. Hierarchical clustering was used to organize genes by expression pattern across samples. Figure 5A is a heat map representing the union of all DEGs found between the three conditions. Taken together, this heat map and its pattern suggests similar gene-activating signatures by R-MT and TCDD, especially when compared to sample-matched untreated controls. The Venn diagram in Figure 5B represents the degree of overlap for genes found to be up-regulated or down-regulated in R-MT-treated cells or TCDD-treated cells relative to controls. Among the up-regulated genes, we noted Cyp1a1 and Cyp1b1 (Supp. Table 1) were both present, confirming an AHR-activating signature for both drugs; there were also 108 genes that were down-regulated in common (Fig. 5B, Supp. Table 1).

IPA reveals a pro-inflammatory transcriptional signature for MSCs treated with 1MT

We next sought to identify the pathways that were uniquely affected by R-MT, but not by

TCDD treatment (715 genes, Supp. Table 2. The 167 genes that were uniquely changed by TCDD are summarized in Supp. Table 3). We performed an Ingenuity Pathway Analysis (IPA) on the genes from Supp. Table 2, those uniquely affected by R-MT, and Figure 5C is a curated list of 24 immunomodulatory pathways most significantly altered, with the bar color indicating if net pathway activation was up, down, or more diversely activated. The most potently-activated pathway from this list was the Nrf2-mediated oxidative stress pathway, which was identified as being overall down-regulated as a result of R-MT treatment. Figure 5D presents a heat map for four of the aforementioned gene sets. To generate this heat map, each patient sample was normalized to its own untreated control, and IPA-pathway genes were assessed for up- or down-regulation on a per-patient basis. This heat map compares TCDD- and R-MT responses side-by-side. Key pathways are observed to be activated or down-regulated by both drugs, but in each case, R-MT was a more robust activator. These pathways are consistent with a cellular response poised towards pro-inflammatory infiltration of tumor tissues. Across all five samples, R-MT downregulates the Nrf2-mediated oxidative stress pathway, which is similar to the down-regulations observed in the paxillin pathway. Also of note was the net up-regulation of gene sets involved with the diapedesis of white blood cells, as well as the pro-inflammatory IL-1 pathway.

Discussion

Previous reports have indicated that the immunosuppressive effects of the IDO enzyme are due to the catabolism of tryptophan and the generation of secondary messenger

metabolites. However, it remains unclear how those molecules may affect leukocytes, such as those that infiltrate a tumor. One such compound, kynurenine, was shown to have a net immunosuppressive effect on the proliferative capacity of inflammatory T cells [27], whereas others have been shown to activate the AHR and induce an pro-inflammatory response in cancer cells [23]. All of these tryptophan derivatives, including 1MT, contain an aromatic ring substituent. We hypothesized that the aromatic moieties in these compounds may rationalize their ability to serve as binding partner for the AHR, classically only appreciated as a receptor for aromatic hydrocarbon toxicants. We sought to characterize the effects of enantiomerically-pure and racemic mixtures because various human, murine and *in vitro* experiments have reported differential tumor clearance or IDO-inhibition for different enantiomeric preparations [24, 28-30]. On-going clinical trials use the enantiomerically-pure compound of D-MT [13, 24], which has been shown *in vitro* to be more effective at reversing tumor-mediated T cell suppression, and better *in vivo* synergy with conventional chemotherapy regimens [28]. Although many *in vitro* studies are conducted with a racemic mixture of R-MT [29], and it has been shown that the L enantiomer is a more effective inhibitor of IDO enzymatic activity [30]. Due to these conflicting reports, we tested the pure enantiomers as well as the racemic mixture, with some of our assays suggesting the racemic mixture was a stronger induce of the AHR response.

Although the present work has utilized a variety of indirect 1MT-to-AHR activation correlates, a direct ligand-binding assay will be necessary to validate the drug actually

ligates the receptor. For example, there may exist an indirect middle actor(s) between the AHR response and treatment with 1MT. Ligand-binding studies such as the electromobility shift assay, as examined with free AHR protein and treatments with radiolabeled TCDD or 1MT would address this question [31].

Through a combination of biochemical, immunologic and bioinformatic methods, we demonstrate the efficacy of 1MT for cancer immunotherapy may be rationalized in part due to its AHR-activation. The tumor microenvironment contains malignant and non-malignant cells, as well as cells that may or may not express IDO. MSCs and their closely-related progeny can be mobilized to a growing tumor and participate in the formation of an immune suppressive microenvironment. Considering their innate ability to express IDO and constitutive expression of AHR, they provide a likely biological target for the pharmacological effects of 1MT. MSCs are touted as a therapeutic cell therapy tool, owing to their immune-suppressive or regenerative capabilities, but these same traits can become maladaptive in a tumor microenvironment. The process by which a tumor expands can be thought of as a chronic, non-healing wound [32]. The inflammatory milieu that attracts endogenous or local MSCs to repair damaged tissues can be usurped by a tumor, and the immune-suppressive effects of MSCs hijacked to help the tumor evade future attack by leukocytes. It is for these reasons that we sought to model the tumor microenvironment with the use of non-transformed MSCs, to understand the balance of inflammatory forces that can be targeted by adjuvant therapies like 1MT. Targeting IDO inhibition (or AHR activation) in a specifically-transformed cancer cell line simply would

not afford the same immunotherapy-relevant insights that we have gained from using MSCs.

RNAseq profiling analyses revealed distinct pro-inflammatory signatures that were activated by 1MT, the most highly-significant of which was Nrf2-mediated oxidative stress. The Nrf2 pathway typically plays a protective role in tissues, mitigating inflammatory damage caused by environmental toxins. However, anti-inflammatory activity in a tumor microenvironment is not a positive-good phenomena; this anti-inflammatory signaling reflects the mechanisms of cancer immune-evasion [33], such as when tumor-infiltrating lymphocytes, or cell-based immunotherapeutics, are reprogrammed to ineffective regulatory cells [34]. The down-regulation of Nrf2 is interesting, as this gene is a known transducer of AHR-mediated signaling, not only for environmental toxins, but also for immune-modifying signals and hematopoietic cues [35]. Various reports have used chromatin-immunoprecipitation and sequencing to show that Nrf2 is an important regulator of anti-oxidant target genes, including HO-1, a key molecule that reduce cellular stresses from reactive oxygen species (ROS) [36-38]. Additionally, the 1MT-induced down regulation of Nrf2 helps explain how anti-inflammatory forces in a tumor microenvironment compete with infiltrating leukocytes to continually evade immune surveillance [34]. Similarly, overexpression of paxillin-family adhesion signaling proteins is a known signature of various tumor types [39, 40], so its down-regulation by 1MT is also consistent with a localized anti-tumor response. Overexpression of paxillin family members is a known signature of various tumor types

[39, 40], so its net down-regulation by 1MT suggests this pathway may also be involved in the 1MT response. This is consistent with the role of 1MT in cancer immunotherapy, which by inhibition of IDO—or shown here as activating the AHR response—primes the immune system to fight tumors. Also of particular interest is the up-regulation of genes involved with extravasation by leukocytes, again consistent with an activated immune system, and tumor infiltration by lymphoid, myeloid or mesenchymal stromal cells.

More than half of the pathways enumerated in Figure 5 contain the pro-inflammatory cytokine IL-1a, and the ERK family kinase MAPK12 is also present at the same frequency. These genes were of interest as mechanisms by which tumor-associated cells could induce an inflammatory response, allowing infiltration by immune cells. Cross-comparisons with the Comparative Toxicogenomics Database revealed that MAPK12 is known to interact with benzopyrene, a toxicant in cigarette smoke, as well as DMBA, both of which are well-characterized AHR ligands known for potent toxicity in mammalian cells [41]. MAPK12 is also known for transducing signals related to cisplatin, etoposide and tamoxifen, three widely-used chemotherapeutic drugs [41]. To strengthen the association that MAPK12 may be transducing 1MT and AHR signals, we developed an *in silico* search algorithm to identify possible AHR response elements upstream of this putative AHR target gene. Our approach is modeled after a 2010 publication which utilized RNA-seq coupled with *in silico* bioinformatics to identify AHRE in target gene promoters, to putatively define them as downstream regulators [42]. Using this technique, Perdew et al. showed the 10kb-promoter region of the pro-inflammatory

cytokine IL-6 contained an AHRE (GCGTG), rationalizing how a synthetic AHR ligand might stimulate the immune system. Notably, our own RNA-seq data reinforces these findings, as we noted an up-regulation of the IL-6 pathway in our R-MT transcriptome pathway analyses (Figure 5C). When we used this same scan-and-score algorithm to analyze the 10kb-promoter regions of MAPK12, we identified ten hypothetical AHR binding sites with sequence GCGTG. Similarly, the pro-inflammatory cytokine IL-1a contained two possible AHR binding sites with GCGTG.

The overlapping signals elicited by AHR toxicants (TCDD), as well as drugs in common usage but with incomplete understanding of their mechanisms of action (1MT) indicate possible steps forward in drug development. Importantly, we cannot be guided by traditional understanding of 1MT (as solely an IDO-inhibitor). It will be important to identify which types of AHR-activating ligands have pro-cancer effects (TCDD), which have anti-cancer effects (1MT), and what downstream activation panels will be most useful in screening compounds for bioactivity, via Cyp1a1/Cyp1b1 induction, Nrf2 repression or activation of MAPK12 or IL-1a.

The present work has utilized conventional biochemical and microscopy-based techniques to show that 1MT may act as an activator of the AHR pathway. However, beyond the identification of this signal, it has been important for us to define the downstream mechanisms by which 1MT may interact with AHR, in order to better characterize and pharmacologically exploit its cancer immunotherapy-augmenting

abilities. By coupling RNAseq bioinformatics and *in silico* prediction modalities, we identified novel downstream actors that may rationalize how and why R-MT augments cancer immunotherapy. The finding that 1MT activates an AHR immune-activating signature—independent of IDO expression—suggests that this drug may have broader indications than previously anticipated. Taken together, this work lays the foundation for wider implementation of AHR-activating molecules, and the screening parameters that may guide further use of these molecules, to synergize immune-activation with conventional cancer treatment modalities.

Materials & Methods

MSC isolation and culture

Human MSCs were isolated from bone marrow aspirates collected from the iliac crest of consenting volunteer subjects [43]. Bone marrow aspirates were diluted 1:2 with PBS and layered onto a Ficoll density gradient to isolate mononuclear cells. The cells were centrifuged at 400 × *g* for 20 min and thereafter plated in complete human MSC medium (α-MEM with L-glutamate, 10% human platelet lysate, 100 U/ml penicillin/streptomycin (Corning International, Corning, NY)) at 200,000 cells/cm^2. Non-adherent hematopoietic cells were removed by changing the medium after 3 d of culture, and MSCs were allowed to expand for 7 d. Thereafter, the cells were passaged weekly and reseeded at 1000 cells/cm^2. After the third passage, the MSC cultures were assayed by flow cytometric analysis for the absence of CD45$^+$ and CD31$^+$ contaminating cells and expression of CD44, CD73, CD90, and CD105 (BD Biosciences, San Jose, CA). Flow cytometry was performed

using a FACSCanto II (BD Biosciences, San Jose, CA) and FlowJo software v9.6 (TreeStar, Ashland, OR). All assays were performed using MSCs between passages 3 and 6. Although culture-expanded in α-MEM, all subsequent tissue culture experimental work was performed in R10 (RPMI 1640 with L-glutamate plus 100 U/ml penicillin/streptomycin, and 10% fetal calf serum) (Corning International, Corning, NY). All cell culture work was performed in standard conditions in a tissue incubator at 37 °C in 5% CO_2 and 95% air.

Immunoblotting

Approximately 1 million MSCs were harvested from a single 75-cm^2 flask at 80% confluency. Cells had been treated for 12h with 50 ng/ml recombinant human IFN-γ (Invitrogen, Carlsbad, CA), and/or 1-methyl-DL-tryptophan, 1-methyl-D-tryptophan, or 1-methyl-L-tryptophan (Sigma-Aldrich, St. Louis, MO). Whole-cell protein lysates were run in a 4-20% polyacrylamide gel electrophoresis apparatus and then transferred to PVDF membrane, which was blocked in 5% non-fat milk in Tris-buffered saline + 0.05% Tween-20. Protein was detected using primary rabbit anti-human IDO1 (1:1000; EMD Millipore Corporation, Billerica, MA), primary mouse anti-human AHR (1:1000; ThermoFisher, Waltham, MA) or primary rabbit anti-human β-actin (1:1000; Cell Signaling Technology, Danvers, MA), and secondary horseradish peroxide-coupled goat anti-rabbit IgG h + l (1:10,000; Bethyl Laboratories, Montgomery, TX). ECL detection system (Amersham Pharmacia Biotech, Piscataway, NJ) was used to detect immunoreactive blots.

q-RT-PCR Analysis

MSCs cultured in the presence or absence of tryptophan derivatives or known AHR agonists were analyzed using quantitative Real-Time PCR. Total RNA was extracted and depleted of genomic DNA using the RNeasy plus mini kit (QIAGEN, Hilden, Germany). Normalized RNA was converted cDNA using Quantitect Reverse Transcription kit (QIAGEN, Hilden, Germany). Perfecta Sybr Green Fast Mix (Quanta Biosciences, Beverly, MA) real-time PCR was performed with the following primer pairs, listed with the forward primer followed by the reverse primer: GAPDH: 5'-CTC-TCT-GCT-CCT-CCT-GTT-CGA-C-3' ; 5'-TGA-GCG-ATG-TGG-CTC-GGC-T-3'. Cyp1b1: 5'-GCT-GCA-GTG-GCT-GCT-CCT-3' ; 5'-CCC-ACG-ACC-TGA-TCC-AAT-TCT-3'. Cyp1a1: 5'-CAC-CAT-CCC-CCA-CAG-CAC-3' ; 5'-ACA-AAG-ACA-CAA-CGC-CCC-TT-3'. An ABI 7500 fast real-time PCR system thermal cycler (ThermoFisher, Waltham, MA) was used for amplification and the Δ-Δ C_T method was employed to calculate the fold change in expression [44]. Data are presented as normalized fold-induction above contemporaneously vehicle-treated controls.

Immunofluorescence microscopy

In a twelve-welled tissue culture plate, 50,000 MSCs were plated onto glass coverslips and allowed to adhere overnight. Media was aspirated and replaced with R10 with/without indicated AHR testing ligand. Drugs: TCDD: 10nM (Supelco, St. Louis, MO), L-MT, D-MT, R-MT all at 1mM (Sigma Aldrich, St. Louis, MO). Cells were treated for 5h, after which media was aspirated and cells were fixed with 4% paraformaldehyde in PBS, then quenched with 50mM NH_4Cl. Cells were permeabilized with 0.2% Triton and stained for AHR protein (1:100, ThermoFisher, Waltham, MA) diluted in 3% BSA in PBS (Sigma Aldrich, St. Louis,

MO). Slips were kept overnight at 4˚C in a humid chamber, washed with PBST, then stained (1:500) with a goat-derived anti-mouse secondary antibody with DyLight-488 (ThermoFisher, Waltham, MA). Isotype-control was a non-specific primary murine-derived IgG1 (BD Biosciences, San Jose, CA), followed by the same secondary. Glass slips were affixed to microscope slides using DAPI-containing VectaShield Dry-Curing mounting medium (Vector, Burlingame, CA) and then imaged using a confocal Zeiss SP8 microscope (Zeiss, Oberkochen, Germany). The Leica LASX software package (Leica, Wetzlar, Germany) was utilized by a treatment-blinded observer to delimit regions of interest, defined by the DAPI-stained nucleus. From these regions, the signal of Alexa488 was computed and normalized per square micron.

Statistics

All graphical data for the project was analyzed using GraphPad Prism version 6.0 (GraphPad, La Jolla, CA), and the statistical tests of significance are noted where indicated, always using an alpha level set at 0.05.

RNA-seq

RNA-Seq analyses were conducted at the Yerkes NHP Genomics Core on five independently-sourced MSC samples. Cells ($1x10^5$) were plated into six-welled tissue culture plates in duplicates and treated with vehicle alone (R10), TCDD (10nM) or a racemic mixture of 1MT (1mM) for 24h. Total RNA was extracted from using QIAGEN RNEasy Mini kits (QIAGEN, Hilden, Germany) and RNA quality assessed using Agilent

Bioanalyzer analysis. Polyadenylated transcripts were purified on oligo-dT magnetic beads, reverse transcribed using random hexamers, fragmented, and incorporated into barcoded complementary DNA libraries based on the Illumina TruSeq platform. Libraries were validated by microelectrophoresis, pooled, and sequenced on an Illumina HiSeq 1000 (101 bp) to an average read depth of 25 million [45]. 58,604 unique mRNA transcripts were identified in the data set. Reads were aligned to human RefSeq hg19 reference using STAR software (v2.3.0e) (http://code.google.com/p/rna-star) [46]. The RNAseq data discussed in this publication have been deposited in NCBI's Gene Expression Omnibus [47] and are accessible through GEO Series accession number GSE95072 (https://www.ncbi.nlm.nih.gov/geo/query/acc.cgi?acc=GSE95072).

RNA-Seq Analyses

To examine differential gene expression in samples, estimates of gene-wise and isoform-wise expression levels for individual genes were performed using DESeq, which normalizes gene expression level estimates across samples and also corrects for nonuniformity in read distributions across each gene [48]. Each patient-sample-set included an untreated control, which was used to measure differential expression above baseline on a per-patient basis. Clustering by covariance PCA and visualization (i.e., heat maps) of expression data were performed in Partek Genomics Suite software (Partek Inc., St Louis, MO). Differentially expressed genes were analyzed for enriched gene families/pathways/ protein interactions using Ingenuity Pathway Analysis (QIAGEN,

Hilden, Germany). Gene set enrichment analysis was performed on the regularized log (rlog) expression table produced by DESeq2 employing a weighted enrichment statistic and Signal2Noise as the ranking metric and using 1000 phenotype permutations. The UCSC Genome browser, loaded with hg19, was used to analyzed the 10-kb promoter regions of MAPK12 and IL1a, prior to the first known exon, and a text-searching Python script employed to identify putative AHREs.

Chapter 2: Figure 1: IDO and AHR expression in resting and IFN-γ-stimulated MSC treated with 1MT

A.
Mesenchymal stromal cells (MSC) were isolated from the marrow of healthy human donors (N=3). Cells were removed from flasks after 5d of growth and stained using a panel approved by the International Society for Cell Therapy. Panel A represents the flow cytometry gating strategies for an isotype control sample, compared to an MSC sample stained with PE-conjugated CD73. These data are representative of all MSC samples utilized in this study.

B.
Panel B represents the sub-gating analysis, interrogating MSC for CD45, CD44, CD73 and CD90 and CD105. In each histogram, the black unfilled-line represents relevant isotype-matched control, and the three gray lines are independent but contemporaneously-analyzed MSC samples.

C.
Untreated, resting (r) MSCs and IFN-γ stimulated (γ), MSCs were analyzed for expression of the IDO protein (IFN-γ: 50 ng/ml for 24 h). Additionally, treatment with (D)-1MT, (L)-1MT or racemic (R) mixture was tested (1 mM each). Figure 1C represents the immunoblotting results of a single membrane that was first blotted for IDO1, then stripped, re-blocked and probed for actin. These are results from an experiment with MSC sample, which was replicated three times.

D.
At baseline, resting MSCs (r) demonstrate presence of the AHR protein. The effects of 24h treatment with IFN- γ (γ), or D-MT, L-MT or R-MT on AHR protein expression was evaluated. IFN-γ: 50 ng/ml; all 1MT: 1mM). AHR is indicated by the arrowhead near the 100 kDa band. Figure 1D represents the immunoblotting results of a single membrane that was cut into two and blotted separately for AHR and actin. These are results from an experiment with one MSC sample, which was replicated three times.

Chapter 2: Figure 1: IDO and AHR expression in resting and IFN-γ-stimulated MSC treated with 1MT

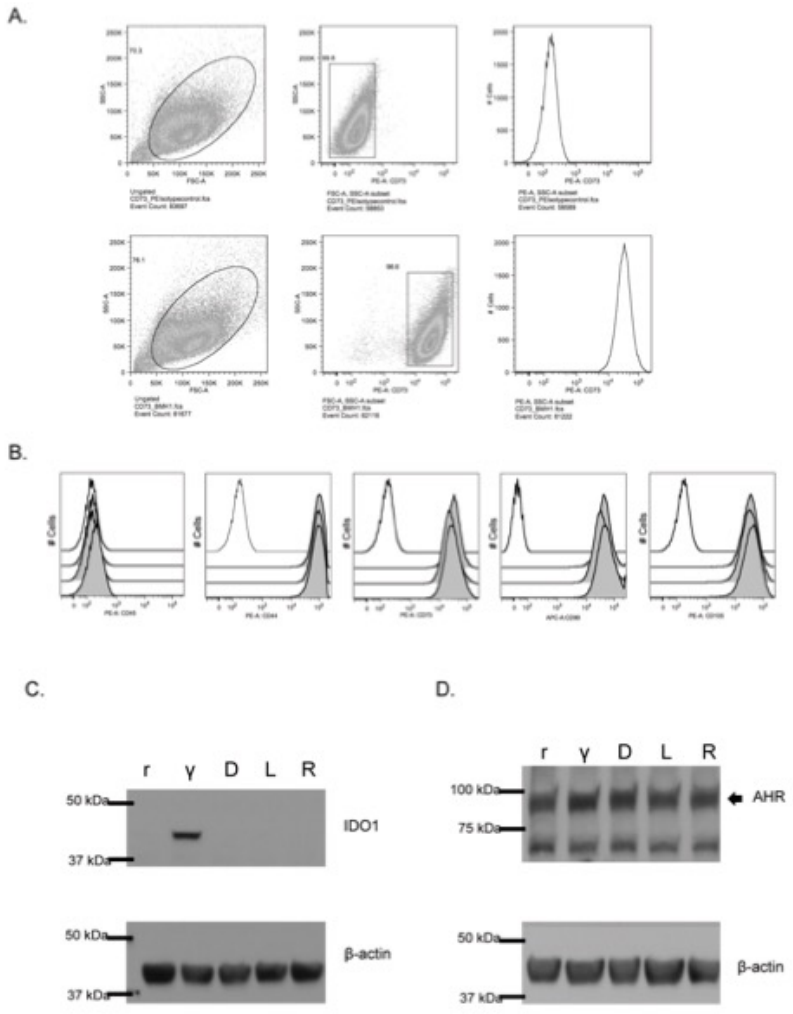

Chapter 2: Figure 2: AHR nucleotransloaction in MSCs treated with 1MT and AHR agonists

A, B.
MSCs were plated onto glass coverslips and allowed to adhere overnight. Media was aspirated and replaced with R10 or the indicated drug. Drugs were left on cells for 5h, after which cells were fixed and AHR was visualized via immunofluorescence; DAPI was used to visualize nuclei. Isotype-control was a non-specific murine-derived IgG. TCDD concentration was 10 nM. Concentrations of D-MT, L-MT, R-MT all at 1mM. These results (A, B) from an experiment with one MSC sample, which was replicated four times with independent MSC samples. All images were taken using a confocal microscope with the same exposure settings.

C.
The bar graph represents the quantified results of nucleotranslocation, as observed via immunofluorsence. The Leica LASX software package was utilized to delimit regions of interest, defined by the DAPI-visualized nucleus. From these regions, the signal of Alexa488 was computed and normalized per μm^2. These data are the cumulative average of three experiments using independent MSC samples, each with an average of twelve enumerations per high-power field. Statistical test performed was one-way ANOVA, P=0.003.

Chapter 2: Figure 2: AHR nucleotransloaction in MSCs treated with 1MT and AHR agonists

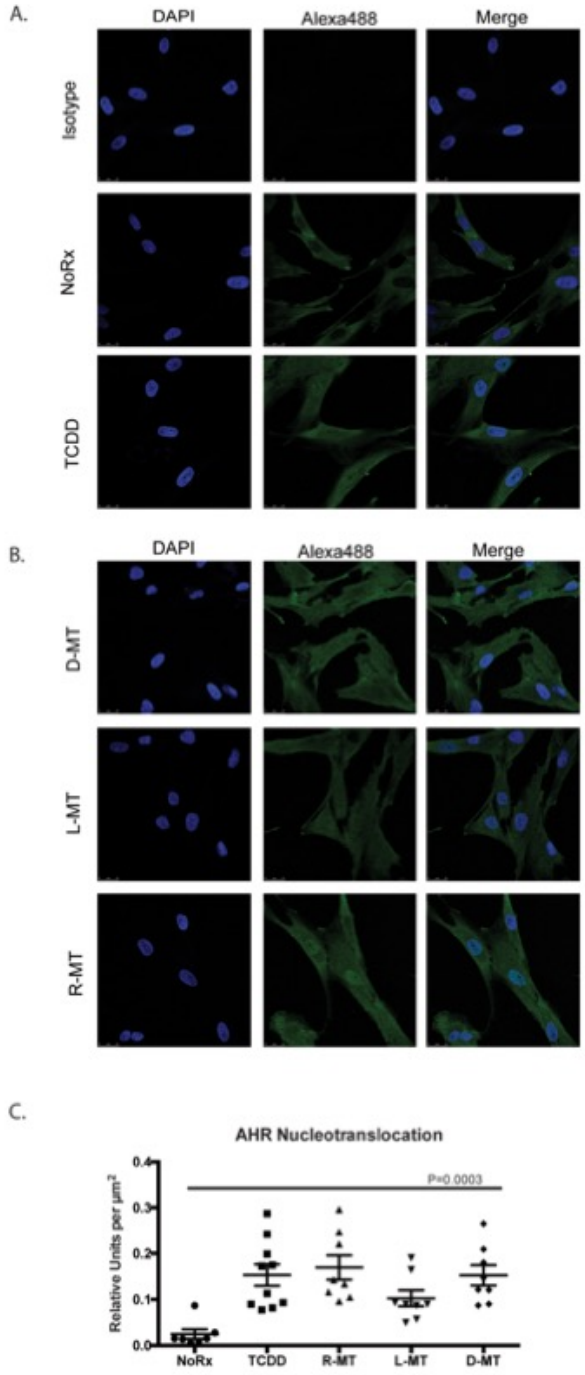

Chapter 2: Figure 3: Known AHR ligands and Trp derivatives activate the AHR response in MSCs

A-D.
MSCs were cultured in the presence of well-characterized AHR-binding ligands or other derivatives of tryptophan. Concentrations used in these fixed-dose studies were FICZ, TCDD: 10nm; Kyn, KynAc: 500 µM, 1MT: 1mM. After 6 or 24h, cells were harvested, lysed and total RNA was extracted, converted to cDNA and analyzed via quantitative real-time PCR. Panels A and C show the relative fold-induction of mRNA for the gene Cytochrome 1a1, calculated using each sample's GAPDH expression, and then normalized to vehicle-treated controls via the delta-delta CT method; panels B and D are the same experiments, plotting Cytochrome 1b1. A one-way ANOVA test was used with Dunnet's correction for multiple comparisons to assess statistical significance between R-MT-treated and untreated cells. These data are the calculated average of four independent experiments using two independent MSC samples.

E.
MSCs were cultured in the presence of racemic 1MT (R-MT), or the pure enantiomer (L)-MT or (D)-MT at varying doses: (0.1 µM to 5000 µM). After 24h, cells were harvested, lysed and total RNA was extracted, converted to cDNA and analyzed via quantitative real-time PCR. Panel E shows the relative fold-induction of mRNA for the gene Cytochrome 1a1, calculated using each sample's GAPDH expression, and then normalized to vehicle-treated controls. Each treatment condition was fitted to a linear regression model, which were then compared by F-test to assess differences in line slope (P=0.009).

Chapter 2: Figure 3: Known AHR ligands and Trp derivatives activate the AHR response in MSCs

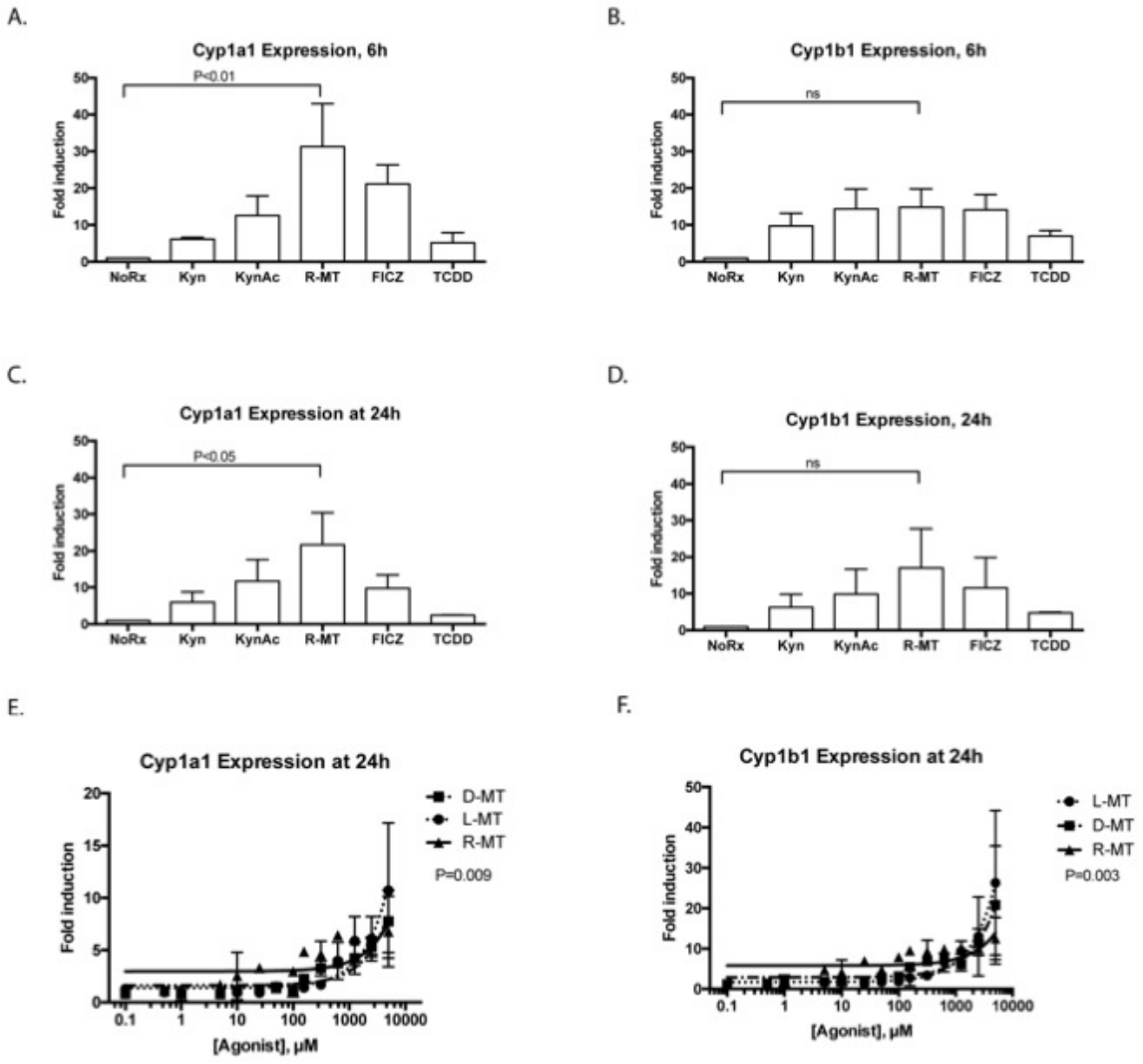

Chapter 2: Figure 4: Interferon-γ licensing of MSCs and AHR response

A.
Resting MSCs (r) and IFN-γ stimulated (γ) MSCs were analyzed for IDO expression after pre-stimulation with a fixed dose of IFN-γ (50 ng/ml), followed by treatment with a fixed 1mM dose of 1MT. Figure represents the immunoblotting results of a single membrane that was first blotted for IDO1, then stripped, re-blocked and probed for actin. Lanes 1-5 represent mono-treated cells. Lanes 6-8 represent 1MT and IFN-γ co-treatment; lanes 9-11 are an IFN-γ pre-stimulation, a PBS wash then 1MT alone. Lanes 12-14 represent a mono-treatment of IFN-γ, followed by 1MT co-treatment. These are results from an experiment with one MSC sample, which was replicated three times.

B, C, D.
MSCs were cultured for 24h in the presence of a variable dose (0.1 μM to 5000μM) of racemic 1MT (R-MT), or the sole enantiomer (L)-MT or (D)-MT. In parallel experiments, MSCs were given 12h of pre-stimulation with IFN-γ, followed by 24h of 1MT treatment, using the same dose-titration curve. After the 1MT treatments, cells were harvested, lysed and total RNA was extracted, converted to cDNA and analyzed via quantitative real-time PCR. Panel B shows the relative fold-induction of mRNA for the gene Cytochrome 1a1, calculated using each sample's GAPDH expression, and then normalized to vehicle-treated controls. Each treatment condition was fitted to a linear regression model, which were then compared by F-test to assess for differences in line slope.

E, F, G.
Panels E, F and G show data from the same experiments as B, C, D, but plot fold-induction of Cytochrome 1b1. As above, each treatment condition was fitted to a linear regression model, which were then compared by F-test to assess for differences in line slope. These six panels are the summary data for nine experiments using two independent MSC samples.

Chapter 2: Figure 4: Interferon-γ licensing of MSCs and AHR

A.

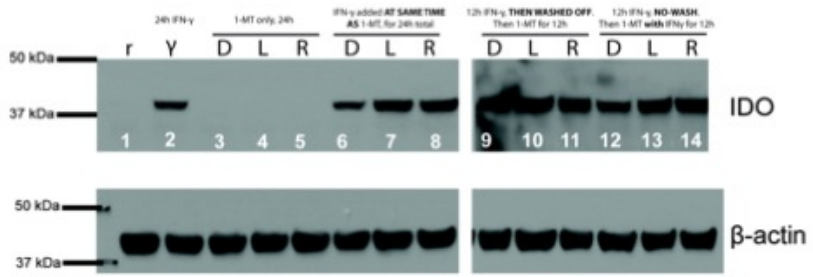

B.

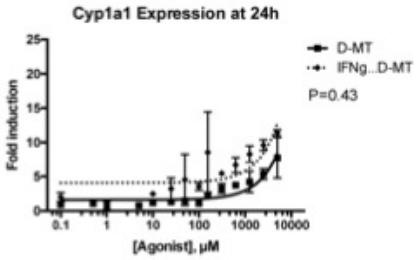

E.

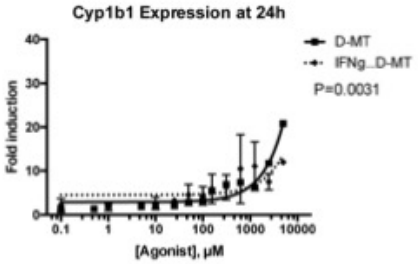

C.

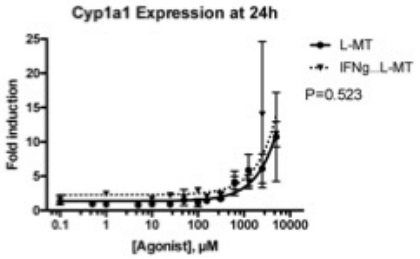

F.

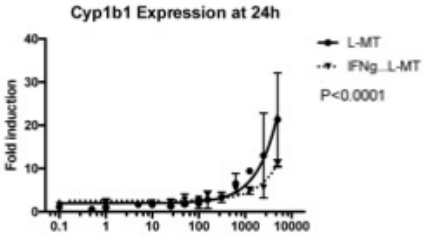

D.

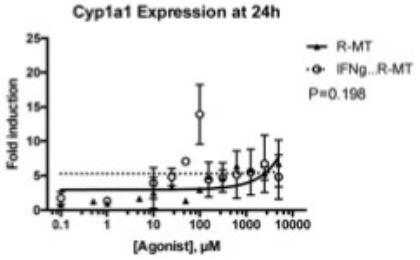

G.

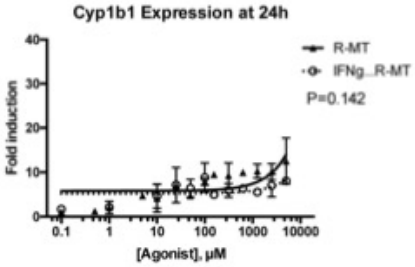

Chapter 2: Figure 5 : RNA-seq analysis of 1MT and TCDD treated MSCs

A.
MSC samples (N=5) were cultured for 24h in vitro in the presence of R-MT (1 mM), TCDD (10 nM), or R10 vehicle (NoRx), and analyzed via mRNA-Seq. Heat map displaying the union of all differentially-expressed genes (DEGs) found between control vehicle treated cells (NoRx) and TCDD treated cells or R-MT treated cells. DEGs were defined as +/-2-fold change and FDR <0.05. Hierarchical clustering was used to organize genes by expression pattern across samples. The color scale shown at bottom is defined as the ratio of each read-count to a gene-centric median, and maximum and minimums defined by a 2-fold upregulation (log2 = +1, red color) or downregulation (log2 = -1, blue color).

B.
Venn diagrams showing degree of overlap of genes found to up-regulated or down-regulated in R-MT treated cells or TCDD treated cells relative to vehicle-treated controls.

C.
Ingenuity Pathway Analysis (IPA) was used to identify sets of functionally-related genes with statistically-significant enrichment in the genes differentially regulated by R-MT. Panel C is a curated list of 24 immunomodulatory pathways from the IPA databases found to be most significantly altered by R-MT, with the bar color indicating if net pathway activation was up, down, or more diversely activated, as determined by IPA Z-scores.

D.
Figure 5D presents a heat map for four of the aforementioned 24 gene sets. To generate this heat map, each MSC sample was normalized to its own untreated control, allowing gene transcripts to be illustrated for up- or down-regulation on a per-MSC sample basis. They were subsequently scaled, whereby a +1.0 is a relative doubling from untreated samples and -1.0 is a relative halving. Patient samples were clustered separately along treatment parameters to compare the TCDD- and R-MT responses side-by-side.

Chapter 2: Figure 5 : RNA-seq analysis of 1MT and TCDD treated MSCs

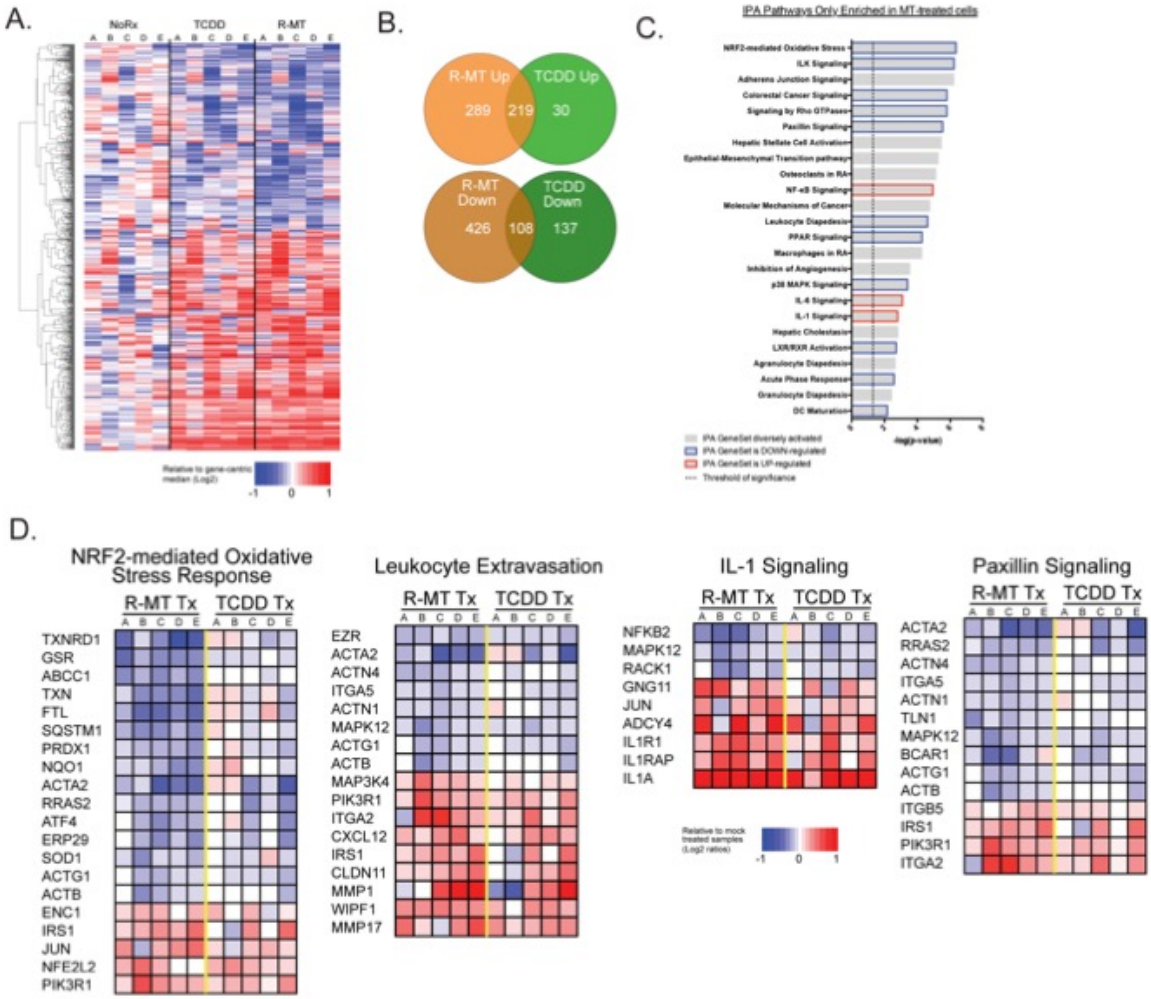

Chapter 2: Figure 6 Supplementary Table 1

(Page 1 of 3)

Differentially Expressed, DOWN-Regulated by BOTH R-MT and TCDD

DE_Up_Both	baseMean	log2FoldChange (DL-MT/NoRx)	pvalue (DL-MT/NoRx)	padj (DL-MT/NoRx)	baseMean	log2FoldChange (TCDD/NoRx)	pvalue (TCDD/NoRx)	padj (TCDD/NoRx)
ABHD11	2197.92	-0.108841	0.000182418	0.015112	1597.82	-0.212796	3.58E-05	0.005810294
ABN	629.158	-0.558899	1.89E-18	1.40E-13	629.158	-0.58088	4.67E-11	2.44E-08
AMM1	9230.32	-0.210435	2.07E-08	3.21E-06	9293.83	-0.17721	1.11E-05	0.002903175
AMMECR1	436.836	-0.28302	5.08E-05	0.003149	436.836	-0.196195	0.006129108	0.069988[illegible]
ATOH8	1297.49	-0.229086	4.21E-05	0.003618179	1297.49	-0.184133	0.008968323	0.084585[illegible]
BDKRB2	63.2095	-0.671174	0.000182113	0.015811	63.2095	-0.538543	0.003364751	0.037587[illegible]
BTG1	927.899	-0.614882	0.000158016	0.014181816	927.899	-0.691727	3.79E-05	0.008309[illegible]
C18orf18	268.566	-0.479444	3.91E-14	1.56E-11	268.566	-0.661691	3.73E-07	0.000[illegible]
C18orf54	1185.28	-0.10544	1.61E-07	1.38E-05	1185.28	-0.139137	8.54E-05	0.013[illegible]
C1orf188	2362.11	-0.614554	1.36E-20	3.86E-15	2362.11	-0.314181	1.33E-05	0.002[illegible]
CANX6L	468.1042	-0.851438	3.88E-07	4.81E-05	449.104	-0.192128	0.008869434	0.080[illegible]
CAV3	15102.3	-0.611078	2.99E-18	1.56E-13	15102.3	-0.191253	3.55E-10	8.10E-08
CDC42EP4	475.368	-0.306431	3.27E-07	3.85E-05	475.368	-0.307503	1.62E-05	0.002[illegible]
CHN1	458.16	-0.210501	2.17E-06	0.000217117	458.16	-0.151126	7.51E-07	0.000[illegible]
CDH13A1	1928.26	-0.668096	1.34E-08	2.87E-06	1928.26	-0.684376	2.41E-07	6.70E-05
CPA4	1586.22	-0.316127	1.89E-08	3.81E-06	1586.22	-0.226829	5.62E-05	0.008[illegible]
CRABP2	6331.78	-0.654795	3.55E-18	6.10E-08	6331.78	-0.429361	3.46E-05	0.005[illegible]
CRYAB	336.39	-0.334546	1.60E-09	2.18E-07	330.95	-0.427092	1.51E-05	0.002[illegible]
CSF1	1871.34	-0.306449	2.41E-18	1.86E-13	1871.34	-0.326488	3.59E-10	1.13E-08
CSPG4	2931.82	-0.610137	8.51E-08	1.38E-06	2931.82	-0.196364	0.008193193	0.0325[illegible]
DKK3	5049.47	-0.378688	8.41E-17	4.48E-12	5049.47	-0.288038	1.51E-10	7.26E-08
DRG1	247.288	-0.317719	0.003072353	0.075[illegible]	247.288	-0.667344	1.27E-10	7.86E-08
DPY5L2	3050.21	-0.177945	5.50E-05	0.003848411	3050.21	-0.153918	0.008129154	0.0347[illegible]
EMP1	932.885	-0.614951	7.87E-14	2.41E-10	932.885	-0.312234	1.17E-05	0.002[illegible]
EPHB4	5168.17	-0.308356	5.16E-10	1.13E-08	5168.17	-0.219726	1.98E-07	5.75E-05
ELL2	2798.75	-0.314523	2.67E-08	4.85E-06	2798.71	-0.206893	0.008244218	0.0269[illegible]
EN01	4799[illegible]	-0.251665	1.17E-08	2.31E-06	47992.9	-0.144126	8.08115775	0.0983[illegible]
ENO2	1936.75	-0.238075	2.48E-05	0.002873314	1936.75	-0.190185	0.008736238	0.0491[illegible]
EPB41	2692.97	-0.608074	1.30E-23	1.31E-20	2692.97	-0.283881	9.36E-06	0.0036[illegible]
ERRFI1	4046.33	-0.42526	2.30E-22	1.81E-18	4046.33	-0.410889	2.94E-20	4.33E-16
FAM129A	277.164	-0.613262	4.86E-18	1.87E-07	271.164	-0.32487	0.008756537	0.0701[illegible]
FBLN2	233.885	-0.68997	2.21E-06	0.000231814	233.885	-0.357192	0.008124307	0.0262[illegible]
FGFR2	481.779	-0.522233	1.61E-12	4.41E-09	481.779	-0.533182	3.57E-12	1.82E-09
FHL1	2975.62	-0.298932	6.77E-07	7.56E-05	2975.62	-0.22184	0.008170196	0.0203[illegible]
FST	706.531	-0.575818	1.01E-22	9.95E-19	706.531	-0.523224	1.31E-10	1.63E-07
GJB2	191.931	-0.710597	2.60E-18	6.81E-08	191.931	-0.421211	0.008147813	0.0178[illegible]
GAS6	3065.02	-0.28082	1.68E-07	2.32E-05	3065.02	-0.170884	0.008993987	0.0082[illegible]
GENT1	1531.99	-0.278614	1.30E-08	2.32E-06	1531.99	-0.257529	1.62E-06	0.000290367
GPR176	1432.07	-0.327513	1.72E-08	3.81E-06	1432.07	-0.228023	0.008149626	0.0173[illegible]
HMGB2	1673.2	-0.273468	0.009114878	0.048[illegible]	1673.2	-0.187731	8.08403337	0.0462[illegible]
HRG1	268.117	-0.657981	5.63E-08	8.32E-06	268.117	-0.326676	0.008622485	0.0198[illegible]
ID1	2080.81	-0.363208	3.95E-07	4.39E-05	2080.81	-0.305035	5.90E-09	2.27E-06
ID3	5583.66	-0.510185	1.46E-15	7.81E-13	5583.66	-0.428018	1.92E-11	1.24E-08
ID4	239.917	-0.454833	1.81E-07	2.27E-05	239.917	-0.414583	1.31E-06	0.000251[illegible]
IGFBP3	409.526	-0.403652	6.51E-05	0.003[illegible]	409.526	-0.368181	0.008121886	0.0295[illegible]
ITGA4	4193.82	-0.278163	8.60E-05	0.004[illegible]	4193.84	-0.186689	0.008503133	0.0499[illegible]
ITGA7	372.909	-0.32358	0.000152545	0.008[illegible]	372.909	-0.342111	6.23E-05	0.0087[illegible]
KCTD10	3366.04	-0.375936	4.42E-08	6.61E-06	3366.04	-0.250086	0.008243095	0.0201[illegible]
KITLG	1476.7	-0.610148	5.05E-24	5.81E-11	1476.7	-0.424784	2.79E-12	1.28E-09
KRT18	835.787	-0.692053	2.42E-20	2.80E-17	835.787	-0.601277	4.55E-09	1.82E-06
LAYN	817.98	-0.303546	1.66E-06	0.000115515	817.98	-0.290871	2.62E-06	0.000362[illegible]
LMCD1	784.498	-0.343451	1.12E-05	0.000920809	784.498	-0.252044	8.08117439	0.0384[illegible]
MAMDC2	59.521	-0.35401	3.20E-06	0.000301814	59.521	-0.370577	2.07E-06	0.000401[illegible]
MAPK13	1090.56	-0.210919	9.50E-05	0.006[illegible]	1090.56	-0.228181	3.92E-05	0.0386[illegible]
MAPK14	808.104	-0.467759	2.57E-18	9.44E-11	808.104	-0.351357	8.09E-09	1.28E-06
MCAM	5367.37	-0.279858	5.25E-12	1.31E-08	5367.37	-0.188019	3.09E-05	0.0017[illegible]
MEST	1950.88	-0.335148	0.004403435	0.020[illegible]	1950.88	-0.335187	0.008230361	0.0230[illegible]
MFAP5	581.636	-0.631776	7.93E-06	0.000381879	581.636	-0.188681	3.59E-05	0.0038[illegible]
MFGE8	447.769	-0.358961	0.003158864	0.018[illegible]	447.769	-0.356161	0.008114303	0.0424[illegible]
MFSD6HL	641.171	-0.378179	7.94E-08	1.10E-05	641.171	-0.258781	0.008116636	0.0240[illegible]
MFRL1	401.2	-0.208112	0.009318918	0.041[illegible]	401.2	-0.298821	0.008242138	0.0359[illegible]
MGAT4	1031.3	-0.614112	3.03E-18	6.86E-08	1031.3	-0.228181	3.53E-06	0.0036[illegible]
MN1	786.914	-0.298502	2.69E-06	0.000261814	786.914	-0.208147	0.008164769	0.0349[illegible]
MPHOSPH6	586.705	-0.316188	2.02E-06	0.000209378	586.705	-0.316884	0.008246850	0.0389[illegible]
MPR1	1190.86	-0.373074	2.86E-06	0.000270518	1190.86	-0.251835	0.008950585	0.0343[illegible]
P2RY2	283.31	-0.413448	1.23E-14	5.38E-12	283.31	-0.276367	6.43E-07	0.000[illegible]
PDE1C	1281.89	-0.695136	1.31E-14	5.37E-12	1281.89	-0.251585	0.008122953	0.0382[illegible]
PEBP4	2137.27	-0.18007	7.41E-18	1.81E-13	2137.27	-0.196781	1.35E-06	0.000297[illegible]
PGF	236.947	-0.449175	1.15E-05	0.000957171	236.947	-0.538722	1.03E-07	4.80E-05
PGK1	12828.2	-0.255039	1.61E-12	4.41E-09	12828.2	-0.141492	0.008162575	0.0153[illegible]
PHGDH	3529.51	-0.352881	3.81E-13	2.20E-12	3529.51	-0.220637	9.30E-07	0.000217[illegible]
PLOD2	258.017	-0.2796	5.30E-05	0.002418[illegible]	258.017	-0.306589	0.008218102	0.0292[illegible]
POSTN	309.909	-0.361248	1.17E-05	0.000960324	309.909	-0.437165	5.42E-07	0.000282[illegible]
PRKD1	695.335	-0.314416	3.40E-07	4.11E-05	695.335	-0.253586	3.96E-05	0.0058[illegible]
PRKAR2B	4687.46	-0.273816	2.30E-12	7.78E-10	4687.46	-0.189576	0.008139081	0.0157[illegible]
PTGFL	5640.49	-0.369906	2.68E-14	1.81E-11	5640.49	-0.181039	0.008243076	0.0208[illegible]
PTPRB	65.3941	-1.01794	3.27E-12	8.46E-09	65.3941	-0.673033	4.92E-05	0.0071[illegible]
PTPRQ	85.7847	-0.48728	0.000801845	0.006[illegible]	85.7847	-0.403899	0.008671283	0.0438[illegible]
PTX3	738.325	-0.916637	1.35E-18	2.85E-08	738.325	-0.526175	0.008136135	0.0394[illegible]
PYGB	3732.08	-0.614788	1.25E-14	5.40E-12	3732.08	-0.217185	3.17E-07	1.78E-05
RANBP3L	1038.59	-0.268923	0.002397162	0.074[illegible]	1038.59	-0.184212	0.008796207	0.0728[illegible]
RALGPS2	1183.05	-0.242236	0.000126708	0.007[illegible]	1183.05	-0.213891	0.008763034	0.0701[illegible]
RCAN1	2424.38	-0.618628	3.12E-22	7.75E-18	2424.38	-0.453095	8.33E-12	5.72E-09
RGS4	1696.29	-0.295718	0.003728679	0.0386[illegible]	1696.29	-0.322287	3.59E-06	5.87E-06
RUNX1	1251.586	-0.625969	7.71E-06	0.000369864	1251.586	-0.593281	8.70E-05	0.0532[illegible]
RND3	1574.39	-0.327644	6.07E-09	1.11E-06	1574.39	-0.252567	7.06E-06	0.0013[illegible]
RP4-555D20.2	679.894	-0.53109	8.50E-12	2.51E-09	679.894	-0.289167	0.008179526	0.0269[illegible]
RXRA	1630.98	-0.227586	0.003167098	0.0[illegible]	1630.98	-0.181257	0.008632789	0.0398[illegible]
SAMD11	535.828	-0.358257	6.41E-05	0.0038[illegible]	535.828	-0.601028	4.52E-06	0.0009[illegible]
SCUBE2	1928.28	-0.495923	2.50E-17	1.44E-14	1928.28	-0.465077	3.69E-10	1.73E-12
SHROOM3	345.396	-0.358126	1.31E-05	0.0010[illegible]	345.396	-0.387479	2.72E-06	0.000955[illegible]
SLIT2	986.579	-0.614757	1.11E-07	1.31E-05	986.579	-0.257927	1.28E-05	0.0031[illegible]
SMOCP1	208.072	-0.608102	6.66E-08	0.000[illegible]	208.072	-0.608187	0.008607628	0.0728[illegible]
SOCS2	51.9776	-0.689519	1.26E-06	0.000[illegible]	51.9776	-0.814914	7.60E-06	0.0014[illegible]
SOX9	1260.94	-0.369557	1.01E-09	3.89E-07	1260.94	-0.243517	3.42E-05	0.0051[illegible]
TBC1D2	1263.89	-0.253637	3.17E-06	0.000287964	1263.89	-0.18782	8.08134675	0.0403[illegible]
THBS1	904.766	-0.236787	0.003195898	0.0[illegible]	904.766	-0.193886	0.008126696	0.0393[illegible]
THBS2	284.004	-0.608883	1.98E-07	2.45E-05	284.004	-0.658681	1.24E-07	4.83E-05
TIMP3	12136.8	-0.277831	8.59E-18	5.31E-13	12136.8	-0.284817	9.35E-11	5.30E-08
TNFAIP3	179.87	-0.695258	5.31E-18	1.36E-07	179.87	-0.343087	0.008449341	0.0701[illegible]
TNFSF10	1270.88	-0.234881	9.66E-06	0.000[illegible]	1270.88	-0.194884	0.008736809	0.0701[illegible]
TNFRSF1B	1029.72	-0.398852	7.56E-05	0.0[illegible]	1029.72	-0.208126963	0.008416963	0.0386[illegible]
TOX	178.163	-0.4824	5.20E-06	0.000465703	178.163	-0.484211	1.13E-05	0.0038[illegible]
TPESL1	155.747	-0.757034	2.01E-13	7.54E-11	155.747	-0.68154	4.05E-10	1.38E-07
TWIST1	338.222	-0.618816	1.71E-05	0.0013[illegible]	338.222	-0.304171	8.83E-05	0.0060[illegible]
VGFAM1	585.19	-0.798438	1.01E-06	1.54E-13	585.19	-0.809166	8.39E-08	2.19E-06
VTG1L	1605.21	-0.12124	0.003238[illegible]	0.0[illegible]	1605.21	-0.126187	8.08197[illegible]	0.0[illegible]
WNT	5253.17	-0.251871	0.004488162	0.0241[illegible]	5253.17	-0.18587	3.98E-05	0.0087[illegible]

Differentially Expressed, UP-Regulated by BOTH R-MT and TCDD

DE_Up_Both	baseMean	log2FoldChange (DL-MT/NoRx)	pvalue (DL-MT/NoRx)	padj (DL-MT/NoRx)	baseMean	log2FoldChange (TCDD/NoRx)	pvalue (TCDD/NoRx)	padj (TCDD/NoRx)
ABL1	4703.77	0.225839	8.20E-07	9.16E-05	4703.77	0.188294	2.88E-05	0.0044[illegible]
AC005740.5	0.635272	13.761	0.001085[illegible]	0.075[illegible]	0.635272	17.4358	4.47E-05	0.0065[illegible]
ADAM10	3438.91	0.227583	0.000156557	0.009[illegible]	3438.91	0.204271	0.0030[illegible]	0.0652[illegible]
ADAM12	14786.1	0.152061	0.002716[illegible]	0.0957[illegible]	14786.1	0.219004	1.58E-05	0.0015[illegible]
ADAMTS1	5627.03	0.202563	4.50E-08	6.72E-06	5627.03	0.248507	1.28E-05	0.0020[illegible]
ADAMTS14	1158.35	1.4473	1.86E-29	3.15E-28	1158.35	1.13592	1.24E-28	1.60E-25
ADAMTS15	106.247	1.38657	6.61E-15	2.97E-12	106.247	1.14859	4.67E-11	2.48E-08
ADAMTS16	159.852	0.414283	0.000205989	0.014[illegible]	159.852	0.559412	8.38E-07	0.0001[illegible]

Figure 6 Supplementary Table 1

A listing of the genes that were identified in the RNAseq analysis for Figure 5 to be differentially expressed upon treatment with R-MT and also by TCDD.

Chapter 2: Figure 6 Supplementary Table 1

(Page 2 of 3)

Differentially Expressed, DOWN-Regulated by BOTH R-MT and TCDD

DE_Up_Both	baseMean	log2FoldChange (DL-MT/NoRx)	pvalue (DL-MT/NoRx)	padj (DL-MT/NoRx)	baseMean	log2FoldChange (TCDD/NoRx)	pvalue (TCDD/NoRx)	padj (TCDD/NoRx)
ABHD11	2197.92	-0.108841	0.000182418	0.015112	1597.82	-0.212796	3.59E-05	0.007810294
ABN	629.164	-0.158899	1.89E-16	1.40E-13	629.164	-0.30388	4.67E-11	2.44E-08
ANKS1	9230.32	-0.210435	2.07E-08	3.21E-06	9293.83	-0.17721	1.11E-05	0.002855775
ANKRD10	416.836	-0.28332	5.08E-05	0.003149	416.836	-0.196195	0.008129108	0.069985
ATOH8	1297.49	-0.229086	4.21E-05	0.003618	1297.49	-0.184133	0.008968322	0.084585
BDKRB2	63.2095	-0.671174	0.000182113	0.015811	63.2095	-0.538543	0.008184751	0.107587
BTG1	927.899	-0.151882	0.000158016	0.014181	927.899	-0.191127	3.79E-05	0.008309916
C10orf10	268.166	-0.479444	3.91E-14	1.56E-11	268.166	-0.161691	3.73E-07	0.000[illegible]
C10orf54	1185.28	-0.10544	1.61E-07	1.38E-05	1185.28	-0.139137	8.54E-05	0.013[illegible]
C1orf188	2362.17	-0.149554	1.36E-09	1.80E-07	2362.17	-0.14181	1.33E-05	0.002[illegible]
CANX1	468.1042	-0.151438	3.68E-07	4.81E-05	449.104	-0.192128	0.008869434	0.080[illegible]
CAV1	15102.3	-0.101178	2.99E-16	1.56E-13	15102.3	-0.101253	1.55E-10	8.10E-08
CDC42EP4	475.368	-0.206431	3.27E-07	3.89E-05	475.368	-0.307503	1.62E-05	0.002[illegible]
CHN1	458.16	-0.210501	2.17E-06	0.000217117	458.16	-0.151126	7.51E-07	0.000[illegible]
COL14A1	1928.26	-0.668096	1.34E-08	2.37E-06	1928.26	-0.804376	2.41E-07	4.70E-05
CPA4	1586.22	-0.316127	1.89E-08	3.01E-06	1586.22	-0.126829	5.62E-05	0.008[illegible]
CRABP2	6331.78	-0.014795	3.55E-16	6.10E-08	6331.78	-0.429161	3.46E-05	0.005[illegible]
CRYAB	336.39	-0.334546	1.60E-09	2.18E-07	330.95	-0.427269	1.51E-05	0.002[illegible]
CSF1	1871.34	-0.306449	2.41E-18	1.86E-15	1871.34	-0.326488	3.59E-13	1.13E-10
CSPG4	2931.82	-0.351137	6.51E-08	1.18E-06	2931.82	-0.196364	0.008193193	0.0325[illegible]
DKK3	5049.47	-0.378688	8.41E-17	4.48E-14	5049.47	-0.288038	1.51E-10	7.26E-08
DRG3	247.288	-0.317719	0.003072353	0.075394	247.288	-0.667344	1.27E-10	7.86E-08
DPYSL2	3050.21	-0.177545	5.59E-05	0.003848	3050.21	-0.153918	0.008129154	0.104[illegible]
EMP1	932.885	-0.614951	7.87E-14	2.41E-12	932.885	-0.312234	1.17E-05	0.002[illegible]
EPHB4	5168.17	-0.303154	1.11E-10	1.11E-08	5168.17	-0.219726	1.98E-07	5.75E-05
ELL2	2798.71	-0.314523	2.67E-08	4.85E-06	2798.71	-0.206893	0.008244218	0.0[illegible]
EN01	47992.9	-0.251695	1.17E-08	2.31E-06	47992.9	-0.144126	8.08115775	0.0[illegible]
ENO2	1936.71	-0.238075	2.48E-05	0.002872314	1936.71	-0.190185	0.008736228	0.0[illegible]
EPB41	2692.97	-0.608074	1.30E-23	1.31E-20	2692.97	-0.283883	9.36E-06	0.00[illegible]
ERRFI1	4046.33	-0.42526	2.30E-22	1.81E-18	4046.33	-0.410889	2.94E-20	4.33E-16
FAM129A	277.164	-0.612262	4.86E-18	1.87E-05	277.164	-0.32487	0.008756537	0.0701[illegible]
FBLN2	233.885	-0.68997	2.21E-06	0.000231814	233.885	-0.337192	0.008124307	0.0[illegible]
FGFR2	483.779	-0.522233	1.41E-12	4.41E-09	483.779	-0.533182	3.57E-12	1.82E-09
FHL1	2975.62	-0.298932	6.77E-07	7.56E-05	2975.62	-0.22184	0.008170196	0.0203[illegible]
FST	706.531	-0.575818	1.01E-22	9.95E-19	706.531	-0.523224	1.31E-10	1.63E-07
GAS1	191.931	-0.751537	2.60E-18	6.81E-06	191.931	-0.421211	0.008147913	0.0[illegible]
GAS6	3065.02	-0.28082	1.68E-07	2.32E-05	3065.02	-0.170884	0.008993987	0.0[illegible]
GENT1	1531.99	-0.278614	1.30E-08	2.32E-06	1531.99	-0.257529	1.62E-06	0.000290367
GPR176	1432.07	-0.327513	1.72E-08	2.81E-06	1432.07	-0.228023	0.008149626	0.0[illegible]
HMGB2	1673.2	-0.273468	0.009114878	0.048956	1673.2	-0.187731	8.08403337	0.0462[illegible]
HRG1	268.117	-0.617981	5.63E-08	8.32E-06	268.117	-0.326676	0.008622485	0.0[illegible]
ID1	2080.81	-0.363208	3.95E-07	4.39E-05	2080.81	-0.305035	5.90E-09	2.27E-06
ID3	5583.66	-0.510185	1.46E-15	7.81E-13	5583.66	-0.428018	1.92E-11	1.24E-08
ID4	239.917	-0.454833	1.81E-07	2.27E-05	239.917	-0.414583	1.31E-05	0.002[illegible]
IGFBP3	409.526	-0.403652	6.51E-05	0.003388	409.526	-0.388181	0.008121886	0.[illegible]
ITGA4	4193.82	-0.178163	8.60E-05	0.004197	4193.84	-0.188489	0.008503133	0.0[illegible]
ITGA7	372.909	-0.32358	0.000152545	0.008129	372.909	-0.342111	6.23E-05	0.008[illegible]
KCTD10	3366.04	-0.375936	4.42E-08	6.61E-06	3366.04	-0.250086	0.008243095	0.0[illegible]
KITLG	1476.7	-0.610148	5.05E-24	5.81E-21	1476.7	-0.424784	2.79E-12	1.28E-09
KRT18	835.787	-0.692053	2.42E-08	2.80E-17	835.787	-0.601277	4.55E-09	1.82E-06
LAYN	617.98	-0.303549	1.66E-06	0.000115515	617.98	-0.290871	2.62E-06	0.000842124
LMCD1	784.698	-0.343451	1.12E-05	0.000920809	784.698	-0.252044	8.08117439	0.0[illegible]
MAMDC2	59.521	-0.35401	3.20E-06	0.000261814	59.521	-0.870577	2.07E-06	0.000401[illegible]
MAPK6	1090.56	-0.210919	9.50E-05	0.006686[illegible]	1090.56	-0.228181	3.92E-05	0.0[illegible]
MAPK10	808.104	-0.467759	2.37E-18	9.44E-11	808.104	-0.351357	8.09E-09	1.28E-06
MCAM	5367.37	-0.279858	5.25E-12	1.31E-08	5367.37	-0.188010	3.09E-05	0.001[illegible]
MEST	1950.88	-0.203148	0.004403435	0.020[illegible]	1950.88	-0.205187	0.008230361	0.02[illegible]
MFAP5	981.636	-0.621776	7.93E-06	0.000[illegible]179	981.636	-0.188681	3.59E-05	0.0[illegible]
MFGE8	417.764	-0.358961	0.003158864	0.0[illegible]4	417.764	-0.356161	0.008114303	0.0[illegible]
MFSD6HL	641.171	-0.378179	7.94E-08	1.10E-05	641.171	-0.258781	0.008116636	0.0[illegible]
MFRL1	401.2	-0.208112	0.009318918	0.0[illegible]877	401.2	-0.298821	0.008242138	0.0[illegible]
MKX1	1031.3	-0.614112	3.03E-18	6.86E-08	1031.3	-0.228181	3.59E-05	0.0[illegible]
MN1	786.914	-0.298502	2.69E-06	0.000261814	786.914	-0.208147	0.008164709	0.0[illegible]
MPRIPA	586.705	-0.316188	2.01E-06	0.000209378	586.705	-0.216884	0.008246850	0.0[illegible]
MPX1	1130.86	-0.373074	2.86E-06	0.000270518	1130.86	-0.251835	0.008969585	0.0[illegible]
P2RY2	283.31	-0.413448	1.23E-14	5.38E-12	283.31	-0.276367	6.43E-07	0.000[illegible]
PDE1C	1281.89	-0.695136	1.31E-14	5.37E-12	1281.89	-0.251585	0.008122953	0.0[illegible]
PEBP4	2137.27	-0.18007	7.41E-16	1.81E-13	2137.27	-0.196781	1.35E-06	0.000297[illegible]
PGF	236.947	-0.449175	1.15E-05	0.000957171	236.947	-0.538722	1.03E-07	4.80E-05
PGK1	12828.2	-0.255039	1.61E-11	4.41E-09	12828.2	-0.141492	0.008162575	0.0[illegible]
PHGDH	3529.51	-0.618881	3.81E-13	2.20E-12	3529.51	-0.220687	9.30E-07	0.000[illegible]
PLOD2	258.017	-0.2796	5.30E-05	0.002418[illegible]	258.017	-0.306589	0.008218102	0.0292[illegible]
POSTN	309.909	-0.361248	1.17E-05	0.000960324	309.909	-0.437165	5.42E-07	0.000[illegible]
PRKD1	695.335	-0.314416	3.40E-07	4.11E-05	695.335	-0.253586	3.96E-05	0.005[illegible]
PRKAR2B	4687.46	-0.273816	2.30E-12	7.78E-10	4687.46	-0.189276	0.008139081	0.0[illegible]
PTGFRN	5640.49	-0.369906	2.68E-14	1.81E-11	5640.49	-0.181039	0.008366376	0.0[illegible]
PTPRB	65.3941	-1.01794	3.27E-12	8.46E-09	65.3941	-0.673033	4.92E-05	0.007[illegible]
PTPRQ	85.7847	-0.48728	0.008001945	0.0[illegible]1081	85.7847	-0.403899	0.008671283	0.0[illegible]
PTX3	738.929	-0.916637	1.35E-18	2.85E-08	738.929	-0.526175	0.008136135	0.0[illegible]
PYGB	3732.08	-0.614788	1.25E-14	5.40E-12	3732.08	-0.217185	3.27E-07	3.76E-05
RANBP3L	1038.59	-0.268923	0.002397162	0.0[illegible]	1038.59	-0.186212	0.008796207	0.0[illegible]
RALGPS2	1183.05	-0.242236	0.000126708	0.00735[illegible]	1183.05	-0.213891	0.008763034	0.0[illegible]
RCAN1	2424.38	-0.618628	3.12E-22	7.75E-18	2424.38	-0.453095	8.33E-12	5.72E-09
RGS4	1696.29	-0.295718	0.003728679	0.0[illegible]128	1696.29	-0.322287	3.59E-05	0.870-06
RUNX1	1251.586	-0.625969	7.71E-06	0.000[illegible]	1251.586	-0.550281	8.70E-05	0.0[illegible]
RND3	1574.39	-0.327644	6.07E-09	1.11E-06	1574.39	-0.252567	7.06E-06	0.001[illegible]
RPA SSSD2.2	679.894	-0.53109	8.50E-12	7.51E-09	679.894	-0.289167	0.008179526	0.0[illegible]
RXRA	1630.98	-0.227586	0.003167098	0.0[illegible]	1630.98	-0.181257	0.008832789	0.0[illegible]
SAMD11	535.828	-0.358257	6.41E-05	0.00[illegible]	535.828	-0.604108	4.52E-06	0.000[illegible]
SCUBE2	1928.28	-0.495923	2.50E-17	1.44E-14	1928.28	-0.465077	3.69E-10	1.73E-07
SHROOM3	345.396	-0.358126	1.31E-05	0.00[illegible]	345.396	-0.387479	2.72E-06	0.000[illegible]
SLIT2	986.579	-0.614757	1.11E-07	1.31E-05	986.579	-0.257927	1.28E-05	0.00[illegible]
SMOCP1	206.072	-0.608182	6.66E-06	0.000[illegible]	206.072	-0.500187	0.008837628	0.0[illegible]
SOCS2	51.9776	-0.689519	1.26E-06	0.000[illegible]	51.9776	-0.814914	7.60E-06	0.00[illegible]
SOX9	1260.94	-0.369557	1.01E-09	1.89E-07	1260.94	-0.243517	3.42E-05	0.005[illegible]
TBC1D2	1263.89	-0.253837	3.17E-06	0.000[illegible]	1263.89	-0.18782	8.08134675	0.0[illegible]
THBS1	904.766	-0.236787	0.003195898	0.0[illegible]	904.766	-0.193886	0.008126086	0.0[illegible]
THBS2	284.004	-0.608883	1.98E-07	2.45E-05	284.004	-0.658681	1.24E-07	4.83E-05
TIMP3	12136.8	-0.277691	8.59E-18	5.31E-15	12136.8	-0.284817	9.35E-11	5.30E-08
TNFAIP3L1	179.87	-0.695258	5.31E-18	1.36E-07	179.87	-0.343087	0.008849341	0.0701[illegible]
TNFSF10	1270.88	-0.234881	9.66E-06	0.000[illegible]	1270.88	-0.194884	0.008736809	0.0701[illegible]
TNFRSF1B	1029.72	-0.398852	7.94E-05	0.00[illegible]	1029.72	-0.208124963	0.008416963	0.0[illegible]
TOX	178.163	-0.4824	5.20E-06	0.000465703	178.163	-0.484211	1.13E-05	0.0[illegible]
TPESL1	155.747	-0.757034	2.01E-13	7.54E-11	155.747	-0.68154	4.05E-10	1.38E-07
TWIST1	338.222	-0.618831	1.71E-05	0.00[illegible]	338.222	-0.304171	8.63E-05	0.0[illegible]
VGFNN1	585.19	-0.798438	1.01E-06	1.54E-13	585.19	-0.809166	8.39E-28	2.19E-16
VTG1L	1805.21	-0.18724	0.003232852	0.0[illegible]	1805.21	-0.126187	8.08197475	0.0[illegible]
WNT	5253.17	-0.251871	0.004488162	0.0[illegible]	5253.17	-0.18587	3.59E-05	0.0[illegible]

Differentially Expressed, UP-Regulated by BOTH R-MT and TCDD

DE_Up_Both	baseMean	log2FoldChange (DL-MT/NoRx)	pvalue (DL-MT/NoRx)	padj (DL-MT/NoRx)	baseMean	log2FoldChange (TCDD/NoRx)	pvalue (TCDD/NoRx)	padj (TCDD/NoRx)
ABL1	4703.77	0.225839	8.20E-07	9.16E-05	4703.77	0.188294	2.88E-05	0.0044[illegible]
AC005740.5	0.635272	13.761	0.001085[illegible]	0.075[illegible]968	0.635272	17.4358	4.47E-05	0.0065[illegible]
ADAM10	3438.91	0.227583	0.000156557	0.0[illegible]852	3438.91	0.204271	0.0[illegible]	0.0[illegible]
ADAM12	14786.1	0.152061	0.002716[illegible]	0.0[illegible]7117	14786.1	0.219004	1.58E-05	0.0[illegible]
ADAMTS1	5627.03	0.202563	4.50E-08	6.72E-06	5627.03	0.248507	1.28E-05	0.0[illegible]
ADAMTS14	1158.35	1.4473	1.86E-29	3.15E-28	1158.35	1.13592	1.24E-28	1.60E-25
ADAMTS15	106.247	1.38657	6.61E-15	2.97E-12	106.247	1.14859	4.67E-11	2.48E-08
ADAMTS16	159.852	0.414283	0.000[illegible]	0.014[illegible]7	159.852	0.559412	8.38E-07	0.00[illegible]

Chapter 2: Figure 6 Supplementary Table 1

(Page 3 of 3)

MEF2A	1056.56	0.514833	4.41E-12	1.34E-08	1056.56	0.385473	2.34E-07	6.58E-05
MKLA2	12717.1	0.235084	4.79E-06	0.00458845	12717.1	0.227452	9.57E-06	0.0038878
MMP14	25624.9	0.203656	8.28E-10	1.71E-07	25624.9	0.188668	1.28E-08	5.09E-06
MMP2	73672	0.206019	1.46E-09	3.01E-07	73672	0.182263	8.83E-08	2.90E-05
MN1	898.696	0.730362	1.49E-27	1.35E-15	898.696	0.772343	4.37E-25	8.89E-22
MPRIP	7501.84	0.184919	1.52E-06	0.00115884	7501.84	0.182629	5.44E-07	0.0001382
MSW01	799.508	0.272853	9.81E-06	0.00853303	799.508	0.217668	0.0004249	0.0434182
MYH10	3016.75	0.236684	1.86E-07	2.61E-05	3016.75	0.155586	0.0006366	0.0617275
NCDH1	380.647	0.367311	2.41E-05	0.0018293	380.647	0.364493	2.75E-05	0.0062438
NCKAP5	102.622	0.818835	1.47E-08	2.49E-06	102.622	0.747574	2.53E-07	6.87E-05
NDN	2221.06	0.409916	9.52E-11	2.37E-08	2221.06	0.298617	3.38E-06	0.000682
NFATC2	99.7468	0.803324	2.50E-08	5.82E-06	99.7468	0.723751	5.22E-07	0.0001355
NFATC4	3124.26	0.411132	2.49E-17	1.44E-14	3124.26	0.289206	3.12E-09	1.49E-06
NGD2	7.68913	1.0846	1.31E-05	0.0010671	7.68913	2.44341	0.0007402	0.0682752
NFTX1	90.1901	1.92723	9.81E-14	2.08E-11	90.1901	1.48581	1.27E-08	5.09E-06
NR2F1	456.207	0.376589	1.13E-06	0.00012285	456.207	0.324553	5.68E-05	0.0080947
NR2F2	1140.77	0.363498	6.72E-10	1.44E-07	1140.77	0.247375	2.83E-05	0.0043555
NRIP	7737.48	0.290414	1.89E-06	0.00020877	7737.48	0.209067	0.0003217	0.0686439
NTM	1562.13	0.441781	1.82E-11	2.94E-08	1562.13	0.255711	9.37E-05	0.0123058
OAS2	129.302	0.865737	2.57E-11	6.97E-09	129.302	0.459826	0.0005537	0.0526209
OLFM2	44.7701	1.10523	3.73E-09	7.04E-07	44.7701	0.782149	0.0006478	0.0624358
OLFML2B	1162.15	1.13544	1.25E-44	4.12E-41	1162.15	0.753721	2.13E-20	3.54E-17
OSBP2	83.0116	0.912854	6.86E-08	8.61E-06	83.0116	0.557356	0.0011725	0.0884967
OSR1	185.863	0.609631	9.45E-09	1.65E-06	185.863	0.620755	3.54E-09	1.50E-06
PADI2	70.0616	1.84368	1.09E-18	8.05E-16	70.0616	1.4423	2.02E-21	6.82E-09
PAFPA	518.741	0.467524	1.13E-06	0.00012523	518.741	0.3317	0.0003225	0.0367748
PALD41	1503.72	0.555043	3.23E-18	2.10E-15	1503.72	0.388425	8.45E-08	2.13E-05
PLA2G4A	267.328	0.681189	1.79E-12	5.62E-10	267.328	0.559803	8.27E-09	3.42E-06
PLAT	1210.6	0.479613	1.54E-24	1.99E-21	1210.6	0.412245	6.18E-10	2.94E-07
PLXNA4	410.331	1.02553	7.36E-30	1.28E-26	410.331	0.787076	5.49E-18	6.11E-15
PMEPA1	1356.54	0.405604	3.54E-12	1.09E-09	1356.54	0.226158	0.000114	0.0142115
POSTN	823.221	0.599687	5.47E-25	5.35E-20	823.221	0.80958	9.99E-24	1.90E-20
PRDM1	67976.8	0.268358	4.82E-08	7.26E-06	67976.8	0.234769	1.27E-05	0.002117
PRDM2	469.223	0.810693	5.80E-24	6.24E-21	469.223	0.782263	2.37E-22	4.05E-19
PTGFRN	1122.32	0.283599	0.000721489	0.0533279	1122.32	0.177103	0.0010872	0.0991164
PTPN13	1858.12	0.332825	7.25E-06	0.00061301	1858.12	0.250103	0.0007578	0.0701969
PYK	1638.17	0.479083	5.71E-16	2.88E-13	1638.17	0.43034	2.63E-13	2.50E-10
RBP1	2286.6	0.370436	7.55E-10	1.60E-07	2286.6	0.259594	1.64E-05	0.0026178
RGS2	605.774	0.875326	2.99E-17	1.23E-14	605.774	0.530794	2.58E-11	1.88E-08
RHOBTB3	3707.54	0.374238	2.97E-21	7.79E-09	3707.54	0.226468	5.59E-05	0.0083932
RP1-102K2.4	9.93115	1.52864	0.00197861	0.0751468	9.93115	1.672	0.0006514	0.0624358
RP11-94A24	66.6528	0.830537	1.25E-09	0.00114872	66.6528	0.770788	8.52E-08	0.001254
RUNX1	1616.17	0.290683	1.87E-08	3.03E-06	1616.17	0.270834	1.78E-07	5.28E-05
S100A3	255.83	0.342581	0.000142389	0.0084986	255.83	0.325605	0.0004582	0.0442381
SECTM1	60.8117	2.99899	2.87E-37	6.18E-34	60.8117	2.12972	1.34E-18	1.59E-15
SERPINA5	1011.02	0.47889	6.44E-10	1.29E-07	1011.02	0.380432	5.24E-07	0.0001358
SERPINB9	8258.33	0.157399	0.000138462	0.00829486	8258.33	0.193674	3.83E-06	0.0007392
SERPINB2	6.25803	2.11237	5.82E-05	0.0039098	6.25803	2.70813	0.0005345	0.0526209
SERPINE2	20337.5	0.131871	0.000342758	0.0418455	20337.5	0.177722	8.28E-06	0.0013185
SERPINF1	1400.59	0.344429	6.32E-24	6.80E-21	1400.59	0.240749	9.57E-09	0.0017491
SHBP4	5012.58	0.326889	2.80E-12	1.05E-10	5012.58	0.312178	3.17E-12	2.46E-09
SHC3	91.2851	0.803516	1.99E-08	3.17E-06	91.2851	0.641448	4.58E-08	1.03E-05
SHISA2	20.5705	1.10472	6.66E-05	0.0044463	20.5705	1.42533	1.16E-05	0.0018754
SIM2	271.853	0.430752	5.30E-06	0.00366413	271.853	0.445318	3.58E-07	0.0001408
SLC12A8	358.13	0.254782	0.001158838	0.0628199	358.13	0.35273	3.37E-05	0.0091091
SLC34A1	1264.78	0.866579	1.56E-17	9.68E-15	1264.78	0.542755	7.68E-07	0.0001839
SLC2A1	5478.8	0.267799	1.80E-07	1.58E-05	5478.8	0.287468	1.07E-08	4.39E-06
SLC2A12	138.1	0.693671	4.24E-07	4.90E-05	138.1	0.456889	0.0009843	0.18468
SLC35F4	307.252	0.498181	1.80E-08	2.95E-06	307.252	0.304574	0.000858	0.062805
SLC4A4	421.688	0.457824	5.11E-06	0.00046317	421.688	0.319071	0.0011684	0.0988852
SLC7A14	128.261	0.8195	4.52E-08	6.72E-06	128.261	0.685755	6.53E-06	0.0012679
SLC8A3	80.9141	1.14102	3.80E-13	1.35E-10	80.9141	0.880588	8.79E-08	2.27E-05
SMIM3	1874.52	0.296681	2.79E-18	1.87E-15	1874.52	0.165506	0.0003026	0.0322436
SNTB1	429.398	0.307427	0.000280627	0.0158561	429.398	0.374283	9.88E-06	0.0018288
SOBP	179.59	0.54545	3.39E-07	4.01E-05	179.59	0.350494	0.0011444	0.0975832
SORCS2	678.975	0.407371	8.52E-10	1.79E-07	678.975	0.296545	8.75E-06	0.0015866
SP581	452.544	0.342188	2.85E-06	0.00028117	452.544	0.295614	5.12E-05	0.0073536
SQLE	1258.1	0.195838	0.001103326	0.0547027	1258.1	0.204951	0.000778	0.0798616
SSH1	3650.28	0.337474	3.28E-09	6.04E-07	3650.28	0.287924	2.73E-07	5.18E-05
SSP5	7929.95	0.244583	5.80E-09	9.53E-07	7929.95	0.196258	2.72E-06	0.0005565
STC2	23265.3	0.59855	3.62E-24	4.46E-21	23265.3	0.630941	1.12E-26	2.62E-23
STN6	228.539	0.484577	4.35E-06	0.00401225	228.539	0.338218	0.0008826	0.0782577
SYN2	3894.68	0.336168	1.61E-10	3.85E-08	3894.68	0.331908	2.72E-10	1.37E-07
TACC1	2338.85	0.335571	6.49E-09	9.04E-08	2338.85	0.235585	0.0001584	0.0189526
TBX3	942.007	0.648086	7.47E-25	7.06E-20	942.007	0.485187	6.94E-14	6.40E-11
TCF7	1004.7	0.646527	1.47E-24	1.98E-21	1004.7	0.448006	1.58E-12	1.27E-09
TENM4	1509.3	0.398927	2.81E-11	6.97E-09	1509.3	0.249266	3.29E-05	0.0058101
TGM2	3251.87	0.346658	1.13E-12	4.60E-11	3251.87	0.227116	1.22E-06	0.000277
TIFAFF	2325.35	1.39068	3.21E-85	5.46E-81	2325.35	1.1921	3.23E-85	1.30E-82
TMEM119	5638.99	0.852947	2.57E-83	1.66E-59	5638.99	0.521983	5.80E-41	5.18E-37
TMEM158	693.876	0.282777	1.76E-06	0.00018226	693.876	0.229775	0.0001068	0.0134157
TRAK1	1333.7	0.238285	5.58E-07	6.52E-05	1333.7	0.18588	9.72E-05	0.0124009
TRIOBP	3793.52	0.214566	1.41E-05	0.00112885	3793.52	0.169674	0.0005987	0.0586767
TTYH3	5463.64	0.298659	2.28E-07	2.67E-05	5463.64	0.245204	2.24E-06	0.0004732
UBASH3B	667.963	0.294929	1.88E-05	0.00090801	667.963	0.300414	7.23E-06	0.0014418
UGCG	1197.34	0.280413	3.34E-06	0.00204835	1197.34	0.287403	1.74E-06	0.0003798
VCAN	23802	0.472671	8.33E-12	1.89E-09	23802	0.328593	1.78E-06	0.0003896
VDR	782.379	0.438436	1.24E-11	3.54E-08	782.379	0.462827	7.06E-13	5.85E-10
VEGFA	9231.41	0.239887	1.83E-09	3.21E-07	9231.41	0.258434	2.01E-09	9.02E-07
WBP11	1357.5	0.288226	2.80E-08	3.18E-06	1357.5	0.250489	1.18E-06	0.000258
WNT5A	4914.26	0.577988	1.20E-25	1.69E-22	4914.26	0.541619	1.68E-22	1.90E-19
WNT5A-AS1	111.563	0.680345	8.30E-05	0.00540471	111.563	0.750158	7.14E-06	0.0013348
WNT7B	802.633	0.66088	4.89E-18	3.22E-15	802.633	0.490503	1.63E-10	8.50E-08
XYLT1	3107.32	0.589386	2.39E-19	1.83E-16	3107.32	0.45484	4.88E-12	3.05E-09
ZBTB21	473.507	0.283054	0.000210744	0.0140857	473.507	0.346416	7.15E-06	0.0013496
ZBTB4	2684.13	0.299511	2.93E-13	7.80E-11	2684.13	0.242814	2.78E-09	1.22E-06
ZFP161	3139.19	0.300878	5.79E-10	2.08E-07	3139.19	0.259277	1.42E-07	4.38E-05
ZFP91	1438.81	0.263515	7.23E-06	0.00061656	1438.81	0.187912	0.0017642	0.0719969
ZFYVE28	139.513	0.831888	3.86E-07	6.28E-05	139.513	0.472558	7.48E-05	0.0188762
ZM221	3968.43	0.159159	0.001133023	0.0546477	3968.43	0.230819	2.14E-05	0.0034441
ZNF423	103.944	0.83852	8.52E-08	1.18E-05	103.944	0.669566	1.72E-05	0.0037268
ZNF503	1143.54	0.378512	9.82E-09	1.67E-06	1143.54	0.330828	2.58E-06	0.0005362

Figure 6 Supplementary Table 1

A listing of the genes that were identified in the RNAseq analysis for Figure 5 to be differentially expressed upon treatment with R-MT and also by TCDD.

Chapter 2: Figure 7 Supplementary Table 2

(Page 1 of 5)

Differentially Expressed, DCMPS Regulated by Only R-MT

DE_Down_DE-MT_Only	baseMean	log2FoldChange (DE-MT/Dmso)	pvalue (DE-MT/Dmso)	padj (DE-MT/Dmso)
AAR1	5210.30	-0.21886	9.17E-09	1.04E-06
ABC1-ADRA0080	46.7987	-0.611511	0.001194802	0.014136
ABCC1	2928.8	-0.267709	8.96E-09	1.14E-06
ABLIM7	2521.03	-0.119763	1.14E-05	0.0013855
ACTA2	18775.2	-0.245619	1.30E-06	0.000128051
ACTA	2750.93	-0.156937	0.000181444	0.015176
ACTG2	27196.2	-0.125369	0.001161012	0.014146
ACTN1	3184.6	-0.121291	0.000783425	0.010111
ACTN4	20816.1	-0.119741	1.13E-05	0.000760214
ADAM12	281.929	-0.110179	0.000951334	0.011124
ADAMTS1	1251.263	-0.198581	0.002587138	0.031167
AHNAK1	8.01.303	-0.449481	1.13E-05	0.000166784
AIP1528	3365.14	-0.203176	0.000114632	0.014147
AKR1A4P26	140.35	-0.414691	0.000734495	0.010875
AKR1C3-AS	10.6918.8	-0.11285	1.87E-05	0.001521121
AKR1D1-17	4503.3	-0.148791	0.002697734	0.047268
AKR1D1-2	1171.24	-0.272668	3.68E-13	8.17E-09
ARHGEF12	6.74.365	-0.247768	0.000461459	0.011511
ARPC1A	3496.11	-0.142018	0.000987082	0.016371
ASNS	4455.42	-0.168958	5.53E-12	1.10E-08
ASPN	1.101.12	-0.115814	0.000116175	0.001511
ASS1	899.394	-0.280361	0.000117534	0.001720291
ATF4	10310.7	-0.214958	0.000116052	0.001716543
ATP2A2	56.19366	-0.513958	0.001278105	0.006847
BCAP31	2121.28	-0.207508	0.000916696	0.0408277
BCAR3	1241.51	-0.168926	0.000441179	0.012132
BOMP81	231.892	-0.406969	2.17E-05	0.001210521
BZW2	3091.97	-0.165142	1.88E-05	0.0053214
BHLHE40	2015.8	-0.214969	0.000200036	0.011481
BIP	551.117	-0.209448	0.001121985	0.0548338
BNIP3	3.536.02	-0.152582	0.002401138	0.0667909
BNIP3L	2894.68	-0.125428	0.001014448	0.0444064
C14orf166	2471.55	-0.150956	0.000691008	0.0314364
C1orf58	11.7928	-1.26097	0.001449957	0.0560881
CABYR-AS1	573.812	-0.298611	0.001154175	0.0525606
CAH9	2101.05	-0.164812	0.000394055	0.0301649
CAK1	1729.48	-0.2869	3.29E-05	0.0014.668
CBLB	3896.496	-0.152677	5.75E-06	0.000514491
CCBE1	3591.8	-0.207953	1.10E-07	1.44E-05
CCDC80	42916.6	-0.273894	1.28E-12	3.61E-09
CDH2-AS1	2012.30	-0.178659	8.13E-05	0.001450614
CGB5	35.7201	-1.39967	0.001171518	0.0517998
CHAC1	1384.72	-0.373428	2.70E-07	3.13E-05
CITED2	2434.97	-0.120116	8.45E-09	1.10E-06
CLTC11	5.34.4816	-0.280988	0.000146214	0.009840.12
CNN3	2317.62	-0.62674	0.002271515	0.062961
COL1A1	9595.93	-0.153237	9.81E-06	0.000776791
COL4A2	5214.96	-0.139928	0.000451176	0.0381881
COTL1	12273.2	-0.18464	4.75E-05	0.001436212
CPM1	2849.2	-0.211961	0.001125644	0.0514978
CRIP2	2761.68	-0.116894	0.002097158	0.0781962
CSRP1	3495.2	-0.172845	1.04E-06	0.000111.6363
CYR61	17918.6	-0.121851	0.000211.6	0.015169
DAAM1	768.898	-0.207863	8.63E-08	1.63E-06
DDIT3	845.408	-0.413612	1.31E-06	0.000111947
DDIT4	1761.21	-0.164988	2.13E-06	0.000136211
DDR1	8.6.982	-0.192693	0.000141171	0.0175.929
DNAJC1	7.6.35.4	-0.232161	0.001114129	0.0111845
DNAJB1-AS2	35.1338	-0.208129	0.000219.553	0.0111563
DNMT3A	9.6.7.56	-0.127454	0.000490618	0.0119988
DOPEY1	287.769	-0.202727	0.001324.84	0.0317361
DPS2	231.284	-0.602984	1.48E-05	3.01E-07
DUPA	296.954	-0.308611	0.001111.7	0.0482585
DUSP1-AS1	3025.95	-0.112535	0.001154.05	0.008.8851
DUSP10P1	638.125	-0.180494	2.74E-05	0.0017.456
DUT-AS	2561.99	-0.176673	0.000287784	0.013385
DUX2	1492.2	-0.125862	0.001125445	0.0175978
DY.211	4011.46	-0.206503	0.000141113	0.0086513
DY.213	3.681.86	-0.128837	0.001251669	0.0067612
DY-AS0P1	2151.87	-0.151125	0.000817512	0.0115647
DYNC1	2556.128	-0.180481	0.000491.124	0.0118.45
DYTYK	2585.67	-0.166665	0.002881515	0.0981.051
DY10	2547.28	-0.189738	0.000119366	0.0112886
DY31	15.6782	-0.750895	4.53E-05	0.001212.551
DY.P28	3556.85	-0.198891	0.000134092	0.0071454
E.T11	2135.57	-0.174756	0.000121422	0.0171613
EAT-1	254.9625	-0.272542	0.001334862	0.0845615
EDN	2539.3	-0.196097	9.36E-06	0.000852.468
EJD-12	634.373	-0.29627	1.78E-06	0.000162979
EMP1	3981.26	-0.148116	5.84E-13	1.11E-07
FAM20A	486.494	-0.230872	0.000204357	0.0046724
FAM210B	867.196	-0.240587	4.90E-05	0.0034.029
FAM43B	391.396	-0.328862	0.001741662	0.065048
FBL	2851.68	-0.2891	2.73E-05	0.0016.862
FGFBP1	2521.92	-0.143361	0.001145918	0.017541
FLNB	11272.2	-0.13717	0.000116414	0.0061885
FLNC	12232.3	-0.282545	3.68E-13	8.17E-09
FNDC1	304.14	-0.618756	2.87E-06	0.000170.18
FTL	55.694.8	-0.26348	1.58E-12	4.41E-09
GAPDH	6387.36	-0.28796	1.10E-06	1.05E-07
GAS2-DT1A	9.7.3.678	-0.185171	4.13E-06	0.000195.55
GAPDH	7.6.773.2	-0.188831	3.55E-06	0.000110861
GBP1	12332.6	-0.221388	6.84E-06	0.000159872
GBAP1	258.552	-0.412726	0.000161348	0.0054.550
GBC1	2527.25	-0.177939	5.34E-08	1.74E-06
GDF15	275.42	-0.183133	0.000634.025	0.0399863
GFRA1	391.338	-0.177.204	1.39E-11	2.12E-08
GLB	136.339	-0.548233	6.25E-06	0.000152563
GOT1	3066.35	-0.10991	5.81E-08	8.13E-06
GPC1	7.5.1.38	-0.154269	2.83E-08	3.12E-06
GPT2	1857.27	-0.29865	1.39E-05	0.0017654
GPX1	3481.67	-0.151341	2.60E-05	0.001487767
GPX4	4.125.28	-0.174477	1.89E-05	0.001450811
GRB10	1857.29	-0.185183	7.14E-05	0.004857.63
GSR	3038.24	-0.305232	5.70E-08	1.05E-06
GTPBP2	2353.64	-0.120986	4.03E-06	0.000179761
HELLS	380.977	-0.277451	0.000660165	0.0314211
HBA71	1483.06	-0.175951	0.000159841	0.0191691
HBB71	731.868	-0.117936	0.000461157	0.0211.612
HCFC2	86.9770	-0.679212	2.16E-05	0.001587.21
HK1	5.396.46	-0.158917	6.88E-06	0.001316.45
HMMT	131.337	-0.188977	4.61E-05	0.001658861
HSPA2	3595.04	-0.121566	1.17E-05	1.15E-05
HSPA5	2487.7	-0.157118	2.83E-05	0.001875.61
HXD	7431.84	-0.185108	9.37E-05	0.0016477.1
IER3	2182.42	-0.168143	0.000511157	0.0268386
IGFBP2	1355.47	-0.171881	0.000214836	0.0161561
IGFBP5	4926.5	-0.231254	2.14E-06	0.000156.65
IL36	232.337	-0.510239	1.10E-07	1.44E-05
INHBA2	356.42	-0.587176	0.000491457	0.018.834
ITGB8	351.37	-0.410341	0.0009498	0.0417261
JAG1	5084.87	-0.132112	0.001135621	0.0517963
JTB45	30798.2	-0.128469	0.000311771	0.0365218
JTB52	2347.28	-0.125621	0.000214157	0.0122728
LBP1	834.896	-0.246442	0.000471648	0.0215145
KCNMA1	2529.57	-0.171788	0.000781755	0.0313459
KIAA0513	385.928	-0.492177	2.63E-05	0.0019541.1

Figure 6 Supplementary Table 2

A listing of the genes that were identified in the RNAseq analysis for Figure 5 to be differentially expressed ONLY upon treatment with R-MT.

Chapter 2: Figure 7 Supplementary Table 2

(Page 2 of 5)

[illegible]	[illegible]	-0.408864	1.17E-06	0.000127572
[illegible]	[illegible]	-0.24628	0.000995163	0.04261832
[illegible]	[illegible]	-0.416184	0.002405916	0.08683344
[illegible]	[illegible]	-0.413817	2.28E-07	2.78E-05
[illegible]	[illegible]	-0.457233	4.57E-05	0.003102863
[illegible]	[illegible]	-0.503237	1.26E-05	0.001692278
[illegible]	[illegible]	-0.113675	0.009134494	0.051193673
[illegible]	[illegible]	-0.117495	0.009151689	0.049905051
[illegible]	[illegible]	-0.110354	0.002831527	0.038118131
[illegible]	[illegible]	-0.109447	1.79E-07	2.19E-05
[illegible]	[illegible]	-0.417598	0.002805927	0.05714344
[illegible]	[illegible]	-0.1741	0.000819402	0.018418914
[illegible]	[illegible]	-0.164898	0.002363184	0.081734[illegible]
[illegible]	[illegible]	-0.203871	1.23E-07	1.51E-05
[illegible]	[illegible]	-0.19861	8.63E-05	0.005410651
[illegible]	[illegible]	-0.145178	0.009471136	0.041725[illegible]
[illegible]	[illegible]	-0.145193	0.009410134	0.0311476
[illegible]	[illegible]	-0.165385	2.54E-05	0.001930845
[illegible]	[illegible]	-0.209176	1.24E-07	1.51E-05
[illegible]	[illegible]	-0.146257	0.001376415	0.0324951
[illegible]	[illegible]	-0.198149	0.000821414	0.0371290
[illegible]	[illegible]	-0.175831	0.009175914	0.0377251
[illegible]	[illegible]	-0.124875	8.23E-05	1.47E-05
[illegible]	[illegible]	-0.186187	0.008151834	0.0390714
[illegible]	[illegible]	-0.129675	4.70E-05	0.003202351
[illegible]	[illegible]	-0.145218	1.18E-13	2.03E-09
[illegible]	[illegible]	-0.107214	0.009165657	0.004575062
[illegible]	[illegible]	-0.183965	0.00185956	0.0372157
[illegible]	[illegible]	-0.198141	0.009118962	0.0373183
[illegible]	[illegible]	-0.126325	0.009146258	0.0368[illegible]741
[illegible]	[illegible]	-0.1611	0.009344111	0.0385
[illegible]	[illegible]	-0.198141	0.009112642	0.0371149
[illegible]	[illegible]	-0.162359	2.18E-13	5.00E-08
[illegible]	[illegible]	-0.164847	1.87E-13	4.45E-08
[illegible]	[illegible]	-0.176125	0.009344426	0.0372578
[illegible]	[illegible]	-0.173386	0.00365367	0.0363121
[illegible]	[illegible]	-0.175215	5.53E-05	0.004180357
[illegible]	[illegible]	-0.157156	0.009878051	0.0393212
[illegible]	[illegible]	-0.157548	0.009171092	0.0372353
[illegible]	[illegible]	-0.110668	0.00385914	0.0454198
[illegible]	[illegible]	-0.180871	4.76E-05	0.003136322
[illegible]	[illegible]	-0.229611	8.23E-05	0.005357843
[illegible]	[illegible]	-0.687134	1.84E-07	2.10E-05
[illegible]	[illegible]	-0.166824	0.009144178	0.0372943
[illegible]	[illegible]	-0.672817	0.002054455	0.0372757
[illegible]	[illegible]	-0.215178	7.39E-08	1.02E-05
[illegible]	[illegible]	-0.317973	0.009144797	0.0396[illegible]639
[illegible]	[illegible]	-0.457878	9.17E-05	0.006602485
[illegible]	[illegible]	-0.154148	0.009145455	0.0398[illegible]222
[illegible]	[illegible]	-0.158461	0.00181177	0.0849929
[illegible]	[illegible]	-0.417581	2.23E-08	4.17E-07
[illegible]	[illegible]	-0.441192	0.009145522	0.0373[illegible]28
[illegible]	[illegible]	-0.29188	0.009495009	0.0344613
[illegible]	[illegible]	-0.220810	7.68E-05	0.005[illegible]885
[illegible]	[illegible]	-0.409284	0.00819955	0.0313[illegible]36
[illegible]	[illegible]	-0.610281	0.009774947	0.0312413
[illegible]	[illegible]	-0.155216	3.69E-12	1.04E-07
[illegible]	[illegible]	-0.157983	1.90E-05	0.001472172
[illegible]	[illegible]	-0.197963	0.00175928	0.0368[illegible]75
[illegible]	[illegible]	-0.219527	0.00147898	0.0368[illegible]574
[illegible]	[illegible]	-0.154575	0.00121711	0.0312[illegible]293
[illegible]	[illegible]	-0.194547	0.00271188	0.0351[illegible]053
[illegible]	[illegible]	-0.328733	1.24E-12	8.92E-06
[illegible]	[illegible]	-0.112953	0.00184364	0.0393[illegible]246
[illegible]	[illegible]	-0.109953	1.13E-05	0.001364413
[illegible]	[illegible]	-0.16368	0.008269561	0.0343[illegible]554
[illegible]	[illegible]	-0.126826	0.009876372	0.0391[illegible]994
[illegible]	[illegible]	-0.210344	0.00141361	0.0351[illegible]781
[illegible]	[illegible]	-0.138176	0.00187407	0.0371[illegible]544
[illegible]	[illegible]	-0.1881	0.009136105	0.0370[illegible]8[illegible]1
[illegible]	[illegible]	-0.174963	0.00247198	0.0385[illegible]763
[illegible]	[illegible]	-0.186697	9.49E-06	0.000[illegible]6[illegible]
[illegible]	[illegible]	-0.178911	0.009124067	0.0372[illegible]964
[illegible]	[illegible]	-0.166726	0.009191509	0.0335[illegible]593
[illegible]	[illegible]	-0.175484	0.00604148	0.0354[illegible]866
[illegible]	[illegible]	-0.141147	0.009[illegible]0[illegible]76	0.0362[illegible]7
[illegible]	[illegible]	-0.217845	4.81E-07	5.11E-05
[illegible]	[illegible]	-0.159142	0.008845[illegible]1	0.0363[illegible]785
[illegible]	[illegible]	-0.178854	0.00141187	0.0387247
[illegible]	[illegible]	-0.146029	0.00301726	0.0441[illegible]982
[illegible]	[illegible]	-0.136663	0.009[illegible]9[illegible]	0.0365[illegible]954
[illegible]	[illegible]	-1.13624	2.23E-08	4.17E-07
[illegible]	[illegible]	-1.61386	0.00174686	0.0380[illegible]968
[illegible]	[illegible]	-0.168912	0.00148178	0.0395[illegible]22
[illegible]	[illegible]	-0.179648	0.009114795	0.0369[illegible]76
[illegible]	[illegible]	-0.101444	0.009117172	0.0371[illegible]997
[illegible]	[illegible]	-0.158918	0.009911267	0.0418[illegible]42
[illegible]	[illegible]	-0.155181	0.009[illegible]7[illegible]	0.0311[illegible]74
[illegible]	[illegible]	-0.149531	0.00119814	0.0365[illegible]33
[illegible]	[illegible]	-0.221836	1.13E-05	-0.000[illegible]0624
[illegible]	[illegible]	-0.189991	0.009415901	0.0311476
[illegible]	[illegible]	-0.208832	0.009114422	0.0371[illegible]67
[illegible]	[illegible]	-0.20522	5.53E-05	0.003417[illegible]78
[illegible]	[illegible]	-0.175445	0.00148868	0.0387954
[illegible]	[illegible]	-0.229487	2.19E-05	0.001[illegible]836
[illegible]	[illegible]	-0.166833	0.008886868	0.0400387
[illegible]	[illegible]	-0.175522	0.009[illegible]8[illegible]02	0.0345968
[illegible]	[illegible]	-0.171984	0.00891644	0.0395[illegible]484
[illegible]	[illegible]	-0.155586	0.00821992	0.0395[illegible]726
[illegible]	[illegible]	-0.195969	0.00181448	0.0444[illegible]08
[illegible]	[illegible]	-0.142668	0.0025156	0.0368[illegible]45
[illegible]	[illegible]	-0.146589	0.00181177	0.0383[illegible]48
[illegible]	[illegible]	-0.188779	0.00171111	0.0375[illegible]96
[illegible]	[illegible]	-0.209149	4.23E-05	0.003[illegible]979
[illegible]	[illegible]	-0.208824	5.83E-05	0.003[illegible]998
[illegible]	[illegible]	-0.16885	0.009490014	0.0342[illegible]5[illegible]
[illegible]	[illegible]	-0.160327	0.00147108	0.0387[illegible]87
[illegible]	[illegible]	-0.186963	0.00249178	0.0388[illegible]29
[illegible]	[illegible]	-0.173863	0.009[illegible]9[illegible]94	0.0345[illegible]5[illegible]
[illegible]	[illegible]	-0.203204	1.50E-05	0.001[illegible]959
[illegible]	[illegible]	-0.177538	0.00871165	0.0381[illegible]79
[illegible]	[illegible]	-0.22721	1.75E-08	0.000[illegible]1[illegible]93
[illegible]	[illegible]	-0.175432	0.00281977	0.0394[illegible]951
[illegible]	[illegible]	-0.209988	0.00841503	0.0316[illegible]83
[illegible]	[illegible]	-0.189909	2.23E-13	5.00E-08
[illegible]	[illegible]	-0.110667	0.009[illegible]8[illegible]09	0.0372[illegible]63
[illegible]	[illegible]	-0.113706	6.68E-05	0.004[illegible]0957
[illegible]	[illegible]	-0.173847	6.63E-05	0.004[illegible]993
[illegible]	[illegible]	-0.151787	0.00128178	0.0382[illegible]945
[illegible]	[illegible]	-0.145588	0.009[illegible]1[illegible]84	0.0368[illegible]847
[illegible]	[illegible]	-0.165138	0.00147105	0.0387[illegible]951
[illegible]	[illegible]	-0.22238	2.89E-08	1.67E-06
[illegible]	[illegible]	-0.195854	0.009[illegible]4[illegible]04	0.0367[illegible]486
[illegible]	[illegible]	-0.181163	0.009[illegible]1[illegible]55	0.0367[illegible]97
[illegible]	[illegible]	-0.208123	1.67E-08	1.17E-06
[illegible]	[illegible]	-0.187518	0.00816171	0.0365[illegible]48
[illegible]	[illegible]	-0.110993	0.00[illegible]0[illegible]09	0.0371[illegible]245
[illegible]	[illegible]	-0.110667	8.89E-05	0.0371[illegible]951
[illegible]	[illegible]	-0.147112	0.00149115	0.0368[illegible]881
[illegible]	[illegible]	-0.11547	0.00161418	0.0316[illegible]54
[illegible]	[illegible]	-0.111764	2.13E-05	0.001[illegible]8[illegible]19
[illegible]	[illegible]	-0.750367	0.009[illegible]4[illegible]02	0.0383[illegible]442
[illegible]	[illegible]	-0.138676	2.13E-08	3.92E-06
[illegible]	[illegible]	-0.101138	0.00121977	0.0384[illegible]60
[illegible]	[illegible]	-0.158838	0.00121192	0.0311[illegible]754
[illegible]	[illegible]	-0.110451	0.00136[illegible]80	0.0491[illegible]87
[illegible]	[illegible]	-0.108257	0.009[illegible]8[illegible]72	0.0317[illegible]986
[illegible]	[illegible]	-0.202736	0.00149172	0.0483[illegible]17
[illegible]	[illegible]	-0.127484	0.009961172	0.0410[illegible]786
[illegible]	[illegible]	-0.101781	6.17E-07	6.97E-05
[illegible]	[illegible]	-0.114852	2.63E-08	0.000[illegible]9[illegible]9
[illegible]	[illegible]	-0.174292	0.009[illegible]8[illegible]78	0.0384[illegible]786

Figure 6 Supplementary Table 2

A listing of the genes that were identified in the RNAseq analysis for Figure 5 to be differentially expressed ONLY upon treatment with R-MT.

Chapter 2: Figure 7 Supplementary Table 2

(Page 3 of 5)

Differentially Expressed, UP-Regulated by Only R-MT

DE_Up_DE-MT_Only	baseMean	log2FoldChange (Ds-MT/NoRx)	pvalue (Ds-MT/NoRx)	padj (Ds-MT/NoRx)
ABCA1	298.1537	0.274424	0.0012614145	0.0917245
ABHD2	3031.06	0.276281	2.15E-05	0.0012292626
ACER3	349.2778	0.243268	0.0023212168	0.0840793
ACSL1	711.3571	0.210845	0.0009147557	0.0541993
ACTB_2	11146.0	1.48827	0.0003471508	0.0115579
ADAMTS1	9524.04	0.148634	0.0008711115	0.0316365
ADAMTS5	296.3571	0.503845	8.90E-05	1.68E-05
ADCY4	5134.004	0.6180333	0.0012864889	0.0719378
ADORA2A	834.2778	0.333826	1.13E-05	1.51E-05
ADURB4	355.7889	0.257842	0.0011171485	0.0364513
AES	267.4278	0.2381	0.0003819128	0.0324328
AIGP1L2	2201.77	0.185736	0.0008664057	0.0313389
AMHR2P1	298.1537	0.2564	0.0011717176	0.0585962
ANGPTL2	855.286	0.204536	0.0008205012	0.0356889.6
ANGPTL4	352.9778	0.513233	1.17E-05	0.0009968586
ANK3	2235.14	0.223841	2.64E-05	1.17E-05
ANKRD17	2281.79	0.283254	0.0012210232	0.0720381
ANKRD35	3138.61	0.767181	0.0018197734	0.0313311
ANTXR1	2865.32	0.136197	0.0012161979	0.0313344
APOD1	2519.078	1.48731	0.0012195057	0.0303668
ARDC1	8455.3	0.148109	0.001138	0.0332299
ARHGAP20	3034.9	0.152863	0.0012114934	0.0295123
ARHGB	731.7556	0.163282	1.15E-05	0.0005108913
ARPP19	2885.23	0.147736	0.0012131152	0.0341614
ARRDC3	1221.23	0.192411	1.13E-05	0.0011401891
BHLHE41	232.5806	0.242953	0.0010810157	0.0711468
BNC1	2595.17	0.218403	8.71E-05	1.13E-05
BTG1	2817.24	0.28711	2.04E-05	1.12E-05
BMP2	2135.12	0.214735	0.0009116187	0.0417517
C1orf151	896.9833	0.508775	2.96E-05	0.0004176793
C1orf73	3.13893	0.689212	0.0017114145	0.0561176
CAV2P26	35.5388	1.26854	6.78E-05	0.0045343
CALU	8.61198	0.131711	0.0002367156	0.0130363
CARD9	1352.22	0.175131	0.0014141153	0.0125851
CACNG7	2512.731	1.87988	0.0008353136	0.0303535
CADPS2	232.2556	0.588615	9.19E-05	0.0039636
CARD18	276.3158	0.257826	5.76E-05	0.0010616
CCND1	5363.133	0.228179	0.0003214411	0.0366159
CD164	5390.82	0.144716	0.0014214303	0.0373653
CD59	1229.5	0.158721	4.93E-05	0.0004304717
CDH13	1267.7	0.218834	0.0012181132	0.0302445
CDH6	361.317	0.169847	1.83E-05	0.0011287
CDK14	916.4667	0.228849	4.14E-05	0.0013505
CDRR2B	712.3538	0.275414	0.0007306158	0.0318126
CDS2	855.3278	0.272592	0.0008903262	0.0321252
CHEB_1	416.3278	0.474803	4.95E-05	0.0004583
CHD7 (1)	635.7944	0.281134	0.0012345555	0.0312864
CLDN11	3.411.57	0.298651	2.43E-05	0.0014349
CLDN23	629.2278	0.189931	0.0012132385	0.0313826
CLDCP	1000.192	0.215168	0.0017151179	0.0373486
CNTN6	795.3886	0.228365	0.0002899536	0.0314517
COL8A1	13849.3	0.228851	2.73E-05	0.0010329
CPEB4	339.3672	0.265541	0.0005189555	0.0352444
CPQ4	1861.87	0.298851	0.0002448592	0.0315941
CPT1C	351.4662	0.223653	0.0012183942	0.0311449
CQ14ORF172	784.75.8	0.25254	0.0005203034	0.0314889
CTNNC2	4763.47	0.298288	3.74E-05	4.34E-05
CUL4B	2461.42	0.221597	2.54E-05	0.0013094
CX3C1L2	3503.63	0.22651	7.19E-05	0.0047586
CYBRD1	2496.06	0.204596	0.0001361517	0.0381988
CYT11	6.13981	1.3117	0.0014118	0.0372968
DABIP	647.25.8	0.25684	0.0005419417	0.0365815
DACH1	2303.29	0.167343	0.0008497152	0.0341832
DCBLD2	5822.18	0.22196	2.29E-05	1.68E-05
DCN	2383.92	0.35710	2.15E-18	5.03E-08
DEPTOR	632.9778	0.641233	0.0003195958	0.0363449
DKK3	2399.25	0.513812	0.0004217174	0.0316811
DNCH24	2351.36	0.18128	0.0014591017	0.0380714
DNJ2	87.41758	0.866305	4.83E-07	5.11E-05
DRP2	360.3444	0.210842	1.85E-06	0.0010513
DSCR5	2081.06	0.253512	0.0002535955	0.0315317
DSP	577.4778	0.28851	0.0003019814	0.0313397
DUSP10	1351.13	0.294651	0.0012411118	0.0313175
EGR1	3031.08	0.273835	1.53E-05	0.0012787
EIF4EP2	3622.79	0.177136	0.0009141152	0.0303836
EPLN2	208.3172	0.289753	0.0006171113	0.0316869
ELP4	286.3357	0.258851	0.0002914	0.0391535
EMB	943.8833	0.189435	1.47E-05	0.118.45
EMP1	871.3511	0.283171	0.0013183034	0.0371128
ENC1	7355.1	0.513892	0.0017193652	0.0320171
EPS8	26.13893	1.23781	6.86E-05	0.0017324
EPHA3	361.3512	0.195892	2.14E-05	0.0017886.7
EPHA5	1.13918	2.1613	2.13E-05	0.0001319967
ETV1	956.4918	0.178841	0.0012171616	0.0363682
FAM107B	326.2294	0.286772	2.44E-05	0.0012174.2
FAM168A	1334.898	0.145821	0.0020293675	0.0349353
FAM203B	485.3622	0.215262	0.0008836161	0.0371884
FAM20A	8114.07	0.141267	0.0012511128	0.0320742
FAM213B	757.168	0.258821	0.0005111152	0.0314423
FBXL5	1686.06	0.21611	0.0008186.5	0.0362459
FGF14	2202.72	0.1164459	0.001435	0.0363742
FHDC1	1044.08	0.257818	0.0008803032	0.0373147
FPR2	125.9556	0.682642	0.0018911837	0.0373739
FLRT2	254.7532	0.486754	1.12E-05	1.02E-05
FLRRP	2322.162	0.168176	0.0007703032	0.0318226
FZD10	896.2772	0.224144	0.0020214.69	0.0734844
FZD6	1054.22	0.134898	0.0001473.82	0.0320441

Chapter 2: Figure 7 Supplementary Table 2

(Page 4 of 5)

Figure 6 Supplementary Table 2

A listing of the genes that were identified in the RNAseq analysis for Figure 5 to be differentially expressed ONLY upon treatment with R-MT.

Chapter 2: Figure 7 Supplementary Table 2

(Page 5 of 5)

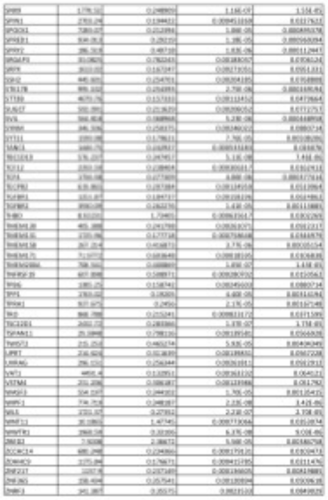

Figure 6 Supplementary Table 2

A listing of the genes that were identified in the RNAseq analysis for Figure 5 to be differentially expressed ONLY upon treatment with R-MT.

Chapter 2: Figure 8 Supplementary Table 3

(Page 1 of 2)

Figure 6 Supplementary Table 3

A listing of the genes that were identified in the RNAseq analysis for Figure 5 to be differentially expressed ONLY upon treatment with TCDD.

Differentially Expressed, DOWN-Regulated by Only TCDD

DE_Down_TCDD_Only	baseMean	log2FoldChange (TCDD/NoRx)	pvalue (TCDD/NoRx)	padj (TCDD/NoRx)
ARSI	839.97	-0.269349	7.73E-05	0.0103953
CABLES1	354.382	-0.266233	0.000722843	0.0680484
COL21A1	21.238	-1.13098	0.000199606	0.0231844
COPRS	1400.07	-0.22993	3.42E-05	0.00513359
DBP	90.5699	-0.590342	7.51E-05	0.0101469
DUSP10	338.437	-0.320009	8.67E-05	0.0114166
EMP1	4235.28	-0.160168	0.000286423	0.0307262
ENPP1	2879.23	-0.232248	9.10E-08	2.97E-05
F2R	1205.32	-0.246765	1.06E-05	0.0018388
FAM180A	147.675	-0.407427	0.000651621	0.0624358
FIBIN	591.462	-0.332667	2.26E-07	6.41E-05
GAS1	151.255	-0.386526	0.000793202	0.0718192
HMOX1	1190.64	-0.191892	0.00115152	0.0978491
IRX3	917.582	-0.25627	0.000276909	0.0299043
LPCAT4	693.752	-0.208964	0.000785808	0.0714753
MCM7	1783.3	-0.193505	0.00117197	0.0984967
MME	346.396	-0.34257	0.000176973	0.0207045
MXRA5	491.159	-0.366878	1.16E-05	0.00197525
NCALD	46.0926	-0.708175	0.000915948	0.080576
PAMR1	876.226	-0.279462	4.11E-06	0.000815035
PCDH18	1015.1	-0.303624	1.83E-05	0.00288177
PFKFB3	1576.22	-0.182764	0.000396437	0.0408976
PLIN2	1487.03	-0.18041	0.000251137	0.0275823
PTGES	752.878	-0.361332	3.80E-06	0.000759239
PTTG1IP	8288.19	-0.122206	0.000487587	0.048895
RP11-61L23.2	0.497737	-24.6307	3.17E-08	1.18E-05
STMN1	2268.52	-0.184102	0.000753939	0.0701576
TMEM106C	639.026	-0.212799	0.000496569	0.0494883
TXNDC17	782.861	-0.220381	0.000918301	0.080576

Differentially Expressed, UP-Regulated by Only TCDD

DE_Up_TCDD_Only	baseMean	log2FoldChange (TCDD/NoRx)	pvalue (TCDD/NoRx)	padj (TCDD/NoRx)
ACKR3	98.6499	0.582509	0.000139749	0.0170283
ALDH3A1	11.421	1.50582	0.00074399	0.0694319
ALPK2	2024.19	0.215206	6.08E-05	0.00845994
CCDC189	6.71161	1.98651	0.000916024	0.080576
COL5A1	88856.2	0.138292	9.43E-05	0.012125

Chapter 2: Figure 8 Supplementary Table 3

(Page 2 of 2)

Figure 6 Supplementary Table 3

A listing of the genes that were identified in the RNAseq analysis for Figure 5 to be differentially expressed ONLY upon treatment with TCDD.

CREBBP	1685.69	0.182581	0.00119225	0.0997348
DHCR7	867.827	0.184757	0.00109138	0.0932294
ECE1	2932.19	0.13111	0.000971136	0.0845228
ERCC6	870.714	0.280867	0.000777822	0.0709616
GPRC5A	228.501	0.460673	1.05E-06	0.000243624
HIPK2	1652.57	0.267114	0.000117332	0.0145717
IER3	2160.39	0.22519	0.000641091	0.0619785
LINC00886	84.9223	0.564159	9.51E-05	0.0121825
LOXL3	2020.68	0.168305	0.000295508	0.0315959
LURAP1L	618.662	0.244792	0.000267279	0.0290587
MLLT1	3035.81	0.182817	6.69E-05	0.00922754
MYADM	5208.3	0.162747	0.000141535	0.0171811
NRXN2	624.658	0.26738	0.00011189	0.0140035
NTN4	563.536	0.330292	7.27E-05	0.0099456
PFKP	7891.61	0.129743	0.000218761	0.0250489
POLR2A	5656.12	0.181195	0.000414926	0.0425332
PPM1H	229.663	0.372097	8.64E-05	0.0114166
PRKCA	3763.64	0.24269	7.86E-05	0.0105281
RP5-1172A22.1	129.704	0.430283	0.000674317	0.0638525
SELPLG	272.996	0.352764	0.000104334	0.0131599
SLC38A5	722.708	0.252375	5.01E-05	0.00721506
SMAD3	3206.32	0.169562	7.45E-05	0.0101135
SULF1	2185.87	0.19608	0.000874714	0.0778821
TENM3	4866.89	0.225699	0.000367324	0.0381379
TRPM2	11.4673	1.38931	0.000978687	0.0849157

Chapter 3: Modeling AHR Ligation In silico

Introduction

A major premise of this MSC-bsed project is that 1MT activates the AHR by functioning as a ligand. We noted that we never demonstrated such directly, with the use of a competitive binding assay. However, we employed an in silico methodology to assess our hypotheses. It is important for us to acknowledge that that 1MT may act via AHR directly or indirect means. We recognize there may exist an indirect middle actor(s) between the AHR response and treatment with 1MT that would confound the drug's status as a true ligand. The authors acknowledge that we did not demonstrate direct ligand-binding to the AHR protein such as using an electromobility shift assay (EMSA) [1]. Such assessments would require radioisotope studies that are not available to our Emory lab. To address the issue of 1MT binding to AHR we instead utilized a computational chemical biology methodology, building from the published reports cited below.

Results

An important issue confronting structural biology of the AHR protein is that its ligand binding domain (the PAS-B domain) has not been solved by x-ray crystallography. However, the research group of Dr. Gary Perdew has used a computational chemical biology approach using another protein, HIF-2α, whose PAS-B domain shares 30% homology with the PAS-B domain of human AHR [2]. In that publication, they utilized PDB code-1p97, which renders an NMR structure for the binding domain of HIF-2α and then

performed hundreds of virtualized ligand screenings, including experimentally-verified AHR ligands, like FICZ and TCDD. They performed molecular docking simulations to compute the ΔG, or change in Gibbs free energy after hypothetical ligation. This approach, using libraries of virtualized ligands to model molecular docking to the AHR protein, has been explored by other research teams as well, who used it to conclude that the access-path to the ligand-binding domain is an important determinant of AHR ligand affinities [3].

In order to provide some theoretical basis for the claim that 1-MT might serve as an AHR ligand, we pursued an analogous strategy to those publications. We utilized the Swiss-Model web server [4] to render the PAS-B domain of human HIF-2α, as was done by the aforementioned papers. We then replaced that sequence with the ligand-binding domain of human AHR (residues 278-390) and threaded these amino acids onto that PDB model. Next, we used the Swiss-Dock platform [5] to perform molecular docking simulations with known and putative AHR ligands, using coded identifiers pulled from the ZINC website [6]. We included the classical ligands TCDD and FICZ, but then also included cinnabarinic acid and kynurenic acid, two novel, endogenous ligands, each of which has been experimentally-validated [7, 8]. Notably, two ZINC codes existed for kynurenic acid, varying on the protonation status of the cyclic nitrogen atom. We chose to model both species independently. We then performed ligand-binding pocket-docking simulations in parallel with the pure enantiomers of 1MT, and recorded the lowest possible value of ΔG (please see chart at top right of this page).

Discussion

These data are solely computational, nonetheless, they support our arguments that 1MT may be acting as an AHR ligand, because the change in free energy falls within the same order of magnitude as other literature-verified ligands. We aknowledge that such studies should be further validated by docking simulations using very large virtualized ligand libraries, as was done in our cited publications.

Chapter 3: Figure 1: In Silico Modeling of AHR Ligation

A. A rendering of D-1-methyl-tryptophan in complex with a simulated x-ray crystal structure of the aryl hydrocarbon receptor.

B. Changes in Gibbs free energy (ΔG) upon simulated ligation with various known and putative AHR ligands.

A.

B.

ZINC Code	Name	Min. ΔG (kcal/mol)
897030	TCDD	-7.43
3871197	FICZ	-6.64
4096852	Cinnabarinic acid	-6.56
8584773	unprot-KynAc	-6.48
19203138	prot-KynAc	-6.45
39101	(L) 1-MT	-6.20
39102	(D) 1-MT	-5.55

Chapter 4: Community Approaches for Diverse Cell Donorship

The culture of blood ex clinico

Sickle cell disease (SCD) is an inherited disorder of red blood cells that is most common in people of color. In the U.S, about one of every 360 African American children is diagnosed with SCD, triggering acute pain crises when sickled cells get trapped in blood vessels throughout the body [1]. Often, these cells block vessels in the brain causing strokes; 50% of pediatric sickle patients have had at least one stroke by the time they turn 18 [2]. Treatment of SCD is largely supportive, including antibiotics and frequent transfusions of donated red cells [3]. Sickle cell is more than twice as prevalent as cystic fibrosis or hemophilia (two genetic diseases common in Caucasians), but suffers from drastically fewer federal dollars for research and clinical care [1]. The only curative therapy for sickle cell disease is a matched hematopoietic stem cell transplant (HSCT). First developed for SCD in 1984, today researchers across the globe are achieving cure rates that approach 90% [4], but these numbers depend strongly upon how well we match the immune systems of the donor and recipient.

As a stem cell therapist seeking to leverage my privileges, I started by reviewing literature to understand the barriers to exploring curative HSCT for SCD. Finding a donor for sickle transplant is challenging, in part because African Americans are underrepresented on the national blood and marrow registries, where the average donor is a college-educated, heterosexual, married white male [3]. There are a number of reasons why African

Americans donate blood and participate in clinical trials at lower rates, including a historically well-founded mistrust of the American medical system [5]. Cell therapy for SCD is at a critical juncture: the science has advanced tremendously, but the bigger, more pressing issue is one of public health outreach. Primary care clinicians, patients and would-be blood cell donors are often unaware that the option for a curative transplant exists, unaware how much we rely on blood cells donated from people of color to effectively treat and cure this disease.

Be-the-Match maintains one of the largest global repositories of stem cell donors, sourced from people asked to provide a small cheek-swabbing at community drive locations, but its demographics reflect a paucity of those with African heritage. A 2013 publication focus-grouped patients in Chicago and Atlanta, seeking to identify community knowledge regarding HSCT availability, and particularly, Be-the-Match donor drives. One participant noted that "*There's a booth set up I think at the state fair for bone marrow but everything around it says cancer or leukemia. I don't see one sickle, no nothing, but it all says cancer."* [2] This scenario is reflective of health disparities observed for people of color with end-stage renal disease (ESRD), on dialysis therapy, awaiting curative kidney transplantation. Dr. Rachel Patzer of the Emory Transplant Center has shown that racially-disparate ESRD outcomes are compounded not only through more time on organ waitlists, but also in the amount of time it takes a primary care clinician to make the initial referrals to even consider transplant [6].

Outreach to the black community for increased donorship must be relevant and participatory to have any efficacy, as basic tenets of social justice admonish against neo-colonial theories of medical pity. The paradigm of misplaced pity is unfortunately persistent in a number of current-day medical outreach programs, particularly those that bring American medical trainees to developing nations for 'service trips.' The lack of participatory reciprocity is a remarkably common issue in such trips, particularly those aimed at the health of marginalized groups or the global South. A 2015 study examined the training and reciprocity practices of medical service trips conducted by 19 American obstetrics/gynecology residency programs. Less than a third of such programs bothered with doing a needs assessment prior to foreign travel, and fewer than 10% trained participants on ethical issues of international medical work [7]. Programs that actively involved local staff during the pre-contemplative phase of trip planning reported higher trainee satisfaction, as well as sustainable growth and training opportunities for in-country staff.

We located one sickle-focused community study that seemed closest to participatory dialogue. In 2002 researchers at Washington University in St. Louis sent a post card, and videotape to 5000 households in the 63115 zip code, presumably chosen for its racial demographics. The videotape featured "a local African American recording artist," who encouraged viewers to donate blood cells in solidarity with the black sickle community. The researchers did note an increase in blood donorship over the first 6 months post-intervention, but this increase was not sustained in subsequent years [8].

Building off these lessons from the literature and the clinic, our team branched out into the Atlanta community, meeting local musicians, artists and politicians who were interested in co-organizing a Be-the-Match community event, centering people of color. The project truly blossomed when we began working with a pair of sickle sisters, one who'd donated marrow to cure the other. Both were impassioned activists, and each had connections to the music and arts scene in Atlanta. Together we organized a music and arts event at two venues in Atlanta's Old Fourth Ward. Sickle warriors spoke from the stage to destigmatize the disease, artists painted sickle-themed graffiti and musicians performed while clinicians, scientists and community activists mingled through intersectional discussions. The cheek-swabbing station was staffed by people of color, all Atlanta-area students, from PhD engineering candidates, to pre-med undergraduates. We all agreed that the persons doing direct-to-community education should be the folks historically marginalized, and contemporarily with most at-stake. In all, the event garnered over a thousand dollars in charity donations for the Sickle Cell Foundation of Georgia, and recruited 31 new stem cell registrants; a huge accomplishment when considering the paucity of black donors on such registries.

Caring for patients with chronic disease requires a multidisciplinary team of clinicians, and in sickle transplant, this team must extend to the African American community writ large. From a sustainability perspective, it is imperative that leadership also reflect the people of color most affected by the sickled cell. To that end, we are working with a team of

undergraduate students at the Atlanta University Center. It is our hope they will build from our template of participatory community outreach, and develop a yearly project. Sickle & Flow hopes that by empowering these communities, we can better translate biological research into meaningful social change that improves lives.

Chapter 4: Figure 1: Translational Stem Cell Therapy

A: Dr. Ned Waller (Emory Hematology/Oncology) and Moji Hassan (Emory Immunology MD/PhD candidate, Sickle & Flow co-director) are featured with Constance Benson, the first person cured of sickle cell by this current protocol. This was her 12-month check-up appointment, at which she exhibited zero clinical signs of graft rejection.

B. Holly Chris Lewis with Constance Benson at the Galipeau lab cell culture facility, discussing mesenchymal stromal cell biology.

C. Moji Hassan at the Waller Lab, teaching Constance Benson how a micropipette is used.

A.

B.

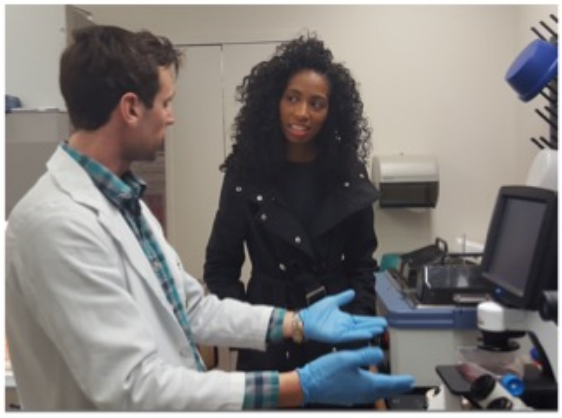

C.

Chapter 4: Figure 2: Sickle & Flow Event June 18, 2016.

A. *Background:* Holly Chris Lewis introduces Georgia State Rep. Park Cannon (D-Atlanta) to deliver the welcome address. Back lot of Peaceful Clouds Smoke Shop, adjacent to Our Lady of Lourdes Catholic Church, Old Fourth Ward, Atlanta.
Midground: Emory immunology PhD Candidate Lisa Mills manages the Be-the-Match cheek swab donation station.
Foreground: Two patients cured of sickle cell by the Emory marrow transplantation teams speak with representatives of the Atlanta Chapter for the National Association for the Advancement of Colored People.

B. Sickle & Flow featured speeches by sickle cell patients, clinicians and scientists, interspersed with live music performances. In this photograph at the Sound Table on Edgewood Avenue, Dr. Margo Rollins (Children's Healthcare of Atlanta, Pediatric Hematology/Oncology, Blood Banking/Transfusion Medicine) addresses the crowd, sharing her personal experiences treating sickle cell patients in Atlanta, emphasizing the importance of stem cell donation.

A.

B.

Chapter 5: Modeling MSC-Based Therapies with Exosomes

Abstract

Introduction: Exosomes from bone marrow (BM)-derived mesenchymal stromal cells (MSCs) support growth of multiple myeloma cells, a plasma cell neoplasm. We recently showed that the secretome of irradiated primary BM-derived MSC maintained survival of human antibody secreting cells (ASC*) ex vivo* (manuscript submitted), but whether exosomes of BM-derived MSCs could also support healthy ASC survival remained elusive.

Methods: Exosomes from irradiated and non-irradiated primary BM-derived MSC were quantified by electron microscopy (EM), CD63 and CD81 immuno-gold staining, and CD9 ELISA. ASC *ex vivo* were cultured with exosomes versus conventional media and IgG ASC Elispots were used to measure survival and function. Finally, contents of the exosome fractions were differentially evaluated by proteomics.

Results: Both irradiated and non-irradiated preparations from BM-derived MSC demonstrated similar quantities of exosomes by EM structural morphology, CD63 and CD81 immuno-gold, and by CD9 staining. Compared to conventional media, which only supported ASC survival and secretion at 7% on day 3, both irradiated and non-irradiated exosome fractions were similar in their ability to support ASC function, 170% and 174% (respectively, day 3). To identify the specific factors that provided *in vitro* ASC support, we compared proteomics of irradiated and non-irradiated exosomes with conventional media. Pathway analysis identified factors involved in the vesicle-mediated delivery of

integrin signaling proteins.

Conclusions: Taken together, these findings indicate that BM-derived MSC exosomes provide an effective support system for ASC survival and immunoglobulin secretion.

Introduction

The interrelationship between bone marrow (BM) mesenchymal stromal cells (MSC) and antibody secreting cells (ASC) has been well-explored in a variety of *in vitro* models, suggesting that MSCs impart various growth factors, cytokines, and chemokines to maintain survival or function of B-derived cells; virtually all such studies have relied upon the use of cancer-derived or otherwise transformed B-lineage cells [1]. The survival mechanisms of the BM microniche are thought to be mediated by local paracrine MSC secretion of IL-6 and VEGF [2-4] as well as adhesion or cell-cell contact [5]. Some of these interactions have been shown to occur via MSC-derived extracellular vesicles, such as exosomes and microvesicles [6]. The ability of MSC-derived exosomes to support the *ex vivo* function of non-transformed peripheral blood-derived ASCs has not been completely described.

MSCs are a low-frequency population in the adult marrow, comprising only one in 10,000 of all mononuclear cells [7-10] that can be isolated in an iliac crest aspirate. Although long-lived plasma cells also take up residence in the BM, they are also quite rare accounting for only 0.05% of all marrow mononuclear cells [11]. Thus, communication between these two such rare BM populations is likely to require cell-cell contact, chemokine gradients,

close paracrine signaling or other cell-contact-independent mechanisms. Recently, the immunomodulatory effects of MSC-based cell therapies rely in part on the release of extracellular vesicles, which may be capable of delivering both soluble and membranous proteins [12, 13]; however, it has been virtually unknown whether marrow communication between the BM MSC and ASC, two relatively rare populations may also occur in a similar manner.

Marrow-derived stromal cells have been shown to provide survival factors in the human BM microniche that support long-lived plasma cell survival [14-17]. Co-culture systems of marrow stromal cells with plasma cells showed that IL-6 and fibronectin (FN1) were two soluble factors needed for effective long-term immunoglobulin secretion [15]. Additionally, IL-6 alone was necessary but not sufficient for antibody production [18]. Subsequent reports have shown contact-dependent signaling, via molecules like CXCL12 and the integrin $\alpha_4\beta_1$ (VLA-4) have also been shown to impart important cues delivered by MSCs, suggesting that cell-cell contact or close proximity may be required in the BM microniche in addition to secreted factors [19-21]. However, our group recently developed a novel in vitro plasma cell survival system that models the BM microniche. It reveals the critical role of the BM-derived MSC in maintaining survival of *ex vivo* ASC for over 60 days in culture (Nguyen D, et al submitted). Most interestingly, cell-cell contact was not required as the MSC secretome, or supernatant, was sufficient to maintain ASC functionality. In pursuit of a reductionist cell-free platform, we sought to address if supernatant-derived extracellular vesicles alone could recapitulate this pheonomena.

Extracellular vesicles are small membranous spheroids that can be released from a variety of cell types. They feature distinctive tetraspanins at their membrane surface (such as CD9, CD63, CD81) and transport cargo over short or long distances, including proteins and RNA. Extracellular vesicles can be secreted from cells as large microvesicles (MVs) (100 to 1000 nm diameter) or as the nano-scale exosomes (30 to 150 nm diameter) [22]. Larger-sized MVs are released from cells as outpouchings of plasma membrane, whereas exosomes have trafficked through the cell's multivesicular body, part of the endosomal sorting complex required for transport (ESCRT), which tags, sorts and matures endosomes with the use of membrane-bound Rab GTPases [23]. A variety of reports have explored MSC-derived exosomes as an avenue for cell-free cell-based therapy, showing therapeutic efficacy in animal models of liver and heart disease [24, 25]. In this study, we demonstrate that MSC-derived exosomes indeed provide a cell-free component to recapitulate the marrow niche and a novel mechanism of communication between hematopoietic stroma and ASC, which thereby enable the *ex vivo* cultures of healthy human plasma cells.

Results

Lipid-disruption of MSC CM abrogates in vitro support to ASCs

Healthy adults were enrolled for BM aspirates and peripheral blood. BM MSC secretomes were prepared from irradiated and non-irradiated BM-derived MSC cultures. In these initial experiments, MSCs were irradiated to arrest the growth of these cells which are typically robustly proliferative. These doses of irradiation do not kill the cells, but rather

preserves their immunomodulatory effects intact [26, 27]; we assessed secreted factors from non-irradiated MSCs in parallel. Antibody secreting cells (ASCs) were FAC sorted (CD19_CD27hiCD38hi) from the peripheral blood of healthy adults and then were cultured in conventional media (RPMI + 10% FCS (R10,), secretomes from MSC cultures, or secretomes pre-treated with the lipid-disrupting agent Cleanascite [28]. Cleanascite is known to not alter protein functionality [29], and we hypothesized this would disrupt the exosome components of the CM. Cells were harvested at days 0, 1, 3, and 7 post-culture and the frequency of IgG-secreting ASCs Elispots were measured. Rapid decline in ASC survival is notable in conventional media compared to the MSC secretome on day 1 (10%). Cleanasite-treated MSC secretomes compared to untreated secretomes decreased survival of ASC from 121% to 51% on day 3 and 82% to 18% by day 7 (P-value 0.02, two-way ANOVA). These results suggested that lipid-membrane bodies (i.e. exosomes) may be an important ASC survival factor.

Electron microscopy shows vesicular size consistent with exosomes

We used electron microscopy (EM), a well-validated methodology to verify the size and morphology of the extracellular vesicles [30]. A phospotungstic acid staining technique was used to stain and visualize a number of exosome preparations from Irradiated and Non-Irradiated MSCs. EM images were counted by trained observers in a blinded, random sequence. Figure 2a,b shows representative whole-field images. Exosome frequencies of 50-100 nm vesicular bodies were higher in rradiated versus non-irradiated MSC exosome factions (p-value 0.0159, Mann-Witney test) (Figure 2c). However, as this preparation

only assessed vesicles based on size, not protein or cargo identity, we sought a more specific method for characterization.

Immunogold electron microscopy confirms exosome markers

We performed immunogold-EM to assess if the vesicles expressed CD63 and CD81, markers known to be found on MSC-derived exosomes [31, 32]. Representative images are shown in Figure 3a,b. The ultrastructure of exosomes were similar in frequency for those derived from Irradiated and Non-Irradiated MSCs. Immunogold-EM is an important tool to assess the presence of known exosome markers, but does not afford a quantitative assessment of exosome yield, as only positively-labeled vesicles are visible in-field.

Irradiation-induced growth arrest does not modify MSC exosome yield

The direct quantification of exosome yield is a challenging; various reports utilize a Bradford or bicinchoninic acid (BCA) assay coupled to spectrophotometric quantification [33-35], but such a technique may be an over-estimate, as it depends on total protein present in the biofluid, rather than exosome-specific protein. To address this, we used the CD9 ExoTest system, which includes professional-grade exosome samples, enabling the generation of a standard curve [36, 37]. The use of CD9 as capture antibody provides an additional checkpoint, as it has been shown to be expressed on the surface of MSC-derived exosomes [38]. Similar CD9-specific exosomes concentrations 200 ng/µL were notable between the irradiated and non-irradiated fractions (p-value 0.84, unpaired t-test) (Figure 4). As this ELISA relies on a specific protein marker for quantification, we

may state with confidence that the irradiation-induced growth arrest did not modify MSC exosome yield.

Exosomes from MSCs support ASC function irrespective of cell growth status

Exosomes derived from either Irradiated or non-Irradiated MSCs were co-cultured with ASC and IgG Elispot assays were performed on day 1, 3 and 7 (Figure 5a,b). Again, we observed rapid drop in ASC survival when the cells were cultured in conventional media, with secreting cells only at 19% at day 1 and 7% by day 3. In contrast, the exosomes derived from non-irradiated MSCs supported ASC function by 194%, 174% and 100% at days 1, 3 and 7, respectively. In a similar fashion, the exosomes from irradiated MSCs were capable of supporting the ASCs at 164%, 170% and 114%, at days 1, 3 and 7. To summarize, we found that exosomes from either cell source were both equally competent in the support of ASC function, when comparing to the vehicle alone (2-way ANOVA, p-value<0.0001).

Exosomes: Proteomics and Ingenuity Pathway Analysis

To identify the protein factors in the exosomes, and how they may mediate ASC survival, we performed proteomic analysis of exosomes, derived from sample-matched pairs of actively-proliferating (No-irrad) or growth-arrested (Irrad) MSCs. As controls, we used vehicle or conventional media (R10). Protein digestion and proteomics were performed with mass spectrophotometry (as described in Methods; complete protein lists are included in Supp. Table 1).Six hundred ninety six and 623 proteins were identified in the

irradiated vs non-irradiated exosome fractions compared to 129 in the controls. Proteins that were uniquely common to both the irradiated and non-irradiated exosome fractions were identified and further analyzed using Ingenuity Pathway Analysis (IPA) (Figure 6A). A curated list featuring five of the most highly-significant pathways associated with the exosome proteomes is presented in Figure 6b (full list may be found in Supp. Table 2). We note significant representation for both caveolar- and clathrin-mediated endocytosis, identified by proteins including clathrin light chain A (CLTA), the coatomer protein complex (COPA), and a number of integrins including the integrin β_1 subunit. IPA also revealed statistically-significant representation for integrin- and integrin-linked kinase signaling, with one important protein identified as cell division control protein 42 (Cdc42). The last pathway we noted to be of significant interest was Phospholipase C (PLC) Signaling, identified by the presence of proteins including the Ras-like proto-oncogenes A and B (RALA, RALB). Taken together, the identification of these proteins and their corresponding pathways suggest that MSC-derived exosomes may be capable of delivering the relevant immune-activing signals to receiver cells such as ASCs.

Discussion

In this study, we demonstrate that exosomes alone in the BM-MSC secretome support and enhance function of human ASC. Irradiation had been initially used to growth-arrest the MSCs, avoiding overgrowth by these robustly-proliferative cells, and we found that irradiation did not alter functional survival-conferring capacity nor differential yields of MSC-derived exosomes. We hypothesized irradiation would modify the secretome of

MSCs relative to replication-competent cells, and that the exosomes derived from these growth-arrested cells might provide differential *in vitro* support to ASCs, but we hereby report that exosomes from either cell source (Irrad or No-Irrad) can be used to support ASCs to equivalent efficacy.

The vesicles generated were subjected to conventional assays including electron microscopy size-validation, and immunogold-EM for markers known to be on MSC-derived exosomes. The quantitative ELISA, coupled to a known exosome surface protein (CD9), provides evidence that these vesicles were indeed exosomes. The therapeutic dosing of exosomes in the cell therapy literature can be challenging to interpret as quantities are often calculated via traditional spectrophotometry, rather than ELISA. One example is a 2013 report from Li *et al*., in which the team used a BCA protein assay to quantify exosomes, noting a therapeutic effect on murine liver inflammation after administration of exosomes at a concentration of 750 ng/µl (but no total dose is provided) [39]. Tomasoni and colleagues in 2013 reported therapeutic effect on renal tissues after dosing mice with exosomes at a concentration of 25 ng/µl, again with no full dose reported [40]. Whereas Li *et al.* used a BCA protein assay, Tomasoni *et al.* used a Bradford protein assay, both of which should be considered as upper bounds of an exosome dose, as ultracentrifugation may carry-over non-exosome proteins. Our exosome preparation contained 200 ng/µl of total CD9-protein, which for a dose of 50 µl, scales to 10 µg of exosomes (pooled from 7 days x 60 ml, or 420 ml of the MSC secretome).

As MSCs and ASCs are both relatively rare populations, we have hypothesized that the release of extracellular vesicles might serve as an intermediary for short- or long-distance signaling. Indeed, our lab has shown that MSCs can take up residence in lung-tissue, whereupon clinical or biologic activity at distant sites can still be observed [41, 42]. These observations led us to hypothesize that exosomes may be a novel model for ASC and MSC interaction.

We note that our proteomic approach was hypothesis-generating in regards to the MSC-derived factors that support ASCs *in vitro*; future analyses may be focused on the mRNA and microRNA carried within the MSC-derived exosome. In analyzing the proteomic and pathway datasets, we sought to model MSC-to-ASC crosstalk, but with the acknowledgment of a one-directional analysis. Agnostic to the transcriptional and translational events occurring within the ASC compartment, our model is best-suited to explore how MSC-derived exosomes may recapitulate the stromal support of the marrow niche. Although known survival factors such as IL-6 and VEGF were not found, either they are not packaged in the exosomes or insensitivity of low abundant proteins may account for their absence. Nonetheless, over 400 candidate proteins in were noted in both irradiated and nonirradiated fractions of exosomes.

Within the exosome proteomes, we note the presence of pathways consistent with vesicular transport and targeted uptake by recipient cells, including the clathrin-mediated and caveolin-mediated signaling pathways. Both of these pathways have been shown to

play a role in the uptake of exosomes by B cell and plasma cells, consistent with exosome-mediated delivery of survival factors derived from stromal cells [43, 44].

The exosomes' proteomic prevalence of integrin and the integrin-linked kinases is an important finding, as these molecules have already been shown as key contact-dependent mechanisms whereby stromal cells support lymphocyte functionality. For instance, the integrin $\alpha_4\beta_1$ has been described as key factor for the experimental generation of long-lived plasma cells [19-21]. Reports show that these cells rely on a combination of soluble and contact-mediated mechanisms to fulfill hematopoietic and immunomodulatory functions [45-47]. Exosomes may help explain these phenomena by parsimony; coated with bioactive integrins, they may be capable of triggering membrane-associated signaling cascades while also delivering soluble protein cargo to target cells. Thus, if integrins, themselves, promote ASC survival or merely deliver packaged survival factors would require further studies.

Plasma membranes, like the surfaces of extracellular vesicles, are composed of a phospholipid bilayer, decorated with a variety of bioactive enzymes, lipids and sugars that enable cellular recognition. Immunlogical cell signaling cascades often begin at the membrane surface, where phospholipid substrates like PIP_2 (Phosphatidylinositol 4,5-bisphosphate) are cleaved by a class of molecules known as the phospholipase C (PLC) family, generating downstream signaling molecules that activate cellular transcription programs for proliferation and differentiation in a variety of cell types, including

lymphocytes [48]. In our proteomic assessment of MSC-derived exosomes, we noted the significance of the PLC signaling pathway, including the presence of the signaling proteins RALA and RALB. These proteins are both guanosine triphosphatases (GTPases) and act in close association with G-protein coupled receptors to transduce signaling events via GTP hydrolysis. RALA and RALB are both important for the proliferation of immune cells as well as membrane trafficking and exocytosis; of particular note, RALA is required to suppress apoptosis [49]. An additional GTPase identified in the MSC-derived exosomes was Cdc42, which activates actin polymerization in target cells, coordinating cell migration, proliferation and survival [50]. Recent reports have shown that Cdc42 to be essential for the activation and function of mature B cells in a mouse model of primary immune deficiency [51]. Again, it is important to stress that these bioinformatic analysis of the MSC-derived exosomes' proteomes would require further studies for validation.

In conclusion, this study shows that exosomes derived from the BM-derived MSC secretome enhance *in vitro* human ASC survival . This mechanisms of the MSC-ASC communication appears to occur in close proximity via local paracrine interactions and over fairly long distances via exosome. Our proteomic analysis suggests that MSC exosome protein cargo contain a number of known molecules related to immune cell proliferation, protein translation, endocytosis and integrin signals. The pathway members identified herein offer possible candidates for short interfering RNA knockdown or antibody-neutralization. Such steps will help narrow the search for key factors that maintain survival of human plasma cells in the long-lived plasma cell niches.

Materials & Methods

Human Subjects

We recruited a total of 14 healthy adults (6 females and 8 males) for either peripheral blood (PBL) samples (n=9) or bone marrow (BM) aspirates (BMA) (N=5) with a mean age of 31 ± 14 years of age. All studies were approved by the Emory University Institutional Review Board Committee. PBL samples were obtained from 9 healthy adult subjects (mean age of 37 ± 13 years old).

MSC isolation and culture

Human MSCs were isolated from bone marrow aspirates collected from the iliac crest of consenting volunteer subjects [52]. Bone marrow aspirates were diluted 1:2 with PBS and layered onto a Ficoll density gradient to isolate mononuclear cells. The cells were centrifuged at 400 × *g* for 20 min and thereafter plated in complete human MSC medium (α-MEM, 10% human platelet lysate (hPL), 100 U/ml penicillin/streptomycin (Corning International, Corning, NY)) at 200,000 cells/cm^2. Non-adherent hematopoietic cells were removed by changing the medium after 3 d of culture at 37 °C in 5% CO_2, and MSCs were allowed to expand for an additional 7 d. Thereafter, the cells were passaged weekly and reseeded at 1000 cells/cm^2; all experiments were performed with MSCs at passage 3 or 4. Although culture-expanded in α-MEM +hPL, all subsequent cultures were performed in M10 (α-MEM with 100 U/ml penicillin/streptomycin, and 10% fetal calf serum) (Corning International, Corning, NY).

Culture medium preparation

MSCs were cultured in a special exosome-depleted culture medium; this medium was α-MEM (+100 U/ml penicillin/streptomycin, and 20% fetal calf serum), or M20. All centrifugations of all liquids in this project occurred with new tubes and caps that had been rinsed twice with 70% ethanol, twice with PBS, and then left to air dry overnight in a biosafety cabinet under constant ultraviolet light exposure. M20 medium was transferred to polyallomer tubes and then spun at 100,000 x G in a Beckman Optima L-80XP Ultra Centrifuge (Brea, CA) at 4˚C for 18h. The pellet, containing serum-derived extracellular vesicles, was discarded, and the supernatant (M20) was extracted using a sterile syringe fitted with a 21G needle. M20 was then mixed 1:1 with sterile serum-free media, to prepare a final mixture of 10% fetal-calf serum α-MEM (M10). This resulting M10 was then passed through a 0.2μM bottle-top vacuum filter system (Corning) and stored at 4˚C until use. All centrifugations occurred at 4˚C unless stated otherwise.

Purification of exosomes from conditioned medium, ELISA

After initial tissue culture expansion as described, MSCs were washed with PBS, trypsinized and resuspended in ice-cold exo-free M10, with some preparations then exposed to a total of 30 Gray irradiation. Cells were then re-plated into new 150 cm^2 tissue culture flasks, at a density of 8.5 x 10^6 cells per flask, and placed into separate tissue incubators. Every 24h, the conditioned medium (CM) from each flask was aspirated and replaced with fresh M10. CM from each irradiation treatment group was pooled into

sterile bottles, collecting together condition-identical CM for seven consecutive days, and stored all week at 4˚C. The pooled CM was transferred into sterile 50 mL polypropylene tubes (Corning) and spun at 300 x G for 10 minutes; the supernatant was collected and then spun again in 50 mL tubes at 2,000 x G for 20 minutes. The resulting supernatant was then transferred to freshly-cleaned polyallomer tubes and spun at 10,000 x G in a Sorvall RC-6 Plus Centrifuge (Waltham, MA). The pellets were discarded, and the supernatant was transferred to freshly-cleaned polyallomer tubes and then spun 100,000 x G in the Beckman Optima L-80XP Ultra Centrifuge for 70 min. We refer to the supernatant resulting from this spin as the Exosome-Depleted CM (Exo-Depl CM), and 500 µl aliquots were taken and stored at -80˚C until used in downstream applications. The pellets from all condition-identical tubes were then washed with sterile PBS, pooled together and spun again at 100,000 x G in the Beckman Optima L-80XP Ultra Centrifuge for 1 hour. The supernatant was aspirated using a sterilized glass Pasteur pipette, with the resulting pellet, which we refer to as Exosomes, resuspended in 600 µL sterile PBS, and stored at -80˚C until use in downstream applications. Our method, which did not use a sucrose gradient, was adapted from other similar publications [30, 53]. Exosomes were quantified using the ExoTest CD9-specific ELISA, which includes reagents for standard curve titration (HansaBioMed, Tallinn, Estonia).

Electron microscopy

Exosome samples were subjected to standard negative-stain electron microscopy. Briefly, a 5 µl of exosome sample was placed on a 400-mesh carbon coated copper grid (Electron

Microscopy Sciences, Hatfield, PA) that was glow discharged for 20 seconds. Exosome samples were allowed to settle on grids for 5 minutes in a covered glass dish. Each grid was then quickly washed on 2 drops deionized water, wicked with filter paper, and then stained with 1% PTA for 20 seconds before wicking dry again with filter paper. Twelve grids were prepared per condition, and imaged by an operator who was blinded to sample-treatments using a JEOL JEM-1400 Transmission Electron Microscope (Tokyo, Japan) equipped with a Gata US1000 CCD camera (Pleasanton, CA). For immungold labeling, primary human-reactive mouse anti-CD63 (Abcam, Cambridge, UK) and mouse anti-CD81 (Santa Cruz Biotechnology, Dallas TX) were used at 10 µg/ml. Colloidal gold (6nm) conjugated goat anti-mouse secondary antibody was diluted in buffer at 1:20.

Peripheral blood mononuclear cell isolation: Briefly, as previously described [54], PBMCs were separated from freshly collected PBL samples by Ficoll-Hypaque (GE Healthcare) or Lymphocyte Separation Medium (LSM; Cellgro/Corning) density-gradient centrifugation where PBS (Ca2+Mg2+free; Cellgro/Corning)-diluted PBL samples (PBL:PBS=1:1) were carefully applied, then centrifuged no brake at 800xg for 20 minutes at RT. The light-weight layer of PBL MNCs (PBMCs) was then gently collected and washed in PBS and RPMI 1640 (with phenol-red and L-Glutamine; Cellgro/Corning). Cells were then washed twice with RPMI 1640 and the resultant unfractionated PBMCs were thereafter manually counted. Cells were then resuspended in MNC medium (MNC-med, or R10), which was made from RPMI 1640 (with phenol-red and L-Glutamine; Cellgro/Corning) completed with 10% heat-inactivated Fetal Bovine Serum (FBS) (Sigma/Atlanta Biologicals) and 1%

Antibiotic-Antimycotic [e.g. 100units/mL penicillin, 100µg/mL streptomycin, and 0.25µg/mL Fungizone (amphotericin B); Thermo Fisher]. T cells and monocytes were magnetically removed by immune magnetic cell selection (magnetic-activated cell sorting; MACS) using conjugated magnetic microbeads targeting T-cell lineage cell surface markers CD3 and CD14 on LS columns and in MACS buffer (Miltenyi), according to the instructions of the manufacturer. The flow-through T-cell depleted PBMC fractions were disaggregated using sterile 35µm filtration (Tube with Cell Strainer Cap; Corning). The negatively selected cellular fractions enriched for B cells and ASC.

Fluorescence-Activated Cell Sorting (FACS). Fresh negatively selected CD3 and CD14 fractions by Miltenyi according to manufacturer's instruction. Initially the cells were blocked with non-specific staining by incubating cells with 5% normal mouse serum (NMS; Jackson ImmunoResearch) in PBS for 10 minutes at RT. Cells were washed and stained with human CD3-PE-Cy5.5, human CD14-PE-Cy5.5 (Life Tech); human CD19-PE-Cy7, human IgD-FITC, human CD27-APC-eFluor780, human CD38-v450, and human CD138-APC (BD Biosciences). After washing, blood ASCs, (CD19+CD27^{hi}CD38^{hi}), were sorted on the FACSAria II sorter (BD Biosciences). The PB populations were generally ~90-95% pure.. Post-sort PBs were cultured immediately.

***In Vitro Cultures for Human Blood ASCs*.** To study ASC survival and IgG-secreting function ex vivo, we used cell-free BM-MSC secretome. Unless otherwise stated, all cultures were performed on 96-well flat-bottom cell culture plates (Nunc/Corning), maintained in ~150-

200uL medium per well, and were set up at 37°C in a humid, 5% CO2 incubator. ASC numbers for each culture well varied (~500 to ~2,036 cells), dependent upon the total post-sort cells from clinical PBL samples. Replicate ASC cultures were maintained without replenishing the BM-MSC secretome or conventional media or vehicle (R10). After days 1, 3, and 6 or 7, each culture harvestedl was washed 4-6 times to remove secreted Ig and ASCs were plated in Elispot wells. Percentage of viable ASCs on day 0, served as 100%.

Cultures with Cleanascite. Cultures of freshly sort-purified blood ASC populations were cultured in the irradiated BM-MSC secretome or treated with cleanascite, a lipid removal reagent and clarification (Biotech Support Group), according to the manufacturer's recommendations. BM-MSC secretome and conventional media (R10) were used as positive and negative controls.

IgG ELISpot Assay. Briefly, Elispot assays were performed as previously described for total igG [54]. Briefly, pre-wetted membrane, MultiScreen flat-bottom 96-well ELISpot plates (Millipore) were coated overnight at 4°C with goat anti-human IgG capture Ab (5µg/mL) or with 2mg/ml BSA (2% in PBS). To prevent non-specific binding, plates were then blocked with RPMI 1640 supplemented with 8% FBS for 2 hrs at 37°C. Subsequently, plates were loaded with cultured blood ASCs and were incubated in ~150-200uL media for ~16-18 hours at 37°C in the air incubator (5% CO2). Then cells were removed and the plates were washed six times with washing buffer using Microplate Washer (Biotek). Secondary goat anti-human IgG alkaline phosphatase-conjugated Ab (1µg/mL, diluted in

PBST+2%BSA), which was incubated for ~2 hrs at RT. Spots were developed and visualized with an enzymatic color reaction using ABC-AP Vector Blue Substrate reagents (Vector Laboratories). Plates were counted on the ELISpot reader (Cellular Technology Limited; CTL) using the ImmunoSpot 5.0.9.21 software.

Exosome Lysis and Protein Digestion

Exosome pellets were lysed through end-to-end rotation at 4 ºC for 45 minutes in RIPA buffer. The supernatant was transferred to new tubes. Proteins were reduced with 5 mM dithiothreitol (DTT) (56 ºC, 30 minutes) and alkylated with 14 mM iodoacetamide (RT, 15 minutes in the dark). Detergent was removed by the methanol-chloroform protein precipitation method. Purified proteins were digested with 10 ng/µL Lys-C (Wako) in 50 mM HEPES pH 8.6, 1.6 M urea, 5% ACN at 31 ºC for 16 hours, then with 8 ng/uL Trypsin (Promega) at 37 ºC for 4 hours.

Peptide Purification and LC-MS/MS Analysis

Protein digestions were quenched by addition of trifluoroacetic acid (TFA) to a final concentration of 0.1%, followed by centrifugation to remove the precipitate. The peptides were desalted using a tC18 Sep-Pak cartridge (Waters) and lyophilized and subjected to LC-MS/MS analysis. Peptides were detected with a data-dependent Top20 method [55] in a hybrid dual-cell quadrupole linear ion trap - Orbitrap mass spectrometer (LTQ Orbitrap Elite, ThermoFisher, with Xcalibur 3.0.63 software). One full MS scan (resolution: 60,000) was performed in the Orbitrap at 10E6 AGC target for each cycle, and up to 20

MS/MS in the LTQ for the most intense ions were recorded. These sequenced ions were excluded from further analysis for 90 seconds. Precursor ions were required to have at least two charges for analysis. Maximum ion accumulation duration was 1000 ms for each full MS scan and 50 ms for MS/MS scans. All MS^2 spectra were searched using the SEQUEST algorithm (version 28) [56]. Spectra were matched against a database containing sequences of all proteins in the UniProt Human (Homo sapiens) database. We used the following parameters for database searching: 20 ppm precursor mass tolerance; fully digested with trypsin; up to three missed cleavages; fixed modification: carbamidomethylation of cysteine (+57.0214); variable modifications: oxidation of methionine (+15.9949). False discovery rates (FDRs) of peptide and protein identifications were evaluated and controlled to less than 1% by the target-decoy method [57] through linear discriminant analysis (LDA). [58] Peptides fewer than seven amino acid residues in length were deleted. We also applied a filter at the protein level to ensure the protein FDR is less than 1%.

Bioinformatics

Protein digestion, proteomic analysis and thresholding were performed as described in Methods, and complete protein lists were generated with the Partek Genomics Suite software (Partek Inc., St Louis, MO, USA). Full protein lists may be found in Supplemental Table 1. As we have observed ASCs to quickly die when grown in vehicle alone, we hypothesized the additive presence of factors might provide a better model for ASC survival (rather than the absence of apoptotic factors). In preparing the input dataset for

pathway analysis, we included proteins that were differentially expressed in exosomes when compared to the vehicle-alone condition, and with a minimum value of 2 total hits per sample. Relative abundance was computed as the ratio of the number of hits of a given protein divided by the total number of hits in that sample. Supplementary Table 1 presents these calculations and the paired datasets that were used as input for Ingenuity Pathway Analysis (IPA) software (QIAGEN, Hilden, Germany). Non-irrad-MSC exosomes afforded 410 such proteins; Irrad-MSC exosomes afforded a list of 460. A standard IPA core analysis was performed using canonical pathways, and full results may be found in Supplementary Table 2. IPA considers the presence of proteins and computes a p-value that connotes the likelihood that a pre-defined molecular biology pathway has been activated. Within this software package, a statistically-significant p-value of 0.05 is equivalent to a –log(p-value) = 1.35.

Statistics

Graphical data for the project was analyzed using GraphPad Prism version 6.0. For Figure 2A, an unpaired t-test was performed. For Figure 2, microscopy staff were blinded to treatment status of preparations; after image collection, two lab technicians were trained on how to identify vesicular bodies in the digital image files, again in a treatment-blinded fashion, using a mouse cursor scaled 50 to 100 nm. HPFs from twelve grids were thusly enumerated. Due to the counted, integer-based nature of these data, a Mann-Whitney test was used to assess significance. Figures 1 and 7 were analyzed via two- way ANOVA; a t-test was used for Figure 4.

Chapter 5: Figure 1: MSC CM maintains in vitro ASC survival, but is abrogated by lipid-disruption

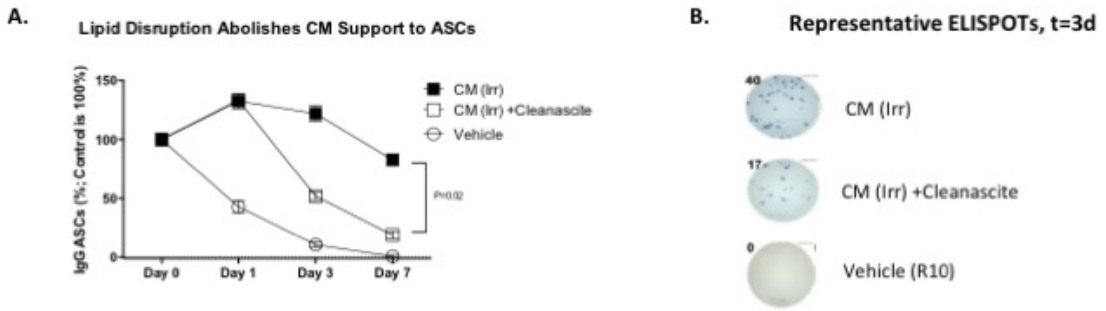

A. Healthy, freshly-sorted blood ASCs were cultured in RPMI + 10 %FCS (R10, or Vehicle), Conditioned medium (CM) from MSC cultures, or MSC CM that had been pre-treated with the lipid disrupting agent Cleanascite. Each condition was set with the same ASC input cell number (approx. 2,000). Cells were harvested at days 0, 1, 3, and 7 post-culture and the frequency of IgG-secreting ASCs were measured by ELISPOT and normalized to Day 0 (100%). A repeated-measures one-way ANOVA afforded a P-value of 0.02,indicating that the lipid disruption statistically abrogated the *in vitro* support to ASCs.

B. Representative photomicrographs of the wells from ELISPOT experiments in panel A.

Chapter 5: Figure 2. Electron microscopy shows CM from irradiated MSCs contains a greater number of exosome-sized extracellular vesicles

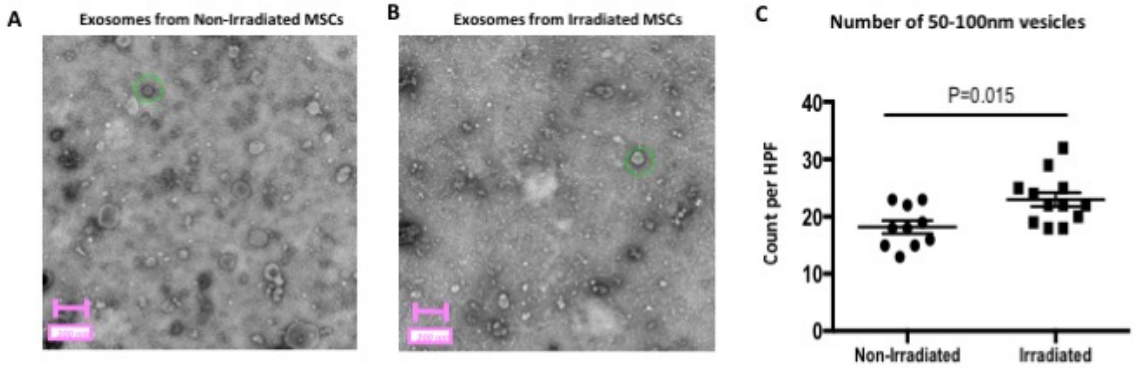

A-B. Negative-staining electron microscopy was performed on exosomal fractions isolated from Irradiated or Non-Irradiated MSCs. Imaging was performed using uranyl-oxalate negative staining and observed using a JEOL Transmission electron microscope. Twelve grids were prepared and imaged by a trained microscopist who was blinded to the samples' radiation-treatment-status. Scale bar indicates 200 nm. Exosomes are 50 to 100 nm in size, and two such putative vesicles are indicated by green dashed lines.

C. Two technicians were trained on what 50-100nm vesicles should look like via electron microscopy, and blinded to radiation-treatment status. They enumerated the number of 50-100nm vesicles that could be appreciated on all twelve of the TEM grids, which were shown to the observer in a randomized sequence. A Mann-Whitney test (employed due to the counted nature of integer-based data) afforded a test statistic of 0.015.

Chapter 5: Figure 3. Immuno-gold electron microscopy confirms presence of known MSC-derived exosome markers

A. CD63 Immunogold

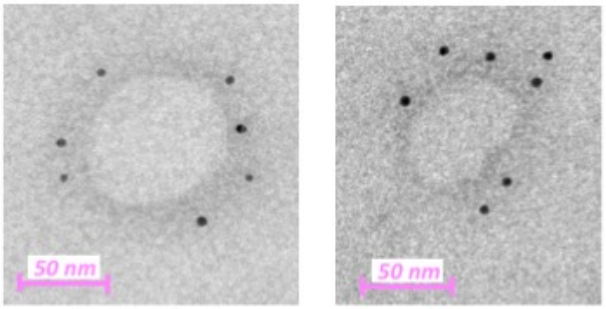

Non-Irradiated Irradiated

B. CD81 Immunogold

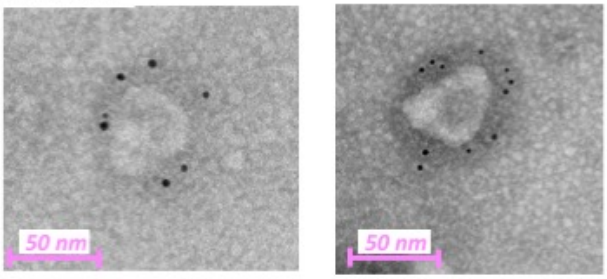

Non-Irradiated Irradiated

A-B.
Immunogold-labeling electron microscopy was utilized to confirm if the 50-100nm vesicles could justifiably be referred to as exosomes. Commercial antibodies for CD63 and CD81 were acquired and conjugated to colloidal gold by trained electron microscopists; both these molecules are known to be present on MSC-derived exosomes. The scale bar indicates 50 nm. As only positively-marked vesicles can be visualized using the immunogold technique, we demur in quantifying the number or proportion of vesicles thusly stained, apart from noting that the ultrastructure of exosomes appeared comparable for those derived from non-irradiated and irradiated MSCs. These micrographs are representative of over two dozen such images, using exosomes derived from three independent patient donors.

Chapter 5: Figure 4. Highly-specific ELISA shows that Irradiated and Non-irradiated MSCs release the same quantity of CD9-positive exosomes

A.

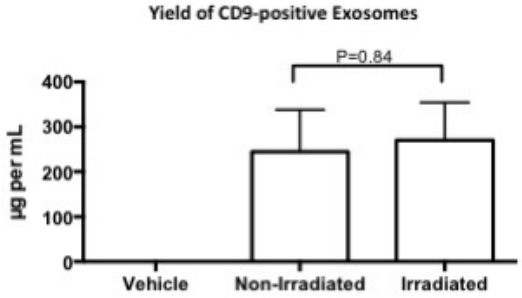

A. Exosomes were collected and isolated using the flowchart in panel A. We obtained an exosome-customized ELISA kit utilizing CD9, a surface protein marker known to be present on MSC-derived exosomes. It uses conventional sandwich ELISA technology, with human CD9 as the capture antibody, and also includes professional-grade exosome standards for the generation of an exact standard curve. Panel B shows the results of this ELISA result, comparing the results of three independent experiments using independent MSC patient donors, each replicated twice. An unpaired t-test was performed, yielding a P value of 0.84, showing an insignificant difference between the amount of CD9-specific exosomes generated from Irradiated or Non-Irradiated MSCs.

Chapter 5: Figure 5: Exosomes from MSCs support ASC function irregardless of irradiation status

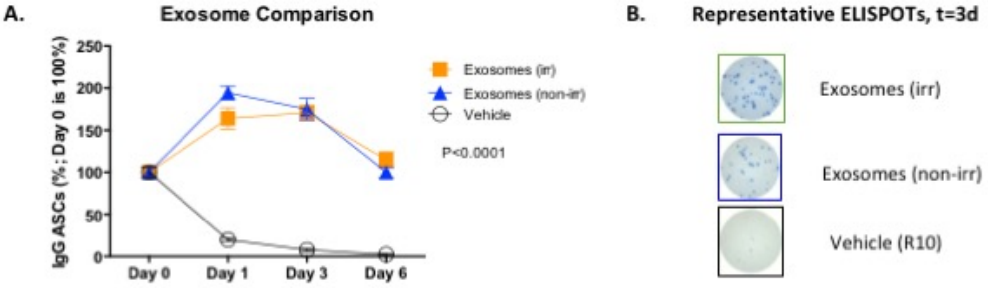

Figure 5: Exosomes from MSCs support ASC function irrespective of irradiation status

A. Figure 5 shows the cumulative data for three independent experiments, plotted in two separate graphs for condition-based comparisons. Panel A shows only exosome samples, in comparison to vehicle alone. We noted that irrespective of irradiation status, exosomes were no different in the support of ASC function, when comparing to the vehicle alone (two-way ANOVA, p-value<0.0001). Figure shows the cumulative data for three independent experiments.

B. Representative photomicrographs of the wells from ELISPOT experiments in panel A.

Chapter 5: Figure 6: Exosome proteomics reveals high significance for exosome-mediated delivery of integrin signaling proteins

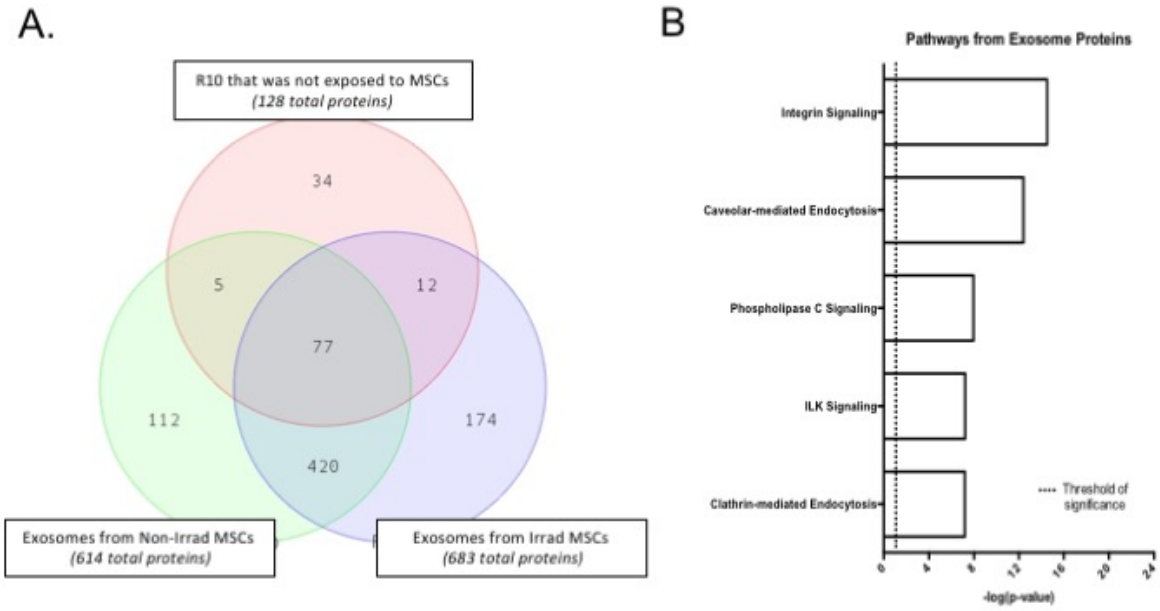

Figure 6: Exosome proteomics reveals high significance for exosome-mediated delivery of integrin signaling proteins

A. After statistical thresholding as described in Methods, the datasets from Supplemental Table 1 were used as input for the IPA software, to generate pathways most highly-associated with those proteins. Only unique proteins present in both exosome samples but absent in the R10 media were used as input for IPA.
B. Panel B presents a curated listing of five of the most significantly-represented pathway lists generated by IPA. Within the IPA platform, a pathway is considered statistically-significant according to the proportion of pathway members present. A statistically-significant p-value of 0.05 is equivalent to a –log(p-value of 1.35, which is indicated on the plot as a vertical dashed line, at the x-value of 1.35.

Chapter 5: Figure 7: Supplemental FlowChart for Generation of Exosomes from MSCs

A.

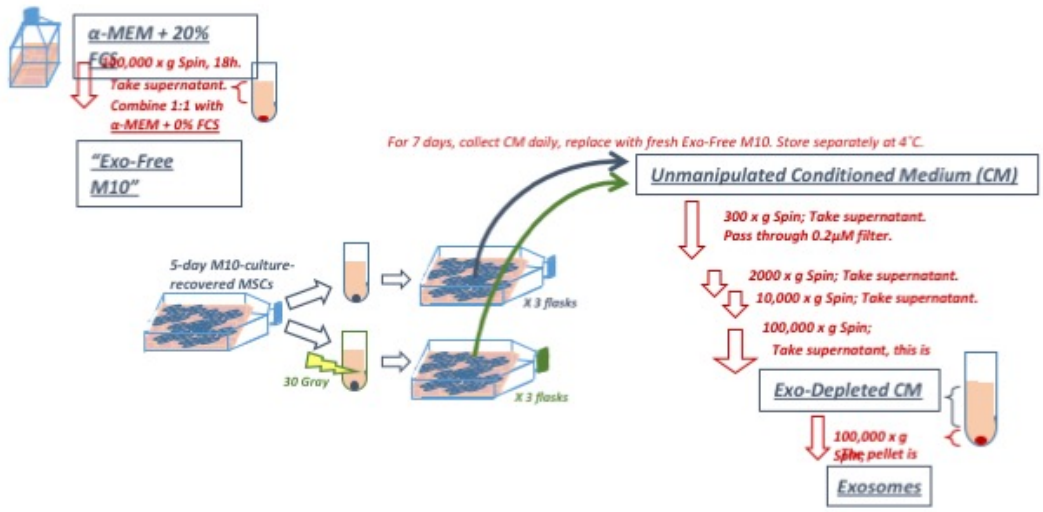

A. This flowchart illustrates how exosomes were generated from MSC conditioned medium (CM). Full details may be found in Methods, but here we wish to point out how the same population of MSCs was passaged and irradiated, and how the subsequent fractionation of CM was performed. It may be helpful to envision the theoretical sum of (Exosomes + Exo-depleted CM) to be relatively equivalent to the overall unmanipulated CM.

Chapter 5: Figure 7 Supplementary Table 1 (Page 1 of 8)

All protein hits from proteomic analysis of the R10 media alone and exosomes derived from Irradiated or Noni-Irradiated MSCs. Greyed-out proteins indicate low-abundance proteins that were excluded in downstream bioinformatic analyses.

Supplemental Table #1: All Proteomic Hits in R10 and Exosomes

Sample #1: R10 Vehicle

	Hits	Gene Reference	Symbol	Rel. Abundance
1	330	sp|P02769|ALBU_BOVIN	ALB	0.420382166
2	102	sp|P12763|FETUA_BOVI	AHSG	0.129936306
3	18	sp|P02768|ALBU_HUMA	ALB	0.022929936
4	13	sp|P02774|VTDB_HUMA	GC	0.01656051
5	10	sp|P08123|CO1A2_HUM	COL1A2	0.012738854
6	10	sp|P04264|K2C1_HUMA	KRT1	0.012738854
7	9	sp|P02751|FINC_HUMA	FN1	0.011464968
8	9	sp|P02771|FETA_HUMA	AFP	0.011464968
9	8	sp|P60709|ACTB_HUMA	ACTB	0.010191083
10	8	sp|P23142|FBLN1_HUM	FBLN1	0.010191083
11	8	sp|P02452|CO1A1_HUM	COL1A1	0.010191083
12	8	sp|P36955|PEDF_HUMA	SERPINF1	0.010191083
13	8	sp|P67809|YBOX1_HUM	YBX1	0.010191083
14	7	sp|P01024|CO3_HUMAN	C3	0.008917197
15	7	sp|P18206|VINC_HUMA	VCL	0.008917197
16	7	sp|P35527|K1C9_HUMA	KRT9	0.008917197
17	7	sp|P19823|ITIH2_HUMA	ITIH2	0.008917197
18	7	sp|P04114|APOB_HUMA	APOB	0.008917197
19	6	sp|P35443|TSP4_HUMA	THBS4	0.007643312
20	5	sp|P02461|CO3A1_HUM	COL3A1	0.006369427
21	5	sp|P07996|TSP1_HUMA	THBS1	0.006369427
22	5	sp|Q15063|POSTN_HUN	POSTN	0.006369427
23	5	sp|P05452|TETN_HUMA	CLEC3B	0.006369427
24	5	sp|P18065|IBP2_HUMA	IGFBP2	0.006369427
25	5	sp|P00734|THRB_HUM	F2	0.006369427
26	5	sp|P49747|COMP_HUM	COMP	0.006369427
27	5	sp|P20908|CO5A1_HUM	COL5A1	0.006369427
28	4	sp|P13645|K1C10_HUM	KRT10	0.005095541
29	4	sp|P62937|PPIA_HUMA	PPIA	0.005095541
30	4	sp|P06396|GELS_HUMA	GSN	0.005095541
31	3	sp|P00761|TRYP_PIG	TRYP_PIG	0.003821656
32	3	sp|P23528|COF1_HUMA	CFL1	0.003821656
33	3	sp|A5A3E0|POTEF_HUM	POTEF	0.003821656
34	3	sp|P05543|THBG_HUM	SERPINA7	0.003821656
35	3	sp|P02788|TRFL_HUMA	LTF	0.003821656
36	3	sp|P01008|ANT3_HUMA	SERPINC1	0.003821656
37	3	sp|P00736|CO4A_HUMA	C4A	0.003821656
38	3	sp|P01023|A2MG_HUMA	A2M	0.003821656
39	3	sp|P69905|HBA_HUMAN	HBA1	0.003821656
40	3	sp|P01344|IGF2_HUMA	IGF2	0.003821656
41	3	sp|P35908|K22E_HUMA	KRT2	0.003821656
42	3	sp|O95497|VNN1_HUM	VNN1	0.003821656
43	3	sp|P0CG47|UBB_HUMA	UBB	0.003821656
44	3	sp|P00747|PLMN_HUMA	PLG	0.003821656
45	3	sp|Q09666|AHNK_HUM	AHNAK	0.003821656
46	2	sp|Q15485|RGN_HUMA	RGN	0.002547771
47	2	sp|P18669|PGAM1_HUM	PGAM1	0.002547771
48	2	sp|P12109|CO6A1_HUM	COL6A1	0.002547771
49	2	sp|Q04756|HGFA_HUMA	HGFAC	0.002547771
50	2	sp|P09486|SPRC_HUMA	SPARC	0.002547771
51	2	sp|P13591|NCAM1_HUM	NCAM1	0.002547771
52	2	sp|P02656|APOC3_HUM	APOC3	0.002547771
53	2	sp|Q9UQB0|PA2G4_HUM	PA2G4	0.002547771
54	2	sp|P62736|ACTA_HUMA	ACTA2	0.002547771
55	2	sp|P04278|SHBG_HUMA	SHBG	0.002547771
56	2	sp|P62942|FKB1A_HUM	FKBP1A	0.002547771
57	2	sp|P40925|MDHC_HUM	MDH1	0.002547771
58	2	sp|P08603|CFAH_HUMA	CFH	0.002547771
59	2	sp|P24593|IBP5_HUMA	IGFBP5	0.002547771
60	2	sp|P35998|PRS7_HUMA	PSMC2	0.002547771
61	2	sp|Q9H299|SH3L3_HUM	SH3BGRL3	0.002547771
62	2	sp|P15259|PGAM2_HUM	PGAM2	0.002547771
63	2	sp|P07339|CATD_HUMA	CTSD	0.002547771
64	2	sp|P55290|CAD13_HUM	CDH13	0.002547771
65	2	sp|P20700|LMNB1_HUN	LMNB1	0.002547771
66	2	sp|P10451|OSTP_HUMA	SPP1	0.002547771
67	2	sp|P06727|APOA4_HUN	APOA4	0.002547771
68	1	sp|Q14118|DAG1_HUM	DAG1	0.001273885
69	1	sp|P00746|CFAD_HUMA	CFD	0.001273885
70	1	sp|Q9HCY8|S10AE_HUM	S100A14	0.001273885
71	1	sp|P51884|LUM_HUMA	LUM	0.001273885
72	1	sp|Q14766|LTBP1_HUM	LTBP1	0.001273885
73	1	sp|P51991|ROA3_HUM	HNRNPA3	0.001273885
74	1	sp|P02458|CO2A1_HUM	COL2A1	0.001273885
75	1	sp|Q96D15|RCN3_HUM	RCN3	0.001273885
76	1	sp|P05156|CFAI_HUMA	CFI	0.001273885
77	1	sp|P04004|VTNC_HUMA	VTN	0.001273885
78	1	sp|P08697|A2AP_HUMA	SERPINF2	0.001273885
79	1	sp|Q8TEA8|DTD1_HUM	DTD1	0.001273885
80	1	sp|P67936|TPM4_HUMA	TPM4	0.001273885
81	1	sp|P63104|1433Z_HUM	YWHAZ	0.001273885
82	1	sp|Q8NBJ4|GOLM1_HUE	GOLM1	0.001273885
83	1	sp|Q06828|FMOD_HUM	FMOD	0.001273885
84	1	sp|Q99497|PARK7_HUN	PARK7	0.001273885
85	1	sp|P02753|RET4_HUMA	RBP4	0.001273885
86	1	sp|Q14624|ITIH4_HUMA	ITIH4	0.001273885

Sample #6: No Irrad MSC Exosomes

	Hits	Gene Reference	Symbol	Rel. Abundance
1	135	sp|P02769|ALBU_BOVIN	ALB	0.042439484
2	131	sp|P02751|FINC_HUMA	FN1	0.041182018
3	102	sp|P12111|CO6A3_HUM	COL6A3	0.032065388
4	89	sp|P12763|FETUA_BOVI	AHSG	0.027978623
5	69	sp|P04264|K2C1_HUMA	KRT1	0.021691292
6	63	sp|P02452|CO1A1_HUM	COL1A1	0.019805093
7	57	sp|P08123|CO1A2_HUM	COL1A2	0.017918893
8	48	sp|P21333|FLNA_HUMA	FLNA	0.015089594
9	38	sp|P35908|K22E_HUMA	KRT2	0.011945929
10	35	sp|Q00610|CLH1_HUMA	CLTC	0.011002829
11	35	sp|P08133|ANXA6_HUM	ANXA6	0.011002829
12	35	sp|O43854|EDIL3_HUMA	EDIL3	0.011002829
13	34	sp|P35527|K1C9_HUMA	KRT9	0.010688463
14	29	sp|P07996|TSP1_HUMA	THBS1	0.00911663
15	29	sp|P13645|K1C10_HUM	KRT10	0.00911663
16	29	sp|P60709|ACTB_HUMA	ACTB	0.00911663
17	28	sp|Q99715|COCA1_HUN	COL12A1	0.008802263
18	26	sp|Q14764|MVP_HUMA	MVP	0.00817353
19	26	sp|P35579|MYH9_HUMA	MYH9	0.00817353
20	22	sp|P13611|CSPG2_HUM	VCAN	0.006916064
21	21	sp|P02461|CO3A1_HUM	COL3A1	0.006601698
22	20	sp|P04406|G3P_HUMAN	GAPDH	0.006287331
23	19	sp|P12109|CO6A1_HUM	COL6A1	0.005972964
24	18	sp|P68363|TBA1B_HUM	TUBA1B	0.005658598
25	18	sp|P11142|HSP7C_HUM	HSPA8	0.005658598
26	17	sp|Q08431|MFGM_HUN	MFGE8	0.005344231
27	17	sp|P14618|KPYM_HUM	PKM	0.005344231
28	17	sp|P13647|K2C5_HUMA	KRT5	0.005344231
29	16	sp|P06733|ENOA_HUM	ENO1	0.005029865
30	16	sp|P08670|VIME_HUMA	VIM	0.005029865
31	16	sp|Q14204|DYHC1_HUN	DYNC1H1	0.005029865
32	16	sp|A6NMY6|AXA2L_HUM	ANXA2P2	0.005029865
33	16	sp|Q08380|LG3BP_HUM	LGALS3BP	0.005029865
34	15	sp|Q07954|LRP1_HUMA	LRP1	0.004715498
35	15	sp|P23142|FBLN1_HUM	FBLN1	0.004715498
36	15	sp|P12110|CO6A2_HUM	COL6A2	0.004715498
37	14	sp|Q9Y490|TLN1_HUMA	TLN1	0.004401132
38	14	sp|P98160|PGBM_HUM	HSPG2	0.004401132
39	14	sp|P15144|AMPN_HUM	ANPEP	0.004401132
40	14	sp|P05023|AT1A1_HUM	ATP1A1	0.004401132
41	13	sp|P07942|LAMB1_HUN	LAMB1	0.004086765
42	13	sp|Q9P2B2|FPRP_HUMA	PTGFRN	0.004086765
43	13	sp|P00558|PGK1_HUMA	PGK1	0.004086765
44	12	sp|P08758|ANXA5_HUM	ANXA5	0.003772399
45	12	sp|P35442|TSP2_HUMA	THBS2	0.003772399
46	12	sp|P04083|ANXA1_HUM	ANXA1	0.003772399
47	12	sp|P04350|TBB4A_HUM	TUBB4A	0.003772399
48	12	sp|P60174|TPIS_HUMAN	TPI1	0.003772399
49	12	sp|P68104|EF1A1_HUM	EEF1A1	0.003772399
50	11	sp|Q09666|AHNK_HUM	AHNAK	0.003458032
51	11	sp|Q15063|POSTN_HUM	POSTN	0.003458032
52	11	sp|P05556|ITB1_HUMAN	ITGB1	0.003458032
53	11	sp|P21589|5NTD_HUMAN	NTSE	0.003458032
54	11	sp|P08238|HS90B_HUM	HSP90AB1	0.003458032
55	11	sp|P29966|MARCS_HUN	MARCKS	0.003458032
56	11	sp|P53675|CLH2_HUMA	CLTCL1	0.003458032
57	10	sp|Q8WUM4|PDCD6I_HU	PDCD6IP	0.003143666
58	10	sp|Q9NZM1|MYOF_HUN	MYOF	0.003143666
59	10	sp|Q01995|TAGL_HUMAN	TAGLN	0.003143666
60	10	sp|P02533|K3C14_HUM	KRT14	0.003143666
61	10	sp|P11047|LAMC1_HUN	LAMC1	0.003143666
62	10	sp|P07093|GDN_HUMAN	SERPINE2	0.003143666
63	10	sp|P06756|ITAV_HUMAN	ITGAV	0.003143666
64	10	sp|P00761|TRYP_PIG	TRYP_PIG	0.003143666
65	10	sp|P02768|ALBU_HUMA	ALB	0.003143666
66	9	sp|P10915|HPLN1_HUM	HAPLN1	0.002829299
67	9	sp|P11021|GRP78_HUM	HSPA5	0.002829299
68	9	sp|O43707|ACTN4_HUM	ACTN4	0.002829299
69	9	sp|Q7Z794|K2C1B_HUM	KRT77	0.002829299
70	9	sp|P13639|EF2_HUMAN	EEF2	0.002829299
71	9	sp|P22413|ENPP1_HUM	ENPP1	0.002829299
72	9	sp|P07900|HS90A_HUM	HSP90AA1	0.002829299
73	9	sp|P17301|ITA2_HUMAN	ITGA2	0.002829299
74	8	sp|P18206|VINC_HUMA	VCL	0.002514932
75	8	sp|P26038|MOES_HUMA	MSN	0.002514932
76	8	sp|P62736|ACTA_HUMA	ACTA2	0.002514932
77	8	sp|P08195|4F2_HUMAN	SLC3A2	0.002514932
78	8	sp|Q6YHK3|CD109_HUN	CD109	0.002514932
79	8	sp|P08779|K3C16_HUM	KRT16	0.002514932
80	8	sp|Q12884|SEPR_HUMAN	FAP	0.002514932
81	8	sp|P50990|TCPQ_HUMA	CCT8	0.002514932
82	8	sp|Q5T749|KPRP_HUMAN	KPRP	0.002514932
83	8	sp|O75083|WDR1_HUM	WDR1	0.002514932
84	8	sp|Q92896|GSLG1_HUM	GSLG1	0.002514932
85	8	sp|P62805|H4_HUMAN	HIST1H4A	0.002514932
86	8	sp|P02774|VTDB_HUMA	GC	0.002514932

Sample #7: Irrad MSC Exosomes

	Hits	Gene Reference	Symbol	Rel. Abundance
1	146	sp|P02769|ALBU_BOVIN_co	ALB	0.041990221
2	132	sp|P02751|FINC_HUMAN	FN1	0.037963762
3	89	sp|P12111|CO6A3_HUMAN	COL6A3	0.025596779
4	83	sp|P02452|CO1A1_HUMAN	COL1A1	0.023871153
5	75	sp|Q99715|COCA1_HUMAN	COL12A1	0.021570319
6	72	sp|P12763|FETUA_BOVIN_co	AHSG	0.020707506
7	67	sp|P08123|CO1A2_HUMAN	COL1A2	0.019269485
8	58	sp|P21333|FLNA_HUMAN	FLNA	0.016681047
9	43	sp|P02461|CO3A1_HUMAN	COL3A1	0.012366983
10	39	sp|P07996|TSP1_HUMAN	THBS1	0.011216566
11	37	sp|P04264|K2C1_HUMAN_co	KRT1	0.010641357
12	36	sp|P35579|MYH9_HUMAN	MYH9	0.010353753
13	34	sp|Q00610|CLH1_HUMAN	CLTC	0.009778545
14	32	sp|O43854|EDIL3_HUMAN	EDIL3	0.009203336
15	32	sp|P60709|ACTB_HUMAN	ACTB	0.009203336
16	31	sp|P08133|ANXA6_HUMAN	ANXA6	0.008915732
17	31	sp|Q14764|MVP_HUMAN	MVP	0.008915732
18	28	sp|P35908|K22E_HUMAN_co	KRT2	0.008052919
19	27	sp|Q09666|AHNK_HUMAN	AHNAK	0.007765315
20	25	sp|P35527|K1C9_HUMAN_co	KRT9	0.007190106
21	24	sp|Q07954|LRP1_HUMAN	LRP1	0.006902502
22	24	sp|Q9Y490|TLN1_HUMAN	TLN1	0.006902502
23	21	sp|P13645|K1C10_HUMAN_c	KRT10	0.006039689
24	20	sp|P13611|CSPG2_HUMAN	VCAN	0.005752085
25	20	sp|P23142|FBLN1_HUMAN	FBLN1	0.005752085
26	20	sp|P12110|CO6A2_HUMAN	COL6A2	0.005752085
27	19	sp|P35442|TSP2_HUMAN	THBS2	0.005464481
28	18	sp|P12109|CO6A1_HUMAN	COL6A1	0.005176877
29	18	sp|P08670|VIME_HUMAN	VIM	0.005176877
30	18	sp|P04083|ANXA1_HUMAN	ANXA1	0.005176877
31	17	sp|P68363|TBA1B_HUMAN	TUBA1B	0.004889272
32	17	sp|P11142|HSP7C_HUMAN	HSPA8	0.004889272
33	16	sp|P14618|KPYM_HUMAN	PKM	0.004601668
34	16	sp|P04406|G3P_HUMAN	GAPDH	0.004601668
35	16	sp|Q14204|DYHC1_HUMAN	DYNC1H1	0.004601668
36	14	sp|P55072|TERA_HUMAN	VCP	0.00402646
37	14	sp|Q9NZM1|MYOF_HUMAN	MYOF	0.00402646
38	14	sp|P35555|FBN1_HUMAN	FBN1	0.00402646
39	14	sp|P05556|ITB1_HUMAN	ITGB1	0.00402646
40	13	sp|A6NMY6|AXA2L_HUMAN	ANXA2P2	0.003738855
41	12	sp|P13639|EF2_HUMAN	EEF2	0.003451251
42	12	sp|P18206|VINC_HUMAN	VCL	0.003451251
43	12	sp|Q08431|MFGM_HUMAN	MFGE8	0.003451251
44	12	sp|Q15149|PLEC_HUMAN	PLEC	0.003451251
45	12	sp|P29966|MARCS_HUMAN	MARCKS	0.003451251
46	12	sp|P04114|APOB_HUMAN	APOB	0.003451251
47	11	sp|P98160|PGBM_HUMAN	HSPG2	0.003163647
48	11	sp|P08253|MMP2_HUMAN	MMP2	0.003163647
49	11	sp|P08758|ANXA5_HUMAN	ANXA5	0.003163647
50	11	sp|O43707|ACTN4_HUMAN	ACTN4	0.003163647
51	11	sp|P20020|AT2B1_HUMAN	ATP2B1	0.003163647
52	11	sp|P02545|LMNA_HUMAN	LMNA	0.003163647
53	11	sp|P10915|HPLN1_HUMAN	HAPLN1	0.003163647
54	11	sp|P01023|A2MG_HUMAN	A2M	0.003163647
55	11	sp|P06733|ENOA_HUMAN	ENO1	0.003163647
56	11	sp|Q8WUM4|PDCD6I_HUMAN	PDCD6IP	0.003163647
57	11	sp|P02768|ALBU_HUMAN_co	ALB	0.003163647
58	10	sp|P00558|PGK1_HUMAN	PGK1	0.002876043
59	10	sp|Q15113|PCOC1_HUMAN	PCOLCE	0.002876043
60	10	sp|P50990|TCPQ_HUMAN	CCT8	0.002876043
61	10	sp|P11047|LAMC1_HUMAN	LAMC1	0.002876043
62	10	sp|Q15582|BGH3_HUMAN	TGFBI	0.002876043
63	10	sp|P04899|GNAI2_HUMAN	GNAI2	0.002876043
64	10	sp|P07900|HS90A_HUMAN	HSP90AA1	0.002876043
65	10	sp|P00761|TRYP_PIG	TRYP_PIG	0.002876043
66	10	sp|P22413|ENPP1_HUMAN	ENPP1	0.002876043
67	9	sp|P27348|1433T_HUMAN	YWHAQ	0.002588438
68	9	sp|Q15063|POSTN_HUMAN	POSTN	0.002588438
69	9	sp|Q01995|TAGL_HUMAN	TAGLN	0.002588438
70	9	sp|P00338|LDHA_HUMAN	LDHA	0.002588438
71	9	sp|P07437|TBB5_HUMAN	TUBB	0.002588438
72	9	sp|P05023|AT1A1_HUMAN	ATP1A1	0.002588438
73	9	sp|P68104|EF1A1_HUMAN	EEF1A1	0.002588438
74	9	sp|O00468|AGRIN_HUMAN	AGRN	0.002588438
75	9	sp|P80723|BASP1_HUMAN	BASP1	0.002588438
76	9	sp|P17302|CXA1_HUMAN	GJA1	0.002588438
77	9	sp|P11021|GRP78_HUMAN	HSPA5	0.002588438
78	9	sp|P53621|COPA_HUMAN	COPA	0.002588438
79	9	sp|P62736|ACTA_HUMAN	ACTA2	0.002588438
80	9	sp|P54289|CA2D1_HUMAN	CACNA2D1	0.002588438
81	9	sp|P02533|K3C14_HUMAN_c	KRT14	0.002588438
82	8	sp|P13647|K2C5_HUMAN_co	KRT5	0.002300834
83	8	sp|P21810|PGS1_HUMAN	BGN	0.002300834
84	8	sp|Q08380|LG3BP_HUMAN	LGALS3BP	0.002300834
85	8	sp|P08195|4F2_HUMAN	SLC3A2	0.002300834
86	8	sp|P60174|TPIS_HUMAN	TPI1	0.002300834

Chapter 5: Figure 7 Supplementary Table 1 (Page 2 of 8)

All protein hits from proteomic analysis of the R10 media alone and exosomes derived from Irradiated or Noni-Irradiated MSCs. Greyed-out proteins indicate low-abundance proteins that were excluded in downstream bioinformatic analyses.

87	1	sp	P29966	MARCS_HUM	MARCKS	0.001273885
88	1	sp	Q9UK55	ZPI_HUMAN	SERPINA14	0.001273885
89	1	sp	P02647	APOA1_HUM	APOA1	0.001273885
90	1	sp	Q13740	CD166_HUM	ALCAM	0.001273885
91	1	sp	P61978	HNRPK_HUM	HNRNPK	0.001273885
92	1	sp	P61970	NTF2_HUMA	NUTF2	0.001273885
93	1	sp	P01042	KNG1_HUMA	KNG1	0.001273885
94	1	sp	O00515	LAD1_HUMA	LAD1	0.001273885
95	1	sp	P02042	HBD_HUMAN	HBD	0.001273885
96	1	sp	P60174	TPIS_HUMAN	TPI1	0.001273885
97	1	sp	P20849	COS9A1_HUM	COL9A1	0.001273885
98	1	sp	Q12805	FBLN3_HUM	EFEMP1	0.001273885
99	1	sp	P26927	HGFL_HUMA	MST1	0.001273885
100	1	sp	O75144	ICOSL_HUM	ICOSLG	0.001273885
101	1	sp	P07195	LDHB_HUMA	LDHB	0.001273885
102	1	sp	P43487	RANG_HUMA	RANBP1	0.001273885
103	1	sp	P20742	PZP_HUMAN	PZP	0.001273885
104	1	##sp	Q07954	LRP1_HUM	##LRP1	0.001273885
105	1	sp	P02748	CO9_HUMAN	C9	0.001273885
106	1	sp	Q13283	G3BP1_HUM	G3BP1	0.001273885
107	1	sp	O60888	CUTA_HUMA	CUTA	0.001273885
108	1	sp	P02538	K2C6A_HUM	KRT6A	0.001273885
109	1	sp	P31947	1433S_HUM	SFN	0.001273885
110	1	sp	P09960	LKHA4_HUM	LTA4H	0.001273885
111	1	sp	P62269	RS18_HUMA	RPS18	0.001273885
112	1	sp	P61026	RAB10_HUM	RAB10	0.001273885
113	1	sp	Q9Y2L5	TPPC8_HUM	TRAPPC8	0.001273885
114	1	sp	O75830	SPI2_HUMA	SERPINI2	0.001273885
115	1	sp	P11940	PABP1_HUM	PABPC1	0.001273885
116	1	sp	P16070	CD44_HUMA	CD44	0.001273885
117	1	sp	P10599	THIO_HUMA	TXN	0.001273885
118	1	sp	P00740	FA9_HUMAN	F9	0.001273885
119	1	sp	P08779	K1C16_HUM	KRT16	0.001273885
120	1	sp	Q13442	HAP28_HUM	PDAP1	0.001273885
121	1	sp	O00757	F16P2_HUM	FBP2	0.001273885
122	1	sp	P00441	SODC_HUM	SOD1	0.001273885
123	1	sp	P54920	SNAA_HUMA	NAPA	0.001273885
124	1	sp	Q9NPH3	IL1AP_HUM	IL1RAP	0.001273885
125	1	sp	P07900	HS90A_HUM	HSP90AA1	0.001273885
126	1	sp	P02795	MT2_HUMAN	MT2A	0.001273885
127	1	sp	P19827	ITIH1_HUMA	ITIH1	0.001273885
128	1	sp	Q8IUL8	CILP2_HUMA	CILP2	0.001273885
129	1	sp	P12107	COBA1_HUM	COL11A1	0.001273885

87	7	sp	P05787	K2C8_HUMA	KRT8	0.002200566
88	7	sp	P07437	TBB1_HUMA	TUBB	0.002200566
89	7	sp	P35613	BASI_HUMAN	BSG	0.002200566
90	7	sp	P02545	LMNA_HUMA	LMNA	0.002200566
91	7	sp	P04114	APOB_HUMA	APOB	0.002200566
92	7	sp	Q04695	K1C17_HUM	KRT17	0.002200566
93	7	sp	P01023	A2MG_HUMA	A2M	0.002200566
94	7	sp	P17987	TCPA_HUMA	TCP1	0.002200566
95	7	sp	P04075	ALDOA_HUM	ALDOA	0.002200566
96	7	sp	P35221	CTNA1_HUM	CTNNA1	0.002200566
97	7	sp	P26022	PTX3_HUMA	PTX3	0.002200566
98	7	sp	P62937	PPIA_HUMAN	PPIA	0.002200566
99	7	sp	P62258	1433E_HUM	YWHAE	0.002200566
100	7	sp	P23528	COF1_HUMA	CFL1	0.002200566
101	7	sp	Q92743	HTRA1_HUM	HTRA1	0.002200566
102	7	sp	P35555	FBN1_HUMA	FBN1	0.002200566
103	7	sp	Q99460	PSMD1_HUM	PSMD1	0.002200566
104	7	sp	Q15582	BGH3_HUMA	TGFBI	0.002200566
105	7	sp	Q16363	LAMA4_HUM	LAMA4	0.002200566
106	7	sp	P01891	1A68_HUMA	HLA-A	0.002200566
107	7	sp	P80723	BASP1_HUM	BASP1	0.002200566
108	7	sp	P04899	GNAI2_HUM	GNAI2	0.002200566
109	6	sp	P54289	CA2D1_HUM	CACNA2D1	0.001886199
110	6	sp	P16070	CD44_HUMA	CD44	0.001886199
111	6	sp	P49368	TCPG_HUMA	CCT3	0.001886199
112	6	sp	P08253	MMP2_HUM	MMP2	0.001886199
113	6	sp	P17302	CKA1_HUMA	GJA1	0.001886199
114	6	sp	P27348	1433T_HUM	YWHAQ	0.001886199
115	6	sp	P50995	ANX11_HUM	ANXA11	0.001886199
116	6	sp	P40227	TCP2_HUMA	CCT6A	0.001886199
117	6	sp	P20020	AT2B1_HUM	ATP2B1	0.001886199
118	6	sp	P06396	GELS_HUMA	GSN	0.001886199
119	6	sp	O60814	H2B1K_HUM	HIST1H2BK	0.001886199
120	6	sp	P62873	GBB1_HUMA	GNB1	0.001886199
121	6	sp	P60842	IF4A1_HUMA	EIF4A1	0.001886199
122	6	sp	P05452	TETN_HUMA	CLEC3B	0.001886199
123	6	sp	Q15149	PLEC_HUMA	PLEC	0.001886199
124	6	sp	Q9UKK3	PARP4_HUM	PARP4	0.001886199
125	6	sp	P35443	TSP4_HUMA	THBS4	0.001886199
126	6	sp	P84095	RHOG_HUMA	RHOG	0.001886199
127	6	sp	P05387	RLA2_HUMA	RPLP2	0.001886199
128	5	sp	O00560	SDCB1_HUM	SDCBP	0.001571833
129	5	sp	P07737	PROF1_HUM	PFN1	0.001571833
130	5	sp	Q15758	AAAT_HUMA	SLC1A5	0.001571833
131	5	sp	P62241	RS8_HUMAN	RPS8	0.001571833
132	5	sp	P08107	HSP71_HUM	HSPA1A	0.001571833
133	5	sp	P21810	PGS1_HUMA	BGN	0.001571833
134	5	sp	P00338	LDHA_HUMA	LDHA	0.001571833
135	5	sp	Q14315	FLNC_HUMA	FLNC	0.001571833
136	5	sp	Q14699	RFTN1_HUM	RFTN1	0.001571833
137	5	sp	P12814	ACTN1_HUM	ACTN1	0.001571833
138	5	sp	P07355	ANXA2_HUM	ANXA2	0.001571833
139	5	sp	A6NNZ2	TBB8L_HUMAN		0.001571833
140	5	sp	Q03405	UPAR_HUMA	PLAUR	0.001571833
141	5	sp	A6NIZ1	RP1BL_HUMAN		0.001571833
142	5	sp	P29144	TPP2_HUMA	TPP2	0.001571833
143	5	sp	P05388	RLA0_HUMA	RPLP0	0.001571833
144	5	sp	Q9H4M9	EHD1_HUM	EHD1	0.001571833
145	5	sp	P15880	RS2_HUMAN	RPS2	0.001571833
146	5	sp	P55072	TERA_HUMA	VCP	0.001571833
147	5	sp	P61247	RS3A_HUMA	RPS3A	0.001571833
148	5	sp	P13010	XRCC5_HUM	XRCC5	0.001571833
149	5	sp	P46940	IQGA1_HUM	IQGAP1	0.001571833
150	5	sp	O14786	NRP1_HUMA	NRP1	0.001571833
151	5	sp	P49747	COMP_HUM	COMP	0.001571833
152	5	sp	Q15113	PCOC1_HUM	PCOLCE	0.001571833
153	5	sp	Q92626	PXDN_HUMA	PXDN	0.001571833
154	5	sp	A5A3E0	POTEF_HUM	POTEF	0.001571833
155	5	sp	Q9NZN4	EHD2_HUM	EHD2	0.001571833
156	4	sp	P20073	ANXA7_HUM	ANXA7	0.001257466
157	4	sp	P05783	K1C18_HUM	KRT18	0.001257466
158	4	sp	P05454	SERPH_HUM	SERPINH1	0.001257466
159	4	sp	P04792	HSPB1_HUM	HSPB1	0.001257466
160	4	sp	Q9Y696	CLIC8_HUMA	CLIC4	0.001257466
161	4	sp	Q9NQC3	RTN4_HUM	RTN4	0.001257466
162	4	sp	A7E3W2	LG3BP_BOV	LGALS3BP	0.001257466
163	4	sp	O14672	ADA10_HUM	ADAM10	0.001257466
164	4	sp	Q02413	DSG1_HUMA	DSG1	0.001257466
165	4	sp	P14923	PLAK_HUMA	JUP	0.001257466
166	4	sp	P46782	RS5_HUMAN	RPS5	0.001257466
167	4	sp	P08648	ITA5_HUMAN	ITGA5	0.001257466
168	4	sp	Q14112	NID2_HUMA	NID2	0.001257466
169	4	sp	P01024	CO3_HUMAN	C3	0.001257466
170	4	sp	P63241	IF5A1_HUMA	EIF5A	0.001257466
171	4	sp	O43175	SERA_HUMA	PHGDH	0.001257466
172	4	sp	P09619	PGFRB_HUM	PDGFRB	0.001257466
173	4	sp	P50914	RL14_HUMA	RPL14	0.001257466
174	4	sp	P09382	LEG1_HUMA	LGALS1	0.001257466
175	4	sp	P07195	LDHB_HUMA	LDHB	0.001257466
176	4	sp	P46777	RL5_HUMAN	RPL5	0.001257466
177	4	sp	Q06830	PRDX1_HUM	PRDX1	0.001257466
178	4	sp	P69905	HBA_HUMAN	HBA1	0.001257466

87	8	sp	P07093	GDN_HUMAN	SERPINE2	0.002300834
88	8	sp	Q14315	FLNC_HUMAN	FLNC	0.002300834
89	8	sp	P15144	AMPN_HUMAN	ANPEP	0.002300834
90	8	sp	P12814	ACTN1_HUMAN	ACTN1	0.002300834
91	8	sp	P04075	ALDOA_HUMAN	ALDOA	0.002300834
92	8	sp	Q9Y696	CLIC4_HUMAN	CLIC4	0.002300834
93	8	sp	Q04695	K1C17_HUMAN	KRT17	0.002300834
94	8	sp	P06756	ITAV_HUMAN	ITGAV	0.002300834
95	8	sp	P05997	CO5A2_HUMAN	COL5A2	0.002300834
96	8	sp	P21589	5NTD_HUMAN	NT5E	0.002300834
97	8	sp	Q16363	LAMA4_HUMAN	LAMA4	0.002300834
98	7	sp	P26038	MOES_HUMAN	MSN	0.00201323
99	7	sp	P08238	HS90B_HUMAN	HSP90AB1	0.00201323
100	7	sp	P07355	ANXA2_HUMAN	ANXA2	0.00201323
101	7	sp	P46940	IQGA1_HUMAN	IQGAP1	0.00201323
102	7	sp	Q14112	NID2_HUMAN	NID2	0.00201323
103	7	sp	P20908	CO5A1_HUMAN	COL5A1	0.00201323
104	7	sp	P24821	TENA_HUMAN	TNC	0.00201323
105	7	sp	P05388	RLA0_HUMAN	RPLP0	0.00201323
106	7	sp	P62258	1433E_HUMAN	YWHAE	0.00201323
107	7	sp	P53675	CLH2_HUMAN	CLTCL1	0.00201323
108	7	sp	P62805	H4_HUMAN	HIST1H4A	0.00201323
109	7	sp	O60701	UGDH_HUMAN	UGDH	0.00201323
110	7	sp	P01891	1A68_HUMAN	HLA-A	0.00201323
111	7	sp	P05452	TETN_HUMAN	CLEC3B	0.00201323
112	7	sp	P08865	RSSA_HUMAN	RPSA	0.00201323
113	7	sp	Q92626	PXDN_HUMAN	PXDN	0.00201323
114	7	sp	O95865	DDAH2_HUMAN	DDAH2	0.00201323
115	7	sp	P33176	KINH_HUMAN	KIF5B	0.00201323
116	7	sp	P02774	VTDB_HUMAN	GC	0.00201323
117	6	sp	P04350	TBB4A_HUMAN	TUBB4A	0.001725626
118	6	sp	P26022	PTX3_HUMAN	PTX3	0.001725626
119	6	sp	P29144	TPP2_HUMAN	TPP2	0.001725626
120	6	sp	P08107	HSP71_HUMAN	HSPA1A	0.001725626
121	6	sp	O43175	SERA_HUMAN	PHGDH	0.001725626
122	6	sp	P08779	K1C16_HUMAN	KRT16	0.001725626
123	6	sp	P63244	GBLP_HUMAN	GNB2L1	0.001725626
124	6	sp	P07942	LAMB1_HUMAN	LAMB1	0.001725626
125	6	sp	P35613	BASI_HUMAN	BSG	0.001725626
126	6	sp	Q13308	PTK7_HUMAN	PTK7	0.001725626
127	6	sp	P00747	PLMN_HUMAN	PLG	0.001725626
128	6	sp	P07737	PROF1_HUMAN	PFN1	0.001725626
129	6	sp	Q92896	GSLG1_HUMAN	GLG1	0.001725626
130	6	sp	P62937	PPIA_HUMAN	PPIA	0.001725626
131	6	sp	P40227	TCP2_HUMAN	CCT6A	0.001725626
132	6	sp	P61247	RS3A_HUMAN	RPS3A	0.001725626
133	6	sp	O00469	PLOD2_HUMAN	PLOD2	0.001725626
134	6	sp	O00560	SDCB1_HUMAN	SDCBP	0.001725626
135	6	sp	Q6YHK3	CD109_HUMAN	CD109	0.001725626
136	6	sp	P09486	SPRC_HUMAN	SPARC	0.001725626
137	6	sp	Q13740	CD166_HUMAN	ALCAM	0.001725626
138	6	sp	O15031	PLXB2_HUMAN	PLXNB2	0.001725626
139	6	sp	P84095	RHOG_HUMAN	RHOG	0.001725626
140	6	sp	P15880	RS2_HUMAN	RPS2	0.001725626
141	6	sp	Q9P2B2	FPRP_HUMAN	PTGFRN	0.001725626
142	5	sp	P50395	GDIB_HUMAN	GDI2	0.001438021
143	5	sp	P35443	TSP4_HUMAN	THBS4	0.001438021
144	5	sp	O00159	MYO1C_HUMAN	MYO1C	0.001438021
145	5	sp	P50995	ANX11_HUMAN	ANXA11	0.001438021
146	5	sp	P06396	GELS_HUMAN	GSN	0.001438021
147	5	sp	P17987	TCPA_HUMAN	TCP1	0.001438021
148	5	sp	P62269	RS18_HUMAN	RPS18	0.001438021
149	5	sp	P39023	RL3_HUMAN	RPL3	0.001438021
150	5	sp	Q06830	PRDX1_HUMAN	PRDX1	0.001438021
151	5	sp	P36578	RL4_HUMAN	RPL4	0.001438021
152	5	sp	P62873	GBB1_HUMAN	GNB1	0.001438021
153	5	sp	O75083	WDR1_HUMAN	WDR1	0.001438021
154	5	sp	P23528	COF1_HUMAN	CFL1	0.001438021
155	5	sp	Q03405	UPAR_HUMAN	PLAUR	0.001438021
156	5	sp	O14950	MYL12B_HUMAN	MYL12B	0.001438021
157	5	sp	O60814	H2B1K_HUMAN	HIST1H2BK	0.001438021
158	5	sp	O00232	PSD12_HUMAN	PSMD12	0.001438021
159	5	sp	P13489	RINI_HUMAN	RNH1	0.001438021
160	5	sp	Q15758	AAAT_HUMAN	SLC1A5	0.001438021
161	5	sp	A5A3E0	POTEF_HUMAN	POTEF	0.001438021
162	5	sp	P01024	CO3_HUMAN	C3	0.001438021
163	5	sp	P62263	RS14_HUMAN	RPS14	0.001438021
164	5	sp	P07814	SYEP_HUMAN	EPRS	0.001438021
165	5	sp	P23396	RS3_HUMAN	RPS3	0.001438021
166	5	sp	P78371	TCPB_HUMAN	CCT2	0.001438021
167	5	sp	O99460	PSMD1_HUMAN	PSMD1	0.001438021
168	5	sp	P02753	RET4_HUMAN	RBP4	0.001438021
169	5	sp	O99832	TCPH_HUMAN	CCT7	0.001438021
170	5	sp	P62753	RS6_HUMAN	RPS6	0.001438021
171	5	sp	P17301	ITA2_HUMAN	ITGA2	0.001438021
172	5	sp	Q9UJI3	HEG1_HUMAN	HEG1	0.001438021
173	5	sp	Q9UKK3	PARP4_HUMAN	PARP4	0.001438021
174	5	sp	P39019	RS19_HUMAN	RPS19	0.001438021
175	5	sp	Q14699	RFTN1_HUMAN	RFTN1	0.001438021
176	5	sp	O00299	CLIC1_HUMAN	CLIC1	0.001438021
177	5	sp	P23634	AT2B4_HUMAN	ATP2B4	0.001438021
178	5	sp	Q15393	SF3B3_HUMAN	SF3B3	0.001438021

Chapter 5: Figure 7 Supplementary Table 1 (Page 3 of 8)

All protein hits from proteomic analysis of the R10 media alone and exosomes derived from Irradiated or Noni-Irradiated MSCs. Greyed-out proteins indicate low-abundance proteins that were excluded in downstream bioinformatic analyses.

179	4	sp|P60033|CD81_HUMA	CD81	0.001257466
180	4	sp|O14818|PSA7_HUMA	PSMA7	0.001257466
181	4	sp|P08134|RHOC_HUMA	RHOC	0.001257466
182	4	sp|P09486|SPRC_HUMA	SPARC	0.001257466
183	4	sp|O00299|CLIC1_HUMA	CLIC1	0.001257466
184	4	sp|O00159|MYO1C_HUM	MYO1C	0.001257466
185	4	sp|Q969P0|IGSF8_HUMA	IGSF8	0.001257466
186	4	sp|P63244|GBLP_HUMA	GNB2L1	0.001257466
187	4	sp|P30050|RL12_HUMA	RPL12	0.001257466
188	4	sp|P00747|PLMN_HUMA	PLG	0.001257466
189	4	sp|P04216|THY1_HUMA	THY1	0.001257466
190	4	sp|Q9P225|SYLC_HUMA	LARS	0.001257466
191	4	sp|O00232|PSD12_HUM	PSMD12	0.001257466
192	4	sp|P61978|HNRPK_HUM	HNRNPK	0.001257466
193	4	sp|Q99832|TCPH_HUMA	CCT7	0.001257466
194	4	sp|P15924|DESP_HUMA	DSP	0.001257466
195	4	sp|P63092|GNAS2_HUM	GNAS	0.001257466
196	4	sp|A6NKZ8|YI016_HUMA	YI016	0.001257466
197	4	sp|P62701|RS4X_HUMA	RPS4X	0.001257466
198	4	sp|P23634|AT2B4_HUM	ATP2B4	0.001257466
199	4	sp|O75369|FLNB_HUMA	FLNB	0.001257466
200	4	sp|Q9ULI3|HEG1_HUMA	HEG1	0.001257466
201	4	sp|P23396|RS3_HUMAN	RPS3	0.001257466
202	4	sp|P39019|RS19_HUMA	RPS19	0.001257466
203	4	sp|P26006|ITA3_HUMA	ITGA3	0.001257466
204	4	sp|P15311|EZRI_HUMAN	EZR	0.001257466
205	4	sp|P0CG47|UBB_HUMA	UBB	0.001257466
206	4	sp|P16401|H15_HUMAN	HIST1H1B	0.001257466
207	4	sp|P62269|RS1B_HUMA	RPS1B	0.001257466
208	4	sp|P14209|CD99_HUMA	CD99	0.001257466
209	4	sp|P31946|1433B_HUM	YWHAB	0.001257466
210	4	sp|Q9H223|EHD4_HUMA	EHD4	0.001257466
211	4	sp|P53396|ACLY_HUMA	ACLY	0.001257466
212	4	sp|Q9NVM1|EVA1B_HU	EVA1B	0.001257466
213	4	sp|P57721|PCBP3_HUM	PCBP3	0.001257466
214	4	sp|P55735|SEC13_HUM	SEC13	0.001257466
215	4	sp|P26641|EF1G_HUMA	EEF1G	0.001257466
216	4	sp|P23381|SYWC_HUMA	WARS	0.001257466
217	4	sp|Q96KG7|MEG10_HU	MEGF10	0.001257466
218	4	sp|P62714|PP2AB_HUM	PPP2CB	0.001257466
219	4	sp|P26373|RL13_HUMA	RPL13	0.001257466
220	4	sp|P09543|CN37_HUMA	CNP	0.001257466
221	3	sp|Q9NRY6|PLS3_HUMA	PLSCR3	0.0009431
222	3	sp|Q6NZI2|PTRF_HUMA	PTRF	0.0009431
223	3	sp|P63104|1433Z_HUM	YWHAZ	0.0009431
224	3	sp|P50395|GDIB_HUMA	GDI2	0.0009431
225	3	sp|P13987|CD59_HUMA	CD59	0.0009431
226	3	sp|P04908|H2A1B_HUM	HIST1H2AB	0.0009431
227	3	sp|O14828|SCAM3_HUM	SCAMP3	0.0009431
228	3	sp|P36955|PEDF_HUMA	SERPINF1	0.0009431
229	3	sp|P18084|ITB5_HUMAN	ITGB5	0.0009431
230	3	sp|P19823|ITIH2_HUMA	ITIH2	0.0009431
231	3	sp|P49588|SYAC_HUMA	AARS	0.0009431
232	3	sp|O60701|UGDH_HUM	UGDH	0.0009431
233	3	sp|P22314|UBA1_HUMA	UBA1	0.0009431
234	3	sp|Q13885|TBB2A_HUM	TUBB2A	0.0009431
235	3	sp|P02771|FETA_HUMA	AFP	0.0009431
236	3	sp|Q8WWI5|CTL1_HUMA	SLC44A1	0.0009431
237	3	sp|P17813|EGLN_HUMA	ENG	0.0009431
238	3	sp|P39023|RL3_HUMAN	RPL3	0.0009431
239	3	sp|P12273|PIP_HUMAN	PIP	0.0009431
240	3	sp|P62263|RS14_HUMA	RPS14	0.0009431
241	3	sp|Q00839|HNRPU_HUM	HNRNPU	0.0009431
242	3	sp|P02649|APOE_HUMA	APOE	0.0009431
243	3	sp|Q10471|GALT2_HUM	GALNT2	0.0009431
244	3	sp|P62888|RL30_HUMA	RPL30	0.0009431
245	3	sp|P01889|1B07_HUMA	HLA-B	0.0009431
246	3	sp|P05543|THBG_HUM	SERPINA7	0.0009431
247	3	sp|P13489|RINI_HUMAN	RNH1	0.0009431
248	3	sp|O00468|AGRIN_HUM	AGRN	0.0009431
249	3	sp|P20908|CO5A1_HUM	COL5A1	0.0009431
250	3	sp|P35222|CTNB1_HUM	CTNNB1	0.0009431
251	3	sp|P25789|PSA4_HUMA	PSMA4	0.0009431
252	3	sp|P30101|PDIA3_HUMA	PDIA3	0.0009431
253	3	sp|P08865|RSSA_HUMA	RPSA	0.0009431
254	3	sp|P62424|RL7A_HUMA	RPL7A	0.0009431
255	3	sp|Q8WWA5|CTL2_HUM	SLC44A2	0.0009431
256	3	sp|P07814|SYEP_HUMA	EPRS	0.0009431
257	3	sp|P62266|RS23_HUMA	RPS23	0.0009431
258	3	sp|Q13308|PTK7_HUMA	PTK7	0.0009431
259	3	sp|P41250|SYG_HUMAN	GARS	0.0009431
260	3	sp|P29317|EPHA2_HUMA	EPHA2	0.0009431
261	3	sp|P62280|RS11_HUMA	RPS11	0.0009431
262	3	sp|Q9Y6C2|EMIL1_HUM	EMILIN1	0.0009431
263	3	sp|Q9H4G4|GAPR1_HUM	GLIPR2	0.0009431
264	3	sp|Q9Y639|NPTN_HUMA	NPTN	0.0009431
265	3	sp|Q9HCD7|TM165_HUM	TMEM165	0.0009431
266	3	sp|Q05682|CALD1_HUM	CALD1	0.0009431
267	3	sp|Q99805|TM9S2_HUM	TMF9SF2	0.0009431
268	3	sp|P43007|SATT_HUMA	SLC1A4	0.0009431
269	3	sp|Q01518|CAP1_HUMA	CAP1	0.0009431
270	3	sp|P11233|RALA_HUMA	RALA	0.0009431

179	5	sp|P13010|XRCC5_HUMAN	SF3B3	0.001438021
180	5	sp|A6NNZ2|TBBBL_HUMAN	TBBBL	0.001438021
181	5	sp|P63092|GNAS2_HUMAN	GNAS	0.001438021
182	5	sp|Q15493|RGN_HUMAN	RGN	0.001438021
183	4	sp|P35221|CTNA1_HUMAN	CTNNA1	0.001150417
184	4	sp|P50454|SERPH_HUMAN	SERPINH1	0.001150417
185	4	sp|P02771|FETA_HUMAN	AFP	0.001150417
186	4	sp|Q13885|TBB2A_HUMAN	TUBB2A	0.001150417
187	4	sp|P21291|CSRP1_HUMAN	CSRP1	0.001150417
188	4	sp|P49588|SYAC_HUMAN	AARS	0.001150417
189	4	sp|P31949|S10AB_HUMAN	S100A11	0.001150417
190	4	sp|P30050|RL12_HUMAN	RPL12	0.001150417
191	4	sp|O75369|FLNB_HUMAN	FLNB	0.001150417
192	4	sp|Q9NVA2|SEP11_HUMAN	SEP11	0.001150417
193	4	sp|P69905|HBA_HUMAN	HBA1	0.001150417
194	4	sp|P62241|RS8_HUMAN	RPS8	0.001150417
195	4	sp|Q9NQC3|RTN4_HUMAN	RTN4	0.001150417
196	4	sp|Q12884|SEPR_HUMAN	FAP	0.001150417
197	4	sp|P61978|HNRPK_HUMAN	HNRNPK	0.001150417
198	4	sp|P41250|SYG_HUMAN	GARS	0.001150417
199	4	sp|P16070|CD44_HUMAN	CD44	0.001150417
200	4	sp|P53396|ACLY_HUMAN	ACLY	0.001150417
201	4	sp|P49368|TCPG_HUMAN	CCT3	0.001150417
202	4	sp|P62424|RL7A_HUMAN	RPL7A	0.001150417
203	4	sp|O43242|PSMD3_HUMAN	PSMD3	0.001150417
204	4	sp|P26373|RL13_HUMAN	RPL13	0.001150417
205	4	sp|P17813|EGLN_HUMAN	ENG	0.001150417
206	4	sp|P23381|SYWC_HUMAN	WARS	0.001150417
207	4	sp|P09382|LEG1_HUMAN	LGALS1	0.001150417
208	4	sp|P32969|RL9_HUMAN	RPL9	0.001150417
209	4	sp|Q96KG7|MEG10_HUMAN	MEGF10	0.001150417
210	4	sp|O14786|NRP1_HUMAN	NRP1	0.001150417
211	4	sp|P62701|RS4X_HUMAN	RPS4X	0.001150417
212	4	sp|P05121|PAI1_HUMAN	SERPINE1	0.001150417
213	4	sp|P62316|SMD2_HUMAN	SNRPD2	0.001150417
214	4	sp|P09619|PGFRB_HUMAN	PDGFRB	0.001150417
215	4	sp|P61981|1433G_HUMAN	YWHAG	0.001150417
216	4	sp|Q10588|BST1_HUMAN	BST1	0.001150417
217	4	sp|P54136|SYRC_HUMAN	RARS	0.001150417
218	4	sp|P49747|COMP_HUMAN	COMP	0.001150417
219	4	sp|P55290|CAD13_HUMAN	CDH13	0.001150417
220	4	sp|P19823|ITIH2_HUMAN	ITIH2	0.001150417
221	4	sp|P62714|PP2AB_HUMAN	PPP2CB	0.001150417
222	4	sp|P62829|RL23_HUMAN	RPL23	0.001150417
223	4	sp|P28300|LYOX_HUMAN	LOX	0.001150417
224	4	sp|P18085|ARF4_HUMAN	ARF4	0.001150417
225	4	sp|P23526|SAHH_HUMAN	AHCY	0.001150417
226	4	sp|P04216|THY1_HUMAN	THY1	0.001150417
227	4	sp|P02788|TRFL_HUMAN	LTF	0.001150417
228	4	sp|Q07955|SRSF1_HUMAN	SRSF1	0.001150417
229	4	sp|P60033|CD81_HUMAN	CD81	0.001150417
230	4	sp|O14672|ADA10_HUMAN	ADAM10	0.001150417
231	4	sp|Q9HC07|TM165_HUMAN	TMEM165	0.001150417
232	4	sp|P05387|RLA2_HUMAN	RPLP2	0.001150417
233	4	sp|P60842|IF4A1_HUMAN	EIF4A1	0.001150417
234	4	sp|Q9CDH2|TTYH3_HUMAN	TTYH3	0.001150417
235	4	sp|Q9Y4L1|HYOU1_HUMAN	HYOU1	0.001150417
236	4	sp|P60981|DEST_HUMAN	DSTN	0.001150417
237	4	sp|P06576|ATPB_HUMAN	ATP5B	0.001150417
238	4	sp|P55735|SEC13_HUMAN	SEC13	0.001150417
239	4	tr|F5H7N9|F5H7N9_HUMAN	MFGE8	0.001150417
240	3	sp|P63104|1433Z_HUMAN	YWHAZ	0.000862813
241	3	sp|Q9Y6C2|EMIL1_HUMAN	EMILIN1	0.000862813
242	3	sp|B5ME19|EIFCL_HUMAN	EIF3CL	0.000862813
243	3	sp|Q9BUF5|TBB6_HUMAN	TUBB6	0.000862813
244	3	sp|A7E3W2|LG3BP_BOVIN_(	LGALS3BP	0.000862813
245	3	sp|P08134|RHOC_HUMAN	RHOC	0.000862813
246	3	sp|O00231|PSD11_HUMAN	PSMD11	0.000862813
247	3	sp|P01008|ANT3_HUMAN	SERPINC1	0.000862813
248	3	sp|Q92743|HTRA1_HUMAN	HTRA1	0.000862813
249	3	sp|O43852|CALU_HUMAN	CALU	0.000862813
250	3	sp|Q96AC1|FERM2_HUMAN	FERMT2	0.000862813
251	3	sp|Q00839|HNRPU_HUMAN	HNRNPU	0.000862813
252	3	sp|P12956|XRCC6_HUMAN	XRCC6	0.000862813
253	3	sp|P13987|CD59_HUMAN	CD59	0.000862813
254	3	sp|O14818|PSA7_HUMAN	PSMA7	0.000862813
255	3	sp|Q01518|CAP1_HUMAN	CAP1	0.000862813
256	3	sp|P36955|PEDF_HUMAN	SERPINF1	0.000862813
257	3	sp|P02649|APOE_HUMAN	APOE	0.000862813
258	3	sp|P10301|RRAS_HUMAN	RRAS	0.000862813
259	3	sp|P35222|CTNB1_HUMAN	CTNNB1	0.000862813
260	3	sp|Q02543|RL18A_HUMAN	RPL18A	0.000862813
261	3	sp|P05543|THBG_HUMAN	SERPINA7	0.000862813
262	3	sp|P04792|HSPB1_HUMAN	HSPB1	0.000862813
263	3	sp|P05106|ITB3_HUMAN	ITGB3	0.000862813
264	3	sp|A6NKZ8|YI016_HUMAN	YI016	0.000862813
265	3	sp|P15311|EZRI_HUMAN	EZR	0.000862813
266	3	sp|P18065|IBP2_HUMAN	IGFBP2	0.000862813
267	3	sp|P13797|PLST_HUMAN	PLS3	0.000862813
268	3	sp|P14625|ENPL_HUMAN	HSP90B1	0.000862813
269	3	sp|P11717|MPRI_HUMAN	IGF2R	0.000862813
270	3	sp|P26006|ITA3_HUMAN	ITGA3	0.000862813

Chapter 5: Figure 7 Supplementary Table 1 (Page 4 of 8)

All protein hits from proteomic analysis of the R10 media alone and exosomes derived from Irradiated or Noni-Irradiated MSCs. Greyed-out proteins indicate low-abundance proteins that were excluded in downstream bioinformatic analyses.

271	3	sp|P08962|CD63_HUMA	CD63	0.0009431
272	3	sp|Q5ZPR3|CD276_HUM	CD276	0.0009431
273	3	sp|O14950|MLL12B_HUN	MYL12B	0.0009431
274	3	sp|A1L4H1|SRCRL_HUM	SSC5D	0.0009431
275	3	sp|P18124|RL7_HUMAN	RPL7	0.0009431
276	3	sp|Q9Y315|DEOC_HUM	DERA	0.0009431
277	3	sp|P17655|CAN2_HUM	CAPN2	0.0009431
278	3	sp|P15559|NQO1_HUM	NQO1	0.0009431
279	3	sp|P07237|PDIA1_HUM	P4HB	0.0009431
280	3	sp|P20618|PSB1_HUMA	PSMB1	0.0009431
281	3	sp|P31943|HNRH1_HUN	HNRNPH1	0.0009431
282	3	sp|P36871|PGM1_HUM	PGM1	0.0009431
283	3	sp|O95865|DDAH2_HUN	DDAH2	0.0009431
284	3	sp|P50281|MMP14_HUN	MMP14	0.0009431
285	3	sp|Q10472|GALT1_HUM	GALNT1	0.0009431
286	3	sp|P00760|TRY1_BOVIN	TRY1_BOVI	0.0009431
287	3	sp|Q13683|ITA7_HUMA	ITGA7	0.0009431
288	3	sp|O15031|PLXB2_HUM	PLXNB2	0.0009431
289	3	sp|Q9UKX5|ITA11_HUM	ITGA11	0.0009431
290	3	sp|P27105|STOM_HUMA	STOM	0.0009431
291	3	sp|P25311|ZA2G_HUMA	AZGP1	0.0009431
292	3	sp|P33176|KINH_HUMA	KIF5B	0.0009431
293	3	sp|P60900|PSA6_HUMA	PSMA6	0.0009431
294	3	sp|Q06033|ITIH3_HUMA	ITIH3	0.0009431
295	3	sp|P62829|RL23_HUMA	RPL23	0.0009431
296	3	sp|Q15517|CD5N_HUMA	CD5N	0.0009431
297	3	sp|P61026|RAB10_HUM	RAB10	0.0009431
298	3	sp|Q8WUJ3|K1199_HUN	KIAA1199	0.0009431
299	2	sp|Q13509|TBB3_HUMA	TUBB3	0.000628733
300	2	sp|P10809|CH60_HUMA	HSPD1	0.000628733
301	2	sp|P06702|S10A9_HUM	S100A9	0.000628733
302	2	sp|P60660|MYL6_HUMA	MYL6	0.000628733
303	2	sp|Q16658|FSCN1_HUM	FSCN1	0.000628733
304	2	sp|Q7Z7G0|TARSH_HUN	ABI3BP	0.000628733
305	2	sp|P78371|TCPB_HUMA	CCT2	0.000628733
306	2	sp|P31944|CASPE_HUM	CASP14	0.000628733
307	2	sp|P01008|ANT3_HUMA	SERPINC1	0.000628733
308	2	sp|P28066|PSA5_HUMA	PSMA5	0.000628733
309	2	sp|P61204|ARF3_HUMA	ARF3	0.000628733
310	2	sp|Q92544|TM9S4_HUN	TM9SF4	0.000628733
311	2	sp|P62753|RS6_HUMAN	RPS6	0.000628733
312	2	sp|P23142-4|FBLN1_HUM	FBLN1	0.000628733
313	2	sp|P54709|AT1B3_HUM	ATP1B3	0.000628733
314	2	sp|Q96AC1|FERM2_HUN	FERMT2	0.000628733
315	2	sp|P01892|1A02_HUMA	HLA-A	0.000628733
316	2	sp|Q07020|RL18_HUMA	RPL18	0.000628733
317	2	sp|P10301|RRAS_HUMA	RRAS	0.000628733
318	2	sp|P62834|RAP1A_HUM	RAP1A	0.000628733
319	2	sp|P62879|GBB2_HUMA	GNB2	0.000628733
320	2	sp|P49327|FAS_HUMAN	FASN	0.000628733
321	2	sp|Q16555|DPYL2_HUM	DPYSL2	0.000628733
322	2	sp|P34932|HSP74_HUM	HSPA4	0.000628733
323	2	sp|O00231|PSD11_HUM	PSMD11	0.000628733
324	2	sp|P11166|GTR3_HUMA	SLC2A1	0.000628733
325	2	sp|Q9C0H2|TTYH3_HUN	TTYH3	0.000628733
326	2	sp|Q99536|VAT1_HUMA	VAT1	0.000628733
327	2	sp|P27635|RL10_HUMA	RPL10	0.000628733
328	2	sp|Q5D862|FILA2_HUM	FLG2	0.000628733
329	2	sp|Q9Y4L1|HYDU1_HUN	HYDU1	0.000628733
330	2	sp|P02792|FRIL_HUMAN	FTL	0.000628733
331	2	sp|Q04917|1433F_HUM	YWHAH	0.000628733
332	2	sp|P14625|ENPL_HUMA	HSP90B1	0.000628733
333	2	sp|Q9BUF5|TBB6_HUMA	TUBB6	0.000628733
334	2	sp|P62195|PRS8_HUMA	PSMC5	0.000628733
335	2	sp|Q96P63|SPB12_HUM	SERPINB12	0.000628733
336	2	sp|P04259|K2C6B_HUM	KRT6B	0.000628733
337	2	sp|Q96QA5|GSDMA_HU	GSDMA	0.000628733
338	2	sp|P02538|K2C6A_HUM	KRT6A	0.000628733
339	2	sp|P23526|SAHH_HUMA	AHCY	0.000628733
340	2	sp|P05997|CO5A2_HUM	COL5A2	0.000628733
341	2	sp|Q02543|RL18A_HUM	RPL18A	0.000628733
342	2	sp|P22090|RS4Y1_HUMA	RPS4Y1	0.000628733
343	2	sp|P05106|ITB3_HUMA	ITGB3	0.000628733
344	2	sp|Q00341|VIGLN_HUM	HDLBP	0.000628733
345	2	sp|P11234|RALB_HUMA	RALB	0.000628733
346	2	sp|P83731|RL24_HUMA	RPL24	0.000628733
347	2	sp|Q99816|TS101_HUM	TSG101	0.000628733
348	2	sp|O60812|HNRC1_HUN	HNRNPC1	0.000628733
349	2	sp|P54136|SYRC_HUMA	RARS	0.000628733
350	2	sp|P23284|PPIB_HUMAN	PPIB	0.000628733
351	2	sp|P06576|ATPB_HUMA	ATP5B	0.000628733
352	2	sp|P05121|PAI1_HUMAN	SERPINE1	0.000628733
353	2	sp|Q8NG11|TSN14_HUN	TSPAN14	0.000628733
354	2	sp|O95980|RECK_HUMA	RECK	0.000628733
355	2	sp|O75340|PDCD6_HUN	PDCD6	0.000628733
356	2	sp|P02753|RET4_HUMA	RBP4	0.000628733
357	2	sp|P02786|TFR1_HUMA	TFRC	0.000628733
358	2	sp|P05109|S10A8_HUM	S100A8	0.000628733
359	2	sp|P61106|RAB14_HUM	RAB14	0.000628733
360	2	sp|P39059|COFA1_HUM	COL15A1	0.000628733
361	2	sp|P10412|H14_HUMAN	HIST1H1E	0.000628733
362	2	sp|P10599|THIO_HUMA	TXN	0.000628733

271	3	sp|Q9NZN4|EHD2_HUMAN	EHD2	0.000862813
272	3	sp|Q99584|S10AD_HUMAN	S100A13	0.000862813
273	3	sp|P30101|PDIA3_HUMAN	PDIA3	0.000862813
274	3	sp|P29317|EPHA2_HUMAN	EPHA2	0.000862813
275	3	sp|Q9UKX5|ITA11_HUMAN	ITGA11	0.000862813
276	3	sp|P30626|SORCN_HUMAN	SRI	0.000862813
277	3	sp|P31946|1433B_HUMAN	YWHAB	0.000862813
278	3	sp|Q99805|TM9S2_HUMAN	TM9SF2	0.000862813
279	3	sp|Q9Y262|EIF3L_HUMAN	EIF3L	0.000862813
280	3	sp|Q9NVM1|EVA1B_HUMAN	EVA1B	0.000862813
281	3	sp|Q15369|ELOC_HUMAN	TCEB1	0.000862813
282	3	sp|Q93052|LPP_HUMAN	LPP	0.000862813
283	3	sp|O00161|SNP23_HUMAN	SNAP23	0.000862813
284	3	sp|P62158|CALM_HUMAN	CALM1	0.000862813
285	3	sp|P31944|CASPE_HUMAN_	CASP14	0.000862813
286	3	sp|Q6NZI2|PTRF_HUMAN	PTRF	0.000862813
287	3	sp|P51149|RAB7A_HUMAN	RAB7A	0.000862813
288	3	sp|P09543|CN37_HUMAN	CNP	0.000862813
289	3	sp|P02786|TFR1_HUMAN	TFRC	0.000862813
290	3	sp|Q99536|VAT1_HUMAN	VAT1	0.000862813
291	3	sp|P14543|NID1_HUMAN	NID1	0.000862813
292	3	sp|Q16555|DPYL2_HUMAN	DPYSL2	0.000862813
293	3	sp|P25789|PSA4_HUMAN	PSMA4	0.000862813
294	3	sp|P15153|RAC2_HUMAN	RAC2	0.000862813
295	3	sp|Q96TA1|NIBL1_HUMAN	FAM129B	0.000862813
296	3	sp|P83731|RL24_HUMAN	RPL24	0.000862813
297	3	sp|P46777|RL5_HUMAN	RPL5	0.000862813
298	3	sp|P32119|PRDX2_HUMAN	PRDX2	0.000862813
299	3	sp|P12107|CO8A1_HUMAN	COL11A1	0.000862813
300	3	sp|P62851|RS25_HUMAN	RPS25	0.000862813
301	3	sp|P46781|RS9_HUMAN	RPS9	0.000862813
302	3	sp|P63167|DYL1_HUMAN	DYNLL1	0.000862813
303	3	sp|Q96597|MYADM_HUMAN	MYADM	0.000862813
304	3	sp|Q9P273|TEN3_HUMAN	TENM3	0.000862813
305	3	sp|P18669|PGAM1_HUMAN	PGAM1	0.000862813
306	3	sp|Q9Y625|GPC6_HUMAN	GPC6	0.000862813
307	2	sp|O14828|SCAM3_HUMAN	SCAMP3	0.000575209
308	2	sp|P49006|MRP_HUMAN	MARCKSL1	0.000575209
309	2	sp|P17655|CAN2_HUMAN	CAPN2	0.000575209
310	2	sp|Q86Y23|HORN_HUMAN_	HRNR	0.000575209
311	2	sp|Q9UBG0|MRC2_HUMAN	MRC2	0.000575209
312	2	sp|P04908|H2A1B_HUMAN	HIST1H2AB	0.000575209
313	2	sp|Q9Y4K0|LOXL2_HUMAN	LOXL2	0.000575209
314	2	sp|P20618|PSB1_HUMAN	PSMB1	0.000575209
315	2	sp|Q05682|CALD1_HUMAN	CALD1	0.000575209
316	2	sp|P09211|GSTP1_HUMAN	GSTP1	0.000575209
317	2	sp|P81605|DCD_HUMAN_co	DCD	0.000575209
318	2	sp|Q9H4G4|GAPR1_HUMAN	GLIPR2	0.000575209
319	2	sp|Q14974|IMB1_HUMAN	KPNB1	0.000575209
320	2	sp|Q969P0|IGSF8_HUMAN	IGSF8	0.000575209
321	2	sp|P01033|TIMP1_HUMAN	TIMP1	0.000575209
322	2	sp|P46782|RS5_HUMAN	RPS5	0.000575209
323	2	sp|P54709|AT1B3_HUMAN	ATP1B3	0.000575209
324	2	sp|Q14192|FHL2_HUMAN	FHL2	0.000575209
325	2	sp|P62917|RL8_HUMAN	RPL8	0.000575209
326	2	sp|P00734|THRB_HUMAN	F2	0.000575209
327	2	sp|P51991|ROA3_HUMAN	HNRNPA3	0.000575209
328	2	sp|P43007|SATT_HUMAN	SLC1A4	0.000575209
329	2	sp|P30086|PEBP1_HUMAN	PEBP1	0.000575209
330	2	sp|P37802|TAGL2_HUMAN	TAGLN2	0.000575209
331	2	sp|Q07020|RL18_HUMAN	RPL18	0.000575209
332	2	sp|P29401|TKT_HUMAN	TKT	0.000575209
333	2	sp|O95183|VAMP5_HUMAN	VAMP5	0.000575209
334	2	sp|Q7Z7G0|TARSH_HUMAN	ABI3BP	0.000575209
335	2	sp|P31939|PUR9_HUMAN	ATIC	0.000575209
336	2	sp|Q14195|DPYL3_HUMAN	DPYSL3	0.000575209
337	2	sp|Q9P121|NTRI_HUMAN	NTM	0.000575209
338	2	sp|Q92629|SGCD_HUMAN	SGCD	0.000575209
339	2	sp|P62879|GBB2_HUMAN	GNB2	0.000575209
340	2	sp|P61026|RAB10_HUMAN	RAB10	0.000575209
341	2	sp|P14868|SYDC_HUMAN	DARS	0.000575209
342	2	sp|O15126|SCAM1_HUMAN	SCAMP1	0.000575209
343	2	sp|P15559|NQO1_HUMAN	NQO1	0.000575209
344	2	sp|P14649|MYL6B_HUMAN	MYL6B	0.000575209
345	2	sp|P16989|YBOX3_HUMAN	YBX3	0.000575209
346	2	sp|P62913|RL11_HUMAN	RPL11	0.000575209
347	2	sp|P61158|ARP3_HUMAN	ACTR3	0.000575209
348	2	sp|P07195|LDHB_HUMAN	LDHB	0.000575209
349	2	sp|Q5D862|FILA2_HUMAN_	FLG2	0.000575209
350	2	sp|Q13683|ITA7_HUMAN	ITGA7	0.000575209
351	2	sp|P11166|GTR1_HUMAN	SLC2A1	0.000575209
352	2	sp|P23284|PPIB_HUMAN	PPIB	0.000575209
353	2	sp|P31150|GDIA_HUMAN	GDI1	0.000575209
354	2	sp|O15143|ARC1B_HUMAN	ARPC1B	0.000575209
355	2	sp|P61204|ARF3_HUMAN	ARF3	0.000575209
356	2	sp|P26639|SYTC_HUMAN	TARS	0.000575209
357	2	sp|P61019|RAB2A_HUMAN	RAB2A	0.000575209
358	2	sp|Q9UBI6|GBG12_HUMAN	GNG12	0.000575209
359	2	sp|Q15365|PCBP1_HUMAN	PCBP1	0.000575209
360	2	sp|Q9Y315|DEOC_HUMAN	DERA	0.000575209
361	2	sp|A6NIZ1|RP1BL_HUMAN	RP1BL	0.000575209
362	2	sp|P10909|CLUS_HUMAN	CLU	0.000575209

Chapter 5: Figure 7 Supplementary Table 1 (Page 5 of 8)

All protein hits from proteomic analysis of the R10 media alone and exosomes derived from Irradiated or Noni-Irradiated MSCs. Greyed-out proteins indicate low-abundance proteins that were excluded in downstream bioinformatic analyses.

363	2	sp|P53621|COPA_HUMA	COPA	0.000628733
364	2	sp|P48643|TCPE_HUMA	CCT5	0.000628733
365	2	sp|P11940|PABP1_HUM	PABPC1	0.000628733
366	2	sp|O75223|GGCT_HUM	GGCT	0.000628733
367	2	sp|P18085|ARF4_HUMA	ARF4	0.000628733
368	2	sp|P07339|CATD_HUMA	CTSD	0.000628733
369	2	sp|P36578|RL4_HUMAN	RPL4	0.000628733
370	2	sp|O00244|ATOX1_HUM	ATOX1	0.000628733
371	2	sp|P62851|RS25_HUMA	RPS25	0.000628733
372	2	sp|P02656|APOC3_HUM	APOC3	0.000628733
373	2	sp|P28070|PSB4_HUMA	PSMB4	0.000628733
374	2	sp|P30086|PEBP1_HUM	PEBP1	0.000628733
375	2	sp|P09496-2|CLCA_HUM	CLTA	0.000628733
376	2	sp|P67809|YBOX1_HUM	YBX1	0.000628733
377	2	sp|P63167|DYL1_HUMA	DYNLL1	0.000628733
378	2	sp|Q13554|KCC2B_HUM	CAMK2B	0.000628733
379	2	sp|P53801|PTTG_HUMA	PTTG1IP	0.000628733
380	2	tr|F5H7N9|F5H7N9_HUM	MFGE8	0.000628733
381	2	sp|P21980|TGM2_HUMA	TGM2	0.000628733
382	2	sp|Q6RW13|ATRAP_HUM	AGTRAP	0.000628733
383	2	sp|Q7KZF4|SND1_HUMA	SND1	0.000628733
384	2	sp|P01033|TIMP1_HUM	TIMP1	0.000628733
385	2	sp|P04632|CPN51_HUM	CAPNS1	0.000628733
386	2	sp|O95183|VAMP5_HUM	VAMP5	0.000628733
387	2	sp|Q93052|LPP_HUMAN	LPP	0.000628733
388	2	sp|P20742|PZP_HUMAN	PZP	0.000628733
389	2	sp|Q8IZB3|A16A1_HUM	ALDH16A1	0.000628733
390	2	sp|P62910|RL32_HUMA	RPL32	0.000628733
391	2	sp|P00734|THRB_HUMA	F2	0.000628733
392	2	sp|Q9Y625|GPC6_HUMA	GPC6	0.000628733
393	2	sp|P84098|RL19_HUMA	RPL19	0.000628733
394	2	sp|P62316|SMD2_HUMA	SNRPD2	0.000628733
395	2	sp|P61313|RL15_HUMA	RPL15	0.000628733
396	2	sp|Q15286|RAB35_HUM	RAB35	0.000628733
397	2	sp|P63027|VAMP2_HUM	VAMP2	0.000628733
398	2	sp|P41252|SYIC_HUMAN	IARS	0.000628733
399	2	sp|P22234|PURG_HUMA	PAICS	0.000628733
400	2	sp|P30041|PRDX6_HUM	PRDX6	0.000628733
401	2	sp|Q9UNM6|PSD13_HUM	PSMD13	0.000628733
402	2	sp|Q86Y23|HORN_HUM	HRNR	0.000628733
403	2	sp|Q14108|SCRB2_HUM	SCARB2	0.000628733
404	2	sp|Q9Y4K0|LOXL2_HUM	LOXL2	0.000628733
405	2	sp|P22531|SPR2E_HUMA	SPRR2E	0.000628733
406	2	sp|P49773|HINT1_HUMA	HINT1	0.000628733
407	2	sp|P50991|TCPD_HUMA	CCT4	0.000628733
408	2	sp|Q13443|ADAM9_HUM	ADAM9	0.000628733
409	2	sp|P46776|RL27A_HUM	RPL27A	0.000628733
410	2	sp|P25705|ATPA_HUMA	ATP5A1	0.000628733
411	1	sp|Q08188|TGM3_HUM	TGM3	0.000314367
412	1	sp|Q9NZT1|CALL5_HUM	CALML5	0.000314367
413	1	sp|Q96597|MYADM_HU	MYADM	0.000314367
414	1	sp|Q9UGM3|DMBT1_HU	DMBT1	0.000314367
415	1	sp|P05534|1A24_HUMA	HLA-A	0.000314367
416	1	sp|P07477|TRY1_HUMA	PRSS1	0.000314367
417	1	sp|P16104|H2AX_HUMA	H2AFX	0.000314367
418	1	sp|P51884|LUM_HUMAN	LUM	0.000314367
419	1	sp|P09972|ALDOC_HUM	ALDOC	0.000314367
420	1	sp|P04004|VTNC_HUMA	VTN	0.000314367
421	1	sp|O15127|SCAM2_HUM	SCAMP2	0.000314367
422	1	sp|P01893|HLAH_HUMA	HLA-H	0.000314367
423	1	sp|P02794|FRIH_HUMA	FTH1	0.000314367
424	1	sp|Q9Y262|EIF3L_HUMA	EIF3L	0.000314367
425	1	sp|P35241|RADI_HUMA	RDX	0.000314367
426	1	sp|P62079|TSN5_HUMA	TSPAN5	0.000314367
427	1	sp|P17980|PRS6A_HUM	PSMC3	0.000314367
428	1	sp|P35998|PRS7_HUMA	PSMC2	0.000314367
429	1	sp|P61981|1433G_HUM	YWHAG	0.000314367
430	1	sp|P06748|NPM_HUMA	NPM1	0.000314367
431	1	sp|P02647|APOA1_HUM	APOA1	0.000314367
432	1	sp|P16035|TIMP2_HUM	TIMP2	0.000314367
433	1	sp|O43657|TSN6_HUMA	TSPAN6	0.000314367
434	1	sp|P24534|EF1B_HUMA	EEF1B2	0.000314367
435	1	sp|P47756|CAPZB_HUM	CAPZB	0.000314367
436	1	sp|P62191|PRS4_HUMA	PSMC1	0.000314367
437	1	sp|P06744|G6PI_HUMA	GPI	0.000314367
438	1	sp|Q16832|DDR2_HUM	DDR2	0.000314367
439	1	sp|Q15043|S39AE_HUM	SLC39A14	0.000314367
440	1	sp|Q9ULC3|RAB23_HUM	RAB23	0.000314367
441	1	sp|P02787|TRFE_HUMA	TF	0.000314367
442	1	sp|A0M8Q6|LAC7_HUM	IGLC7	0.000314367
443	1	sp|P40925|MDHC_HUM	MDH1	0.000314367
444	1	sp|O14817|TSN4_HUMA	TSPAN4	0.000314367
445	1	sp|Q9UBI6|GBG12_HUM	GNG12	0.000314367
446	1	sp|O95218|ZRAB2_HUM	ZRANB2	0.000314367
447	1	sp|P61626|LYSC_HUMAN	LYZ	0.000314367
448	1	sp|Q92819|HYAS2_HUMA	HAS2	0.000314367
449	1	sp|P11413|G6PD_HUMA	G6PD	0.000314367
450	1	sp|Q6ZVX7|FBXS0_HUM	NCCRP1	0.000314367
451	1	sp|P13164|IFM1_HUMA	IFITM1	0.000314367
452	1	sp|Q9H1J7|WNT5B_HUM	WNT5B	0.000314367
453	1	sp|P31949|S10AB_HUM	S100A11	0.000314367
454	1	sp|Q9H444|CHM4B_HU	CHMP4B	0.000314367

363	2	sp|P49591|SYSC_HUMAN	SARS	0.000575209
364	2	sp|O95980|RECX_HUMAN	RECK	0.000575209
365	2	sp|Q92544|TM9S4_HUMAN	TM9SF4	0.000575209
366	2	sp|P10124|SRGN_HUMAN	SRGN	0.000575209
367	2	sp|Q15436|SC23A_HUMAN	SEC23A	0.000575209
368	2	sp|Q9Y639|NPTN_HUMAN	NPTN	0.000575209
369	2	sp|P18084|ITB5_HUMAN	ITGB5	0.000575209
370	2	sp|O75340|PDCD6_HUMAN	PDCD6	0.000575209
371	2	sp|Q9Y265|RUVB1_HUMAN	RUVBL1	0.000575209
372	2	sp|P18124|RL7_HUMAN	RPL7	0.000575209
373	2	sp|P50914|RL14_HUMAN	RPL14	0.000575209
374	2	sp|Q00341|VIGLN_HUMAN	HDLBP	0.000575209
375	2	sp|O14979|HNRDL_HUMAN	HNRNPDL	0.000575209
376	2	sp|Q14108|SCRB2_HUMAN	SCARB2	0.000575209
377	2	sp|P46776|RL27A_HUMAN	RPL27A	0.000575209
378	2	sp|P60953|CDC42_HUMAN	CDC42	0.000575209
379	2	sp|P12273|PIP_HUMAN	PIP	0.000575209
380	2	sp|P29692|EF1D_HUMAN	EEF1D	0.000575209
381	2	sp|P62888|RL30_HUMAN	RPL30	0.000575209
382	2	sp|P35998|PRS7_HUMAN	PSMC2	0.000575209
383	2	sp|P27635|RL10_HUMAN	RPL10	0.000575209
384	2	sp|O60812|HNRCL_HUMAN	HNRNPCL1	0.000575209
385	2	sp|P08962|CD63_HUMAN	CD63	0.000575209
386	2	sp|O15427|MOT4_HUMAN	SLC16A3	0.000575209
387	2	sp|P27824|CALX_HUMAN	CANX	0.000575209
388	2	sp|P62266|RS23_HUMAN	RPS23	0.000575209
389	2	sp|P16035|TIMP2_HUMAN	TIMP2	0.000575209
390	2	sp|Q8WUJ3|K1199_HUMAN	KIAA1199	0.000575209
391	2	sp|Q15942|ZYX_HUMAN	ZYX	0.000575209
392	2	sp|Q92734|TFG_HUMAN	TFG	0.000575209
393	2	sp|Q8N1N4|K2C7B_HUMAN	KRT7B	0.000575209
394	2	sp|P47756|CAPZB_HUMAN	CAPZB	0.000575209
395	2	sp|Q12805|FBLN3_HUMAN	EFEMP1	0.000575209
396	2	sp|P11234|RALB_HUMAN	RALB	0.000575209
397	2	sp|Q16270|IBP7_HUMAN	IGFBP7	0.000575209
398	2	sp|P25786|PSA1_HUMAN	PSMA1	0.000575209
399	2	sp|P06744|G6PI_HUMAN	GPI	0.000575209
400	2	sp|P02042|HBD_HUMAN	HBD	0.000575209
401	2	sp|P46778|RL21_HUMAN	RPL21	0.000575209
402	2	sp|P61353|RL27_HUMAN	RPL27	0.000575209
403	2	sp|P61225|RAP2B_HUMAN	RAP2B	0.000575209
404	2	sp|P15924|DESP_HUMAN_o	DSP	0.000575209
405	2	sp|P06748|NPM_HUMAN	NPM1	0.000575209
406	2	sp|P07237|PDIA1_HUMAN	P4HB	0.000575209
407	2	sp|Q10472|GALT1_HUMAN	GALNT1	0.000575209
408	2	sp|P08648|ITA5_HUMAN	ITGA5	0.000575209
409	2	sp|P10412|H14_HUMAN	HIST1H1E	0.000575209
410	2	sp|P22626|ROA2_HUMAN	HNRNPA2B1	0.000575209
411	2	sp|P41252|SYIC_HUMAN	IARS	0.000575209
412	2	sp|P01892|1A02_HUMAN	HLA-A	0.000575209
413	2	sp|P00441|SODC_HUMAN	SOD1	0.000575209
414	2	sp|Q99439|CNN2_HUMAN	CNN2	0.000575209
415	2	sp|P09525|ANXA4_HUMAN	ANXA4	0.000575209
416	2	sp|Q04756|HGFA_HUMAN	HGFAC	0.000575209
417	2	sp|P60228|EIF3E_HUMAN	EIF3E	0.000575209
418	2	sp|O15511|ARPC5_HUMAN	ARPC5	0.000575209
419	2	sp|P46779|RL28_HUMAN	RPL28	0.000575209
420	2	sp|P62249|RS16_HUMAN	RPS16	0.000575209
421	2	sp|P48643|TCPE_HUMAN	CCT5	0.000575209
422	2	sp|Q9Y230|RUVB2_HUMAN	RUVBL2	0.000575209
423	2	sp|P61769|B2MG_HUMAN	B2M	0.000575209
424	2	sp|P25398|RS12_HUMAN	RPS12	0.000575209
425	2	sp|P41091|IF2G_HUMAN	EIF2S3	0.000575209
426	2	sp|P62333|PRS10_HUMAN	PSMC6	0.000575209
427	2	sp|P22090|RS4Y1_HUMAN	RPS4Y1	0.000575209
428	2	sp|P15531|NDKA_HUMAN	NME1	0.000575209
429	2	sp|P05186|PPBT_HUMAN	ALPL	0.000575209
430	2	sp|P05534|1A24_HUMAN	HLA-A	0.000575209
431	2	sp|P62191|PRS4_HUMAN	PSMC1	0.000575209
432	2	sp|P11233|RALA_HUMAN	RALA	0.000575209
433	2	sp|P21980|TGM2_HUMAN	TGM2	0.000575209
434	2	sp|Q9H223|EHD4_HUMAN	EHD4	0.000575209
435	2	sp|P02656|APOC3_HUMAN	APOC3	0.000575209
436	2	sp|P26232|CTNA2_HUMAN	CTNNA2	0.000575209
437	2	sp|Q92819|HYAS2_HUMAN	HAS2	0.000575209
438	2	sp|P26641|EF1G_HUMAN	EEF1G	0.000575209
439	2	sp|Q98RK5|CAB45_HUMAN	SDF4	0.000575209
440	2	sp|P13497|BMP1_HUMAN	BMP1	0.000575209
441	2	sp|Q9Y224|CN166_HUMAN	C14orf166	0.000575209
442	2	sp|P09496-2|CLCA_HUMAN	CLTA	0.000575209
443	2	sp|Q99497|PARK7_HUMAN	PARK7	0.000575209
444	2	sp|P62910|RL32_HUMAN	RPL32	0.000575209
445	2	sp|P67809|YBOX1_HUMAN	YBX1	0.000575209
446	2	sp|P58546|MTPN_HUMAN	MTPN	0.000575209
447	2	sp|O75487|GPC4_HUMAN	GPC4	0.000575209
448	2	sp|P61313|RL15_HUMAN	RPL15	0.000575209
449	2	sp|P67870|CSK2B_HUMAN	CSNK2B	0.000575209
450	2	sp|P02458|CO2A1_HUMAN	COL2A1	0.000575209
451	2	sp|P00736|C1R_HUMAN	C1R	0.000575209
452	2	sp|P50148|GNAQ_HUMAN	GNAQ	0.000575209
453	2	sp|Q04941|PLP2_HUMAN	PLP2	0.000575209
454	2	sp|A6ND8|RB43L_HUMAN	RB43L	0.000575209

Chapter 5: Figure 7 Supplementary Table 1 (Page 6 of 8)

All protein hits from proteomic analysis of the R10 media alone and exosomes derived from Irradiated or Noni-Irradiated MSCs. Greyed-out proteins indicate low-abundance proteins that were excluded in downstream bioinformatic analyses.

455	1	sp|P51149|RAB7A_HUM	RAB7A	0.000314367
456	1	tr|H7C2F2|H7C2F2_HUM	CD99	0.000314367
457	1	sp|P40926|MDHM_HUM	MDH2	0.000314367
458	1	sp|Q9BQE3|TBA1C_HUM	TUBA1C	0.000314367
459	1	sp|Q13263|TIF1B_HUM	TRIM28	0.000314367
460	1	sp|P51991|ROA3_HUM	HNRNPA3	0.000314367
461	1	sp|Q8N1N4|K2C78_HUM	KRT78	0.000314367
462	1	sp|O75367|H2AY_HUM	H2AFY	0.000314367
463	1	sp|P29323|EPHB2_HUM	EPHB2	0.000314367
464	1	sp|P14866|HNRPL_HUM	HNRNPL	0.000314367
465	1	sp|P02788|TRFL_HUM	LTF	0.000314367
466	1	sp|Q15063-3|POSTN_HU	POSTN	0.000314367
467	1	sp|P62913|RL11_HUM	RPL11	0.000314367
468	1	sp|Q8IVS2|FABD_HUM	MCAT	0.000314367
469	1	sp|P29992|GNA11_HUM	GNA11	0.000314367
470	1	sp|P58546|MTPN_HUM	MTPN	0.000314367
471	1	sp|P18065|IBP2_HUM	IGFBP2	0.000314367
472	1	sp|P62979|RS27A_HUM	RPS27A	0.000314367
473	1	sp|P19827|ITIH1_HUM	ITIH1	0.000314367
474	1	sp|O43242|PSMD3_HUM	PSMD3	0.000314367
475	1	sp|P18621|RL17_HUM	RPL17	0.000314367
476	1	sp|Q9P273|TEN3_HUM	TENM3	0.000314367
477	1	sp|B5ME19|EIF3L_HUM	EIF3CL	0.000314367
478	1	sp|P16989|YBOX3_HUM	YBX3	0.000314367
479	1	sp|Q9UIQ6|LCAP_HUM	LNPEP	0.000314367
480	1	sp|Q9UNH7|SNX6_HUM	SNX6	0.000314367
481	1	sp|P37802|TAGL2_HUM	TAGLN2	0.000314367
482	1	sp|P62917|RL8_HUMAN	RPL8	0.000314367
483	1	sp|P34741|SDC2_HUMA	SDC2	0.000314367
484	1	sp|Q9H9H4|VP37B_HUM	VPS37B	0.000314367
485	1	sp|Q92734|TFG_HUMAN	TFG	0.000314367
486	1	sp|Q14103|HNRPD_HUM	HNRNPD	0.000314367
487	1	sp|Q3SYB4|K2C71_HUM	KRT71	0.000314367
488	1	sp|Q9NVA2|SEP11_HUM	SEP11	0.000314367
489	1	sp|P55290|CAD13_HUM	CDH13	0.000314367
490	1	sp|P14543|NID1_HUMA	NID1	0.000314367
491	1	sp|P07093-2|GDN_HUM	SERPINE2	0.000314367
492	1	sp|P47755|CAZA2_HUM	CAPZA2	0.000314367
493	1	sp|P46778|RL21_HUMA	RPL21	0.000314367
494	1	sp|P05386|RLA1_HUMA	RPLP1	0.000314367
495	1	sp|Q01813|6PFP_HUMA	PFKP	0.000314367
496	1	sp|P61163|ACT2_HUMA	ACTR1A	0.000314367
497	1	sp|P19338|NUCL_HUMAN	NCL	0.000314367
498	1	sp|O15365|PCBP1_HUM	PCBP1	0.000314367
499	1	sp|Q9P121|NTRI_HUMAN	NTM	0.000314367
500	1	sp|P60981|DEST_HUMA	DSTN	0.000314367
501	1	sp|Q99439|CNN2_HUM	CNN2	0.000314367
502	1	sp|P47914|RL29_HUMA	RPL29	0.000314367
503	1	sp|P62906|RL10A_HUM	RPL10A	0.000314367
504	1	sp|P27449|VATL_HUMA	ATP6V0C	0.000314367
505	1	sp|Q16270|IBP7_HUMA	IGFBP7	0.000314367
506	1	sp|O43852|CALU_HUM	CALU	0.000314367
507	1	sp|Q13813|SPTN1_HUM	SPTAN1	0.000314367
508	1	sp|Q13748|TBA3C_HUM	TUBA3C	0.000314367
509	1	sp|Q12805|FBLN3_HUM	EFEMP1	0.000314367
510	1	sp|P51153|RAB13_HUM	RAB13	0.000314367
511	1	sp|P49257|LMAN1_HUM	LMAN1	0.000314367
512	1	sp|P00736|C1R_HUMAN	C1R	0.000314367
513	1	sp|P38117|ETFB_HUMA	ETFB	0.000314367
514	1	sp|P27824|CALX_HUMA	CANX	0.000314367
515	1	sp|O43491|E41L2_HUM	EPB41L2	0.000314367
516	1	sp|Q13155|AIMP2_HUM	AIMP2	0.000314367
517	1	sp|P08697|A2AP_HUMA	SERPINF2	0.000314367
518	1	sp|P63000|RAC1_HUMA	RAC1	0.000314367
519	1	sp|O95837|GNA14_HUM	GNA14	0.000314367
520	1	sp|O15126|SCAM1_HUM	SCAMP1	0.000314367
521	1	sp|O60506|HNRPQ_HUM	SYNCRIP	0.000314367
522	1	sp|P62158|CALM_HUM	CALM1	0.000314367
523	1	sp|P26927|HGFL_HUMA	MST1	0.000314367
524	1	sp|P09525|ANXA4_HUM	ANXA4	0.000314367
525	1	sp|P52943|CRIP2_HUM	CRIP2	0.000314367
526	1	sp|P49755|TMED8A_HUM	TMED10	0.000314367
527	1	sp|P15153|RAC2_HUMA	RAC2	0.000314367
528	1	sp|Q86VP6|CAND1_HUM	CAND1	0.000314367
529	1	sp|Q96TA1|NIBL1_HUM	FAM129B	0.000314367
530	1	sp|P01040|CYTA_HUMA	CSTA	0.000314367
531	1	sp|O10588|BST1_HUMA	BST1	0.000314367
532	1	sp|Q14520|HABP2_HUM	HABP2	0.000314367
533	1	sp|A6NDJ8|RB43L_HUM	RB43L	0.000314367
534	1	sp|P18669|PGAM1_HUM	PGAM1	0.000314367
535	1	sp|Q99829|CPNE1_HUM	CPNE1	0.000314367
536	1	sp|Q12860|CNTN1_HUM	CNTN1	0.000314367
537	1	sp|P07951-2|TPM2_HUM	TPM2	0.000314367
538	1	sp|O00469|PLOD2_HUM	PLOD2	0.000314367
539	1	sp|P52565|GDIR1_HUM	ARHGDIA	0.000314367
540	1	sp|P51148|RAB5C_HUM	RAB5C	0.000314367
541	1	sp|Q13200|PSMD2_HUM	PSMD2	0.000314367
542	1	sp|Q9NRX5|SERC1_HUM	SERINC1	0.000314367
543	1	sp|P62854|RS26_HUMA	RPS26	0.000314367
544	1	sp|P60953|CDC42_HUM	CDC42	0.000314367
545	1	sp|P01344|IGF2_HUMAN	IGF2	0.000314367
546	1	sp|P22626|ROA2_HUM	HNRNPA2B	0.000314367

455	2	sp|P62834|RAP1A_HUMAN	RAP1A	0.000575209
456	2	sp|O43795|MYO1B_HUMAN	MYO1B	0.000575209
457	2	sp|P40121|CAPG_HUMAN	CAPG	0.000575209
458	2	sp|P62750|RL23A_HUMAN	RPL23A	0.000575209
459	2	sp|O95197|RTN3_HUMAN	RTN3	0.000575209
460	2	sp|P26583|HMGB2_HUMAN	HMGB2	0.000575209
461	1	sp|P01834|IGKC_HUMAN	IGKC	0.000287604
462	1	sp|P84157|MXRA7_HUMAN	MXRA7	0.000287604
463	1	sp|P20073|ANXA7_HUMAN	ANXA7	0.000287604
464	1	sp|O95967|FBLN4_HUMAN	EFEMP2	0.000287604
465	1	sp|P28070|PSB4_HUMAN	PSMB4	0.000287604
466	1	sp|Q5T749|KPRP_HUMAN_c	KPRP	0.000287604
467	1	sp|Q9ULC3|RAB23_HUMAN	RAB23	0.000287604
468	1	sp|P05386|RLA1_HUMAN	RPLP1	0.000287604
469	1	sp|Q9NRY6|PLS3_HUMAN	PLSCR3	0.000287604
470	1	sp|P63241|IF5A1_HUMAN	EIF5A	0.000287604
471	1	sp|P57721|PCBP3_HUMAN	PCBP3	0.000287604
472	1	sp|P28066|PSA5_HUMAN	PSMA5	0.000287604
473	1	sp|Q13557|KCC2D_HUMAN	CAMKK2D	0.000287604
474	1	sp|P09972|ALDOC_HUMAN	ALDOC	0.000287604
475	1	sp|P78324|SHPS1_HUMAN	SIRPA	0.000287604
476	1	sp|P02794|FRIH_HUMAN	FTH1	0.000287604
477	1	sp|Q6DD88|ATL3A3_HUMAN	ATL3	0.000287604
478	1	sp|Q15043|S39AE_HUMAN	SLC39A14	0.000287604
479	1	sp|P84098|RL19_HUMAN	RPL19	0.000287604
480	1	sp|Q13509|TBB3_HUMAN	TUBB3	0.000287604
481	1	sp|P04632|CPNS1_HUMAN	CAPNS1	0.000287604
482	1	tr|H7BZJ3|H7BZJ3_HUMAN	PDIA3	0.000287604
483	1	sp|Q13554|KCC2B_HUMAN	CAMK2B	0.000287604
484	1	sp|P27797|CALR_HUMAN	CALR	0.000287604
485	1	sp|P40925|MDHC_HUMAN	MDH1	0.000287604
486	1	sp|Q01970|PLCB3_HUMAN	PLCB3	0.000287604
487	1	sp|P17858|K6PL_HUMAN	PFKL	0.000287604
488	1	sp|P01893|HLAH_HUMAN	HLA-H	0.000287604
489	1	sp|P43686|PRS6B_HUMAN	PSMC4	0.000287604
490	1	sp|Q14766|LTBP1_HUMAN	LTBP1	0.000287604
491	1	sp|Q96QD8|S38A2_HUMAN	SLC38A2	0.000287604
492	1	sp|P36871|PGM1_HUMAN	PGM1	0.000287604
493	1	sp|P78527|PRKDC_HUMAN	PRKDC	0.000287604
494	1	sp|P02647|APOA1_HUMAN	APOA1	0.000287604
495	1	sp|Q08554|DSC1_HUMAN_c	DSC1	0.000287604
496	1	sp|P55209|NP1L1_HUMAN	NAP1L1	0.000287604
497	1	sp|P53999|TCP4_HUMAN	SUB1	0.000287604
498	1	sp|P01344|IGF2_HUMAN	IGF2	0.000287604
499	1	sp|Q6RW13|ATRAP_HUMAN	AGTRAP	0.000287604
500	1	sp|Q9H444|CHMP4B_HUMAN	CHMP4B	0.000287604
501	1	sp|P62195|PRS8_HUMAN	PSMC5	0.000287604
502	1	sp|O00468-3|AGRIN_HUMA	AGRIN	0.000287604
503	1	sp|Q969X1|LFG3_HUMAN	TMBIM1	0.000287604
504	1	sp|O43491|E41L2_HUMAN	EPB41L2	0.000287604
505	1	sp|P60660|MYL6_HUMAN	MYL6	0.000287604
506	1	sp|Q9NVD7|PARVA_HUMAN	PARVA	0.000287604
507	1	sp|O43583|DENR_HUMAN	DENR	0.000287604
508	1	sp|P22692|IBP4_HUMAN	IGFBP4	0.000287604
509	1	sp|P61254|RL26_HUMAN	RPL26	0.000287604
510	1	sp|Q15181|IPYR_HUMAN	PPA1	0.000287604
511	1	sp|Q12874|SF3A3_HUMAN	SF3A3	0.000287604
512	1	sp|Q9NZT1|CALL5_HUMAN	CALML5	0.000287604
513	1	sp|P04004|VTNC_HUMAN	VTN	0.000287604
514	1	sp|Q16658|FSCN1_HUMAN	FSCN1	0.000287604
515	1	sp|O75131|CPNE3_HUMAN	CPNE3	0.000287604
516	1	sp|Q9H9H4|VP37B_HUMAN	VPS37B	0.000287604
517	1	sp|P02787|TRFE_HUMAN	TF	0.000287604
518	1	sp|O15400|STX7_HUMAN	STX7	0.000287604
519	1	tr|H7C2F2|H7C2F2_HUMAN	CD99	0.000287604
520	1	sp|P38646|GRP75_HUMAN	HSPA9	0.000287604
521	1	sp|P23142-4|FBLN1_HUMAN	FBLN1	0.000287604
522	1	sp|P49419|AL7A1_HUMAN	ALDH7A1	0.000287604
523	1	sp|P05156|CFAI_HUMAN	CFI	0.000287604
524	1	sp|Q15019|SEPT2_HUMAN	SEPT2	0.000287604
525	1	sp|Q96CW1|AP2M1_HUMAN	AP2M1	0.000287604
526	1	sp|P35241|RADI_HUMAN	RDX	0.000287604
527	1	sp|Q16832|DDR2_HUMAN	DDR2	0.000287604
528	1	sp|P61163|ACT2_HUMAN	ACTR1A	0.000287604
529	1	sp|Q15370|ELOB_HUMAN	TCEB2	0.000287604
530	1	sp|P35606|COPB2_HUMAN	COPB2	0.000287604
531	1	sp|P05090|APOD_HUMAN	APOD	0.000287604
532	1	sp|P62306|RUXF_HUMAN	SNRPF	0.000287604
533	1	sp|P47914|RL29_HUMAN	RPL29	0.000287604
534	1	sp|P24534|EF1B_HUMAN	EEF1B2	0.000287604
535	1	sp|P55060|XPO2_HUMAN	CSE1L	0.000287604
536	1	sp|Q02878|RL6_HUMAN	RPL6	0.000287604
537	1	sp|P45974|UBP5_HUMAN	USP5	0.000287604
538	1	sp|P47755|CAZA2_HUMAN	CAPZA2	0.000287604
539	1	sp|P11766|ADHX_HUMAN	ADH5	0.000287604
540	1	sp|Q14195-2|DPYL3_HUMAN	DPYSL3	0.000287604
541	1	sp|P00749|UROK_HUMAN	PLAU	0.000287604
542	1	sp|Q99961|SH3G1_HUMAN	SH3GL1	0.000287604
543	1	sp|Q4ZHG4|FNDC1_HUMAN	FNDC1	0.000287604
544	1	sp|P80303|NUCB2_HUMAN	NUCB2	0.000287604
545	1	sp|P61201|CSN2_HUMAN	COPS2	0.000287604
546	1	sp|Q9UBQ7|GRHPR_HUMAN	GRHPR	0.000287604

Chapter 5: Figure 7 Supplementary Table 1 (Page 7 of 8)

All protein hits from proteomic analysis of the R10 media alone and exosomes derived from Irradiated or Noni-Irradiated MSCs. Greyed-out proteins indicate low-abundance proteins that were excluded in downstream bioinformatic analyses.

547	1	sp	Q15417	CNN3_HUMA	CNN3	0.000314367
548	1	sp	P02042	HBD_HUMAN	HBD	0.000314367
549	1	sp	Q969E2	SCAM4_HUM	SCAMP4	0.000314367
550	1	sp	Q01546	K22O_HUMA	KRT76	0.000314367
551	1	sp	O14979	HNRDL_HUM	HNRNPDL	0.000314367
552	1	sp	Q9UBQ7	GRHPR_HUM	GRHPR	0.000314367
553	1	sp	P00740	FA9_HUMAN	F9	0.000314367
554	1	sp	P21291	CSRP1_HUM	CSRP1	0.000314367
555	1	sp	P13804	ETFA_HUMA	ETFA	0.000314367
556	1	sp	Q04941	PLP2_HUMA	PLP2	0.000314367
557	1	sp	O60831	PRAF2_HUM	PRAF2	0.000314367
558	1	sp	P04279	SEMG1_HUM	SEMG1	0.000314367
559	1	sp	Q9UNP9	PPIE_HUMA	PPIE	0.000314367
560	1	sp	Q13867	BLMH_HUM	BLMH	0.000314367
561	1	##sp	Q4G0M1	F1329_H	##FAM132	0.000314367
562	1	sp	Q04756	HGFA_HUMA	HGFAC	0.000314367
563	1	sp	P13591	NCAM1_HUM	NCAM1	0.000314367
564	1	sp	P0CD55	H2A2_HUMA	H2AFZ	0.000314367
565	1	sp	O75131	CPNE3_HUM	CPNE3	0.000314367
566	1	sp	Q4VRL6	TM119_HUM	TMEM119	0.000314367
567	1	sp	Q9Y265	RUVB1_HUM	RUVBL1	0.000314367
568	1	sp	P81605	DCD_HUMAN	DCD	0.000314367
569	1	sp	P10909	CLUS_HUMA	CLU	0.000314367
570	1	sp	P35268	RL22_HUMA	RPL22	0.000314367
571	1	sp	A6NHL2	TBAL3_HUM	TUBAL3	0.000314367
572	1	sp	Q13133-2	NR1H3_HU	NR1H3	0.000314367
573	1	sp	P14174	MIF_HUMAN	MIF	0.000314367
574	1	sp	Q96K17	BTF3L4_HUM	BTF3L4	0.000314367
575	1	sp	P14868	SYDC_HUMA	DARS	0.000314367
576	1	sp	Q9NUP9	LINC7C_HUM	LIN7C	0.000314367
577	1	sp	P28074	PSB5_HUMA	PSMB5	0.000314367
578	1	sp	Q028D9	PLOD1_HUM	PLOD1	0.000314367
579	1	sp	Q04721	NOTC2_HUM	NOTCH2	0.000314367
580	1	sp	Q9NR12	PDLI7_HUM	PDLIM7	0.000314367
581	1	sp	P00491	PNPH_HUMA	PNP	0.000314367
582	1	sp	P09936	UCHL1_HUM	UCHL1	0.000314367
583	1	sp	P11362	FGFR1_HUM	FGFR1	0.000314367
584	1	##tr	H7C2V6	H7C2V6_HUMAN		0.000314367
585	1	sp	O15145	ARPC3_HUM	ARPC3	0.000314367
586	1	##sp	O00219	HYAS3_HU	##HAS3	0.000314367
587	1	sp	P61254	RL26_HUMA	RPL26	0.000314367
588	1	sp	Q96EY5	MB12A_HUM	MVB12A	0.000314367
589	1	sp	Q02878	RL6_HUMAN	RPL6	0.000314367
590	1	sp	O00161	SNP23_HUM	SNAP23	0.000314367
591	1	sp	P62841	RS15_HUMA	RPS15	0.000314367
592	1	sp	Q9Y230	RUVB2_HUM	RUVBL2	0.000314367
593	1	sp	P68431	H31_HUMAN	HIST1H3A	0.000314367
594	1	sp	Q9H3Z4	DNJC5_HUM	DNAJC5	0.000314367
595	1	##sp	Q724N2	TRPM1_H	##TRPM1	0.000314367
596	1	sp	Q15493	RGN_HUMA	RGN	0.000314367
597	1	sp	P15151	PVR_HUMAN	PVR	0.000314367
598	1	sp	P14314	GLU2B_HUM	PRKCSH	0.000314367
599	1	sp	P67870	CSK2B_HUM	CSNK2B	0.000314367
600	1	sp	P01111	RASN_HUM	NRAS	0.000314367
601	1	sp	Q16563	SYPL1_HUM	SYPL1	0.000314367
602	1	sp	P35625	TIMP3_HUM	TIMP3	0.000314367
603	1	sp	O95967	FBLN4_HUM	EFEMP2	0.000314367
604	1	sp	P00441	SODC_HUM	SOD1	0.000314367
605	1	sp	O95445	APOM_HUM	APOM	0.000314367
606	1	sp	P10114	RAP2A_HUM	RAP2A	0.000314367
607	1	sp	Q9NPH3	IL1AP_HUM	IL1RAP	0.000314367
608	1	sp	P08243	ASNS_HUMA	ASNS	0.000314367
609	1	sp	Q14141	SEPT6_HUM	SEPT6	0.000314367
610	1	sp	P61353	RL27_HUMA	RPL27	0.000314367
611	1	sp	O95819	MAK4_HUM	MAPK4	0.000314367
612	1	sp	P26639	SYTC_HUMA	TARS	0.000314367
613	1	sp	O15427	MOT4_HUM	SLC16A3	0.000314367
614	1	sp	Q9UK57	IKZF2_HUM	IKZF2	0.000314367
615	1	sp	P32119	PRDX2_HUM	PRDX2	0.000314367
616	1	sp	P06899	H2B1J_HUM	HIST1H2BJ	0.000314367
617	1	##sp	Q9UL26	RB22A_HU	##RAB22A	0.000314367
618	1	sp	Q14195	DPYL3_HUM	DPYSL3	0.000314367
619	1	sp	Q15942	ZYX_HUMAN	ZYX	0.000314367
620	1	sp	P84103	SRSF3_HUM	SRSF3	0.000314367
621	1	sp	O75695	XRP2_HUM	RP2	0.000314367
622	1	sp	Q9Y4P8	WIP2_HUM	WIPI2	0.000314367
623	1	##tr	E2QRG3	E2QRG3_H	##KIF6	0.000314367

547	1	sp	P22314	UBA1_HUMAN	UBA1	0.000287604
548	1	sp	P02538	K2C6A_HUMAN	KRT6A	0.000287604
549	1	sp	P07305	H10_HUMAN	H1F0	0.000287604
550	1	sp	Q15517	CDSN_HUMAN	CDSN	0.000287604
551	1	sp	O43776	SYNC_HUMAN	NARS	0.000287604
552	1	sp	P42677	RS27_HUMAN	RPS27	0.000287604
553	1	sp	Q9UJ70	NAGK_HUMAN	NAGK	0.000287604
554	1	sp	P55884	EIF3B_HUMAN	EIF3B	0.000287604
555	1	sp	O75955	FLOT1_HUMAN	FLOT1	0.000287604
556	1	sp	P29373	RABP2_HUMAN	CRABP2	0.000287604
557	1	sp	Q9B5J8	ESYT1_HUMAN	ESYT1	0.000287604
558	1	sp	P61106	RAB14_HUMAN	RAB14	0.000287604
559	1	sp	Q01082	SPTB2_HUMAN	SPTBN1	0.000287604
560	1	sp	P49755	TMEDA_HUMAN	TMED10	0.000287604
561	1	sp	Q96EY5	MB12A_HUMAN	MVB12A	0.000287604
562	1	sp	P67936	TPM4_HUMAN	TPM4	0.000287604
563	1	sp	P01857	IGHG1_HUMAN	IGHG1	0.000287604
564	1	sp	P54578	UBP14_HUMAN	USP14	0.000287604
565	1	sp	Q92616	GCN1L_HUMAN	GCN1L1	0.000287604
566	1	sp	P51148	RAB5C_HUMAN	RAB5C	0.000287604
567	1	sp	P62979	RS27A_HUMAN	RPS27A	0.000287604
568	1	sp	Q8IWA5	CTL2_HUMAN	SLC44A2	0.000287604
569	1	sp	P05976	MYL1_HUMAN	MYL1	0.000287604
570	1	sp	Q01844	EWS_HUMAN	EWSR1	0.000287604
571	1	sp	Q969E2	SCAM4_HUMAN	SCAMP4	0.000287604
572	1	sp	P62847	RS24_HUMAN	RPS24	0.000287604
573	1	sp	P08697	A2AP_HUMAN	SERPINF2	0.000287604
574	1	sp	Q01105	SET_HUMAN	SET	0.000287604
575	1	sp	P35080	PROF2_HUMAN	PFN2	0.000287604
576	1	sp	Q6UWP8	SBSN_HUMAN	SBSN	0.000287604
577	1	sp	P06702	S10A9_HUMAN	S100A9	0.000287604
578	1	sp	Q10471	GALT2_HUMAN	GALNT2	0.000287604
579	1	sp	O75367	H2AY_HUMAN	H2AFY	0.000287604
580	1	sp	P07951-2	TPM2_HUMAN	TPM2	0.000287604
581	1	sp	O95837	GNA14_HUMAN	GNA14	0.000287604
582	1	sp	P60900	PSA6_HUMAN	PSMA6	0.000287604
583	1	sp	P05109	S10A8_HUMAN	S100A8	0.000287604
584	1	sp	Q15063-3	POSTN_HUMA	POSTN	0.000287604
585	1	sp	P30041	PRDX6_HUMAN	PRDX6	0.000287604
586	1	sp	P04278	SHBG_HUMAN	SHBG	0.000287604
587	1	sp	P07585	PGS2_HUMAN	DCN	0.000287604
588	1	sp	P30044	PRDX5_HUMAN	PRDX5	0.000287604
589	1	sp	P16104	H2AX_HUMAN	H2AFX	0.000287604
590	1	sp	Q14624	ITIH4_HUMAN	ITIH4	0.000287604
591	1	sp	Q9HCJ1	ANKH_HUMAN	ANKH	0.000287604
592	1	sp	Q14847	LASP1_HUMAN	LASP1	0.000287604
593	1	sp	P62140	PP1B_HUMAN	PPP1CB	0.000287604
594	1	sp	P18621	RL17_HUMAN	RPL17	0.000287604
595	1	sp	Q9NR31	SAR1A_HUMAN	SAR1A	0.000287604
596	1	sp	P14923	PLAK_HUMAN_c	JUP	0.000287604
597	1	sp	P16401	H15_HUMAN	HIST1H1B	0.000287604
598	1	sp	Q01546	K22O_HUMAN_c	KRT76	0.000287604
599	1	sp	P33527	MRP1_HUMAN	ABCC1	0.000287604
600	1	sp	P35659	DEK_HUMAN	DEK	0.000287604
601	1	sp	P62491	RB11A_HUMAN	RAB11A	0.000287604
602	1	sp	Q8NCA5	FA98A_HUMAN	FAM98A	0.000287604
603	1	sp	P01040	CYTA_HUMAN_ce	CSTA	0.000287604
604	1	sp	P07093-2	GDN_HUMAN	SERPINE2	0.000287604
605	1	sp	O75874	IDHC_HUMAN	IDH1	0.000287604
606	1	sp	Q9Y3UB	RL36_HUMAN	RPL36	0.000287604
607	1	sp	P31689	DNJA1_HUMAN	DNAJA1	0.000287604
608	1	sp	A8MT33	SYC1L_HUMAN	SYCE1L	0.000287604
609	1	sp	P13591	NCAM1_HUMAN	NCAM1	0.000287604
610	1	sp	P98172	EFNB1_HUMAN	EFNB1	0.000287604
611	1	sp	Q96C34	RUND1_HUMAN	RUNDC1	0.000287604
612	1	sp	Q9Y3Q3	TMED3_HUMAN	TMED3	0.000287604
613	1	sp	P49773	HINT1_HUMAN	HINT1	0.000287604
614	1	sp	P46783	RS10_HUMAN	RPS10	0.000287604
615	1	sp	P02748	CO9_HUMAN	C9	0.000287604
616	1	##sp	P51532	SMCA4_HUMA	##SMARCA4	0.000287604
617	1	sp	Q15836	VAMP3_HUMAN	VAMP3	0.000287604
618	1	sp	P29992	GNA11_HUMAN	GNA11	0.000287604
619	1	sp	O75387	LAT3_HUMAN	SLC43A1	0.000287604
620	1	sp	P62841	RS15_HUMAN	RPS15	0.000287604
621	1	sp	Q9P2F6	RHG20_HUMAN	ARHGAP20	0.000287604
622	1	sp	Q12841	FSTL1_HUMAN	FSTL1	0.000287604
623	1	sp	O15404	RSU1_HUMAN	RSU1	0.000287604
624	1	sp	O15145	ARPC3_HUMAN	ARPC3	0.000287604
625	1	sp	Q96QK1	VPS35_HUMAN	VPS35	0.000287604
626	1	sp	Q4V9L6	TM119_HUMAN	TMEM119	0.000287604
627	1	sp	Q7LGA3	HS2ST_HUMAN	HS2ST1	0.000287604
628	1	sp	Q04917	1433F_HUMAN	YWHAH	0.000287604
629	1	sp	Q13443	ADAM9_HUMAN	ADAM9	0.000287604
630	1	sp	P14174	MIF_HUMAN	MIF	0.000287604
631	1	sp	Q12904	AIMP1_HUMAN	AIMP1	0.000287604
632	1	sp	Q9UNP9	PPIE_HUMAN	PPIE	0.000287604
633	1	sp	A2A3N6	PIPSL_HUMAN	PIPSL	0.000287604
634	1	##sp	Q15428	SF3A2_HUMA	##SF3A2	0.000287604
635	1	sp	P19827	ITIH1_HUMAN	ITIH1	0.000287604
636	1	sp	O15431	COPT1_HUMAN	SLC31A1	0.000287604
637	1	sp	P10768	ESTD_HUMAN	ESD	0.000287604
638	1	sp	Q15084	PDIA6_HUMAN	PDIA6	0.000287604

Chapter 5: Figure 7 Supplementary Table 1 (Page 8 of 8)

All protein hits from proteomic analysis of the R10 media alone and exosomes derived from Irradiated or Noni-Irradiated MSCs. Greyed-out proteins indicate low-abundance proteins that were excluded in downstream bioinformatic analyses.

639	1	sp|P15259|PGAM2_HUMAN	PGAM2	0.000287604
640	1	sp|P25788|PSA3_HUMAN	PSMA3	0.000287604
641	1	sp|P08603|CFAH_HUMAN	CFH	0.000287604
642	1	sp|Q01813|K6PP_HUMAN	PFKP	0.000287604
643	1	sp|P21796|VDAC1_HUMAN	VDAC1	0.000287604
644	1	sp|P05362|ICAM1_HUMAN	ICAM1	0.000287604
645	1	sp|P08754|GNAI3_HUMAN	GNAI3	0.000287604
646	1	sp|P61224|RAP1B_HUMAN	RAP1B	0.000287604
647	1	##sp|Q9UL26|RB22A_HUMA	##RAB22A	0.000287604
648	1	sp|P62857|RS28_HUMAN	RPS28	0.000287604
649	1	sp|Q6UB99|IG2AS_HUMAN	IGF2-AS	0.000287604
650	1	sp|P52907|CAZA1_HUMAN	CAPZA1	0.000287604
651	1	sp|Q9H3Z4|DNJC5_HUMAN	DNAJC5	0.000287604
652	1	sp|P13693|TCTP_HUMAN	TPT1	0.000287604
653	1	sp|Q13103|SPP24_HUMAN	SPP2	0.000287604
654	1	sp|P11940|PABP1_HUMAN	PABPC1	0.000287604
655	1	sp|Q9NPH3|IL1AP_HUMAN	IL1RAP	0.000287604
656	1	sp|P62244|RS15A_HUMAN	RPS15A	0.000287604
657	1	sp|P22061|PIMT_HUMAN	PCMT1	0.000287604
658	1	sp|Q7Z3B1|NEGR1_HUMAN	NEGR1	0.000287604
659	1	sp|O15460|P4HA2_HUMAN	P4HA2	0.000287604
660	1	sp|P31943|HNRH1_HUMAN	HNRNPH1	0.000287604
661	1	sp|P0CG47|UBB_HUMAN	UBB	0.000287604
662	1	sp|Q9Y2A7|NCKP1_HUMAN	NCKAP1	0.000287604
663	1	sp|Q86VP6|CAND1_HUMAN	CAND1	0.000287604
664	1	sp|O00244|ATOX1_HUMAN	ATOX1	0.000287604
665	1	sp|P09493|TPM1_HUMAN	TPM1	0.000287604
666	1	sp|P62826|RAN_HUMAN	RAN	0.000287604
667	1	sp|P55285|CADH6_HUMAN	CDH6	0.000287604
668	1	sp|P09496|CLCA_HUMAN	CLTA	0.000287604
669	1	sp|A7E2Y1|MYH7B_HUMAN	MYH7B	0.000287604
670	1	tr|H7C4W4|H7C4W4_HUMA	FSTL1	0.000287604
671	1	sp|Q14520|HABP2_HUMAN	HABP2	0.000287604
672	1	sp|P0CD55|H2AZ_HUMAN	H2AFZ	0.000287604
673	1	sp|P48059|LIMS1_HUMAN	LIMS1	0.000287604
674	1	sp|P15151|PVR_HUMAN	PVR	0.000287604
675	1	sp|P13674|P4HA1_HUMAN	P4HA1	0.000287604
676	1	sp|P10599|THIO_HUMAN	TXN	0.000287604
677	1	sp|O95297|MPZL1_HUMAN	MPZL1	0.000287604
678	1	sp|P10809|CH60_HUMAN	HSPD1	0.000287604
679	1	sp|O94979|SC31A_HUMAN	SEC31A	0.000287604
680	1	sp|Q9BQY6-2|WFDC6_HUM	WFDC6	0.000287604
681	1	sp|P18077|RL35A_HUMAN	RPL35A	0.000287604
682	1	sp|P19338|NUCL_HUMAN	NCL	0.000287604
683	1	sp|P21926|CD9_HUMAN	CD9	0.000287604
684	1	sp|P37837|TALDO_HUMAN	TALDO1	0.000287604
685	1	sp|O14744|ANM5_HUMAN	PRMT5	0.000287604
686	1	sp|Q8TB61|S35B2_HUMAN	SLC35B2	0.000287604
687	1	sp|Q7KZF4|SND1_HUMAN	SND1	0.000287604
688	1	sp|Q06033|ITIH3_HUMAN	ITIH3	0.000287604
689	1	##sp|Q96EY7|PTCD3_HUMA	##PTCD3	0.000287604
690	1	sp|P49257|LMAN1_HUMAN	LMAN1	0.000287604
691	1	sp|P11387|TOP1_HUMAN	TOP1	0.000287604
692	1	##sp|Q06203|PUR1_HUMAN	##PPAT	0.000287604
693	1	sp|P06899|H2B1J_HUMAN	HIST1H2BJ	0.000287604
694	1	sp|P25705|ATPA_HUMAN	ATP5A1	0.000287604
695	1	sp|Q9Y3I0|RTCB_HUMAN	RTCB	0.000287604
696	1	##sp|Q8WZ42|TITIN_HUMA	##TTN	0.000287604

Chapter 5: Figure 8 Supplementary Table 2 (Page 1 of 3)

After thresholding as described in Methods, datasets from Supp.Table 1 were used as input for the IPA software, to generate pathways most highly-associated with the exosomes' proteomes. Supp.Table 2 presents the unredacted list of all pathways identified by the IPA software, along with the –log(p-value) for each pathway. Pathways with –log(p-value) below the significance value of 1.35 are greyed-out. The adjacent column indicates the Pathway Ratio, which the IPA software computes; it is a proportion of how many proteins were found in the sample (then names them in the adjacent column) based on the company's proprietary list of the proteins they have identified to be in that pathway. The immunology-relevant pathways of interest to our team are shaded yellow.

Supplemental Table #2: Ingenuity Pathway Analysis of All Exosome Proteomes

No.	Ingenuity Canonical Pathway Name	-log(p-value)	Pathway Ratio	Proteins Present in the Sample Connoting Pathway Activity
1	EIF2 Signaling	3.68E+01	0.27	RPL11,RPS23,RPL21,HSPA5,RPL13,RPL19,RPL21,RPS2,RPL10,RPL3,RRAS,RPS8,RPL26,RPL11,RPL15,RPS6,RPL8,RPL10,RPL6,RPS25,RPS6,RPL24,RPL7,RPS16,RPL26,RPL7A,RPL7,RPS8,RPL27A,RPL19,RPL14,RPL18A,RPS3,RPS3,RPL18,RPL9,RPL17,RPL30,RPL21,RPL27,RPS15,RHAS,RPS4Y1,EIF4A1,RPS27A,RPL15,EIF3L,RPL9,RPS14
2	Integrin Signaling	1.45E+01	0.13	RAC2,RALA,PFN1,TLN1,ITGB1/ITGA3,RHOG,ITGA11,ARF6,ITGAV,ARPC5,ITGB5,MYL12B,ACTN1/ITGB1,RRAS,RHOC,RALB,ITGA2,ITGA5,RAP1A,CAPNS1,CDC42,ARF1,ZYX,GMFG2,ACTN4,ITGA7
3	Regulation of eIF4 and p70S6K Signaling	1.33E+01	0.15	ITGB1,RPS19,RPS18,RHAS,RPS8,RPS23,ITGA2,ITGA3,RPS4X,RPS6,PPP2CB,RPS15,RPS4Y1,ITGA3,EIF4A1,RPS27A,RPS25,RPS2,RPS5,RPS3,EIF3L,RPS14,RPS6
4	Remodeling of Epithelial Adherens Junctions	1.26E+01	0.27	TUBA1B,TUBB3,RALA,RABSC,TUBB2A,RAB7A,CTNNA1,IQGAP1,TUBB,TUBB6,ARPC3,ZYX,TUBB4A,ACTN4,CTNNB1,ACTN1
5	Caveolae-mediated Endocytosis Signaling	1.24E+01	0.23	ITGB1,FLNB,RABSC,HLA-A,ITGA3,COPA,ITGA3,ITGB3,ITGA3,FLNC,FLNA,ITGA11,ITGAV,PTRF,ITGA7,ITGB5
6	Axonal Guidance Signaling	1.21E+01	0.09	DPYSL2,TUBA1B,RAC2,PFN1,MYL9,PDIA1,DNA11,RACK1,GNA14,TUBB,GNB1/ITGA3,ARPC3,TUBB4A,PLXNB2,GNG12,MYL12B,ITGB1,TUBB3,GNAS,RRAS,ITGA2,TUBB2A,ITGAS,MMP2,RAP1A,GNA12,SOCBP,TUBB6,CDC42,GNB2,RTN4,ADAM10,EPHA2,ADAM9,NRP1
7	RhoGDI Signaling	1.15E+01	0.13	ITGB1,GNAS,MYL9,RHOC,GNA11,RACK1,ITGA2,RDX,EDD2,ITGAS,GNA14,GNA12,GNB2/ITGA3,RHOD,CDC42,EZR,GNB2,ARPC3,GNG12,MYL12B,MSN
8	Virus Entry via Endocytic Pathways	1.09E+01	0.17	ITGB1,FLNB,RAC2,RRAS,HLA-A,ITGA2,CLTC,ITGAS,ITGB3,ITGA3,CDC42,FLNA,FLNC,CLTA,CLTC11,TFRC,ITGB1
9	Leukocyte Extravasation Signaling	1.06E+01	0.11	ITGB1,CD99,RAC2,MYL6,ITGA2,RDX,CTNNA1,ITGA3,THY1,MMP2,RAP1A,ITGB1,DNA1/ITGA3,EDA,S,TIMP1,CDC42,EZR,ACTN4,CTNNB1,ACTN1,TIMP2,MSN
10	Germ Cell-Sertoli Cell Junction Signaling	1.06E+01	0.12	ITGB1,TUBA1B,RAC2,TUBB3,RRAS,RHOC,TUBB2A,ITGA2,CTNNA1,IQGAP1,TUBB,ITGA3,RHOG,TUBB6,CDC42,ZYX,TUBB4A,ACTN4,IQF,CTNNB1,ACTN1
11	Epithelial Adherens Junction Signaling	1.02E+01	0.13	TUBA1B,TUBB3,MYH9,MYL6,RRAS,TUBB2A,CTNNA1,IQGAP1,TUBB,RAP1A,TUBB6,CDC42,ZYX,ARPC3,TUBB4A,ACTN4,IQF,CTNNB1,ACTN1
12	Ephrin Receptor Signaling	9.67E+00	0.12	ITGB1,RAC2,GNAS,RRAS,GNA11,RACK1,ITGA2,ITGAS,GNA14,RAP1A,GNAQ,GNB1/ITGA3,SOCBP,CDC42,ADAM10,GNB2,ARPC3,EPHA2,GNG12
13	mTOR Signaling	9.42E+00	0.11	RPS19,RPS18,RRAS,RHOC,RPS8,RPS23,RPS4X,RPS6,PPP2CB,RPS15,RPS4Y1,RHOG,EIF4A1,RPS27A,RPS25,RPS2,RPS5,RPS3,EIF3L,RPS14,RPS6
14	Signaling by Rho Family GTPases	9.18E+00	0.09	ITGB1,GNAS,MYL9,RHOC,GNA11,RACK1,ITGA2,RDX,ITGAS,VIM,GNA14,IQGAP1,GNA12,GNB1/ITGA3,RHOG,CDC42,EZR,GNB2,ARPC3,GNG12,MYL12B,MSN
15	Actin Cytoskeleton Signaling	8.34E+00	0.09	ITGB1,RAC2,PFN1,MYH9,MYL6,RRAS,ITGA2,RDX,ITGAS,TLN1,IQGAP1,ITGA3/CDC42,FLNA,EZR,ARPC3,ACTN4,GNG12,MYL12B,ACTN1,MSN
16	Protein Ubiquitination Pathway	8.19E+00	0.09	PSMB8,PSMA6,HLA-A,PSMA7,HSPA1A/HSPA1B,PSMD3,HSPD1,HSPA5,PSMC5,HSPA8,PSMD11,PSMC1,HSP90B1,DNAJC5,HSP90AB1,PSMA5,PSMD12,PSMA4,PSMB1,PSMD1,UBA1,HSPB1
17	Regulation of Cellular Mechanics by Calpain Protease	7.95E+00	0.18	ITGB1/ITGA3,CAPNS1,RRAS,EZR,ITGA2/ITGA5,CAPN2,TLN1,ACTN4,ACTN1
18	Phospholipase C Signaling	7.95E+00	0.09	ITGB1,PEBP1,CALM1,S,RALA,GNAS,MYL6,RRAS,RHOC,RALB,RACK1,ITGA2/ITGA5,ARPC3,A,TGM2,GNB1,CALM1/ITGA3,RHOG,GNB2,GNG12,MYL12B
19	Sertoli Cell-Sertoli Cell Junction Signaling	7.87E+00	0.10	ITGB1,TUBA1B,TUBB3,RRAS,TUBB2A,ITGA2,CTNNA1,ITGAS,YBX3,TUBB,ITGA5,TUBB6,CDC42,TUBB4A,ACTN4,IQF,CTNNB1,ACTN1
20	Ephrin B Signaling	7.79E+00	0.16	GNB1,GNA12,RAC2,GNAS,CDC42,RACK1,GNA11,GNB2,CAP1,GNA14,CTNNB1,GNG12
21	Glycolysis I	7.65E+00	0.31	PGK1,ENO1,GPI,PKM,GAPDH,ALDOA,PFKP,ALDOC
22	Phagosome Maturation	7.64E+00	0.11	TUBA1B,TUBB3,RABSC,PRDX1,HLA-A,TUBB2A,RAB7A,CANX,TUBB,PRDX6,DYNC1H1,DYNLL1,TUBB6,VPS37B,TUBB4A,PRDX2
23	14-3-3-mediated Signaling	7.42E+00	0.12	TUBA1B,TUBB3,YWHAG,YWHAE,YWHAH,YWHAB,RRAS,PDIA3,TUBB2A,VIM,TUBB,YWHAQ,TUBB6,TUBB4A,PDCD6IP
24	Paxillin Signaling	7.36E+00	0.12	ITGB1,RRAS,ITGA2/ITGA5,TLN1,ITGB3/ITGA3,CDC42,ITGA11,ITGAV,ACTN4,ITGA7,ITGB5,ACTN1
25	IL8 Signaling	7.22E+00	0.09	ITGB1,FLNB,MYH9,MYL6,RHOC,FERMT2,VIM,ITGB3,PPP2CB,RHOG,FLNC,CDC42,FLNA,ACTN4,CTNNB1,ITGB5,DSP,ACTN1
26	Clathrin-mediated Endocytosis Signaling	7.18E+00	0.09	ITGB1,APOE,RABSC,CLTC,RAB7A,ITGAS,ITGB3,HSPA8,TF,CDC42,CLTA,CLTC11,TFRC,APOC3,S100A8,CSNK2B,ITGB5,CLU
27	Agrin Interactions at Neuromuscular Junction	7.05E+00	0.16	LAMC1/ITGB1,RAC2/ITGA3,RRAS,CDC42,ITGA2,LAMB1/ITGAS,AGRN/ITGB3
28	Breast Cancer Regulation by Stathmin1	6.98E+00	0.09	TUBA1B,TUBB3,CALM1S,GNAS,RRAS,RACK1,TUBB2A,TUBB,GNA12,GNB1,PPP2CB,CALM1 (includes others),TUBB6,CDC42,GNB2,TUBB4A,GNG12,CAMK2B
29	PI3K/AKT Signaling	6.85E+00	0.11	ITGB1,YWHAQ,YWHAE,YWHAH,YWHAB,RRAS,ITGA2,ITGAS,YWHAZ,PPP2CB,ITGA3/HSP90B1,HSP90AB1,CTNNB1
30	Regulation of Actin-based Motility by Rho	6.70E+00	0.13	ITGB1,RAC2,ITGA3,PFN1,RHOG,MYL6,RHOC,CDC42,ITGA2,ITGAS,ARPC3,MYL12B
31	tRNA Charging	6.15E+00	0.21	WARS,RARS,GARS,DARS,AARS,TARS,IARS,EPRS
32	Protein Kinase A Signaling	6.05E+00	0.06	FLNB,CALM1S,GNB1,YWHAQ,MYL6,YWHAH,YWHAE,YWHAB,PDIA3,RACK1,RAP1A,GNB2,HIST1H1E,YWHAZ,GNB2,CALM1 (includes others),HIST1H1D,FLNC,FLNA,GNB2,CTNNB1,GNG12,MYL12B,CAMK2B
33	Glioma Invasiveness Signaling	6.00E+00	0.14	RHOG,RRAS,TIMP1,RHOC,ITGAV,PLAUR,MMP2,ITGB1,TIMP2,ITGB3
34	Actin Nucleation by ARP-WASP Complex	5.90E+00	0.16	ITGB1/ITGA3,RHOG,RRAS,RHOC,CDC42,ITGA2,ITGAS,ARPC3
35	Huntington's Disease Signaling	5.88E+00	0.07	HSPA1A/HSPA1B,GNAS1,RACK1,CLTC,GNA14,HSPA5,TGM2,GNB1,HSPA8,CAPNS1,DNAJC5,ATP5B,CLTA,CLTC11,GNB2,CAPN2,CASP14,GNG12
36	IL-8 Signaling	5.77E+00	0.08	RAC2,GNAS,RRAS,RHOC,RACK1,MMP2,IQGAP1,ITGB3,GNB1,GNA12,RHOG,ITGAS,GNB2,GNG12/ITGB3,MYL12B
37	Cardiac Hypertrophy Signaling	5.40E+00	0.07	CALM1S,GNAS,MYL6,RRAS,PDIA3,RHOC,GNA11,RACK1,GNA14,GNB1,GNA12,CALM1 (includes others),RHOG,GNB2,GNG12,MYL12B,HSPB1
38	Tec Kinase Signaling	5.19E+00	0.06	ITGB1,GNA12,GNB1/ITGA3,GNAS,RHOG,RHOC/ITGA2,RACK1,GNA11,GNB2/ITGAS,GNA14/ITGA3
39	G Beta Gamma Signaling	5.08E+00	0.11	GNB1,GNA12,GNAS,RRAS,CDC42,RACK1,GNA11,GNB2,GNA14,GNG12
40	Gluconeogenesis I	5.08E+00	0.23	PGK1,ENO1,GPI,GAPDH,ALDOA,ALDOC
41	Inhibition of Matrix Metalloproteinases	5.04E+00	0.18	HSPG2,TIMP1,RECK,THBS2,ADAM10,MMP2,TIMP2
42	Granulocyte Adhesion and Diapedesis	4.99E+00	0.08	ITGB1,CD99,ITGA2,RDX,ITGAS,THY1,MMP2,ITGB3,GJC1,GNA12/ITGA3,EZR,MSN,HSP90B1
43	Thrombin Signaling	4.94E+00	0.07	GNAS,MYL6,RRAS,PDIA3,RHOC,GNA11,RACK1,GNA14,GNB1,GNA12,RHOG,GNB2,MYL12B,GNG12,CAMK2B
44	CXCR4 Signaling	4.66E+00	0.08	GNAS,MYL6,RRAS,RHOC,GNA11,RACK1,GNA14,GNB1,GNA12,RHOG,GNB2,MYL12B,GNG12
45	PKCθ Signaling in Neutrophils	4.60E+00	0.09	GNB1,GNA12,CALM1 (includes others),CALM1S,GNAS,RRAS,CDC42,RACK1,GNB2,ARPC3,GNG12
46	Role of Tissue Factor in Cancer	4.56E+00	0.09	ITGB1,PAR1B/ITGA3,RRAS,CDC42,GNA11,ITGAV,PLAUR,GNA14/ITGB5,ITGB3
47	ERK/MAPK Signaling	4.42E+00	0.07	ITGB1,RAC2,YWHAQ,PAR1B/ITGA3,YWHAE,YWHAB,RRAS,ITGA2/ITGAS,TLN1,RAP1A,YWHAZ,PPP2CB/ITGA3,YWHAH
48	γ-TBSK Signaling	4.30E+00	0.10	GNB1,GNA12,CALM1 (includes others),CALM1S,GNAS,RRAS,RACK1,GNB2,GNG12
49	p70S6K Signaling	4.28E+00	0.08	RPS6,GNAQ,YWHAQ,PPP2CB,YWHAQ,YWHAH,YWHAE,EIF2,YWHAB,RRAS,PDIA3
50	CCR5 Signaling in Macrophages	4.24E+00	0.12	GNB1,GNA12,CALM1 (includes others),CALM1S,GNAS,RACK1,GNB2,GNG12

No.	Ingenuity Canonical Pathway Name	-log(p-value)	Pathway Ratio	Proteins Present in the Sample Connoting Pathway Activity
51	Androgen Signaling	4.20E+00	0.09	GNB1,GNA12,CALM1 (includes others),CALM1S,GNAS,RACK1,GNA11,GNB2,GNA14,GNG12
52	CREB Signaling in Neurons	4.16E+00	0.07	CALM1S,GNAS,RRAS,PDIA3,GNA11,RAC1,GNA14,GNB1,GNA12,CALM1 (includes others),GNB2,GNG12,CAMK2B
53	Unfolded protein response	4.09E+00	0.13	HSPA8,PAHB,HSP90B1,VCP,HSPA1A/HSPA1B,CANX,HSPA5
54	Agranulocyte Adhesion and Diapedesis	4.04E+00	0.07	ITGB1,GNAQ,CD99,ITGA3,MYH9,MYL6,ITGA2,RDX,ITGAS,MMP2,GJC1,MSN
55	PTEN Signaling	3.94E+00	0.08	ITGB1,RAC2,ITGA3,YWHAH,RRAS,CDC42,ITGA2,ITGAS,CSNK2B,PDGFRB
56	Gα12 Signaling	3.91E+00	0.08	GNB1,GNA12,RALA,GNAS,RRAS,RACK1,RALB,GNB2,RAP1A,GNG12
57	Molecular Mechanisms of Cancer	3.82E+00	0.05	ITGB1,RAC2,RALA,GNAS,RRAS,RHOC,GNA11,ITGA2,RALB,CTNNA1,ITGAS,GNA14,RAP1A,GNA12/ITGA3,RHOG,CDC42,CTNNB1,CAMK2B
58	PAK Signaling	3.80E+00	0.09	ITGB1/ITGA3,RRAS,ITGA2,CDC42/ITGA2/ITGAS,MYL12B,PDGFRB
59	NF-κB Activation by Viruses	3.56E+00	0.09	ITGB1/ITGA3,RRAS,ITGA2,ITGAV/ITGA5/ITGB5,ITGB3
60	Role of NFAT in Regulation of the Immune Response	3.54E+00	0.06	GNB1,GNA12,CALM1 (includes others),CALM1S,GNAS,RRAS,HLA-A,RACK1,GNA11,GNB2,GNA14,GNG12
61	Gαq Signaling	3.51E+00	0.07	GNB1,CALM1 (includes others),CALM1S,GNAS,RHOG,RHOC,RAC1,GNA11,GNB2,GNA14,GNG12
62	Neuregulin Signaling	3.49E+00	0.09	ITGB1,RPS6,HSP90B1/ITGA3,HSP90AB1,RRAS,ITGA2/ITGAS
63	G-Protein Signaling Mediated by Tubby	3.45E+00	0.16	GNB1,GNAS,RACK1,GNB2,GNG12
64	IL-1 Signaling	3.39E+00	0.09	GNB1,GNA12,GNAS,RACK1,GNA11,GNB2/GNA14,GNG12
65	Cdc42 Signaling	3.35E+00	0.07	ITGB1/ITGA3,RALA,MYL6,HLA-A,CDC42/ITGA2/ITGAS,ARPC3,IQGAP1,MYL12B
66	Gap Junction Signaling	3.28E+00	0.06	GNA12,TUBA1B,TUBB3,GNB1,TUBB6,RRAS,PDIA3,TUBB2A,TUBB4A,CTNNB1,TUBB
67	Semaphorin Signaling in Neurons	3.25E+00	0.11	DPYSL2/ITGB1,RHOG,RHOC,DPYSL3/NRP1
68	CD40 Signaling	3.15E+00	0.08	LAMC1/ITGB1,PPP2CB/ITGA3,GNAS,RRAS,TLN1,LAMB1
69	FGF Signaling	3.15E+00	0.08	ITGB1/ITGA3,LAPN11,RRAS/ITGA2/ITGAS,CAPN2,TLN1
70	Calcium Transport I	3.10E+00	0.30	ATP1B1,ANXA5,ATP2B4
71	Hepatic Fibrosis / Hepatic Stellate Cell Activation	3.02E+00	0.06	COL1A2,MYH9,COL6A2,COL6A3,MYL6,TIMP1,COL12A1,MMP2,SERPINE1,TIMP2,PDGFRB
72	Macropinocytosis Signaling	2.99E+00	0.09	ITGB1,RRAS,CDC42/ITGA3,ACTN4/ITGB1,ITGB3
73	CCR3 Signaling in Eosinophils	2.99E+00	0.07	GNB1,GNA12,CALM1 (includes others),CALM1S,GNAS,RRAS,RACK1,GNB2,GNG12
74	IGF-1 Signaling	2.95E+00	0.08	YWHAQ,YWHAG,YWHAH,YWHAE,YWHAB,RRAS,CSNK2B,IGFBP7
75	ERK5 Signaling	2.85E+00	0.10	YWHAQ,YWHAG,YWHAH,YWHAE,YWHAB,RRAS
76	Role of NFAT in Cardiac Hypertrophy	2.85E+00	0.06	GNB1,GNA12,CALM1 (includes others),CALM1S,GNAS,RRAS,PDIA3,RAC1,GNB2,GNG12,CAMK2B
77	Aldosterone Signaling in Epithelial Cells	2.80E+00	0.06	HSPA8,HSP90B1,DNAJC5,HSP90AB1,PDIA3,HSPA1A/HSPA1B,HSPD1,HSPA5,AHCY,HSPB1
78	Ran Signaling	2.68E+00	0.07	ITGB1/ITGA3,RRAS,CDC42/ITGA2/ITGAS,ARPC3,IQGAP1
79	Myc Mediated Apoptosis Signaling	2.62E+00	0.09	YWHAQ,YWHAG,YWHAH,YWHAE,YWHAB,RRAS
80	Synaptic Long Term Potentiation	2.61E+00	0.07	CALM1 (includes others),CALM1S,RRAS,PDIA3,GNA11,GNA14,RAP1A,CAMK2B
81	Cell Cycle: G1/M DNA Damage Checkpoint Regulation	2.59E+00	0.10	YWHAQ,YWHAG,YWHAH,YWHAE,YWHAB
82	Relaxin Signaling	2.52E+00	0.06	GNB1,GNA12,GNAS,RACK1,GNA11,GNB2/GNA14,RAP1A,GNG12
83	P2Y Purigenic Receptor Signaling Pathway	2.36E+00	0.06	GNB1,GNA12,RRAS,PDIA3,RACK1,GNB2,GNG12/ITGB3
84	GPCR-Mediated Nutrient Sensing in Enteroendocrine Cells	2.20E+00	0.07	GNA12,GNAS,PDIA3,GNA11,GNA14,GNG12
85	mTOR signaling	2.15E+00	0.07	YWHAQ,PPP2CB,YWHAQ,YWHAH,YWHAE,YWHAB
86	HGF Signaling	2.13E+00	0.06	ITGB1/ITGA3,RRAS/CDC42/ITGA2/ITGAS,RAP1A
87	HER-2 Signaling in Breast Cancer	2.13E+00	0.07	ITGB1,RRAS,CDC42,ARPC3/ITGB1/ITGB3
88	PPARγ/RXRγ Activation	2.08E+00	0.05	CAND1,HSP90B1,GNAS,HSP90AB1,RRAS,PDIA3,GNA11,GNA14/ITGB5
89	Calcium Signaling	2.08E+00	0.05	CALM1 (includes others),CALM1S,MYH9,MYL6,ATP2B1,TFM1,RAP1A,ATP2B4,CAMK2B
90	Hypoxia Signaling in the Cardiovascular System	2.06E+00	0.08	PAHB,HSP90B1,HSP90AB1,NQO1,LDHA
91	Reelin Signaling in Neurons	2.04E+00	0.07	ITGB1,APOE/ITGA3/ITGA2/ITGAS/ITGB3
92	RhoA Signaling	2.00E+00	0.06	PFN1,MYL6,EZR,RDX,ARPC3,MYL12B,MSN
93	Phagosome Formation	2.00E+00	0.06	ITGB1/ITGA3,RHOG,RHOC,PDIA3/ITGA2/ITGAS
94	eNOS Signaling	1.95E+00	0.05	HSPA8,CALM1 (includes others),CALM1S,HSP90B1,GNAS,HSP90AB1,HSPA1A/HSPA1B,HSPB1
95	Sucrose Degradation V (Mammalian)	1.90E+00	0.22	ALDOA,ALDOC
96	Melatonin Signaling	1.90E+00	0.07	GNA12,CALM1 (includes others),CALM1S,PDIA3,CAMK2B
97	Chemokine Signaling	1.90E+00	0.07	GNA12,CALM1 (includes others),CALM1S,RRAS,CAMK2B
98	nNOS Signaling in Neurons	1.88E+00	0.06	CALM1 (includes others),CALM1S,CAPN1,CAPN2
99	GPCR-Mediated Integration of Enteroendocrine Signaling Exemplified by an L Cell	1.88E+00	0.07	GNA12,GNAS,PDIA3,GNA11,GNA14
100	GNRH Signaling	1.88E+00	0.05	GNA12,GNAS,RRAS,CDC42,GNA11,GNA14,CAMK2B

Chapter 5: Figure 8 Supplementary Table 2 (Page 2 of 3)

After thresholding as described in Methods, datasets from Supp.Table 1 were used as input for the IPA software, to generate pathways most highly-associated with the exosomes' proteomes. Supp.Table 2 presents the unredacted list of all pathways identified by the IPA software, along with the –log(p-value) for each pathway. Pathways with –log(p-value) below the significance value of 1.35 are greyed-out. The adjacent column indicates the Pathway Ratio, which the IPA software computes; it is a proportion of how many proteins were found in the sample (then names them in the adjacent column) based on the company's proprietary list of the proteins they have identified to be in that pathway. The immunology-relevant pathways of interest to our team are shaded yellow.

101	Cellular Effects of Sildenafil (Viagra)	1.86E+00	0.05	CALM1 (includes others),CALML5,MYH9,GNAI3,MYL6,PDIA3,MYL12B
102	Antiproliferative Role of Somatostatin Receptor 2	1.81E+00	0.07	GNB1,RRAS,RACK1,GNB2,GNG12
103	Acetyl-CoA Biosynthesis III (from Citrate)	1.71E+00	1.00	ACLY
104	Gαq Signaling	1.70E+00	0.06	GNB1,GNAS,RACK1,GNB2,RAP1A,GNG12
105	Colorectal Cancer Metastasis Signaling	1.63E+00	0.04	GNB1,GNAS,RHOG,RRAS,RHOC,RACK1,GNB2,MMP2,CTNNB1,GNG12
106	Synaptic Long Term Depression	1.61E+00	0.05	GNAI2,PPP2CB,GNAS,RRAS,PDIA3,GNA11,GNA14
107	Glutamate Receptor Signaling	1.60E+00	0.07	GNB1,CALM1 (includes others),CALML5,SLC1A4
108	Role of IL-17A in Psoriasis	1.59E+00	0.15	S100A9,S100A8
109	Colanic Acid Building Blocks Biosynthesis	1.53E+00	0.14	GPI,UGDH
110	Sphingosine-1-phosphate Signaling	1.47E+00	0.05	GNAI2,RHOG,RHOC,PDIA3,CASP14,PDGFRB
111	Telomere Extension by Telomerase	1.47E+00	0.13	HNRNPA2B1,XRCC5
112	nNOS Signaling in Skeletal Muscle Cells	1.47E+00	0.13	CALM1 (includes others),CALML5
113	Fcγ Receptor-mediated Phagocytosis in Macrophages and Monocytes	1.45E+00	0.05	RAC2,CDC42,IZ9,ARPC3,TLN1
114	NRF2-mediated Oxidative Stress Response	1.45E+00	0.04	DNAJC5,RRAS,PRDX1,PPIB,VCP,NQO1,CCT7,FTH1
115	Glioblastoma Multiforme Signaling	1.44E+00	0.04	RHOG,RRAS,RHOC,PDIA3,CDC42,CTNNB1,PDGFRB
116	Antigen Presentation Pathway	1.43E+00	0.08	PDIA3,HLA-A,CANX
117	UDP-D-xylose and UDP-D-glucuronate Biosynthesis	1.41E+00	0.50	UGDH
118	PI3K Signaling in B Lymphocytes	1.40E+00	0.05	CD81,CALM1 (includes others),CALML5,RRAS,PDIA3,CAMK2B
119	Calcium-induced T Lymphocyte Apoptosis	1.40E+00	0.06	CALM1 (includes others),CALML5,HLA-A,CAPN2
120	TR/RXR Activation	1.37E+00	0.05	ENO1,SLC16A3,SLC2A1,COL6A3,PFKP
121	CTLA4 Signaling in Cytotoxic T Lymphocytes	1.35E+00	0.05	PPP2CB,HLA-A,CLTA,CLTCL1,CLTC
122	Tight Junction Signaling	1.34E+00	0.04	PPP2CB,MYH9,MYL6,CDC42,CTNNA1,YBX3,CTNNB1
123	Cardiac β-adrenergic Signaling	1.28E+00	0.04	GNB1,PPP2CB,GNAS,RACK1,GNB2,GNG12
124	Granzyme A Signaling	1.24E+00	0.10	HIST1H1B,HIST1H1E
125	Diphthamide Biosynthesis	1.24E+00	0.33	EEF2
126	NADH Repair	1.24E+00	0.33	GAPDH
127	Hypusine Biosynthesis	1.24E+00	0.33	EIF5A
128	Oxidized GTP and dGTP Detoxification	1.24E+00	0.33	RUVBL2
129	Endoplasmic Reticulum Stress Pathway	1.21E+00	0.10	HSP90B1,HSPA5
130	Glioma Signaling	1.19E+00	0.05	CALM1 (includes others),CALML5,RRAS,PDGFRB,CAMK2B
131	Corticotropin Releasing Hormone Signaling	1.18E+00	0.05	GNAI2,CALM1 (includes others),CALML5,GNAS,RAP1A
132	B Cell Receptor Signaling	1.15E+00	0.04	RAC2,CALM1 (includes others),CALML5,RRAS,CDC42,RAP1A,CAMK2B
133	Renal Cell Carcinoma Signaling	1.13E+00	0.05	SLC2A1,RRAS,CDC42,RAP1A
134	Endothelin-1 Signaling	1.13E+00	0.04	GNAI2,GNAS,RRAS,PDIA3,GNA11,GNA14,CASP14
135	Uracil Degradation II (Reductive)	1.12E+00	0.25	DPYSL2
136	Glutathione Redox Reactions II	1.12E+00	0.25	PDIA3
137	Thymine Degradation	1.12E+00	0.25	DPYSL2
138	Amyloid Processing	1.11E+00	0.06	CAPN51,CAPN2,CSNK2B
139	Production of Nitric Oxide and Reactive Oxygen Species in Macrophages	1.07E+00	0.04	APOE,PPP2CB,RHOG,RHOC,S100A8,RAP1A,CLU
140	Role of Osteoblasts, Osteoclasts and Chondrocytes in Rheumatoid Arthritis	1.07E+00	0.03	ITGB1,CALM1 (includes others),CALML5,ITGA3,ITGA2,ITGA5,CTNNB1,ITGB3
141	Lipid Antigen Presentation by CD1	1.04E+00	0.08	PDIA3,CANX
142	Serine Biosynthesis	1.03E+00	0.33	PHGDH
143	Eumelanin Biosynthesis	1.03E+00	0.33	MIF
144	Crosstalk between Dendritic Cells and Natural Killer Cells	1.02E+00	0.04	HLA-A,FSCN1,TLN1,CAMK2B
145	Apoptosis Signaling	1.02E+00	0.04	CAPN51,RRAS,LMNA,CAPN2
146	Dopamine DARPP32 Feedback in cAMP Signaling	1.01E+00	0.04	GNAI2,PPP2CB,CALM1 (includes others),CALML5,GNAS,PDIA3
147	Sperm Motility	1.01E+00	0.04	CALM1 (includes others),CALML5,GNAS,PDIA3,PTK7
148	Nur77 Signaling in T Lymphocytes	9.68E-01	0.05	CALM1 (includes others),CALML5,HLA-A
149	PPAR Signaling	9.65E-01	0.04	HSP90B1,HSP90AB1,RRAS,PDGFRB
150	Glucocorticoid Receptor Signaling	9.58E-01	0.03	HSPA8,HSP90B1,YWHAH,HSP90AB1,RRAS,ANXA1,HSPA1A/HSPA1B,SERPINE1,HSPA5
151	Gα12/13 Signaling	9.56E-01	0.04	MYL6,RRAS,CDC42,CTNNB1,MYL12B
152	Pyruvate Fermentation to Lactate	9.53E-01	0.17	LDHA
153	GDP-mannose Biosynthesis	9.53E-01	0.17	GPI
154	Prostate Cancer Signaling	9.53E-01	0.04	HSP90B1,HSP90AB1,RRAS,CTNNB1
155	Ephrin A Signaling	9.51E-01	0.05	CDC42,ADAM10,EPHA2
156	CD28 Signaling in T Helper Cells	9.46E-01	0.04	CALM1 (includes others),CALML5,HLA-A,CDC42,ARPC3
157	HMGB1 Signaling	9.25E-01	0.04	RHOG,RRAS,RHOC,CDC42,SERPINE1
158	Superpathway of Serine and Glycine Biosynthesis I	8.90E-01	0.14	PHGDH
159	Endometrial Cancer Signaling	8.90E-01	0.05	RRAS,CTNNA1,CTNNB1
160	Mitotic Roles of Polo-Like Kinase	8.65E-01	0.05	PPP2CB,HSP90B1,HSP90AB1
161	Aryl Hydrocarbon Receptor Signaling	8.58E-01	0.04	TGM2,HSP90B1,HSP90AB1,NQO1,HSPB1
162	VEGF Signaling	8.48E-01	0.04	YWHAE,RRAS,ACTN4,ACTN1
163	SAPK/JNK Signaling	8.37E-01	0.04	GNB1,RAC2,RRAS,CDC42
164	Airway Pathology in Chronic Obstructive Pulmonary Disease	8.37E-01	0.13	MMP2
165	Superoxide Radicals Degradation	8.37E-01	0.13	NQO1
166	Coagulation System	8.29E-01	0.06	PLAUR,SERPINE1
167	Complement System	7.90E-01	0.05	C1R,CD59
168	GDP-glucose Biosynthesis	7.90E-01	0.11	PGM1
169	GM-CSF Signaling	7.69E-01	0.04	RRAS,RACK1,CAMK2B
170	Telomerase Signaling	7.68E-01	0.04	PPP2CB,HSP90B1,HSP90AB1,RRAS
171	Glucose and Glucose-1-phosphate Degradation	7.48E-01	0.10	PGM1
172	Nitric Oxide Signaling in the Cardiovascular System	7.47E-01	0.04	CALM1 (includes others),CALML5,HSP90B1,HSP90AB1
173	Thyroid Cancer Signaling	7.38E-01	0.05	RRAS,CTNNB1
174	Neuroprotective Role of THDP1 in Alzheimer's Disease	7.38E-01	0.05	YWHAE,HLA-A
175	HIF1α Signaling	7.29E-01	0.03	SLC2A1,RRAS,MMP2,LDHA
176	Mechanisms of Viral Exit from Host Cells	7.21E-01	0.05	CHMP4B,PDCD6IP
177	UDP-N-acetyl-D-galactosamine Biosynthesis II	7.11E-01	0.09	GPI
178	NGF Signaling	7.11E-01	0.03	RHOG,RRAS,CDC42,RAP1A
179	Regulation of IL-2 Expression in Activated and Anergic T Lymphocytes	7.00E-01	0.04	CALM1 (includes others),CALML5,RRAS
180	Glycogen Degradation II	6.77E-01	0.08	PGM1
181	LXR/RXR Activation	6.76E-01	0.03	APOE,TF,S100A8,CLU
182	NOS Signaling	6.75E-01	0.05	CALM1 (includes others),CALML5
183	ICOS-ICOSL Signaling in T Helper Cells	6.68E-01	0.03	CALM1 (includes others),CALML5,HLA-A,CAMK2B
184	Guanosine Nucleotides Degradation III	6.46E-01	0.08	NT5E
185	Acute Phase Response Signaling	6.30E-01	0.03	C1R,ITIH3,TF,RRAS,SERPINE1
186	Wnt/β-catenin Signaling	6.30E-01	0.03	PPP2CB,GJA1,RUVBL2,CSNK2B,CTNNB1
187	Atherosclerosis Signaling	6.28E-01	0.03	APOE,S100A8,CLU,GLO1
188	TGF-β Signaling	6.19E-01	0.03	RRAS,CDC42,SERPINE1
189	DNA Double-Strand Break Repair by Non-Homologous End Joining	6.18E-01	0.07	XRCC5
190	Glycogen Degradation III	6.18E-01	0.07	PGM1
191	Urate Biosynthesis/Inosine 5'-phosphate Degradation	6.18E-01	0.07	NT5E
192	Chondroitin Sulfate Degradation (Metazoa)	5.92E-01	0.07	CEMIP
193	Vitamin C Transport	5.92E-01	0.07	SLC2A1
194	PDGF Signaling	5.91E-01	0.03	RRAS,CSNK2B,PDGFRB
195	TKC-θ Signaling in T Lymphocytes	5.91E-01	0.03	RAC2,RRAS,HLA-A,CAMK2B
196	Death Receptor Signaling	5.74E-01	0.03	PARP4,LMNA,HSPB1
197	cAMP-mediated signaling	5.70E-01	0.03	GNAI2,CALM1 (includes others),CALML5,GNAS,RAP1A,CAMK2B
198	Dermatan Sulfate Degradation (Metazoa)	5.68E-01	0.06	CEMIP
199	γ-glutamyl Cycle	5.68E-01	0.06	ANPEP
200	Triacylglycerol Degradation	5.58E-01	0.04	AARS,PRDX6

Chapter 5: Figure 8 Supplementary Table 2 (Page 3 of 3)

After thresholding as described in Methods, datasets from Supp.Table 1 were used as input for the IPA software, to generate pathways most highly-associated with the exosomes' proteomes. Supp.Table 2 presents the unredacted list of all pathways identified by the IPA software, along with the –log(p-value) for each pathway. Pathways with –log(p-value) below the significance value of 1.35 are greyed-out. The adjacent column indicates the Pathway Ratio, which the IPA software computes; it is a proportion of how many proteins were found in the sample (then names them in the adjacent column) based on the company's proprietary list of the proteins they have identified to be in that pathway. The immunology-relevant pathways of interest to our team are shaded yellow.

201	G-Protein Coupled Receptor Signaling	5.51E-01	0.03	GNAI2,GNAS,RRAS,GNA11,GNA14,RAP1A,CAMK2B
202	Adenosine Nucleotides Degradation II	5.46E-01	0.06	NTSE
203	Methionine Degradation I (to Homocysteine)	5.46E-01	0.06	AHCY
204	Sumoylation Pathway	5.41E-01	0.03	RHOG,RHOC,GOI2
205	AMPK Signaling	5.11E-01	0.03	PPP2CB,GNAS,SLC2A1,EEF2,PFKP
206	Ovarian Cancer Signaling	5.10E-01	0.03	GJA1,RRAS,MMP2,CTNNB1
207	Cysteine Biosynthesis III (mammalia)	5.06E-01	0.05	AHCY
208	Cholecystokinin/Gastrin-mediated Signaling	5.02E-01	0.03	RHOG,RRAS,RHOC
209	IL-12 Signaling and Production in Macrophages	4.98E-01	0.03	APOE,RAB7A,S100A8,CLU
210	UVA-Induced MAPK Signaling	4.95E-01	0.03	RRAS,PDIA3,PARP4
211	Purine Nucleotides Degradation II (Aerobic)	4.88E-01	0.05	NTSE
212	Maturity Onset Diabetes of Young (MODY) Signaling	4.70E-01	0.05	GAPDH
213	PCP pathway	4.58E-01	0.03	PFN1,HSPB1
214	Polyamine Regulation in Colon Cancer	4.54E-01	0.05	CTNNB1
215	Cell Cycle: G1/S Checkpoint Regulation	4.49E-01	0.03	RPL11,RPL5
216	IL-2 Signaling	4.49E-01	0.03	RRAS,CSNK2B
217	T Cell Receptor Signaling	4.47E-01	0.03	CALM1 (includes others),CALML5,RRAS
218	Amyotrophic Lateral Sclerosis Signaling	4.34E-01	0.03	CAPNS1,RAB5C,CAPN2
219	Glutathione Redox Reactions I	4.24E-01	0.04	PRDX6
220	Role of Macrophages, Fibroblasts and Endothelial Cells in Rheumatoid Arthritis	4.01E-01	0.02	CALM1 (includes others),MIF,CALML5,RRAS,PDIA3,CTNNB1,CAMK2B
221	NAD Salvage Pathway II	3.97E-01	0.04	NTSE
222	IL-15 Production	3.85E-01	0.04	PTK7
223	STAT3 Pathway	3.79E-01	0.03	RRAS,PDGFRB
224	TR/RXR Signaling	3.66E-01	0.03	ITGB1,ITGA5
225	GDNF Family Ligand-Receptor Interactions	3.59E-01	0.03	RRAS,CDC42
226	Heparan Sulfate Biosynthesis (Late Stages)	3.59E-01	0.03	AARS,PRDX6
227	Neurotrophin/TRK Signaling	3.59E-01	0.03	RRAS,CDC42
228	Glutathione-mediated Detoxification	3.51E-01	0.03	ANPEP
229	FXR/RXR Activation	3.51E-01	0.02	APOE,TF,CLU
230	IL-6 Signaling	3.46E-01	0.02	RRAS,CSNK2B,HSPB1
231	Cytotoxic T Lymphocyte-mediated Apoptosis of Target Cells	3.30E-01	0.03	HLA-A
232	Superpathway of Methionine Degradation	3.30E-01	0.03	AHCY
233	MIF-mediated Glucocorticoid Regulation	3.21E-01	0.03	MIF
234	Heparan Sulfate Biosynthesis	3.16E-01	0.02	AARS,PRDX6
235	Oncostatin M Signaling	3.12E-01	0.03	RRAS
236	Inhibition of Angiogenesis by TSP1	3.12E-01	0.03	HSPG2
237	Xenobiotic Metabolism Signaling	3.11E-01	0.02	PPP2CB,HSP90B1,HSP90AB1,RRAS,NQO1,CAMK2B
238	IL-17 Signaling	3.05E-01	0.02	RRAS,TIMP1
239	Cell Cycle Regulation by BTG Family Proteins	3.03E-01	0.03	PPP2CB
240	B Cell Development	3.03E-01	0.03	HLA-A
241	LPS-stimulated MAPK Signaling	3.00E-01	0.02	RRAS,CDC42
242	Regulation of the Epithelial Mesenchymal Transition Pathway	2.97E-01	0.02	RRAS,MMP2,CTNNB1,PDGFRB
243	Bladder Cancer Signaling	2.94E-01	0.02	RRAS,MMP2
244	Dendritic Cell Maturation	2.94E-01	0.02	DDR2,PDIA3,HLA-A,FSCN1
245	VEGF Family Ligand-Receptor Interactions	2.89E-01	0.02	RRAS,NRP1
246	IL-4 Signaling	2.84E-01	0.02	RRAS,HLA-A
247	Hereditary Breast Cancer Signaling	2.80E-01	0.02	NPM1,RRAS,H2AFX
248	Human Embryonic Stem Cell Pluripotency	2.76E-01	0.02	GNAS,CTNNB1,PDGFRB
249	Acute Myeloid Leukemia Signaling	2.74E-01	0.02	RRAS,JUP
250	Netrin Signaling	2.71E-01	0.03	RAC2
251	Ceramide Signaling	2.65E-01	0.02	PPP2CB,RRAS
252	MIF Regulation of Innate Immunity	2.56E-01	0.02	MIF
253	Melanocyte Development and Pigmentation Signaling	2.56E-01	0.02	GNAS,RRAS
254	UVC-Induced MAPK Signaling	2.50E-01	0.02	RRAS
255	Pyrimidine Ribonucleotides Interconversion	2.43E-01	0.02	ANXA1
256	Role of p14/p19ARF in Tumor Suppression	2.43E-01	0.02	NPM1
257	ErbB Signaling	2.43E-01	0.02	RRAS,CDC42
258	Pyrimidine Ribonucleotides De Novo Biosynthesis	2.31E-01	0.02	ANXA1
259	RANK Signaling in Osteoclasts	2.30E-01	0.02	CALM1 (includes others),CALML5
260	Autoimmune Thyroid Disease Signaling	2.19E-01	0.02	HLA-A
261	Graft-versus-Host Disease Signaling	2.14E-01	0.02	HLA-A
262	TNFR1 Signaling	2.08E-01	0.02	CDC42
263	Cancer Drug Resistance By Drug Efflux	2.08E-01	0.02	RRAS

Chapter 6: Conclusions and Next Steps

Introduction: Lessons from the Node

It is our hope that by studying the cellular biology of the MSC, we may be able to better understand the mechanisms by which these cells function in the human body, and thereby better develop cell-based therapies. Though a number of encouraging clinical studies have been undertaken in recent years, key questions remain, most importantly, precise definitions of the immunologic correlates of MSC efficacy. In vaccinology, particularly in the elusive search for an HIV vaccine, extensive immunology research is on-going at Emory and other places, investigating the role of helper T cells, different B cell subsets or the virus itself. These follow logically from the same premise, that the more we understand the basic biology, chemistry, and virology, the better we can develop new therapies.

The present work has been basic in scope, seeking to understand how MSCs use the IDO protein for tolerance-signaling, and had originally developed from inquiries into the key correlates of MSC-based immunotherapy. As sometime happens in basic research, we discovered unforeseen connections, notably to the field of toxicology and oncology, linking carcinogenesis to the signals transduced by aromatic hydrocarbons. As an MD slash PhD student, I have come to appreciate how existing at the nodes, or crossing-points, of different fields, one can leverage innovative perspectives, gained from listening

to and learning from experts outside one's tradition. This has been my experience, studying chemistry as an undergraduate, joining an immunology lab in medical school and developing collaborations at the Rollins School of Public Health. It was through these connections that I conceived of and wrote for our lab a sizeable grant (awarded through the National Institute for Environmental Health Sciences), and then went on to attend the Society of Toxicology' annual meeting. These scientific techniques truly blossomed after that conference, as I corresponded extensively with some of these scientists (who graciously shared reagents and detailed methods with our lab). Theretofore, these scientists may not have ever heard of MSC cell therapy, or appreciate the huge value that AHR signaling in tissue-resident stem cells may have for clinical oncology.

In a similar fashion, I was excited to help spearhead efforts to better understand the biology of the MSC when our lab's attention first turned to investigate exosomes. When interviewing for MD/PhD programs, I first met Dr. Mary Galinski, inspired by her integrative approach to systems biology, vaccine immunology and global health. It was during my first Emory rotation at her lab, working closely with Stacey Lapp, deep in the woods of Yerkes, when I first read of these membranous vesicles laden with immunologic potential. Originally defined as a way for developing red blood cells to extrude 'useless' components, exosomes are now understood as part of the secretome of a variety of cells. For example, exosomes have been shown to be released by primate and murine cells infected with *Toxoplasmosis gondii* and *Plasmodia* spp., leading in some cases to innovative exosome-based vaccination strategies for congenital toxoplasmosis and

malaria [1-3]. Relatedly, I developed some of the herein-described exosome protocols during my time at Yerkes, characterizing parasite proteins in exosomes derived from the red blood cells of Rhesus macaques infected with *Plasmodium cynomolgi* (See Chapter 6: Figure 1). By integrating these diverse experiences along those nodes, this dissertation has made important contributions to MSC biology, cell therapy, and perhaps even applicable to infectious disease vaccinology.

AHR Signaling in MSCs: Contributions from This Dissertation

Environmental exposure to aryl hydrocarbon toxins and signaling via AHR have been well-explored, due to patent links to a number of human disease states [4]. However, less has been discovered about endogenous AHR ligands, such as the byproducts of tryptophan metabolism, and how these signaling pathways may overlap. We hypothesized that environmental and endogenously-generated AHR ligands may share signaling modalities in the microstroma of human tissues; that these events could be modeled using patient-derived tissue-resident stem cells; and that characterizing AHR ligand metabolism in biologic systems can afford new insight on how aryl hydrocarbon metabolism is linked to dysregulated and pathologic immune responses.

As discussed in chapter 2, our lab and others have demonstrated that indoleamine 2,3-dioxygenase (IDO) is a crucial determinant of the immunomodulatory and regenerative abilities of MSCs. MSCs are the basis of more than 100 clinical trials worldwide, but the mechanisms whereby MSCs mediate immunomodulatory effects are incompletely

described [5]. In MSCs and other IDO-expressing cells, 1-methyl tryptophan (1-MT) has been historically described as an enzymatic inhibitor of IDO, and is currently the focus of eight clinical trials, aimed at augmenting an anti-tumor response.

Tissue-Resident Stem Cells and Inflammation

In the marrow, MSCs interact with hematopoietic stem cells, neuron terminals and microvasculature to coordinate the development of new blood cells; it is in the marrow that their classical immunomodulation has been described [6]. However, in parenchymal (non-hematopoietic) organs, MSCs have been shown to exert similar immunomodulatory effects, most prominently in inflammatory immune responses. Through an assortment of Toll-like receptors, chemokines and other as yet-undefined sensors, MSCs are exquisitely poised to integrate diverse stimuli and orchestrate both an inflammatory response as well as the post-inflammatory resolution/repair pathways, through interactions with tissue-resident stroma as well as immigrant leukocytes [7].

A paradigm in clinical medicine is the cycle by which environmentally-acquired toxicants induce localized damage, inciting a dysregulated immune response, leading to chronic or otherwise irreversible inflammatory change. Such a pattern has been well-described for aflatoxin- or organochloride-induced liver fibrosis, cigarette toxins in both lung and urothelial cancers, and pleural inflammation arising from exposure to asbestos or beryllium [8-10]. Given their ubiquity in many tissues, MSCs have been observed as part of the stromal component of a number of diseases, including malignant and non-

malignant pathologies [11]. Lung-resident MSCs have been noted to play a pro-inflammatory role in interstitial pulmonary fibrosis, a dysregulated remodeling of pulmonary tissues common after exposures such as coal dust or vanadium oxide (V2O5) poisoning [12]. The presence of MSCs can be readily noted; however, the relative contribution by MSCs to disease (i.e. pro-inflammatory or anti-inflammatory) is not uniformly observed[13].

Despite their role in the post-injury inflammation to environmental toxins, there are no published studies exploring the interactions between AHR ligands and lung-resident MSCs.

AHR, Stem Cells and the Immune System

The present dissertation is perhaps one of the first studies to link 1-MT, immune signaling of stem cells and the AHR pathway, a novel contribution that has emerged along the nodes of innovation. Much of our understanding of aryl hydrocarbons have arisen from studies with TCDD, or dioxin. First described as a dioxin receptor, AHR associates with the AHR nuclear translocator (AHRnt) upon ligand binding, activating transcription at AHR response elements (AHREs) [14]. Signaling at AHREs has been implicated in carcinogenesis using aromatic hydrocarbons like benzopyrene. In such studies, ligand-activation of AHR is often shown by the upregulation of cytochrome p450 (Cyp) enzymes, Cyp1a1 and Cyp1b1. However, the evolutionary conservation of AHR signaling (including invertebrates with no such hepatic biotransformation of toxins suggests a broader

physiologic function for AHR signaling. To our knowledge, the present dissertation is the first to use MSCs in such analyses, linking environmental toxicology to the mechanisms of immune tolerance.

Recently, it was shown that two prototypic AHR ligands, TCDD and 6-formylindolo[3,2-b]carbazole (FICZ), can differentially modulate the activity of IDO+ DCs [15]. In a mouse model of multiple sclerosis, it was shown that TCDD-treated DCs generated anti-inflammatory Tregs, but FICZ treatments generated inflammatory Th17 cells [16]. Transfer of the inflammatory Th17 cells exacerbated disease in the mice, whereas transfer of the Treg population ameliorated symptoms [16]. This is a crucial finding, as it suggests that different classes of AHR ligand (through AHRE activation at disparate genetic loci) can have vastly differential impact on disease. One such example is in the activation of IL6, a cytokine known to be involved in Treg/Th17 polarization. Dr. Gary Perdew (noted toxicologist the first author first met in San Diego at SOT 2015) has shown that the promoter of IL6 contains imperfect AHREs, with sequence homology that permits ligand-activated recruitment of AHR [17]. Dr. Perdew showed that AHR-mediated activity at the IL6 promoter results in dismissal of histone deacetylase-1, and recruitment of nuclear factor-κB (NFκB), both described as examples of pro-inflammatory signaling in tissue microenvironments.

Mechanistic understanding of how different AHR ligands induce disparate immune responses remains incomplete, but studying these ligands in a clinically-relevant model

(patient-derived stem cells) has afforded us important new perspectives on how they may be used in clinical oncology.

AHR and Stem Cell Innovation

The present work has addressed two distinct, yet complementary goals: (i) characterize the transcriptional events initiated by aryl hydrocarbons; and (ii) interrogate the metabolic and functional effects of AHR ligands on the immunomodulatory properties of MSCs. We investigated these mechanisms through the use of MSCs, but this study has important implications for other immune cell types (i.e. dendritic cells, macrophages) that can express IDO in a tissue microenvironment. This work involved primary human stem cell culture, immunologic, and biochemical assay systems, all standard techniques at the Galipeau lab; our transcriptomic and bioinformatic studies were pursued with various lab collaborators.

Linking small molecule catalysis and the signals of immune plasticity is hugely important to developing integrative new therapeutics. The paramount importance of IDO in modulating the immune response has been well-understood; several well-financed clinical trials are underway with an enzymatic inhibitor that aims to augment the anti-tumor response. However, it is unknown what role is played by exogenous and endogenous aryl hydrocarbons, especially in the case of tissue-resident MSCs. The current dissertation has drawn upon the rich literature of molecular toxicology, as well as the expertise of clinically-relevant stem cell biologists at Emory University and Georgia Tech.

Through a collaborative process, this project elucidated how environmental toxins and stem cell signaling can together be leveraged to better develop cancer immunotherapy.

AHR and Stem Cells: Experimental Next Steps

While we await the 1-MT/AHR manuscript's full-press release, I hope that it will foster future inquiries, and have reverberations beyond the field of MSC therapy, inspiring others to test our observations. Notably, EMSA-based ligand-binding studies will need to be performed, as my *in silico* structural chemistry work, while important, is not yet definitive-enough for 1-MT to be termed as a *bona fide* AHR ligand. An additional key set of experiments should involve the use of short interfering RNA knockdown (for IDO and/or AHR), to further corroborate that the 1-MT drug can stimulate an anti-tumor immune response even in the absence of IDO expression.

It is my sincere hope that the *Oncotarget* paper will be read and appreciated by clinicians using IDO-inhibitor drugs for cancer therapy. As mentioned in Chapter 2, it may become an important clinical rationalization to broaden the indications for these drugs, based on their AHR- and immune-stimulating activity. Although few of these IDO clinical trials directly involve MSCs, the node-based innovation of this work demonstrates how basic science can be leveraged to better harness the power of the body's immune system, and prime its endogenous cancer-fighting abilities. A new revolution in cancer cures has emerged following the 2001 FDA approval of imatinib, the first biochemically-rationalized chemotherapeutic. In clinical oncology research, it is always advantageous to use a more

precise pharmacologic approach, especially in frail patients with other co-morbidities. Innovative and ever-more-targeted therapies will continue to give scientists, clinicians and patients reason to hope for a cure.

MSC-Derived Exosomes: Contributions from This Dissertation

As described in Chapter 5, MSC-derived exosomes have generated considerable excitement among basic and translational researchers. One of the touted advantages of such vesicles is their 'universal' application, as they may permit the infusion of a cell-free cellular product, theoretically avoiding issues with donor-patient immune compatibility. Our laboratory has not pursued this avenue for our clinical trials, in part because of extant literature showing third-party MSCs already have a very low risk for graft rejection, being *de facto* universal in their application [18]. However, as we have observed during biodistribution assays that infused MSCs can sometimes lodge in the lung vasculature, we hypothesized that exosomes may explain how the cells can have distant effects in a paracrine nature without actually migrating to inflamed tissues.

Additionally, the observations that soluble as well as contact-dependent factors are implicated in the bioactive mechanism of MSC have often been based on tissue culture work using conditioned medium (CM). We hypothesized that the CM ultra-concentrate, with its exosomes, might explain the bioactive effect, enabling therapeutic delivery of a small exosome dose, rather than injecting large quantities of CM into animals or patients (a volume-based game that is virtually impossible).

The studies in Chapter 5 truly blossomed when we began collaborating with a laboratory interested in understanding the role of MSC-derived factors in supporting plasma cell function. They had already developed an in vitro system using CM to keep non-cancerous plasma cells alive for a month, which is innovative and exciting on its own. Our contributions, that exosomes may rationalize some of this phenomenon, adds important new knowledge to the fields of exosomes, cell therapy and vaccinology. It is crucial for vaccine development to better-understand the cues that enable B cells to develop long-lasting antibodies, just as it is important to develop cell platforms to expand B cells outside of the body. As for MSCs, the studies in this dissertation may help explain by parsimony the dual dependence of soluble and contact-mediated factors in MSC bioactivity.

A Note on Modeling, Epistemology, and Chemical Physics

Chapter 5 is an extensive characterization of the proteins found in MSC-derived exosomes, leveraging bioinformatic techniques to develop a hypothesis, as a first-order model that rationalizes how exosomes may support the *ex vivo* functionality of healthy plasma cells. Although such may appear at first pass to be "mere description," as a person who pursued a secondary bachelor's training in the historical and literary analysis of Romance-language texts, I would ask the reader to critically examine such a premise. Epistemology is the study of how we create new knowledge, and in particular, how that new knowledge is justified according to known or accepted premises. From an epistemological perspective, I posit that the exosome story as written should not suffer

any lack of scientific credibility because it sought to explicate a phenomenon by modeling along a one-dimensional axis (the MSC exosomes' proteomes).

Contemporary political philosopher John Derring explains that any "mere description" of a phenomena carries with it a preconceived bias, a premise from which hypotheses can be formulated [19]. These ideas, classically elaborated by sociologist Jean Baudrillard in *Le Système des objets* (*The System of Objects*) describe how the effort to understand an object by description is non-trivial at best, and inextricably problematic at worst. Baudrillard would contend that a person can only perform signification (naming) in reference to other known identities [20]. As each new referential frame arises from *a priori* assumptions of relationality, the effort towards 'mere description' is not only non-objective, it becomes critical, theoretical, and important for future scholars to continue to break apart for further study (just as we do in biological reproducibility studies).

To take a step back into the realms of conventional biomedicine, I recall my Harvard coursework in chemical physics, involving a great deal of multivariate calculus and linear algebra, such as the Hamiltonian operator and its corollary, the more colloquially-understood Schrödinger equation (namesake of the proverbial cat that is both alive and dead at the same time). Briefly, as one mathematically describes a wave function (a 3-dimensional probability distribution) to model the *x-y-z* location of an electron, it becomes impossible to ascertain the particle's velocity, which is rigorously defined as the cross-product of speed (a scalar) and direction (a vector). In essence, there is no such

thing as mere description, for every frame of reference we establish is relativistic, biased by framing the question from the perspective of quantum mechanics, linguistics, cell therapy or toxicology.

MSC-Derived Exosomes: Next Steps for Next-Gen Cell Therapy

Chapter 5 was an effort to build off of our established home field of MSC cell therapy and leverage widely-established proteomic techniques to identify immune pathways, thereby developing a first-pass model to explain the observed phenomena. It is essential to state, as we did in the Discussion for Chapter 5, that the bioinformatic techniques used to explore MSC and B cell relationality will need to be assessed in follow-up experiments.

To my estimation, the most important studies to pursue will be a complete profiling of the exosomes themselves, as well as the intact MSC cell. I learned during my time with Dr. Galinski's Malaria Host-Pathogen Interaction Center that the best way to perform systems biology is through extensive collaborations that seek to understand lipidomics and metabolomics, in addition to conventional mRNA (and microRNA) transcriptomics and proteomics. All of these factors will have inter-related effects, especially when it comes to unleashing the potential of these membranous spheroids laden with bioactive molecules.

Importantly, these same parameters should be performed on the antibody-secreting plasma cells; our collaborating lab is already well under-way in characterizing the ASCs'

RNA and protein contents. It is through such a rigorous description that mathematical modeling and bioinformatic techniques can begin to unravel the bi-directional stem cell and B cell signals in the human marrow that maintain an immune repertoire. Indeed, the (conditioned) medium is the message.

Chapter 6: Figure 1: Exosomes from Rhesus Macaques

Figure 1: Exosomes from Rhesus Macaques

A. Photomicrograph of exosomes derived from the red blood cells from a Rhesus macaque infected with *Plasmodium cynomolgi*. Exosomes were fixed in 2% paraformaldehyde (PFA) o.n. at 4˚C. Fixed exosomes were deposited onto formvar grids for 20 min. Grids were then fixed in glutaraldehyde 1% for 5 min, washed in distilled water and negatively stained for 5 min with a solution of uranyl-oxalate (pH = 7) and for 10 min at 4˚C with uranyl acetate (4%)-methyl cellulose (2%). After thoroughly drying, grids were observed with a JEOL 1010 transmission electron microscope. Micrographs were used to quantify the diameter of exosomes; scale bar is 100 nm.

A.

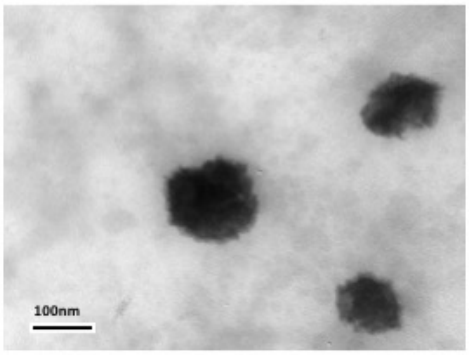

Lewis CN, Lapp, Breding, Galinski.
Unpublished data, 2013.

Chapter 6: Figure 2 Exosomes from AHR+ MSCs

Figure 2: Exosomes from AHR+ MSCs

Tattooed artistic renderings, designed by Holly Chris Lewis, based on images in Chapter 2: Figure 2 and injected by Dustin Swinks of Memorial Tattoo Shop, East Atlanta. Panel portrays green holly leaves interspersed with GFP- and DAPI-colored MSCs. Perinuclear stippling is noted in a distribution consistent with the subcellular location of the AHR protein. Panel also includes the antecubital fossa of Holly Chris Lewis, is the site typically used for peripheral blood phlebotomy. This tattoo portrays an MSC releasing multi-colored exosomes shaped like holly berries.

References (Separated by Chapter)

References for Chapter 1: Introduction

1. Anthony, B.A. and D.C. Link, *Regulation of hematopoietic stem cells by bone marrow stromal cells.* Trends Immunol, 2014. **35**(1): p. 32-7.
2. Dalal, J., K. Gandy, and J. Domen, *Role of mesenchymal stem cell therapy in Crohn's disease.* Pediatr Res, 2012. **71**(4 Pt 2): p. 445-51.
3. Katayama, Y., et al., *Signals from the sympathetic nervous system regulate hematopoietic stem cell egress from bone marrow.* Cell, 2006. **124**(2): p. 407-21.
4. Omatsu, Y., et al., *The essential functions of adipo-osteogenic progenitors as the hematopoietic stem and progenitor cell niche.* Immunity, 2010. **33**(3): p. 387-99.
5. Mendez-Ferrer, S., et al., *Mesenchymal and haematopoietic stem cells form a unique bone marrow niche.* Nature, 2010. **466**(7308): p. 829-34.
6. Greenbaum, A., et al., *CXCL12 in early mesenchymal progenitors is required for haematopoietic stem-cell maintenance.* Nature, 2013. **495**(7440): p. 227-30.
7. Murphy, M.B., K. Moncivais, and A.I. Caplan, *Mesenchymal stem cells: environmentally responsive therapeutics for regenerative medicine.* Exp Mol Med, 2013. **45**: p. e54.
8. Kobayashi, M., et al., *PRL2/PTP4A2 phosphatase is important for hematopoietic stem cell self-renewal.* Stem Cells, 2014. **32**(7): p. 1956-67.
9. Keller JR, O.M., Ruscetti FW., *Steel factor (c-kit ligand) promotes the survival of hematopoietic stem/progenitor cells in the absence of cell division.* Blood, 1994. **86**(5): p. 1757-1764.

10. Jaeger S, F.B., Ferrier P, *Epigenetic aspects of lymphocyte antigen receptor gene rearrangement or 'when stochasticity completes randomness'.* Immunology, 2012. **139**: p. 141-150.

11. Liu, G., et al., *Umbilical cord-derived mesenchymal stem cells regulate thymic epithelial cell development and function in Foxn1(-/-) mice.* Cell Mol Immunol, 2014. **11**(3): p. 275-84.

12. Lin, Z.B., et al., *Isolation, characterization and cardiac differentiation of human thymus tissue derived mesenchymal stromal cells.* J Cell Biochem, 2014.

13. Deschaseaux, F., et al., *Regulation and function of immunosuppressive molecule human leukocyte antigen G5 in human bone tissue.* FASEB J, 2013. **27**(8): p. 2977-87.

14. Naji, A., et al., *Concise review: combining human leukocyte antigen G and mesenchymal stem cells for immunosuppressant biotherapy.* Stem Cells, 2013. **31**(11): p. 2296-303.

15. J, S.J.a.G., *Mechanisms of Immune Modulation by Mesenchymal Stromal Cells and Clinical Translation.* Current Molecular Medicine, 2013. **13**: p. 856-867.

16. Raphaelle Romieu-Mourez, D.L.C., Jacques Galipeau, *The immune plasticity of mesenchymal stromal cells from mice and men: concordances and discrepancies.* Frontiers in Bioscience, 2012. **E4**: p. 824-837.

17. da Silva Meirelles, L., P.C. Chagastelles, and N.B. Nardi, *Mesenchymal stem cells reside in virtually all post-natal organs and tissues.* J Cell Sci, 2006. **119**(Pt 11): p. 2204-13.

18. David S Kwon, X.G., Yong Bo Liu, Deborah S Dulchavsky, Andrew L Danyluk, Mona Bansal, Michael Chopp, Kevin McIntosh, Ali S Arbab, Scott A Dulchavsky, Subhash C Gautam, *Treatment with bone marrow-derived stromal cells accelerates wound healing in diabetic rats.* International Wound Journal, 2008. **5**: p. 453-463.

19. Mackenzie, T.C. and A.W. Flake, *Human mesenchymal stem cells persist, demonstrate site-specific multipotential differentiation, and are present in sites of wound healing and tissue regeneration after transplantation into fetal sheep.* Blood Cells Mol Dis, 2001. **27**(3): p. 601-4.

20. Liwen Chen, E.E.T., Philip Y. G. Wu, Yaojiong Wu, *Paracrine Factors of Mesenchymal Stem Cells Recruit Macrophages and Endothelial Lineage Cells and Enhance Wound Healing.* PloS One, 2008. **3**(4): p. e1886.

21. Murray, I.R., et al., *Natural history of mesenchymal stem cells, from vessel walls to culture vessels.* Cellular and Molecular Life Sciences, 2013. **71**(8): p. 1353-1374.

22. Andrea Zaniboni, C.B., Marco Alessandri, Chiara Mangano, Augusta Zannoni, Francesca Bianchi, Giuseppe Sarli, Laura Calzà, Maria Laura Bacci, and Monica Forni, *Cells derived from porcine aorta tunica media show mesenchymal stromal-like cell properties in in vitro culture.* Am J Physiol Cell Physiol 2014. **306**: p. C322-C333.

23. Turner, C.G., et al., *Craniofacial repair with fetal bone grafts engineered from amniotic mesenchymal stem cells.* J Surg Res, 2012. **178**(2): p. 785-90.

24. Moshaverinia, A., et al., *Application of stem cells derived from the periodontal ligament or gingival tissue sources for tendon tissue regeneration.* Biomaterials, 2014. **35**(9): p. 2642-50.

25. Götherström C, W.M., Shaw SW, Aström E, Biswas A, Byers PH, Mattar CN, Graham GE, Taslimi J, Ewald U, Fisk NM, Yeoh AE, Lin JL, Cheng PJ, Choolani M, Le Blanc K, Chan JK., *Pre- and postnatal transplantation of fetal mesenchymal stem cells in osteogenesis imperfecta: a two-center experience.* Stem Cells Translational Medicine, 2014. **3**(2): p. 255-264.

26. Moutih Rafei, J.H., Simon Fortier, MengYang Li, Shala Yuan, Elena Birman, Kathy Forner, Marie-Noelle Boivin, Karen Doody, Michel Tremblay, Borhane Annabi and Jacques Galipeau, *Mesenchymal stromal cell derived CCL2 suppresses plasma cell immunoglobulin production via STAT3 inactivation and PAX5 induction.* Blood, 2008. **112**: p. 4991-4998.

27. Corcione, A., et al., *Human mesenchymal stem cells modulate B-cell functions.* Blood, 2006. **107**(1): p. 367-72.

28. Ma, L., et al., *Immunosuppressive function of mesenchymal stem cells from human umbilical cord matrix in immune thrombocytopenia patients.* Thromb Haemost, 2012. **107**(5): p. 937-50.

29. Diz-Küçükkaya, R., et al., *Chapter 119. Thrombocytopenia*, in *Williams Hematology, 8e*, M.A. Lichtman, et al., Editors. 2010, The McGraw-Hill Companies: New York, NY.

30. Kipps, T.J., *Chapter 5. The Organization and Structure of Lymphoid Tissues*, in *Williams Hematology, 8e*, M.A. Lichtman, et al., Editors. 2010, The McGraw-Hill Companies: New York, NY.

31. Hubert, F.X., et al., *Aire regulates the transfer of antigen from mTECs to dendritic cells for induction of thymic tolerance.* Blood, 2011. **118**(9): p. 2462-72.

32. Shi, L.Z., et al., *HIF1alpha-dependent glycolytic pathway orchestrates a metabolic checkpoint for the differentiation of TH17 and Treg cells.* J Exp Med, 2011. **208**(7): p. 1367-76.

33. Im, K.I., et al., *Induction of Mixed Chimerism Using Combinatory Cell-Based Immune Modulation with Mesenchymal Stem Cells and Regulatory T Cells for Solid-Organ Transplant Tolerance.* Stem Cells Dev, 2014.

34. Roemeling-van Rhijn, M., et al., *Effects of Hypoxia on the Immunomodulatory Properties of Adipose Tissue-Derived Mesenchymal Stem cells.* Front Immunol, 2013. **4**: p. 203.

35. Cuerquis, J., et al., *Human mesenchymal stromal cells transiently increase cytokine production by activated T cells before suppressing T-cell proliferation: effect of interferon-gamma and tumor necrosis factor-alpha stimulation.* Cytotherapy, 2014. **16**(2): p. 191-202.

36. Chinnadurai, R., et al., *IDO-independent suppression of T cell effector function by IFN-gamma-licensed human mesenchymal stromal cells.* J Immunol, 2014. **192**(4): p. 1491-501.

37. Ribeiro, A., et al., *Mesenchymal stem cells from umbilical cord matrix, adipose tissue and bone marrow exhibit different capability to suppress peripheral blood B, natural killer and T cells.* Stem Cell Res Ther, 2013. **4**(5): p. 125.

38. Bocelli-Tyndall, C., et al., *Human bone marrow mesenchymal stem cells and chondrocytes promote and/or suppress the in vitro proliferation of lymphocytes stimulated by interleukins 2, 7 and 15.* Ann Rheum Dis, 2009. **68**(8): p. 1352-9.

39. Engela, A.U., et al., *Mesenchymal stem cells control alloreactive CD8(+) CD28(-) T cells.* Clin Exp Immunol, 2013. **174**(3): p. 449-58.

40. Singer, N.G. and A.I. Caplan, *Mesenchymal stem cells: mechanisms of inflammation.* Annu Rev Pathol, 2011. **6**: p. 457-78.

41. Uccelli, A., L. Moretta, and V. Pistoia, *Mesenchymal stem cells in health and disease.* Nat Rev Immunol, 2008. **8**(9): p. 726-36.

42. Le Blanc, K. and D. Mougiakakos, *Multipotent mesenchymal stromal cells and the innate immune system.* Nat Rev Immunol, 2012. **12**(5): p. 383-96.

43. Schmid, M. and D.A. Carson, *Chapter 13. Cell-Cycle Regulation and Hematologic Disorders*, in *Williams Hematology, 8e*, M.A. Lichtman, et al., Editors. 2010, The McGraw-Hill Companies: New York, NY.

44. Corthay, A., *Does the immune system naturally protect against cancer?* Front Immunol, 2014. **5**: p. 197.

45. Afshar-Sterle, S., et al., *Fas ligand-mediated immune surveillance by T cells is essential for the control of spontaneous B cell lymphomas.* Nat Med, 2014. **20**(3): p. 283-90.

46. Tu, M.M., et al., *Ly49 family receptors are required for cancer immunosurveillance mediated by natural killer cells.* Cancer Res, 2014. **74**(14): p. 3684-94.

47. Akbay, E.A., et al., *Activation of the PD-1 pathway contributes to immune escape in EGFR-driven lung tumors.* Cancer Discov, 2013. **3**(12): p. 1355-63.

48. Dai, S., et al., *The PD-1/PD-Ls pathway and autoimmune diseases.* Cell Immunol, 2014. **290**(1): p. 72-79.

49. Dong, H., et al., *Tumor-associated B7-H1 promotes T-cell apoptosis: a potential mechanism of immune evasion.* Nat Med, 2002. **8**(8): p. 793-800.

50. Yvette Latchman, C.R.W., Tatyana Chernova, Divya Chaudhary, Madhuri Borde, Irene Chernova, Yoshiko Iwai, Andrew J. Long, Julia A. Brown, Raquel Nunes, Edward A. Greenfield, Karen Bourque,Vassiliki A. Boussiotis, Laura L. Carter, Beatriz M. Carreno, Nelly Malenkovich, Hiroyuki Nishimura,Taku Okazaki, Tasuku Honjo, Arlene H. Sharpe, and Gordon J. Freeman., *PD-L2 is a second ligand for PD-1 and inhibits T cell activation.* Nature Immunology, 2001. **2**(3): p. 261-268.

51. Fumiya Hirano, K.K., Hideto Tamura, Haidong Dong, Shengdian Wang, Masao Ichikawa, Cecilia Rietz, Dallas B. Flies, Julie S. Lau, Gefeng Zhu, Koji Tamada, and Lieping Chen, *Blockade of B7-H1 and PD-1 by Monoclonal Antibodies Potentiates Cancer Therapeutic Immunity.* Cancer Research, 2005. **65**: p. 1089-1096.

52. Iwai, Y., et al., *Involvement of PD-L1 on tumor cells in the escape from host immune system and tumor immunotherapy by PD-L1 blockade.* Proc Natl Acad Sci U S A, 2002. **99**(19): p. 12293-7.

53. Sundar, R., et al., *Immunotherapy in the treatment of non-small cell lung cancer.* Lung Cancer, 2014. **85**(2): p. 101-109.

54. Tang, P.A. and D.Y. Heng, *Programmed death 1 pathway inhibition in metastatic renal cell cancer and prostate cancer.* Curr Oncol Rep, 2013. **15**(2): p. 98-104.

55. Westin, J.R., et al., *Safety and activity of PD1 blockade by pidilizumab in combination with rituximab in patients with relapsed follicular lymphoma: a single group, open-label, phase 2 trial.* The Lancet Oncology, 2014. **15**(1): p. 69-77.

56. FDA, U.S., *FDA approves Keytruda for advanced melanoma.* 2014.

57. Augello, A., et al., *Bone marrow mesenchymal progenitor cells inhibit lymphocyte proliferation by activation of the programmed death 1 pathway.* Eur J Immunol, 2005. **35**(5): p. 1482-90.

58. Sheng, H., et al., *A critical role of IFNgamma in priming MSC-mediated suppression of T cell proliferation through up-regulation of B7-H1.* Cell Res, 2008. **18**(8): p. 846-57.

59. Luz-Crawford, P., et al., *Mesenchymal stem cells repress Th17 molecular program through the PD-1 pathway.* PLoS One, 2012. **7**(9): p. e45272.

60. Luz-Crawford, P., et al., *Mesenchymal stem cells generate a CD4+CD25+Foxp3+ regulatory T cell population during the differentiation process of Th1 and Th17 cells.* Stem Cell Res Ther, 2013. **4**(3): p. 65.

61. Prendergast, G.C., et al., *Indoleamine 2,3-dioxygenase pathways of pathogenic inflammation and immune escape in cancer.* Cancer Immunol Immunother, 2014. **63**(7): p. 721-35.

62. Abumaree, M.H., et al., *Trophoblast debris modulates the expression of immune proteins in macrophages: a key to maternal tolerance of the fetal allograft?* J Reprod Immunol, 2012. **94**(2): p. 131-41.

63. Sucher, R., et al., *IDO and regulatory T cell support are critical for cytotoxic T lymphocyte-associated Ag-4 Ig-mediated long-term solid organ allograft survival.* J Immunol, 2012. **188**(1): p. 37-46.

64. Williams, E.B.a.D., *The Metabolism of tryptophan in patients suffering from cancer of the bladder.* Biochemical Journal, 1956. **64**(3): p. 578-582.

65. Pallotta, M.T., et al., *Indoleamine 2,3-dioxygenase is a signaling protein in long-term tolerance by dendritic cells.* Nat Immunol, 2011. **12**(9): p. 870-8.

66. Health, N.I.o., www.clinicaltrials.gov. 2014.

67. Wen, L., et al., *Immunomodulatory effects of bone marrow-derived mesenchymal stem cells on pro-inflammatory cytokine-stimulated human corneal epithelial cells.* PLoS One, 2014. **9**(7): p. e101841.

68. Olga DelaRosa, E.L., Aitor Beraza, Pablo Mancheño-Corvo, Cristina Ramirez, Ramón Menta, Laura Rico, Eva Camarillo, Laura García, José Luis Abad, Cesar Trigueros, Mario Delgado, and Dirk Büscher., *Requirement of IFN-c–Mediated Indoleamine 2,3-Dioxygenase Expression in the Modulation of Lymphocyte Proliferation by Human Adipose–Derived Stem Cells.* Tissue Engineering: Part A, 2009. **15**(10): p. 2795-2806.

69. Croitoru-Lamoury, J., et al., *Interferon-gamma regulates the proliferation and differentiation of mesenchymal stem cells via activation of indoleamine 2,3 dioxygenase (IDO).* PLoS One, 2011. **6**(2): p. e14698.

70. Francois, M., et al., *Human MSC suppression correlates with cytokine induction of indoleamine 2,3-dioxygenase and bystander M2 macrophage differentiation.* Mol Ther, 2012. **20**(1): p. 187-95.

71. Nemeth, K., et al., *Bone marrow stromal cells attenuate sepsis via prostaglandin E(2)-dependent reprogramming of host macrophages to increase their interleukin-10 production.* Nat Med, 2009. **15**(1): p. 42-9.

72. Geng, Y., et al., *Mesenchymal stem cells ameliorate rhabdomyolysis-induced acute kidney injury via the activation of M2 macrophages.* Stem Cell Res Ther, 2014. **5**(3): p. 80.

73. Fahy, N., et al., *Human osteoarthritic synovium impacts chondrogenic differentiation of mesenchymal stem cells via macrophage polarisation state.* Osteoarthritis Cartilage, 2014.

74. Meisel, R., et al., *Human bone marrow stromal cells inhibit allogeneic T-cell responses by indoleamine 2,3-dioxygenase-mediated tryptophan degradation.* Blood, 2004. **103**(12): p. 4619-21.

75. Jui HY, L.C., Hsu WT, Liu YR, Hsu RB, Chiang BL, Tseng WY, Chen MF, Wu KK, Lee CM., *Autologous mesenchymal stem cells prevent transplant arteriosclerosis by enhancing local expression of interleukin-10, interferon-γ, and indoleamine 2,3-dioxygenase.* Cell Transplantation, 2012. **21**(5): p. 971-984.

76. Ge, W., et al., *Regulatory T-cell generation and kidney allograft tolerance induced by mesenchymal stem cells associated with indoleamine 2,3-dioxygenase expression.* Transplantation, 2010. **90**(12): p. 1312-20.

77. Warren, J.S. and P.A. Ward, *Chapter 17. The Inflammatory Response*, in *Williams Hematology, 8e*, M.A. Lichtman, et al., Editors. 2010, The McGraw-Hill Companies: New York, NY.

78. Smith LC, A.K., Nonaka M, *Complement systems in invertebrates. The ancient alternative and lectin pathways.* Immunopharmacology, 1999. **42**(1-3): p. 107-20.

79. Schraufstatter, I.U., et al., *C3a and C5a are chemotactic factors for human mesenchymal stem cells, which cause prolonged ERK1/2 phosphorylation.* J Immunol, 2009. **182**(6): p. 3827-36.

80. Moll, G., et al., *Mesenchymal stromal cells engage complement and complement receptor bearing innate effector cells to modulate immune responses.* PLoS One, 2011. **6**(7): p. e21703.

81. Conte, M.P., et al., *Adherent-invasive Escherichia coli (AIEC) in pediatric Crohn's disease patients: phenotypic and genetic pathogenic features.* BMC Res Notes, 2014. **7**: p. 748.

82. van den Akker, F., S.C. de Jager, and J.P. Sluijter, *Mesenchymal stem cell therapy for cardiac inflammation: immunomodulatory properties and the influence of toll-like receptors.* Mediators Inflamm, 2013. **2013**: p. 181020.

83. Delarosa, O., W. Dalemans, and E. Lombardo, *Toll-like receptors as modulators of mesenchymal stem cells.* Front Immunol, 2012. **3**: p. 182.

84. Liotta, F., et al., *Toll-like receptors 3 and 4 are expressed by human bone marrow-derived mesenchymal stem cells and can inhibit their T-cell modulatory activity by impairing Notch signaling.* Stem Cells, 2008. **26**(1): p. 279-89.

85. Romieu-Mourez, R., et al., *Cytokine modulation of TLR expression and activation in mesenchymal stromal cells leads to a proinflammatory phenotype.* J Immunol, 2009. **182**(12): p. 7963-73.

86. Mosmann TR, C.H., Bond MW, Giedlin MA, Coffman RL., *Two types of murine helper T cell clone. I. Definition according to profiles of lymphokine activities and secreted proteins.* Journal of Immunology, 1986. **136**(7): p. 2348-57.

87. Krampera, M., et al., *Role for interferon-gamma in the immunomodulatory activity of human bone marrow mesenchymal stem cells.* Stem Cells, 2006. **24**(2): p. 386-98.

88. Ryan, J.M., et al., *Interferon-gamma does not break, but promotes the immunosuppressive capacity of adult human mesenchymal stem cells.* Clin Exp Immunol, 2007. **149**(2): p. 353-63.

89. Olga DelaRosa, E.L., Aitor Beraza, Pablo Mancheño-Corvo, Cristina Ramirez, Ramón Menta, Laura Rico, Eva Camarillo, Laura García, José Luis Abad, Cesar Trigueros, Mario Delgado, and Dirk Büscher., *Requirement of IFN-γ–Mediated Indoleamine 2,3-Dioxygenase Expression in the Modulation of Lymphocyte Proliferation by Human Adipose–Derived Stem Cells.* TISSUE ENGINEERING: Part A, 2009. **15**(10): p. 2795-2806.

90. Raphaëlle Romieu-Mourez, M.F., Marie-Noëlle Boivin, John Stagg, and Jacques Galipeau, *Regulation of MHC Class II Expression and Antigen Processing in Murine and Human Mesenchymal Stromal Cells by IFN-γ, TGF-β, and Cell Density.* Journal of Immunology, 2007. **179**(3): p. 1549-58.

91. Beutler B, G.D., Hulmes JD, Chang M, Pan YC, Mathison J, Ulevitch R, Cerami A., *Identity of tumour necrosis factor and the macrophage-secreted factor cachectin.* Nature, 1985. **316**(6028): p. 552-4.

92. Piao, J.H., et al., *TNF Receptor-Associated Factor 2-Dependent Canonical Pathway Is Crucial for the Development of Peyer's Patches.* The Journal of Immunology, 2007. **178**(4): p. 2272-2277.

93. Furtado, G.C., et al., *TNFalpha-dependent development of lymphoid tissue in the absence of RORgammat(+) lymphoid tissue inducer cells.* Mucosal Immunol, 2014. **7**(3): p. 602-14.

94. Kaushansky, K., *Chapter 14. Signal Transduction Pathways*, in *Williams Hematology, 8e*, M.A. Lichtman, et al., Editors. 2010, The McGraw-Hill Companies: New York, NY.

95. Dorronsoro, A., et al., *Human mesenchymal stromal cells modulate T-cell responses through TNF-alpha-mediated activation of NF-kappaB.* Eur J Immunol, 2014. **44**(2): p. 480-8.

96. Jansen, A.H., E.A. Reits, and E.M. Hol, *The ubiquitin proteasome system in glia and its role in neurodegenerative diseases.* Front Mol Neurosci, 2014. **7**: p. 73.

97. Shen M, S.S., Buac D, Dou QP, *Targeting the ubiquitin–proteasome system for cancer therapy.* Expert Opinion on Therapeutic Targets, 2013. **17**(9): p. 1091-1108.

98. Song, X.T., et al., *A20 is an antigen presentation attenuator, and its inhibition overcomes regulatory T cell-mediated suppression.* Nat Med, 2008. **14**(3): p. 258-65.

99. Lee TH, W.H., Vilcek J., *A novel secretory tumor necrosis factor-inducible protein (TSG-6) is a member of the family of hyaluronate binding proteins, closely related to the adhesion receptor CD44.* Journal of Cell Biology, 1992. **116**(2): p. 545-57.

100. Lee, R.H., et al., *Intravenous hMSCs improve myocardial infarction in mice because cells embolized in lung are activated to secrete the anti-inflammatory protein TSG-6.* Cell Stem Cell, 2009. **5**(1): p. 54-63.

101. Choi, H., et al., *Anti-inflammatory protein TSG-6 secreted by activated MSCs attenuates zymosan-induced mouse peritonitis by decreasing TLR2/NF-kappaB signaling in resident macrophages.* Blood, 2011. **118**(2): p. 330-8.

102. Ren, G., et al., *Mesenchymal stem cell-mediated immunosuppression occurs via concerted action of chemokines and nitric oxide.* Cell Stem Cell, 2008. **2**(2): p. 141-50.

103. Romieu-Mourez, R., et al., *Mesenchymal stromal cells expressing ErbB-2/neu elicit protective antibreast tumor immunity in vivo, which is paradoxically suppressed by IFN-gamma and tumor necrosis factor-alpha priming.* Cancer Res, 2010. **70**(20): p. 7742-7.

104. Galipeau, J., *The mesenchymal stromal cells dilemma--does a negative phase III trial of random donor mesenchymal stromal cells in steroid-resistant graft-versus-host disease represent a death knell or a bump in the road?* Cytotherapy, 2013. **15**(1): p. 2-8.

105. François M, R.-M.R., Stock-Martineau S, Boivin M, Bramson JL, and Galipeau J., *Mesenchymal stromal cells cross-present soluble exogenous antigens as part of their antigen-presenting cell properties.* Blood, 2009. **114**(13): p. 2632-8.

106. Najar, M., et al., *Immune-related antigens, surface molecules and regulatory factors in human-derived mesenchymal stromal cells: the expression and impact of inflammatory priming.* Stem Cell Rev, 2012. **8**(4): p. 1188-98.

107. Raicevic, G., et al., *Influence of inflammation on the immunological profile of adult-derived human liver mesenchymal stromal cells and stellate cells.* Cytotherapy, 2015. **17**(2): p. 174-85.

108. Li, H., et al., *CCR7 guides migration of mesenchymal stem cell to secondary lymphoid organs: a novel approach to separate GvHD from GvL effect.* Stem Cells, 2014. **32**(7): p. 1890-903.

109. Brooke, G., et al., *Molecular trafficking mechanisms of multipotent mesenchymal stem cells derived from human bone marrow and placenta.* Stem Cells Dev, 2008. **17**(5): p. 929-40.

110. Li, H., et al., *CCR7 Expressing Mesenchymal Stem Cells Potently Inhibit Graft-versus-Host Disease by Spoiling the Fourth Supplemental Billingham's Tenet.* PLoS One, 2014. **9**(12): p. e115720.

111. Ringkowski, S., P.S. Thomas, and C. Herbert, *Interleukin-12 family cytokines and sarcoidosis.* Front Pharmacol, 2014. **5**: p. 233.

112. Barros, F.M., et al., *Possible Association between Th1 Immune Polarization and Epithelial Permeability with Toll-Like Receptors 2 Dysfunction in the Pathogenesis of the Recurrent Aphthous Ulceration.* Ulcers, 2010. **2010**: p. 1-11.

113. Martin PJ, U.J., Soiffer RJ, Klingemann H, Waller EK, Daly AS, Herrmann RP, Kebriaei P. , *Prochymal improves response rates in patients with steroid-refractory acute graft versus host disease (SR-GVHD) involving the liver and gut: Results of a randomized, placebo-controlled, multicenter phase III trial in GVHD. .* Biology of Blood and Marrow Transplantation, 2010. **16**(S169e70).

114. Prasad, V.K., et al., *Efficacy and safety of ex vivo cultured adult human mesenchymal stem cells (Prochymal) in pediatric patients with severe refractory acute graft-versus-host disease in a compassionate use study.* Biol Blood Marrow Transplant, 2011. **17**(4): p. 534-41.

115. Ragoonanan, V., A. Hubel, and A. Aksan, *Response of the cell membrane-cytoskeleton complex to osmotic and freeze/thaw stresses.* Cryobiology, 2010. **61**(3): p. 335-44.

116. Castelo-Branco MT, S.I., Lopes DV, Buongusto F, Martinusso CA, do Rosario A Jr, Souza SA, Gutfilen B, Fonseca LM, Elia C, Madi K, Schanaider A, Rossi MI, Souza HS., *Intraperitoneal but Not Intravenous Cryopreserved Mesenchymal Stromal Cells Home to the Inflamed Colon and Ameliorate Experimental Colitis.* PloS One, 2012. **7**(3): p. e33360.

117. Chinnadurai, R., et al., *Actin Cytoskeletal Disruption following Cryopreservation Alters the Biodistribution of Human Mesenchymal Stromal Cells In Vivo.* Stem Cell Reports, 2014. **3**(1): p. 60-72.

118. Waltz, E., *Mesoblast acquires Osiris' stem cell business.* Nat Biotech, 2013. **31**(12): p. 1061-1061.

119. Meldrum, J., *Mesoblast provides update on clinical programs of prochymal® for crohn's disease and acute graft versus host disease.*

120. Kim, N., et al., *Mesenchymal stem cells for the treatment and prevention of graft-versus-host disease: experiments and practice.* Ann Hematol, 2013. **92**(10): p. 1295-308.

121. Introna, M. and A. Rambaldi, *Mesenchymal stromal cells for prevention and treatment of graft-versus-host disease: successes and hurdles.* Curr Opin Organ Transplant, 2015. **20**(1): p. 72-8.

122. Ball, L.M., et al., *Multiple infusions of mesenchymal stromal cells induce sustained remission in children with steroid-refractory, grade III-IV acute graft-versus-host disease.* Br J Haematol, 2013. **163**(4): p. 501-9.

123. Kuzmina, L.A., et al., *Multipotent Mesenchymal Stromal Cells for the Prophylaxis of Acute Graft-versus-Host Disease-A Phase II Study.* Stem Cells Int, 2012. **2012**: p. 968213.

124. Hahn, B.H., *Chapter 319. Systemic Lupus Erythematosus*, in *Harrison's Principles of Internal Medicine, 18e*, D.L. Longo, et al., Editors. 2012, The McGraw-Hill Companies: New York, NY.

125. Carrion F, N.E., Ruiz C, Diaz F, Inostroza C, Rojo D, Monckeberg G and Figueroa FE, *Autologous mesenchymal stem cell treatment increased T regulatory cells with no effect on disease activity in two systemic lupus erythematosus patients.* Lupus, 2010. **19**: p. 317-322.

126. Dandan Wang, H.Z., Jun Liang, Xia Li, Xuebing Feng, Hong Wang, Bingzhu Hua, Bujun Liu, Liwei Lu, Gary S. Gilkeson, Richard M. Silver, Wanjun Chen, Songtao Shi, and Lingyun Sun, *Allogeneic Mesenchymal Stem Cell Transplantation in Severe and Refractory Systemic Lupus Erythematosus: 4 Years of Experience.* Cell Transplantation, 2013. **22**: p. 2267-2277.

127. Wang, D., et al., *A CD8 T cell/indoleamine 2,3-dioxygenase axis is required for mesenchymal stem cell suppression of human systemic lupus erythematosus.* Arthritis Rheumatol, 2014. **66**(8): p. 2234-45.

128. Friedman, S. and R.S. Blumberg, *Chapter 295. Inflammatory Bowel Disease*, in *Harrison's Principles of Internal Medicine, 18e*, D.L. Longo, et al., Editors. 2012, The McGraw-Hill Companies: New York, NY.

129. Blumberg, R.S. and S.B. Snapper, *Chapter 2. Inflammatory Bowel Disease: Immunologic Considerations & Therapeutic Implications*, in *CURRENT Diagnosis & Treatment: Gastroenterology, Hepatology, & Endoscopy, 2e*, N.J. Greenberger, R.S. Blumberg, and R. Burakoff, Editors. 2012, The McGraw-Hill Companies: New York, NY.

130. Duijvestein, M., et al., *Autologous bone marrow-derived mesenchymal stromal cell treatment for refractory luminal Crohn's disease: results of a phase I study.* Gut, 2010. **59**(12): p. 1662-9.

<u>References for Chapter 2: AHR Signaling</u>

1. Lechner MG, Megiel C, Russell SM, Bingham B, Arger N, Woo T and Epstein AL. Functional characterization of human CD33+ and CD11b+ myeloid-derived suppressor cell subsets induced from peripheral blood mononuclear cells co-cultured with a diverse set of human tumor cell lines. Journal of Translational Medicine. 2011; 9:90.

2. Francois M, Romieu-Mourez R, Li M and Galipeau J. Human MSC suppression correlates with cytokine induction of indoleamine 2,3-dioxygenase and bystander M2 macrophage differentiation. Molecular Therapy. 2012; 20(1):187-195.

3. Yu J, Du W, Yan F, Wang Y, Li H, Cao S, Yu W, Shen C, Liu J and Ren X. Myeloid-derived suppressor cells suppress antitumor immune responses through IDO expression and correlate with lymph node metastasis in patients with breast cancer. Journal of Immunology. 2013; 190(7):3783-3797.

4. Pallotta MT, Orabona C, Volpi C, Vacca C, Belladonna ML, Bianchi R, Servillo G, Brunacci C, Calvitti M, Bicciato S, Mazza EM, Boon L, Grassi F et al. Indoleamine 2,3-dioxygenase is a signaling protein in long-term tolerance by dendritic cells. Nature Immunology. 2011; 12(9):870-878.

5. Mezrich JD, Fechner JH, Zhang X, Johnson BP, Burlingham WJ and Bradfield CA. An interaction between kynurenine and the aryl hydrocarbon receptor can generate regulatory T cells. Journal of Immunology. 2010; 185(6):3190-3198.

6. Eguchi H, Ikuta T, Tachibana T, Yoneda Y, and Kawajiri K. A Nuclear Localization Signal of Human Aryl Hydrocarbon Receptor Nuclear Translocator/Hypoxia-inducible Factor 1 Is a Novel Bipartite Type Recognized by the Two Components of Nuclear Pore-targeting Complex. Journal of Biological Chemistry. 1997.

7. Smith KJ, Murray IA, Tanos R, Tellew J, Boitano AE, Bisson WH, Kolluri SK, Cooke MP, Perdew GH. Identification of a high-affinity ligand that exhibits complete aryl hydrocarbon receptor antagonism. Journal of Pharmacology and Experimental Therapeutics. 2011; 338(1):318-327.

8. Chi AC, Appleton K, Henriod JB, Krayer JW, Marlow NM, Bandyopadhyay D, Sigmon RC and Kurtz DT. Differential induction of CYP1A1 and CYP1B1 by benzo[a]pyrene in oral squamous cell carcinoma cell lines and by tobacco smoking in oral mucosa. Oral Oncology. 2009; 45(11):980-985.

9. Pinpin L, Han C, Tsai WT, Wu MH, Liao YS, Chen JT and Su JM. Overexpression of Aryl Hydrocarbon Receptor in Human Lung Carcinomas. Toxicologic Pathology. 2003; 31(1):22-30.

10. McFadyen MC, Rooney PH, Melvin WT and Murray GI. Quantitative analysis of the Ah receptor/cytochrome P450 CYP1B1/CYP1A1 signalling pathway. Biochemical Pharmacology. 2003; 65(10):1663-1674.

11. Hao N and Whitelaw ML. The emerging roles of AhR in physiology and immunity. Biochemical Pharmacology. 2013; 86(5):561-570.

12. Nguyen NT, Kimura A, Nakahama T, Chinen I, Masuda K, Nohara K, Fujii-Kuriyama Y and Kishimoto T. Aryl hydrocarbon receptor negatively regulates dendritic cell

immunogenicity via a kynurenine-dependent mechanism. Proceedings of the National Academy of Sciences of the United States of America. 2010; 107(46):19961-19966.

13. NewLinkGeneticsCorp. Study of the IDO Pathway Inhibitor, Indoximod, and Temozolomide for Pediatric Patients With Progressive Primary Malignant Brain Tumors. ClinicalTrials.gov [Internet] Bethesda (MD): National Library of Medicine. 2017; http://clinicaltrials.gov/ct2/show/NCT02502708

14. Lu Y, Giver C, Sharma A, Li JM, Darlak KA, Owens LM, Roback JD, Galipeau J and Waller EK. "IFN-γ and indoleamine 2,3-dioxygenase signaling between donor dendritic cells and T cells regulates graft versus host and graft versus leukemia activity. Blood. 2012; 119(4):1075-1085.

15. Wuchter P, Bieback K, Schrezenmeier H, Bornhauser M, Muller LP, Bonig H, Wagner W, Meisel R, Pavel P, Tonn T, Lang P, Muller I, Renner M et al. Standardization of Good Manufacturing Practice-compliant production of bone marrow-derived human mesenchymal stromal cells for immunotherapeutic applications. Cytotherapy. 2015; 17(2):128-139.

16. Romieu-Mourez R, Francois M, Boivin MN, Stagg J and Galipeau J. Regulation of MHC Class II Expression and Antigen Processing in Murine and Human Mesenchymal Stromal Cells by IFN- , TGF- , and Cell Density. Journal of Immunology. 2007; 179(3):1549-1558.

17. Tkachenko A, Henkler F, Brinkmann J, Sowada J, Genkinger D, Kern C, Tralau T, Luch A. The Q-rich/PST domain of the AHR regulates both ligand-induced nuclear transport and nucleocytoplasmic shuttling. Scientific Reports. 2016; 6:32009.

18. Davarinos N and Pollenz R. Aryl Hydrocarbon Receptor Imported into the Nucleus following Ligand Binding Is Rapidly Degraded via the Cytosplasmic Proteasome following Nuclear Export. Journal of Biological Chemistry. 1999; 274(40):28708-28715.

19. Tsuji N, Fukuda K, Nagata Y, Okada H, Haga A, Hatakeyama S, Yoshida S, Okamoto T, Hosaka M, Sekine K, Ohtaka K, Yamamoto S, Otaka M et al. The activation mechanism of the aryl hydrocarbon receptor (AhR) by molecular chaperone HSP90. FEBS Open Bio. 2014; 4:796-803.

20. Cui Z, Li P, Liu J and Liu S. Induction of CYP1A1 expression of H4IIE cell after treated with the water organic pollutants from the Yangtze River and Jialing River. Journal of Hygiene Research (Wei Sheng Yan Jiu). 2008; 37(5):540-542.

21. Elshenawy OH and El-Kadi AO. Modulation of aryl hydrocarbon receptor-regulated enzymes by trimethylarsine oxide in C57BL/6 mice: In vivo and in vitro studies. Toxicology Letters. 2015; 238(1):17-31.

22. Wincent E, Kubota A, Timme-Laragy A, Jonsson ME, Hahn ME and Stegeman JJ. Biological effects of 6-formylindolo[3,2-b]carbazole (FICZ) in vivo are enhanced by loss of CYP1A function in an Ahr2-dependent manner. Biochemical Pharmacology. 2016; 110-111:117-129.

23. DiNatale BC, Murray IA, Schroeder JC, Flaveny CA, Lahoti TS, Laurenzana EM, Omiecinski CJ and Perdew GH. Kynurenic acid is a potent endogenous aryl hydrocarbon receptor ligand that synergistically induces interleukin-6 in the presence of inflammatory signaling. Toxicological Sciences. 2010; 115(1):89-97.

24. Soliman HH, Minton SE, Han HS, Ismail-Khan R, Neuger A, Khambati F, Noyes D, Lush R, Chiappori AA, Roberts JD, Link C, Vahanian NN, Mautino M et al. A phase I study of indoximod in patients with advanced malignancies. Oncotarget. 2016; 7(16):22928-22938.

25. Dunham RM, Gordon SN, Vaccari M, Piatak M, Huang Y, Deeks SG, Lifson J, Franchini G and McCune JM. Preclinical Evaluation of HIV Eradication Strategies in the Simian Immunodeficiency Virus-Infected Rhesus Macaque: A Pilot Study Testing Inhibition of Indoleamine 2,3-Dioxygenase. AIDS research and human retroviruses. 2013; 29(2):207-214.

26. Huang Q, Zheng M, Yang S, Kuang C, Yu C and Yang Q. Structure-activity relationship and enzyme kinetic studies on 4-aryl-1H-1,2,3-triazoles as indoleamine 2,3-dioxygenase (IDO) inhibitors. European Journal of Medicinal Chemistry. 2011; 46(11):5680-5687.

27. Chinnadurai R, Copland IB, Patel SR and Galipeau J. IDO-independent suppression of T cell effector function by IFN-gamma-licensed human mesenchymal stromal cells. Journal of Immunology. 2014; 192(4):1491-1501.

28. Hou DY, Muller AJ, Sharma MD, DuHadaway J, Banerjee T, Johnson M, Mellor AL, Prendergast GC and Munn DH. Inhibition of indoleamine 2,3-dioxygenase in dendritic cells by stereoisomers of 1-methyl-tryptophan correlates with antitumor responses. Cancer Res. 2007; 67(2):792-801.

29. Jia L, Schweikart K, Tomaszewski J, Page JG, Noker PE, Buhrow SA, Reid JM, Ames MM and Munn DH. Toxicology and pharmacokinetics of 1-methyl-d-tryptophan: absence

of toxicity due to saturating absorption. Food and Chemical Toxicology. 2008; 46(1):203-211.

30. Qian F, Villella J, Wallace PK, Mhawech-Fauceglia P, Tario JD, Jr., Andrews C, Matsuzaki J, Valmori D, Ayyoub M, Frederick PJ, Beck A, Liao J, Cheney R et al. Efficacy of levo-1-methyl tryptophan and dextro-1-methyl tryptophan in reversing indoleamine-2,3-dioxygenase-mediated arrest of T-cell proliferation in human epithelial ovarian cancer. Cancer Research. 2009; 69(13):5498-5504.

31. Soshilov AA and Denison MS. (2014). DNA Binding (Gel Retardation Assay) Analysis for Identification of Aryl Hydrocarbon (Ah) Receptor Agonists and Antagonists. In: Caldwell GW YZ, ed. Optimization in Drug Discovery: In Vitro Methods. (New York City, NY: Springer Science+Business Media).

32. Shi Y, Du L, Lin L and Wang Y. Tumour-associated mesenchymal stem/stromal cells: emerging therapeutic targets. Nature Reviews Drug Discovery. 2017; 16(1):35-52.

33. Swann JB and Smyth MJ. Immune surveillance of tumors. Journal of Clinical Investigation. 2007; 117(5):1137-1146.

34. Beavis PA, Slaney CY, Kershaw, MH, Gyorki D, Neeson PJ and Darcy PK. Reprogramming the tumor microenvironment to enhance adoptive cellular therapy. Seminars in Immunology. 2016; 28(1):64-72.

35. Ahmed SM, Luo L, Namani A, Wang XJ and Tang X. Nrf2 signaling pathway: Pivotal roles in inflammation. Biochimica et Biophysica Acta. 2016; 1863(2):585-597.

36. Zhu J, Wang H, Chen F, Fu J, Xu Y, Hou Y, Kou HH, Zhai C, Nelson MB, Zhang Q, Andersen ME and Pi J. An overview of chemical inhibitors of the Nrf2-ARE signaling

pathway and their potential applications in cancer therapy. Free Radical Biology and Medicine. 2016; 99:544-556.

37. Li L, Dong H, Song E, Xu X, Liu L and Song Y. Nrf2/ARE pathway activation, HO-1 and NQO1 induction by polychlorinated biphenyl quinone is associated with reactive oxygen species and PI3K/AKT signaling. Chemico-Biological Interactions. 2014; 209:56-67.

38. Li N, Alam J, Venkatesan MI, Eiguren-Fernandez A, Schmitz D, Di Stefano E, Slaughter N, Killeen E, Wang X, Huang A, Wang M, Miguel AH, Cho A et al. Nrf2 Is a Key Transcription Factor That Regulates Antioxidant Defense in Macrophages and Epithelial Cells: Protecting against the Proinflammatory and Oxidizing Effects of Diesel Exhaust Chemicals. The Journal of Immunology. 2004; 173(5):3467-3481.

39. Kanteti R, Batra SK, Lennon FE and Salgia R. FAK and paxillin, two potential targets in pancreatic cancer. Oncotarget. 2016; 7(21):31586-31601.

40. Mowers EE, Sharifi MN and Macleod KF. Novel insights into how autophagy regulates tumor cell motility. Autophagy. 2016; 12(9):1679-1680.

41. Davis AP, Grondin CJ, Johnson RJ, Sciaky D, King BL, McMorran R, Wiegers J, Wiegers TC and Mattingly CJ. The Comparative Toxicogenomics Database: update 2017. Nucleic Acids Research. 2017; 45(D1):D972-D978.

42. DiNatale BC, Schroeder JC, Francey LJ, Kusnadi A and Perdew GH. Mechanistic insights into the events that lead to synergistic induction of interleukin 6 transcription upon activation of the aryl hydrocarbon receptor and inflammatory signaling. Journal of Biological Chemistry. 2010; 285(32):24388-24397.

43. Chinnadurai R, Copland IB, Garcia MA, Petersen CT, Lewis CN, Waller EK, Kirk AD and Galipeau J. Cryopreserved Mesenchymal Stromal Cells Are Susceptible to T-Cell Mediated Apoptosis Which Is Partly Rescued by IFNgamma Licensing. Stem Cells. 2016; 34(9):2429-2442.

44. Livak KJ and Schmittgen TD. Analysis of relative gene expression data using real-time quantitative PCR and the 2(-Delta Delta C(T)) Method. Methods. 2001; 25(4):402-408.

45. Marioni JC, Mason CE, Mane SM, Stephens M and Gilad Y. RNA-seq: an assessment of technical reproducibility and comparison with gene expression arrays. Genome Research. 2008; 18(9):1509-1517.

46. Dobin A, Davis CA, Schlesinger F, Drenkow J, Zaleski C, Jha S, Batut P, Chaisson M and Gingeras TR. STAR: ultrafast universal RNA-seq aligner. Bioinformatics. 2013; 29(1):15-21.

47. Edgar R, Domrachev M and Lash AE. Gene Expression Omnibus: NCBI gene expression and hybridization array data repository. Nucleic Acids Research. 2002; 30(1):207-210.

48. Golden MR, Ashley-Morrow R, Swenson P, Hogrefe WR, Handsfield HH and Wald A. Herpes Simplex Virus Type 2 (HSV-2) Western Blot Confirmatory Testing Among Men Testing Positive for HSV-2 Using the Focus Enzyme-Linked Immunosorbent Assay in a Sexually Transmitted Disease Clinic. Sexually Transmitted Diseases. 2005; 32(12):771-777.

References for Chapter 3: Modeling AHR Ligation in Silico

1. Soshilov AA and Denison MS. (2014). DNA Binding (Gel Retardation Assay) Analysis for Identification of Aryl Hydrocarbon (Ah) Receptor Agonists and Antagonists. In: Caldwell GW YZ, ed. Optimization in Drug Discovery: In Vitro Methods. (New York City, NY: Springer Science+Business Media).

2. Perkins A, Phillips JL, Kerkvliet NI, Tanguay RL, Perdew GH, Kolluri SK and Bisson WH. A Structural Switch between Agonist and Antagonist Bound Conformations for a Ligand-Optimized Model of the Human Aryl Hydrocarbon Receptor Ligand Binding Domain. Biology (Basel). 2014; 3(4):645-669.

3. Szollosi D, Erdei A, Gyimesi G, Magyar C, Hegedus T. Access Path to the Ligand Binding Pocket May Play a Role in Xenobiotics Selection by AhR. PLoS One. 2016; 11(1):e0146066.

4. Biasini M, Bienert S, Waterhouse A, Arnold K, Studer G, Schmidt T, Kiefer F, Gallo Cassarino T, Bertoni M, Bordoli L, Schwede T. SWISS-MODEL: modelling protein tertiary and quaternary structure using evolutionary information. Nucleic Acids Research. 2014; 42(Web Server issue):W252-258.

5. Grosdidier A, Zoete V and Michielin O. SwissDock, a protein-small molecule docking web service based on EADock DSS. Nucleic Acids Research. 2011; 39(Web Server issue):W270-277.

6. Irwin JJ, Schweikart T, Mysinger MM, Bolstad ES and Coleman RG. ZINC: a free tool to discover chemistry for biology. Journal of Chemical Information and Modeling. 2012; 52(7):1757-1768.

7. Lowe MM, Mold JE, Kanwar B, Huang Y, Louie A, Pollastri MP, Wang C, Patel G, Franks DG, Schlezinger J, Sherr DH, Silverstone AE, Hahn ME and McCune JM. . Identification of Cinnabarinic Acid as a Novel Endogenous Aryl Hydrocarbon Receptor Ligand That Drives IL-22 Production. PLoS One. 2014; 9(2):e87877.

8. DiNatale BC, Murray IA, Schroeder JC, Flaveny CA, Lahoti TS, Laurenzana EM, Omiecinski CJ and Perdew GH. Kynurenic acid is a potent endogenous aryl hydrocarbon receptor ligand that synergistically induces interleukin-6 in the presence of inflammatory signaling. Toxicological Sciences. 2010; 115(1):89-97.

References for Chapter 4: Community Approaches for Diverse Cell Donorship

1. Grosse, S.D., et al., Models of comprehensive multidisciplinary care for individuals in the United States with genetic disorders. Pediatrics, 2009. 123(1): p. 407-12.

2. Shenoy, S., Hematopoietic stem-cell transplantation for sickle cell disease: current evidence and opinions. Therapeutic Advances in Hematology, 2013. 4(5): p. 335–344.

3. Shaz, B.H., et al., Blood donation and blood transfusion: special considerations for African Americans. Transfusion Medicine Review, 2008. 22(3): p. 202-14.

4. Arnold, S.D., et al., Haematopoietic stem cell transplantation for sickle cell disease - current practice and new approaches. British Journal of Haematology, 2016. 174(4): p. 515-25.

5. Washington, H., Medical Apartheid: The Dark History of Medical Experimentation on Black Americans from Colonial Times to the Present 2007, New York: Doubleday.

6. Patzer, R.E., et al., A Randomized Trial to Reduce Disparities in Referral for Transplant Evaluation. Journal of the American Society of Nephrology, 2017. 28(3): p. 935-942.

7. Zaidi, M.Y., L. Haddad, and E. Lathrop, Global Health Opportunities in Obstetrics and Gynecology Training: Examining Engagement Through an Ethical Lens. Am J Trop Med Hyg, 2015. 93(6): p. 1194-200.

8. Price, C.L., et al., Mailing of a sickle cell disease educational packet increases blood donors within an African American community. Transfusion, 2006. 46(8): p. 1388-93.

References for Chapter 5: Modeling MSC-Based Therapies with Exosomes

1. Roccaro, A.M., et al., *BM mesenchymal stromal cell-derived exosomes facilitate multiple myeloma progression.* J Clin Invest, 2013. **123**(4): p. 1542-55.

2. Gupta, D., et al., *Adherence of multiple myeloma cells to bone marrow stromal cells upregulates vascular endothelial growth factor secretion: therapeutic applications.* Leukemia, 2001. **15**(12): p. 1950-61.

3. Kumar, S., et al., *Bone marrow angiogenic ability and expression of angiogenic cytokines in myeloma: evidence favoring loss of marrow angiogenesis inhibitory activity with disease progression.* Blood, 2004. **104**(4): p. 1159-65.

4. Chauhan, D., et al., *Multiple myeloma cell adhesion-induced interleukin-6 expression in bone marrow stromal cells involves activation of NF-kappa B.* Blood, 1996. **87**(3): p. 1104-12.

5. Uchiyama, H., et al., *Adhesion of human myeloma-derived cell lines to bone marrow stromal cells stimulates interleukin-6 secretion.* Blood, 1993. **82**(12): p. 3712-20.

6. Wang, J., et al., *Bone marrow stromal cell-derived exosomes as communicators in drug resistance in multiple myeloma cells.* Blood, 2014. **124**(4): p. 555-66.

7. Campeau, P.M., et al., *Mesenchymal stromal cells engineered to express erythropoietin induce anti-erythropoietin antibodies and anemia in allorecipients.* Mol Ther, 2009. **17**(2): p. 369-72.

8. Stagg J, G.G., *Mechanisms of immune modulation by mesenchymal stromal cells and clinical translation.* Current Molecular Medicine, 2013. **13**(5): p. 856-67.

9. Galipeau, J., *The mesenchymal stromal cells dilemma--does a negative phase III trial of random donor mesenchymal stromal cells in steroid-resistant graft-versus-host disease represent a death knell or a bump in the road?* Cytotherapy, 2013. **15**(1): p. 2-8.

10. Dalal, J., K. Gandy, and J. Domen, *Role of mesenchymal stem cell therapy in Crohn's disease.* Pediatr Res, 2012. **71**(4 Pt 2): p. 445-51.

11. Halliley, J.L., et al., *Long-Lived Plasma Cells Are Contained within the CD19(-)CD38(hi)CD138(+) Subset in Human Bone Marrow.* Immunity, 2015. **43**(1): p. 132-45.

12. Richardson JD, N.A., Zannettino AC, Gronthos S, Worthley SG, Psaltis PJ., *Optimization of the cardiovascular therapeutic properties of mesenchymal stromal/stem cells-taking the next step.* Stem Cell Rev, 2013. **9**(3): p. 281-302.

13. Tan SS, Y.Y., Lee T, Lai RC, Yeo RW, Zhang B, Choo A, Lim SK., *Therapeutic MSC exosomes are derived from lipid raft microdomains in the plasma membrane.* Journal of Extracellular Vesicles, 2013. **2**: p. 22614-22625.

14. Bonnaure, G., C. Gervais-St-Amour, and S. Neron, *Bone Marrow Mesenchymal Stem Cells Enhance the Differentiation of Human Switched Memory B Lymphocytes into Plasma Cells in Serum-Free Medium.* J Immunol Res, 2016. **2016**: p. 7801781.

15. Roldán E, G.-P.A., Brieva JA., *VLA-4-Fibronectin Interaction Is Required for the Terminal Differentiation of Human Bone Marrow Cells Capable of Spontaneous and High Rate Immunoglobulln Secretion.* Journal of Experimental Medicine, 1992. **175**(6): p. 1739-47.

16. Tabera, S., et al., *The effect of mesenchymal stem cells on the viability, proliferation and differentiation of B-lymphocytes.* Haematologica, 2008. **93**(9): p. 1301-9.

17. Dallos T, K.M., Chorazy-Massalska M, Warnawin E, Zánová E, Rudnicka W, Radzikowska A, Maśliński W., *BAFF from bone marrow-derived mesenchymal stromal cells of rheumatoid arthritis patients improves their B-cell viability-supporting properties.* Folia Biologica (Praha). 2009. **55**(5): p. 166-76.

18. Roldán E, R.C., Navas G, Parra C, Brieva JA., *Cytokine network regulating terminal maturation of human bone marrow B cells capable of spontaneous and high rate Ig secretion in vitro.* Journal of Immunology, 1992. **149**(7): p. 2367-71.

19. Keller JR, O.M., Ruscetti FW., , *Steel factor (c-kit ligand) promotes the survival of hematopoietic stem/progenitor cells in the absence of cell division.* Blood, 1994. **86(5)**: p. 1757-1764.

20. Kobayashi, M., et al., *PRL2/PTP4A2 phosphatase is important for hematopoietic stem cell self-renewal.* Stem Cells, 2014. **32**(7): p. 1956-67.

21. Omatsu, Y., et al., *The essential functions of adipo-osteogenic progenitors as the hematopoietic stem and progenitor cell niche.* Immunity, 2010. **33**(3): p. 387-99.

22. Balbi C, P.M., Barile L, Papait A, Armirotti A, Principi E, Reverberi D, Pascucci L, Becherini P, Varesio L Mogni M, Coviello D, Bandiera T, Pozzobon M, Cancedda R, Bollini S., *First Characterization of Human Amniotic Fluid Stem Cell Extracellular Vesicles as a Powerful Paracrine Tool Endowed with Regenerative Potential.* Stem Cells Transl Med, 2017.

23. Schmidt, O. and D. Teis, *The ESCRT machinery.* Curr Biol, 2012. **22**(4): p. R116-20.

24. Wen S, D.M., Cheng Y, Papa E, Del Tatto M, Pereira M, Deng Y, Goldberg L, Aliotta J, Chatterjee D, Stewart C, Carpanetto A, Collino F, Bruno S, Camussi G, Quesenberry P., *Mesenchymal stromal cell-derived extracellular vesicles rescue radiation damage to murine marrow hematopoietic cells.* Leukemia, 2016. **30**(11): p. 2221-2231.

25. Battiwalla M, B.A., *Bone marrow mesenchymal stromal cells to treat complications following allogeneic stem cell transplantation.* Tissue Eng Part B Rev, 2014. **20**(3): p. 211-7.

26. Nicolay NH, S.E., Lopez R, Wirkner U, Trinh T, Sisombath S, Debus J, Ho AD, Saffrich R, Huber PE., *Mesenchymal stem cells retain their defining stem cell characteristics after exposure to ionizing radiation.* Int J Radiat Oncol Biol Phys, 2013. **87**(5): p. 1171-8.

27. Fekete N, E.A., Amann EM, Furst D, Rojewski MT, Langonne A, Sensebe L, Schrezenmeier H, Schmidtke-Schrezenmeier G., *Effect of high-dose irradiation on human bone-marrow-derived mesenchymal stromal cells.* Tissue Eng Part C Methods, 2015. **21**(2): p. 112-22.

28. Castro AR, M.W.a.P.V., *Lipid Removal from Human Serum Samples.* Clinical and Diagnostic Laboratory Immunology, 2000. **7**(2): p. 197-199.

29. Megger, D.A., et al., *One Sample, One Shot - Evaluation of sample preparation protocols for the mass spectrometric proteome analysis of human bile fluid without extensive fractionation.* J Proteomics, 2017. **154**: p. 13-21.

30. Helwa, I., et al., *A Comparative Study of Serum Exosome Isolation Using Differential Ultracentrifugation and Three Commercial Reagents.* PLoS One, 2017. **12**(1): p. e0170628.

31. Madrigal M, R.K., Riordan NH, *A review of therapeutic effects of mesenchymal stem cell secretions and induction of secretory modification by different culture methods.* Journal of Translational Medicine, 2014. **12**(260): p. s12967-014-0260-8.

32. Nong, K., et al., *Hepatoprotective effect of exosomes from human-induced pluripotent stem cell-derived mesenchymal stromal cells against hepatic ischemia-reperfusion injury in rats.* Cytotherapy, 2016. **18**(12): p. 1548-1559.

33. Giri, P.K., et al., *Proteomic analysis identifies highly antigenic proteins in exosomes from M. tuberculosis-infected and culture filtrate protein-treated macrophages.* Proteomics, 2010. **10**(17): p. 3190-202.

34. Zhao, Z., et al., *A microfluidic ExoSearch chip for multiplexed exosome detection towards blood-based ovarian cancer diagnosis.* Lab Chip, 2016. **16**(3): p. 489-96.

35. Kim, J., Z. Tan, and D.M. Lubman, *Exosome enrichment of human serum using multiple cycles of centrifugation.* Electrophoresis, 2015. **36**(17): p. 2017-26.

36. Foster, B.P., et al., *Extracellular vesicles in blood, milk and body fluids of the female and male urogenital tract and with special regard to reproduction.* Crit Rev Clin Lab Sci, 2016. **53**(6): p. 379-95.

37. Zarovni, N., et al., *Integrated isolation and quantitative analysis of exosome shuttled proteins and nucleic acids using immunocapture approaches.* Methods, 2015. **87**: p. 46-58.

38. Tan, S.S., et al., *Therapeutic MSC exosomes are derived from lipid raft microdomains in the plasma membrane.* J Extracell Vesicles, 2013. **2**.

39. Li T, Y.Y., Wang B, Qian H, Zhang X, Shen L, Wang M, Zhou Y, Zhu W, Li W, Xu W., *Exosomes Derived from Human Umbilical Cord Mesenchymal Stem Cells Alleviate Liver Fibrosis.* Stem Cells and Development, 2013. **22**(6): p. 845-54.

40. Tomasoni S, L.L., Rota C, Morigi M, Conti S, Gotti E, Capelli C, Introna M, Remuzzi G, Benigni A., *Transfer of Growth Factor Receptor mRNA Via Exosomes Unravels the Regenerative Effect of Mesenchymal Stem Cells.* Stem Cells and Development, 2013. **22**(5): p. 772-80.

41. Chinnadurai R, N.S., Velu V, Galipeau J., *Challenges in animal modelling of mesenchymal stromal cell therapy for in ammatory bowel disease.* World J Gastroenterol 2015. **21**(16): p. 4779-4787.

42. Chinnadurai R, G.M., Sakurai Y, Lam WA, Kirk AD, Galipeau J, Copland IB., *Actin cytoskeletal disruption following cryopreservation alters the biodistribution of human mesenchymal stromal cells in vivo.* Stem Cell Reports, 2014. **3**(1): p. 60-72.

43. Mulcahy, L.A., R.C. Pink, and D.R. Carter, *Routes and mechanisms of extracellular vesicle uptake.* J Extracell Vesicles, 2014. **3**.

44. Malhotra, S., et al., *B cell antigen receptor endocytosis and antigen presentation to T cells require Vav and dynamin.* J Biol Chem, 2009. **284**(36): p. 24088-97.

45. HM, M.H.a.M., *Mesenchymal Stem Cell Therapy for Autoimmune Disease: Risks and Rewards.* Stem Cells and Development, 2015. **24**(18): p. 2091-2100.

46. Introna M, R.A., *Mesenchymal stromal cells for prevention and treatment of graft-versus-host disease: successes and hurdles.* Current Opinion in Organ Transplantation, 2015. **20**(1): p. 72-78.

47. Mendez-Ferrer, S., et al., *Mesenchymal and haematopoietic stem cells form a unique bone marrow niche.* Nature, 2010. **466**(7308): p. 829-34.

48. Lattanzio, R., M. Piantelli, and M. Falasca, *Role of phospholipase C in cell invasion and metastasis.* Adv Biol Regul, 2013. **53**(3): p. 309-18.

49. Shirakawa, R. and H. Horiuchi, *Ral GTPases: crucial mediators of exocytosis and tumourigenesis.* J Biochem, 2015. **157**(5): p. 285-99.

50. Burbage M, K.S., Gasparrini F, Martínez-Martín N, Gaya M, Feest C, Domart MC, Brakebusch C, Collinson L, Bruckbauer A, and Batista FD., *Cdc42 is a key regulator of B cell di erentiation and is required for antiviral humoral immunity.* Journal of Experimental Medicine, 2014. **212**(1): p. 53-72.

51. Gerasimcik N, D.C., Baptista MAP, Massaad MJ, Geha RS, Westerberg LS, Severinson E., *The Rho GTPase Cdc42 Is Essential for the Activation and Function of Mature B Cells.* Journal of Immunology. **194**: p. 4750-4758.

52. Chinnadurai, R., et al., *Cryopreserved Mesenchymal Stromal Cells Are Susceptible to T-Cell Mediated Apoptosis Which Is Partly Rescued by IFNgamma Licensing.* Stem Cells, 2016. **34**(9): p. 2429-42.

53. Szatanek, R., et al., *Isolation of extracellular vesicles: Determining the correct approach (Review).* Int J Mol Med, 2015. **36**(1): p. 11-7.

54. Halliley, J.L., et al., *Peak frequencies of circulating human influenza-specific antibody secreting cells correlate with serum antibody response after immunization.* Vaccine, 2010. **28**(20): p. 3582-7.

55. Chen WX, S.J., Wu RH., *Enhancing the mass spectrometric identification of membrane proteins by combining chemical and enzymatic digestion methods.* Journal of Proteome Research, 2014. **13**: p. 1466-1473.

56. Eng JK, M.A., Yates JR., *An approach to correlate tandem mass spectral data of peptides with amino acid sequences in a protein database.* Journal of the American Society of Mass Spectrometry, 1994. **5**(11): p. 976-89.

57. Elias JE, G.S., *Target-decoy search strategy for increased confidence in large-scale protein identifications by mass spectrometry.* Nature Methods, 2007. **4**(3): p. 207-14.

58. Käll L, C.J., Weston J, Noble WS, MacCoss MJ., *Semi-supervised learning for peptide identification from shotgun proteomics datasets.* Nature Methods, 2007. **4**(11): p. 923-5.

References for Chapter 6: Conclusions and Next Steps

1. Schorey, J.S. and S. Bhatnagar, *Exosome function: from tumor immunology to pathogen biology.* Traffic, 2008. **9**(6): p. 871-81.

2. Martin-Jaular, L., et al., *Exosomes from Plasmodium yoelii-infected reticulocytes protect mice from lethal infections.* PLoS One, 2011. **6**(10): p. e26588.

3. Beauvillain, C., et al., *Exosomes are an effective vaccine against congenital toxoplasmosis in mice.* Vaccine, 2009. **27**(11): p. 1750-7.

4. Pinpin, L., et al., *Overexpression of Aryl Hydrocarbon Receptor in Human Lung Carcinomas.* Toxicologic Pathology, 2003. **31**(1): p. 22-30.

5. Munir, H. and H.M. McGettrick, *Mesenchymal Stem Cell Therapy for Autoimmune Disease: Risks and Rewards.* Stem Cells Dev, 2015. **24**(18): p. 2091-100.

6. Anthony, B.A. and D.C. Link, *Regulation of hematopoietic stem cells by bone marrow stromal cells.* Trends Immunol, 2014. **35**(1): p. 32-7.

7. Stagg J, G.G., *Mechanisms of immune modulation by mesenchymal stromal cells and clinical translation.* Current Molecular Medicine, 2013. **13**(5): p. 856-67.

8. Bhadkamkar, N.A., et al., *Chapter 19. Hepatobiliary Malignancies*, in *The MD Anderson Manual of Medical Oncology, 2e*, H.M. Kantarjian, R.A. Wolff, and C.A. Koller, Editors. 2011, The McGraw-Hill Companies: New York, NY.

9. Konety, B.R.C., Peter R., *Chapter 21. Urothelial Carcinoma: Cancers of the Bladder, Ureter, & Renal Pelvis*, in *Smith & Tanagho's General Urology, 18e*, J.W. McAninch and T.F. Lue, Editors. 2013, The McGraw-Hill Companies: New York, NY.

10. Teitelbaum, D.T., *Chapter 56. Introduction to Toxicology: Occupational & Environmental*, in *Basic & Clinical Pharmacology, 12e*, B.G. Katzung, S.B. Masters, and A.J. Trevor, Editors. 2012, The McGraw-Hill Companies: New York, NY.

11. Lin, J.T., et al., *Colon cancer mesenchymal stem cells modulate the tumorigenicity of colon cancer through interleukin 6.* Exp Cell Res, 2013. **319**(14): p. 2216-29.

12. Bonner, J.C., *Mesenchymal cell survival in airway and interstitial pulmonary fibrosis.* Fibrogenesis Tissue Repair, 2010. **3**: p. 15.

13. Pierro, M. and B. Thebaud, *Mesenchymal stem cells in chronic lung disease: culprit or savior?* Am J Physiol Lung Cell Mol Physiol, 2010. **298**(6): p. L732-4.

14. Smith KJ, M.I., Tanos R, Tellew J, Boitano AE, Bisson WH, Kolluri SK, Cooke MP, Perdew GH., *Identification of a high-affinity ligand that exhibits complete aryl*

hydrocarbon receptor antagonism. Journal of Pharmacology and Experimental Therapeutics, 2011. **338**(1): p. 318-27.

15. Mezrich, J.D., et al., *An interaction between kynurenine and the aryl hydrocarbon receptor can generate regulatory T cells.* Journal of Immunology, 2010. **185**(6): p. 3190-8.

16. Quintana, F.J., et al., *Control of T(reg) and T(H)17 cell differentiation by the aryl hydrocarbon receptor.* Nature, 2008. **453**(7191): p. 65-71.

17. DiNatale, B.C., et al., *Mechanistic insights into the events that lead to synergistic induction of interleukin 6 transcription upon activation of the aryl hydrocarbon receptor and inflammatory signaling.* Journal of Biological Chemistry, 2010. **285**(32): p. 24388-97.

18. Maccario R, P.M., Moretta A, Cometa A, Comoli P, Montagna D, Daudt L, Ibatici A, Piaggio G, Pozzi S, Frassoni F, Locatelli F., *Interaction of human mesenchymal stem cells with cells involved in alloantigen-specific immune response favors the differentiation of CD4+ T-cell subsets expressing a regulatory/suppressive phenotype.* Haematologica, 2015. **90**: p. 516-525.

19. Gerring, J., *Mere Description.* British Journal of Political Science, 2012. **42**(4): p. 721-46.

20. Baudrillard, J., *Le Système Des Objets*. 1968, Paris.: Gallimard.